Optimal Strategies for Electrical Stimulation with Implantable Neuromodulation Devices

Steffen Eickhoff, MSc, BEng

A thesis submitted in partial fulfilment of the requirements of

Liverpool John Moores University for the degree of

Doctor of Philosophy

This research programme was carried out in collaboration with

MED-EL Medical Electronics

July 2020

DECLARATION

This dissertation was written by me and is the result of my own work. It has not been previously submitted, in part or whole, to any university of institution for any degree, diploma, or other qualification.

Signed: 

Steffen Eickhoff, MSc, BEng

Liverpool, 07.07.2020

ABSTRACT

Electrical stimulation (ES) is a neuromodulation technique that uses electrical pulses to modulate the activity of excitable cells to provide a therapeutic effect. Many past and present ES applications use rectangular current waveforms that have been well studied and are easy to generate. However, an extensive body of scientific literature describes different stimulation waveforms and their potential benefits. A key measure of stimulation performance is the amplitude required to reach a certain percentual threshold of activation, as it directly influences important ES parameters such as energy consumption per pulse and charge density. The research summarized in this thesis was conducted to re-examine some of the most-commonly suggested ES waveform variations in a rodent *in-vivo* nerve-muscle preparation. A key feature of our experimental model is the ability to test stimulation with both principal electrode configurations, monopolar and bipolar, under computer control and in randomized order. Among the rectangular stimulation waveforms, we investigated the effect of interphase gaps (IPGs), asymmetric charge balanced pulses, and subthreshold conditioning pre-pulses. For all these rectangular waveforms, we surprisingly observed opposite effects in the monopolar compared to the bipolar stimulation electrode configuration. The rationale for this consistent observation was identified by analyzing electroneurograms (ENGs) of the stimulated nerve. In the monopolar configuration, biphasic pulses first evoked compound action potentials (eCAPs) as a response to the first field transition. In the bipolar electrode configuration, that is the mode in which many contemporary ES devices, including the envisioned miniaturized *electroceuticals*, operate, eCAPs were first elicited at the return electrode in response to the middle field transition of biphasic pulses. As all rectangular waveform variations achieve their effect by modulating the amplitude and timing of cathodic (excitatory) and anodic (inhibitory) field transitions, the inverted current profile at the bipolar return electrode explains these observed opposite effects.

Further we investigated the claimed benefits of non-rectangular, Gaussian stimulation waveforms in our animal model. In our study only moderate energy savings of up to 17% were observed, a finding that is surprising in light of the predicted range of benefits of up to 60% energy savings with this novel waveform in question. Additionally, we identified a major disadvantage in terms of substantially increased maximum instantaneous power requirements with Gaussian compared to rectangular stimuli.

We examined physiological changes in fast twitch muscle following motor nerve injury, and optimal stimulation strategies for activation of denervated muscle. While a high frequency doublet has previously been identified to enhance stimulation efficiency of healthy fast twitch muscle, an effect that has been termed *"doublet effect"*, we here show that this benefit is gradually lost in muscle during denervation. Lastly, the effect of long duration stimulation pulses, that are required to activate denervated muscle, on nerve is examined. We show that these long pulses can activate nerves up to three times when the three field transition within the biphasic pulses are separated by more than (i.e., when the phase width is above) the refractory period of that nerve. This observation challenges state-of-the-art computational models of extracellular nerve stimulation that do not seem to predict such multiple activations. Further, an undesired up to threefold co-activation of innervated structures nearby the denervated stimulation target warrants further research to study whether these co-activations can be lessened with alternative stimulation waveforms such as ramped *sawtooth* pulses.

ACKNOWLEDGEMENTS

With this I would like to express my thanks and gratitude to all those who supported me on my PhD journey. First and foremost, I want to thank my supervisory team, led by my director of studies Professor Jonathan Jarvis. His tireless, detail-oriented work mentality as well as his genuine passion to solve complex research questions have been an inspiration throughout my PhD studies. I remain in admiration of Jonathan's deep subject knowledge both of muscle physiology and biomedical engineering to which I was provided access in countless meetings and discussions. The guidance and feedback that I received from Jonathan accelerated my academic and personal development and I continue to profit from my time in his research group. Further, my gratitude is towards the extended supervisory team: I thank my second supervisor Professor Gabor Barton, Professor Winfried Mayr from the Center for Medical Physics and Biomedical Engineering at Medical University of Vienna, and Werner Lindenthaler who is leading the emerging applications division of MED-EL Medical Electronics, our industrial partner. I thank Dr Hazel Sutherland and Mark Viggars for all their help with the animal experiments. Further I am grateful to Steve Broadfoot and his team for their help with animal care and handling, and I acknowledge that their practical support and experience was crucial to guarantee successful data collection. I thank Professor Frank Rattay and Dr Andreas Fellner from the Institute of Analysis and Scientific Computing at Vienna University of Technology for the many most stimulating discussions and their collaboration in an ongoing research project. I am thankful for the joint research project with Dr Daniel Owens and Andrew Nolan and the opportunity to get valuable insights in a new area of research, applying electrical stimulation to muscle cell cultures. I thank my former host family Phil and Kate Hammersley, who welcomed me in when I was a stranger in Liverpool, supported me in so many ways and became very good friends. Finally, I want to thank my family and especially my wife Emma for all her encouragement and support throughout the many challenges that accompanied us on my PhD journey. Thank you all so much!

CONTENTS

LIST OF TABLES

LIST OF FIGURES

LIST OF ABBREVIATIONS AND ACRONYMS

°C	Degree Celsius
Ω	Ohm
Å	Angstrom
A-band	Anisotropic band
AC	Alternating current
ACh	Acetylcholine
ANOVA	Analysis of variance
AP	Action potential
ARP	Absolute refractory period
ATP	Adenosine triphosphate
Ca^{2+}	Calcium ion
CAP	Compound action potential
Ca_V	Voltage gated calcium ion channel
c_e	Extracellular ion concentration
CE	Contractile element (in Hill-type muscle model)
c_i	Intracellular ion concentration
Cl^-	Chloride ion
Cl_e	Extracellular chloride concentration
Cl_i	Intracellular chloride concentration
CNS	Central nervous system
CPN	Common peroneal nerve
CSC	Charge storage capacity
DBS	Deep brain stimulation
DC	Direct current
DPP	Depolarizing pre-pulse
e	Euler constant
E	Electrical energy
eCAP	Electrically evoked compound action potential
EDL	Extensor digitorum longus muscle
e.g.	Latin: "*exempli gratia*" – for example
E_m	Transmembrane potential
EMG	Electromyogram
ENG	Electroneurogram
epp	endplate potential

ES	Electrical stimulation
E_{th}	Threshold energy
F	Faraday constant
FTI	Force time integral
G	Gauge
GA	Genetic algorithm
GHK	Goldman-Hodgkin-Katz (equation)
g_K, g_{Na}, g_{Cl}	Membrane conductance to potassium, sodium, chloride
h	Sodium channel inactivation variable
HPP	Hyperpolarizing pre-pulse
Hz	Hertz
I, I_{stim}	Current, Stimulation amplitude
$I_{50\%}$, $I_{95\%}$	50%, 95% Threshold current
I_{an}	Amplitude of anodic phase
I-band	Isotropic band
I_{ca}	Amplitude of cathodic phase
i.e.	Latin: "*id est*" – that is
IPG	Interphase gap
IPI	Inter pulse interval
I_r	Rheobase
I_{th}	Threshold current
J	Joule
k	Adjustable parameter
K	Kelvin
K^+	Potassium ion
K_e	Extracellular potassium concentration
kg	Kilogram
KHFAC	Kilohertz frequency alternating current
K_i	Intracellular potassium concentration
kS	Kilo-sample = 1,000 samples
K_V	Voltage gated potassium ion channel
L	Litre
ln	Natural logarithm
$\log_{10}$	Common logarithm
mAChR	Muscarinic acetylcholine receptors
mepp	Miniature endplate potential

MFCV	Muscle fibre conduction velocity
MS	Mega-sample = 1,000,000 sample
N	Newton
Na^+	Sodium ion
nAChR	Nicotinic acetylcholine receptors
Na_e	Extracellular sodium concentration
Na_i	Intracellular sodium concentration
NA/K-ATPase	Sodium-potassium adenosine triphosphatase
Na_V	Voltage gated sodium ion channel
nFTI	Normalized force time integral
NMJ	Neuromuscular junction
NoR	Node of Ranvier
OPA	Operational Amplifier
P	Power
PE	Parallel elastic element (in Hill-type muscle model)
PhW	Phase width
P_K, P_{Na}, P_{Cl}	Membrane permeabilities to Potassium, Sodium, Chloride
PNS	Peripheral nervous system
PPL	Home Office project licence
pps	Pulses per second
PSC	Perisynaptic Schwann cell
PW	Pulse width
Q	Electric charge
Q_{th}	Threshold charge
R	Gas constant
RMS	Room mean square
RRP	Relative refractory period
SD	Standard deviation
SE	Series elastic element (in Hill-type muscle model)
SEM	Standard error of the mean
SI	International System of Units (Système international d'unités)
T	Temperature
T_C	Chronaxie
t-SNARE	Target-soluble N-ethylmaleimide sensitive fusion attachment protein receptor
T-tubules	Transverse tubules

V	Volt
$V_{e,n}$, $V_{e,n-1}$, $V_{e,n+1}$	Extracellular potential at the central, previous, and next node of Ranvier
v-SNARE	Vesicle-soluble N-ethylmaleimide sensitive fusion attachment protein receptor
W	Watt
Z	Impedance
Z-disc	German: "*Zwischenscheibe*" - the disc in between the I-bands

LIST OF APPENDICES

1 INTRODUCTION

1.1 Motivation and structure of the thesis

Many medical devices and treatments use electrical stimulation (ES) to achieve a therapeutic effect. Often, especially when the ES equipment is battery powered, as is the case with many wearable or implanted devices, energy efficient stimulation is of paramount importance. Optimization of the waveform used for stimulation can influence the amount of electrical energy consumed per pulse and a number of rectangular and non-rectangular waveform variations have been suggested in scientific literature to improve efficiency of ES. However, these published experimental and computational studies about the effect of many stimulation waveforms are unclear and report contradictory findings. Further, most authoritative literature on such pulse shaping strategies only investigated the monopolar electrode configuration that is different from the bipolar mode in which many contemporary ES devices operate. Thus, this PhD project aimed to comprehensively re-examine commonly suggested ES waveforms in an *in-vivo* animal model with a particular focus on the influence of the stimulation electrode configuration.

After providing the essential background knowledge about the neuromuscular system (Section 1.2) and electrical stimulation (Section 1.3), Chapter 2 describes the development and refinement of a rodent nerve-muscle model, suitable to answer the relevant research questions outlined above. This model includes a sophisticated instrumentational setup for neural stimulation and recording, and effective methods for data normalization, as well as analysis of complex bioelectric signals.

In Chapter 3, three studies arising from the examination of rectangular and non-rectangular stimulation waveform variations are presented:

- Subthreshold conditioning pre-pulses (Section 3.1)
- Interphase gaps and asymmetric pulses (Section 3.2)
- Gaussian shaped pulses (Section 3.3)

A set of experimental observations on muscle surface stimulation with standard rectangular pulses in healthy (innervated) and impaired preparations with different time courses of denervation is presented in Chapter 4. These experiments raise fundamental questions on differences in recruitment behaviour with nerve and muscle surface stimulation and warrant further research.

The study presented in Chapter 5 closely examines a series of experiments on the influence of long phase width stimuli, such as are used for stimulation of partially or complete denervated muscle, on nerve. This investigation is of interest since in many scenarios of denervated muscle stimulation, nearby innervated structures may be affected by these long duration ES pulses.

1.2 The neuromuscular system

Neuromuscular systems can even be found in some of the lowest developed multicellular organisms with differentiated tissues. Sedentary sea anemones, for example, possess cell networks that combine sensory reception with locomotive response, enabling the organism to catch food or withdraw as defence (Katz, 1966).

There are two principal methods of communication within living organisms. The first way of conveying information relies on transmission of chemical messenger substances, the hormones. Following a specific stimulus, the transmitter organ A releases the hormones, e.g. into the blood stream, which then travel through the system until they find the receiver organs B and C that are equipped with the corresponding receptors. While communication via hormones plays a critical role in numerous systemic regulatory and metabolic processes, it is inappropriate for many functions that required fast and accurate transmission of information. The second path of communication relies on the transmission of electrical signals and meets these demands for speed and accuracy. The nervous system provides the necessary infrastructure for this electrical communication. The nervous system of vertebrates consists of the peripheral nervous system (PNS) and the central nervous system (CNS), which is the organisms central processing unit. The CNS is comprised of the brain and spinal cord, both these delicate structures are safely suspended in a shock absorbing fluid inside their bony protective shells, the skull and the

spinal canal. The PNS is a network of conductive pathways, the nerve fibres or *axons*, that connect the CNS to every other part of the organism. While the PNS contains some peripheral processing units, the ganglia, its two main tasks are providing sensory input to the CNS, via *afferent* fibres, and transmitting commands from the CNS to the periphery via *efferent* fibres. The structural base units fulfilling these tasks are the individual neurons.

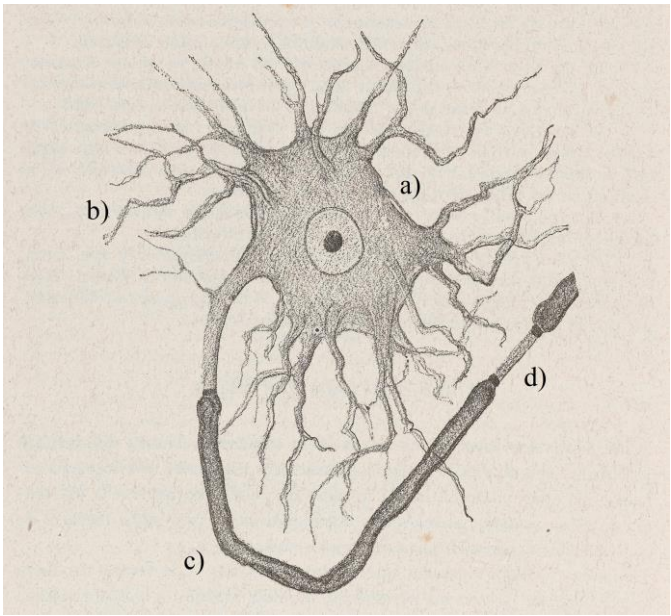

Figure 1.1 The neuron is the structural unit of the nervous system. Dendritic processes (b) and the myelinated axon (c) originate from the cell soma (a). Myelination is interrupted at nodes of Ranvier (d), where the axonal membrane is exposed. (Ramón y Cajal, 1911) Copyright by Wellcome Collection. CC BY. Adapted with permission.

Neurons are comprised of a cell body, the *soma*, from which a network of fine processes is spreading in various directions and is contacting neighbouring cells (Figure 1.1). A neuron can be seen as a miniature nervous system itself: It receives input via synapses on the cell body and the nearby dendritic processes, integrates these received input data, and generates an output signal, an action potential, which it sends along its efferent pathway to its axonal terminals. On both sides, the dendritic/somatic input and the terminal output, the neuron is in close contact with its neighbouring cells. Further, most nerves cells are almost entirely enveloped by tightly connected satellite cells, like the Schwann cells that form an insulating myelin sheath around most mammalian nerve axons. The intimate nature of these cell interactions divided late 19th and early 20th century physiologists into two schools of thinking. One group, championed by Italian biologist Camillo Golgi, thought the cells are penetrating each other, forming a smooth reticular network, while

the other group famously represented by Spanish scientist Santiago Ramón y Cajal, maintained that the individual nerve cells are, albeit the close contact with other cells, structurally separated[1]. Later findings of electron microscope investigations proved Ramón y Cajal right and revealed that the gaps between a neuron and its neighbouring and satellite cells are as small as a hundred angstrom[2].

In the neuromuscular systems of many vertebrates, many functional complexes are formed by neurons interacting with adjacent cells. The following list highlights some key complexes formed by neurons and other cells and is far from being exhaustive:

- Motor units consist of a motor neuron and several skeletal muscle fibres that are innervated by terminal branches of that neuron (Liddell and Sherrington, 1925).
- Neuromuscular junctions (NMJ) are tripartite synapse complexes consisting of a pre-synaptic terminal nerve process of a motor nerve, a post-synaptic muscle fibre and a perisynaptic Schwann cell (PSC).
- Myelination of a peripheral nerve axon is formed by Schwann cells wrapping around the axon concentrically (Figure 1.2), interrupted in regular intervals by small patches of exposed nerve membrane, so called nodes of Ranvier (NoR).
- Muscle spindles and Golgi tendon organs are proprioceptive sensory receptors that sense changes in muscle length and tension and provide constant feedback to the CNS. They are comprised of afferent sensory fibres interacting with muscle and tendon tissue.

1.2.1 The motor neuron

Axons leaving the CNS form bundles of fibres, the nerves, that are running together to the region they innervate. These peripheral nerve trunks are enclosed by the epineurium, a dense connective tissue layer, and are typically comprised of multiple distinct nerve fascicles, small arterioles and venules, fibroblasts, mast cells, and occasional lymphocytes (Bertorini, 2008). The fascicles have an outer connective tissue layer, the perineurium,

[1] Ramón y Cajal and Golgi received the 1906 Nobel Prize in Physiology or Medicine jointly for their work on the structure of the nervous system. “The two scientific adversaries met only in Stockholm. Golgi aggressively championed his belief in ‘reticular’ [smooth] neural networks in his Nobel lecture, which Ramón y Cajal characterized in his autobiography as an ‘extravagant lucubration.’” (Bentivoglio, 2014).

[2] The angstrom (Å) is a metric unit of length, named after Swedish physicist Anders Jonas Ångström, and is equal to 10^{-10}m or 0.1nm.

and are bundles of individual axons. The individual nerve axons have yet another thin connective tissue sheath wrapped around them, the endoneurium (Figure 1.2).

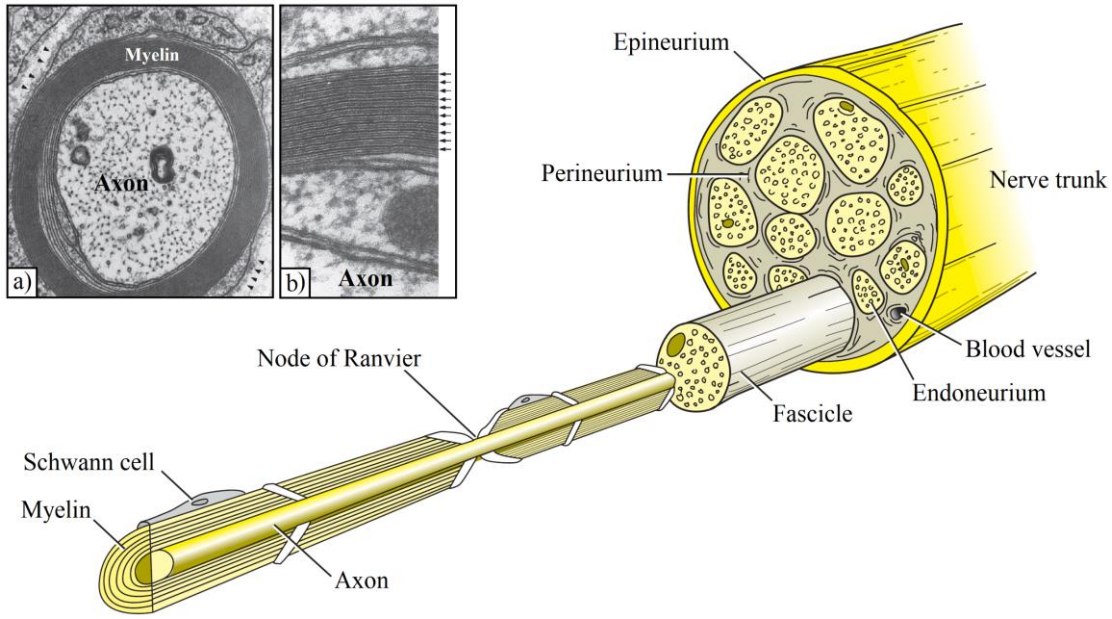

Figure 1.2 The peripheral nerve and its components. (Bertorini, 2008) Copyright by Elsevier. Adapted with permission. Insets: Electron micrograph illustrating the ultrastructure of the myelin sheath. a) Transverse section of an axon with myelination composed of multiple layers of Schwann cell membrane (arrowheads). b) Examination of the myelin sheath at higher magnification. (Johns, 2014) Copyright by Elsevier. Adapted with permission.

Peripheral nerves typically contain a distribution of small and large, unmyelinated and myelinated fibres of different fibre types. One fibre type most relevant to the neuromuscular system is the group of large diameter myelinated Aα fibres that innervate muscle fibres and thus form the motor units. Table 1.1 summarizes the key characteristics of Aα and other nerve and muscle fibre types. The myelination is an insulating multilayer structure, formed by Schwann cells concentrically wrapped around the axon (Figure 1.2). The myelin sheath of large Aα nerve fibres is normally composed of 80 to 160 individual myelin lamellae (Bertorini, 2008). In regular intervals, at the nodes of Ranvier, the insulation myelin sheath is interrupted and the axonal nerve membrane is exposed.

Table 1.1 Nerve and muscle fibre types. [a] (Bertorini, 2008; Marani and Lakke, 2012)

Nerve fibre types

Classification		Myelination	Diameter (µm) // conduction velocity (m/s)	Function and associated cells
Aα		myelinated	12-20 // 70-120	motor somatic muscle fibre
Aα	Ia	myelinated	12-20 // 70-120	proprioception; muscle spindle annulospiral
Aα	Ib	myelinated	12-20 // 70-120	proprioception; Golgi tendon organ
Aβ	II	myelinated	5-12 // 30-70	proprioception; muscle spindle flower spray
Aβ	II	myelinated	5-12 // 30-70	exteroception; touch and pressure
Aγ		myelinated	2-8 // 10-50	motor somatic muscle spindle
Aδ	III	myelinated	1-5 // 3-30	exteroception; pain temperature (some) touch
B		unmyelinated	1-3 // 3-15	motor autonomic preganglionic
C	IV	unmyelinated	<1 // <2	exteroception; pain reflex responses
C		unmyelinated	<1 // <2	motor autonomic postganglionic sympathetic

Muscle fibre types

Type	Speed	Strength	Fatigability	ATPase	Colour	Motor unit	Axon
I	slow	weak	fatigue resistant	low	red	slow	small
IIB	fast	strong	fatigable	high	white	fast, fatigable	large
IIA	fast	intermediate	fatigue resistant	high	red	fast, fatigue resistant	large

[a] Note that these numbers are means from several publications.

The nerve membrane

In order to understand the generation and propagation of electrical signals, the action potentials, in the nervous system, a brief description of the nerve membrane structure, its electrical potential and the function of its transmembrane ion channels will be given below.

The plasma membrane of excitable cells not only provides structural integrity, but it is crucial in maintaining a concentration gradient between the intracellular and extracellular space and controls the cells nutrient supply and waste disposal. The membrane is built from carbohydrates, lipids, and proteins. The lipid bilayer is formed of phospholipids, glycolipids, and contains cholesterol molecules (Koester, 1985a) and prevents large water-soluble molecules to pass across the membrane. To allow for the passage of specific water-soluble molecules and ions across the lipid bilayer, channel proteins are situated in

the membrane, connecting the intracellular and extracellular space over a water filled channel or pore. Some forms of transmembrane transport involve carrier proteins that bind to a substance, undergo a conformational change, and release the substance on the other side of the membrane.

Some special types on transmembrane channel proteins, that enable selective passage of electrical charge carrying ions, are fundamentally important for the generation and propagation of action potentials in nervous tissue (Koester, 1985b). Some channels, the so-called *leak* channels, are in an open state when the nerve membrane is at rest and let specific ions pass the membrane following their electrical and/or concentration gradient. Other channels undergo a conformational change when a specific neurotransmitter binds to them and thus change from the closed to the open state (or vice versa). This group of channels is called *ligand-gated* and an example is the nicotinic acetylcholine receptor (nAChR) that is of central importance for the excitation-contraction coupling at the neuromuscular junction. *Voltage-gated* channels change their conformation to open or closed state based on local changes of the transmembrane potential. A common and helpful notation for voltage-gated ion channels is a subscript $_v$ behind the ions symbol as example Na_V for voltage gated sodium ion channels or K_V for voltage gated potassium channels. Besides these *passive* ion transport mechanisms, that do not require energy for operation, *active* transport mechanisms use energy, e.g. chemical energy in form of adenosine triphosphate (ATP), to move ions against their concentration gradient across the cell membrane. For nerve cells to maintain their resting potential, the sodium-potassium pump (Na-K ATPase pump) is an important example of active transmembrane transport (Bertorini, 2008).

The membrane resting potential

In 1868, Julius Bernstein published his famous Bernstein-hypothesis (Bernstein, 1868) and advanced it in 1902 with his “membrane theory” (Bernstein, 1902), proposing that the intracellular space of living cells contains ions at different concentrations than the extracellular space. Bernstein hypothesized that the thin, relatively impermeable cell membrane prevents the ions to follow their concentration gradient and that the interior space of excitable cells is at rest more negative than the extracellular space.

Today, more than a century after his original proposal, Bernstein’s hypothesis of transmembrane ionic concentration gradients is still the prevailing paradigm in neurophysiology. In excitable cells, the concentration and electrical gradients of

osmotically active particles create a membrane resting potential. Depending on the specific cell type, the cell interior is between approximately 60 to 90mV more negative than the extracellular space. The concentration gradient causes ions on both sides of the membrane to try to equilibrate. In the intracellular space large polyanionic[3] proteins and positive charge carrying potassium ions K^+ are present in high concentrations (Table 1.2). Following their *concentration gradient* K^+ ions tend to move, or *leak*, into the extracellular space. This loss of positive charge creates an *electrical gradient* across the membrane that counteracts the tendency of K^+ ions to leave the cell. The transmembrane potential at which the K^+ outflux due to the concentration gradient is balanced by the K^+ influx following the electrical gradient, i.e. the potential at which no net K^+ flux occurs across the membrane, is called the *equilibrium potential*.

Table 1.2 Distribution of osmotically active particles in a peripheral nerve and its surrounding fluid (Dwyer, 2018). Copyright by Elsevier. Reprint with permission.

		Free ion concentration		
Ion	**Molecular charge**	**Intracellular**	**Extracellular**	**Equilibrium potential (mV)**
Sodium	+1	10mM	142mM	+70
Potassium	+1	100mM	4mM	-86
Calcium	+2	0.0001mM	1.2mM	+126
Chloride	-1	5.5mM	103mM	-78
Protein	Polyanion [-x]	200-300mg/mL	Cerebrospinal fluid: 0.2-0.5mg/mL Interstitium: ~20mg/mL Plasma: 55-80mg/mL	None possible

The equilibrium membrane potential E_m for individual ion types can be calculated using the Nernst equation:

$$\boldsymbol{E_m = \frac{R \cdot T}{z \cdot F} \cdot \ln\left(\frac{c_e}{c_i}\right) = 2.303 \cdot \frac{R \cdot T}{z \cdot F} \cdot \log_{10}\left(\frac{c_e}{c_i}\right)}, \qquad (1.1)$$

where R is the gas constant (8.31446 J K^{-1} mol^{-1}), T the temperature, F the Faraday's constant (96.485 J V^{-1} mol^{-1}), z the charge of the ion, c_e the extracellular ion concentration, and c_i the intracellular ion concentration. At a physiological temperature of 37°C

$$\boldsymbol{2.303 \cdot \frac{R \cdot T}{F} = 61.1\,mV}, \qquad (1.2)$$

[3] Polyanions are complexes that have multiple negative charges.

and thus, the Nernst equation (1.1) can be simplified with (1.2) at this temperature:

$$E_m = \frac{61.6\text{mV}}{z} \cdot \log_{10}\left(\frac{c_e}{c_i}\right). \quad (1.3)$$

Thereby we can determine the equilibrium potential for a specific ion, for example, for chloride:

$$\boldsymbol{E_m = \frac{61.6\text{mV}}{-1} \cdot \log_{10}\left(\frac{103}{5.5}\right) = -78\text{mV}}. \quad (1.4)$$

The membrane potential of nerves, which at rest is between -70 and -80mV, depends not only on the gradients and net flux of a single type of ions but is the sum of multiple potentials caused by different osmotically active particles. The main osmotically active ions contributing to the transmembrane potential are sodium, potassium, and chloride (Table 1.2). Based on the Nernst-Planck equation, Goldman, Hodgkin and Katz derived the GHK equation (Goldman, 1943; Hodgkin and Katz, 1949) describing the membrane potential E_m

$$\boldsymbol{E_m = \frac{R \cdot T}{F} \cdot \ln \frac{P_K \cdot K_e + P_{Na} \cdot Na_e + P_{Cl} \cdot Cl_i}{P_K \cdot K_i + P_{Na} \cdot Na_i + P_{Cl} \cdot Cl_e}}, \quad (1.5)$$

which at temperatures of 37°C can be simplified with (1.2) to

$$\boldsymbol{E_m = 61.6\text{mV} \cdot \log_{10} \frac{P_K \cdot K_e + P_{Na} \cdot Na_e + P_{Cl} \cdot Cl_i}{P_K \cdot K_i + P_{Na} \cdot Na_i + P_{Cl} \cdot Cl_e}}, \quad (1.6)$$

where P_K, P_{Na}, and P_{Cl} are the ion-specific membrane permeabilities, K_e, Na_e, and Cl_e are the extracellular ion concentration and K_i, Na_i, and Cl_i are the intracellular ion concentrations. Absolute membrane permeabilities are difficult to measure and are thus, based on experimental findings, commonly substituted in the GHK equation (1.5) by the relative permeability of P_{Na}/P_K=1/100 (Dwyer, 2018). Further, as we will show below, to determine the membrane resting potential with (1.5) the contribution of Cl^- ions can be neglected. With the ion concentrations given in Table 1.2 we can thus calculate the membrane resting potential

$$\boldsymbol{E_m \cong 61.6\text{mV} \cdot \log_{10}\left(\frac{4 + \frac{1}{100} \cdot 142}{100 + \frac{1}{100} \cdot 10}\right) = -78\text{mV}}, \quad (1.7)$$

At this resting potential of -78mV, which is the equilibrium potential for chloride (compare (1.4)), no net flux of chloride occurs and thus the assumption leading to the simplified GHK equation is valid when the cell membrane is at rest. To maintain a steady

membrane potential, at rest the influx of sodium and outflux of potassium ions is actively reversed by the sodium-potassium pump (Na-K ATPase pump).

The action potential

Action potentials (APs) are the principal signals with which the nervous system operates, brief and defined periods of membrane potential discharge, or *depolarization*, that propagate along the membrane of excitable tissue. The first recording of these electrical signals was published by Bernstein in 1868 (Figure 1.3.a), long before many fundamental properties of the nerve membrane were fully understood. Due to slow response recordings possible with the galvanometers of his days, Bernstein developed the differential rheotome that enabled him to integrate the transmembrane potential responses to several stimuli and thus reconstruct the AP (Carmeliet, 2019). The invention of the thermionic amplifier and the cathode ray oscilloscope in the early 20th century enabled electrophysiologists like Hodgkin and Huxley (Figure 1.3.b) or Curtis and Cole (Figure 1.3.c) to do direct and accurate measurements of the AP.

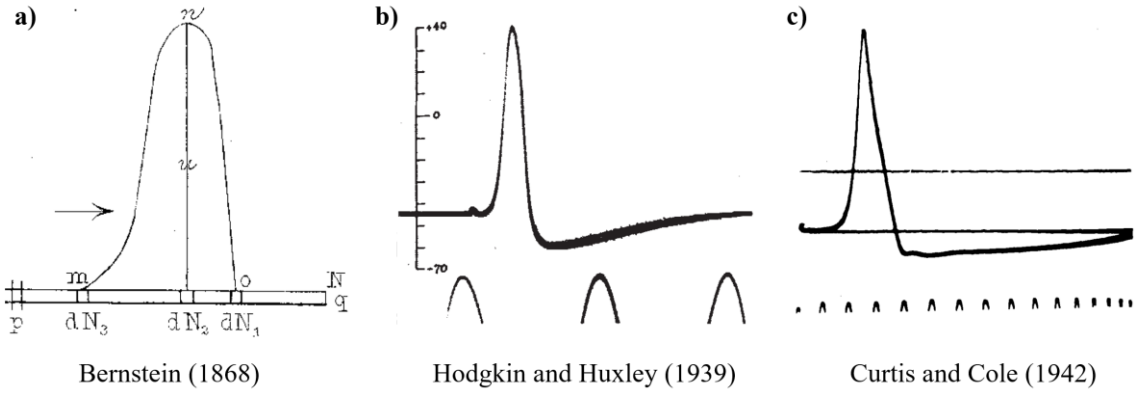

Figure 1.3 Historical recordings of the action potential by **a)** (Bernstein, 1868), **b)** (Hodgkin and Huxley, 1939), and **c)** (Curtis and Cole, 1942). a) and b) Copyright by Springer Nature. c) Copyright by John Wiley and Sons. Reprint with permission.

The cylindrical fibres of nerve and muscle cells can be considered as electrical cables: an electrolytic, conductive interior is surrounded by the insulating cell membrane. The poor cable properties of these cells would, due to resistive and conductive losses, result in strong signal distortion and attenuation within a few mm. However, experimental observations with varying separation between stimulation source and site of recording show that APs can travel long distances without any distortion (Katz, 1966). This discrepancy of insufficient cable properties of nerve and muscle fibres and observations of APs being conveyed over long distances without attenuation suggests that other mechanisms must be involved in AP propagation.

The search for these mechanisms was the driving force behind the electrophysiology research of the early 20th century. In 1952, Hodgkin, Huxley, and Katz published five papers summarizing a series of experimental findings that represent a breakthrough in our understanding of the action potential (Hodgkin and Huxley, 1952a, 1952c, 1952d, 1952b; Hodgkin, Huxley and Katz, 1952). The large diameter of the unmyelinated squid giant axon of up to 1mm allowed Hodgkin, Huxley, and Katz to apply the voltage clamp technique and insert an intracellular electrode and measure the transmembrane voltage while injecting charge into the nerve cell. Thus, they were able to separately determine the voltage dependent transmembrane permeabilities to sodium and potassium ions. Further, they developed a mathematical model that describes these nonlinear ionic conductances as functions of voltage and time and correlates them to discrete ion channels with different gating states. Numerical solution of that model (Figure 1.4.a) enabled Hodgkin and Huxley to reconstruct the action potential quantitatively (Hodgkin and Huxley, 1952a).

While a voltage gated potassium K_V channel, that is modelled as pore with an *activation gate*, can either be "open" or "closed", due to the additional *deactivation gate,* the voltage gated sodium Na_V channel can exist in a third, "inactivated" state. For the following discussion of the gating processes leading to the generation of an AP, it is important to keep in mind that the voltage dependent conformational changes of ion channels are probabilistic events. This means as the transmembrane potential changes, the probability for individual ion channels to transition to another gating state changes. Applied to the large number of voltage gated ion channels in the membrane, the probabilities can also be considered as fractions of channels that transition to a specific state.

At rest, most Na_V and K_V activation gates are closed and most Na_V deactivation gate are open (Figure 1.4.b). Upon membrane depolarization, that is a reduction of the negative transmembrane resting potential, the Na_V activation gates rapidly open and Na^+ ions, following their electrical and concentration gradient, enter the intracellular space. This influx of positive charged Na^+ ions further depolarizes the membrane. However, the reduced negative transmembrane potential also leads to a steady opening of K_V activation gates, causing a gradual outflux of K^+ ions. If the net influx of Na^+ exceeds the outflux of K^+ sufficiently to depolarize the membrane to the *threshold potential* of approximately -55mV, a rapid opening of all Na_V activation gates causes a strong Na^+ influx and membrane depolarization gives rise to an action potential (Figure 1.4.c). Dependent on time and voltage the Na_V deactivation gates close, stopping further influx of Na^+, and the

continuing outflux of K^+ leads to a *repolarization* of the membrane. During this period of repolarization, the Na_V channels gradually return to their resting state, closing their activation gates and opening their deactivation gates (Figure 1.4.d). Due to the slower closing behaviour of K^+ activation gates, that can as analogy be considered as heavy (and thus inert) doors, K^+ outflux continues for a relatively long time causing a hyperpolarization of the membrane (Figure 1.4.e). Once the K_V activation gates are closed the membrane returns to its resting potential.

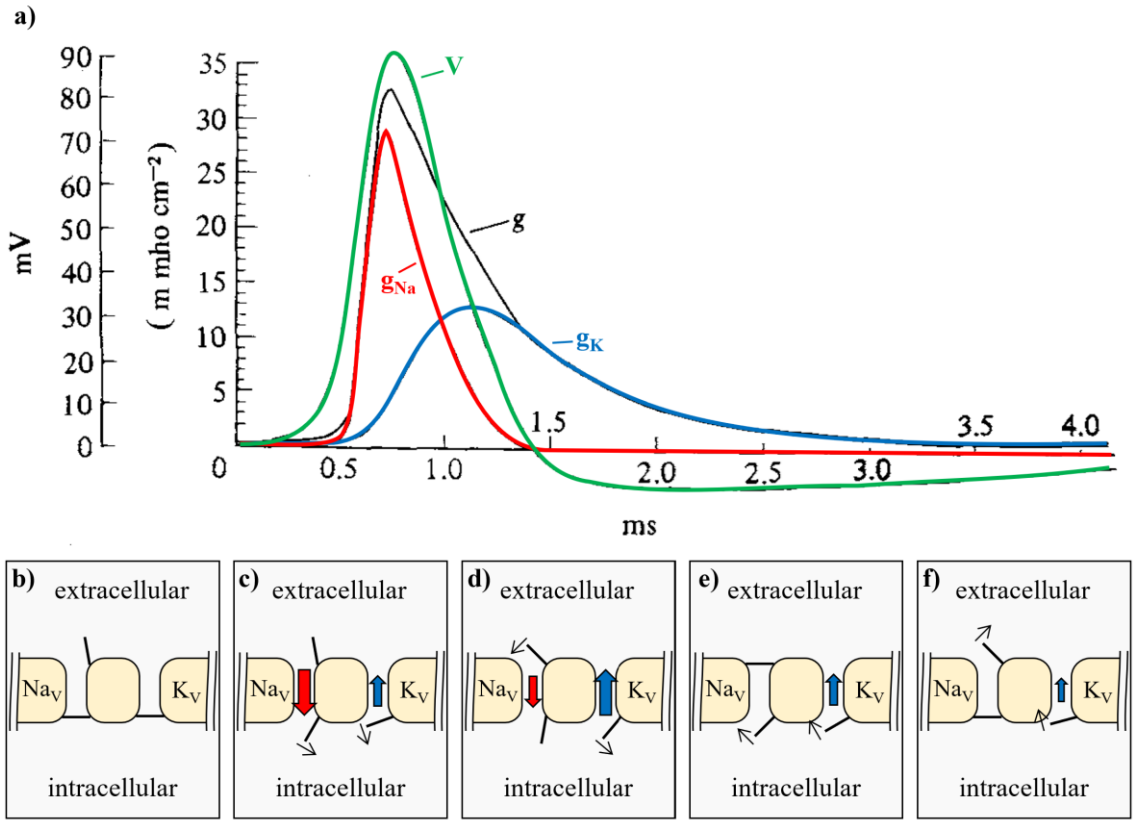

Figure 1.4 Membrane conductances during the action potential. a) Numerical solution of Hodgkin and Huxley membrane model reconstructs the voltage profile V of an action potential quantitatively. g is the total ionic conductance across the membrane, g_{Na} the sodium conductance, and g_K the potassium conductance. (Hodgkin and Huxley, 1952b) Copyright by John Wiley and Sons. Reprint with permission, colouration added. **b)** At rest, the activation gates of Na_V and K_V channels are closed, while the Na_V deactivation gate is open. **c)** A depolarization of the membrane rapidly opens the Na_V activation gate, allowing Na^+ to the enter the cell. K_V activation gates open more slowly, resulting in moderate potassium outflux. **d)** Repolarization of the membrane is initiated by the gradual closing of the Na_V deactivation gate, whereas the K_V activation gate remains open, allowing K^+ ions to leave the cell. **e)** The membrane hyperpolarizes when it is not conductive to Na^+ ions anymore, while K^+ ions still leave the cell. **f)** The membrane restores its resting potential by closing the Na_V and K_V activation gates and opening the Na_V deactivation gate.

Physiologically, the initial stimulus of gradual membrane depolarization occurs at the neuron's cell body. Here many subthreshold input signals, that arrive via synapses either at the dendrites or at the cell soma membrane, are integrated and, if the integrated input signal reaches the threshold, an action potential is triggered. From there the AP propagates along the axon, leaving the membrane that it passed in a state of refractoriness. During what is called the *absolute refractory period* (ARP), the Na_V deactivation gates are closed and the membrane cannot be excited to trigger a second AP (Figure 1.4.e). Once the Na_V deactivations gates are open again but the K_V activation gates are not yet completely shut, the membrane is in the *relative refractory period* (RRP). During this period, the membrane can be excited a second time but the increased outflux of K^+ (with respect to the fully recovered membrane at rest) leads to an increased threshold for AP generation (Figure 1.4.f). These refractory periods, especially the ARP, are responsible for the unidirectional propagation of APs in the nervous system. APs triggered at the cell soma travel along the peripheral axon to the axonal terminals where they release neurotransmitters to convey the signal to neighbouring cells. APs do not reflect or "bounce back" since the membrane behind the spike is in an ARP and only the membrane region in front of the spike can be excited to convey the AP in this forward direction.

This propagation occurs in a *saltatory*, i.e. "jumping", manner in myelinated axons. Due to the insulating myelin sheath, that reduces the internodal membrane capacitance and increases its resistance, APs can only be triggered at the nodes of Ranvier where the membrane is exposed (Huxley and Stämpfli, 1949). This saltatory propagation results in increased conduction velocities of myelinated compared to unmyelinated nerve fibres (compare Table 1.1).

1.2.2 The neuromuscular junction

At the neuromuscular junction (NMJ), also called *motor endplate*, the presynaptic action potential of a motor nerve terminal is conveyed, via release of the neurotransmitter acetylcholine ACh, to a skeletal muscle fibre, where the postsynaptic action potential propagates along the muscle membrane and initiates muscle contraction. Besides the muscle fibre and the motor nerve terminal, which are separated by a synaptic cleft of approximately 50nm, the third element of the tripartite NMJ is the perisynaptic Schwann cell that caps the synapse. In general, each skeletal muscle fibre is innervated by a single terminal branch of a motor neuron and the NMJ is typically located in the middle of that muscle fibre (Figure 1.5.a).

While the axons of motor nerves are myelinated, the terminal regions are only capped by a single layer of the perisynaptic Schwann cell. The terminal motor nerve branches into grape-like varicosities, the *synaptic boutons*, that contain vesicles of the neurotransmitter ACh. These vesicles cluster around regions of specialized presynaptic membrane, the active zones, where voltage gated Ca^{2+} channels prevail with an increased density. The active zones are located opposite of junctional folds in the postsynaptic muscle membrane, where also an increased density of ACh receptors is found (Figure 1.5.b). The precise alignments of Ca_V channels at the presynaptic active zones and the ACh receptors at the junctional folds are important for the performance of signal transmission at the NMJ.

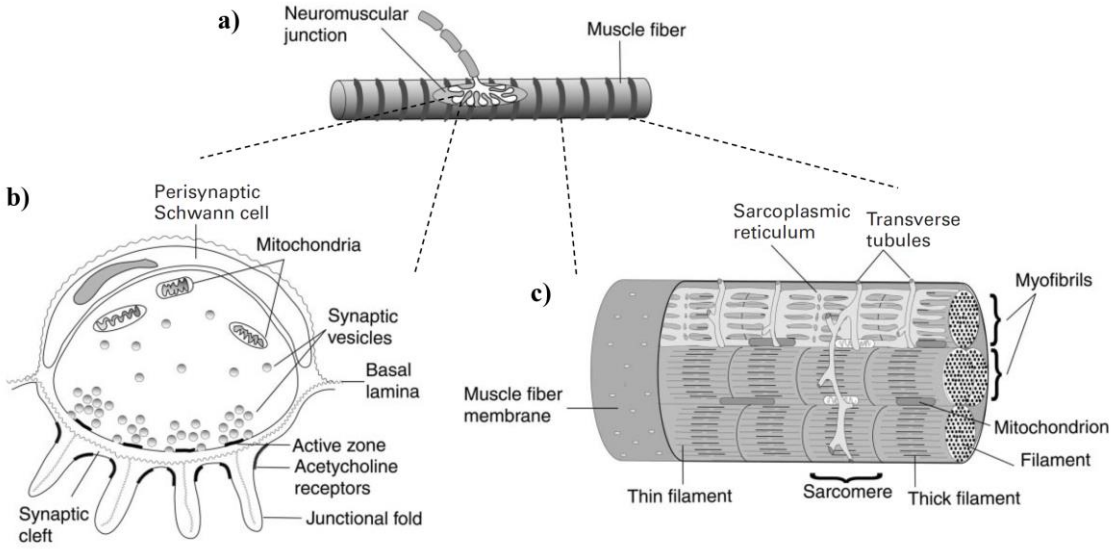

Figure 1.5 Schematic representation of the neuromuscular system. a) The neuromuscular junction where the terminal branch of a motor nerve is in synaptic contact with a single muscle fibre. **b)** Cross-sectional representation of a synaptic bouton at the neuromuscular junction. **c)** An electron microscopic representation of a longitudinal section of a single muscle fibre segment. (Ko, 2001) Copyright by Elsevier. Reprint with permission.

Upon arrival of a motor nerve action potential at the presynaptic membrane, the changes in transmembrane potential increase the conductance of the Ca_V channels at the active zones and Ca^{2+} enters the synaptic bouton following both its electrical and concentration gradient. Increased presynaptic Ca^{2+} concentration triggers an exocytosis of synaptic ACh vesicles, which involves binding of specialized proteins in the vesicle membrane, called v-SNARES, with their counter parts in the nerve terminal membrane, called t-SNARES. After release of the neurotransmitter ACh into the synaptic cleft, the membranes of the empty vesicles are retrieved in a process called endocytosis. This transmitter release is a quantal process that can either happen upon arrival of a motor nerve AP, in which case

many vesicles release ACh almost simultaneously, creating a strong endplate potential (epp) that is sufficient to trigger an AP in the postsynaptic muscle membrane, or randomly with a much lower probability (Katz, 1966). In this later case, which is thought to happen at a frequency of about 1Hz, a single vesicle releases approximately 10,000 acetylcholine molecules into the synaptic cleft and produces a miniature endplate potential (mepp) of about 0.5mV (Ko, 2001).

Both mepps and epps are caused by binding of the released ACh to nicotinic[4] acetylcholine receptors (nAChRs) in the muscle membrane. A nAChR is a non-selective ligand gated cation channel that, when two ACh molecules bind to its two α-subunits, becomes permeable to Na^+ and K^+. The increased permeability of the postsynaptic muscle membrane to Na^+ and K^+, results in changes of the transmembrane potential. When the sum of the depolarizing epps reaches the threshold potential, as outlined above on the example of a nerve membrane depolarization (Chapter 1.2.1), a self-propagating action potential is triggered in the muscle membrane. Through a protein called agrin, which is synthesized by the motor neuron and released in the extracellular matrix at the NMJ, the presence of the motor nerve terminal triggers an aggregation of nAChRs at the endplates. Here the receptors prevail at a density of approximately 10,000 per μm^2, a spatial concentration much higher than at the rest of the muscle membrane, where less than 10 nAChRs are found in a space of 1 μm^2 (Ko, 2001). This aggregation of nAChR at the endplates is lost following nerve damage, i.e. in denervated muscle, where the receptors disperse evenly over the muscle membrane, a phenomenon which is termed *denervation supersensitivity*.

Besides agrin, the extracellular matrix at the NMJ, which is also called the *basal lamina*, contains further important molecules such as the laminin glycoproteins that play an important role in in nerve growth and nerve terminal differentiation. Another crucial molecule of the basal lamina is the enzyme acetylcholinesterase, which hydrolyses ACh molecules that did not bind to nAChRs, and thus prevents those receptors to become desensitized through continuous exposure to ACh.

[4] nAChR receptors belong to the group of nicotinic receptors that can be activated by nicotine derived from the tobacco plant. They are thus distinguished from muscarinic acetylcholine receptors (mAChRs) that are more sensitive to the mushroom derived muscarine than to nicotine.

1.2.3 Skeletal muscle contraction

Skeletal muscles consist of multiple bundles (fascicles) of individual muscle fibres. Human muscle fibres are multinucleated myocytes with diameters of 10-100µm and lengths between 1mm (stapedius muscle) and 30cm (sartorius muscle). Each muscle fibre consists of many *myofibrils*, longitudinal contractile elements, in parallel. The myofibrils are chains of repeated contractile units, the *sarcomeres*, that are composed of thin actin and thick myosin filaments. Actin and myosin filaments are arranged in parallel, partially overlapping each other, and together form the so-called *A-band*. The *I-Band* is composed of actin, the Z-discs, and the elastic titin elements, which are connected in series to the thick myosin filaments. The repetitive pattern of A and I bands gives the skeletal muscle, when viewed under the microscope, a striated appearance which is why it is also referred to as *striated muscle* (Figure 1.5.c).

The transmission of electrical action potentials at the muscle membrane to contractions is termed *excitation-contraction coupling* and relies on the release of Ca^{2+} into the cytoplasm. The motor nerve action potential is transmitted at the NMJ via ACh release to trigger an action potential in the postsynaptic muscle membrane. The AP propagates along the membrane invaginations, called transverse tubules (or T-tubules), where it initiates Ca^{2+} release from the sarcoplasmic reticulum into the cytosol. According to the *sliding filament theory* (Huxley and Hanson, 1954; Huxley and Niedergerke, 1954), Ca^{2+} causes conformational changes of tropomyosin complexes, unblocking actin binding sides and enabling the myosin power stroke. This process is referred to as *crossbridge cycle* and it is the basis for muscle contraction. Once the Ca^{2+} is pumped back into the sarcoplasmic reticulum the actin binding site are blocked again and the muscle relaxes. Thus, calcium is not only essential for the ACh release at the NMJ, but it is also of central importance in the excitation-contraction coupling.

In isometric condition, the mechanical muscle response to a stimulus can be modelled with a three-element Hill muscle model (Hill, 1938). The absolute muscle force is the sum of the active, or developed, muscle twitch force of the contractile element CE and the passive muscle tension. The developed contractile tension is a function of muscle length as it influences the relative amount of actin and myosin filament overlap and the proportion of myosin heads that can perform the power stroke. The two model components contributing to the length-dependent passive tension are the elastic series element SE and the elastic parallel element PE (Figure 1.6.a). While the SE represents the passive tension of the elastic titin element in the sarcomere units and the mainly

collagenous connective tissue of the tendons, the PE models connective tissue that is parallel to the sarcomeres. As both the active and the passive muscle tension depend on muscle length, there is an ideal isometric muscle length where the developed muscle twitch force is maximal while the passive tension is not yet excessively increasing (Figure 1.6.b).

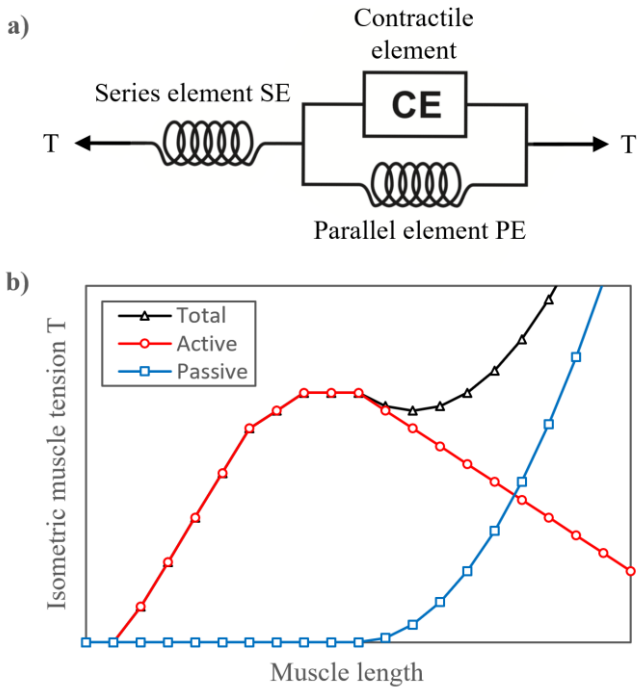

Figure 1.6 Skeletal muscle model. a) Three element Hill-type muscle model consists of a contractile element CE and an elastic element in series SE and an elastic element in parallel PE. **b)** The isometric muscle tension is the is the sum of the active, or developed, twitch force and the passive tension. Both elements that contribute to total muscle tension are functions of muscle length.

1.3 Electrical stimulation

Electrical stimulation (ES) is a neuromodulation technique that finds application in a broad array of therapeutic fields and medical devices including:

- the cardiac pacemaker,
- auditory prosthesis for deaf subjects,
- visual prosthesis for blind subjects,
- chronic pain treatment,
- improving bladder control in paraplegics,
- restoration of locomotive functions for paralysed subjects,
- and muscle rehabilitation and recovery.

Beside these contemporary applications of ES, recent advances in nanoelectronics give rise to promising research and developments in the emerging field of bioelectronic devices. These miniaturized devices, also called *electroceuticals*, are envisioned to be placed minimally invasively to the central or peripheral nervous system and to deliver ES to provide treatment for a range of diseases including type 2 diabetes (Sacramento *et al.*, 2018; Fjordbakk *et al.*, 2019), renal fibrosis, and hypertension (Okusa, Rosin and Tracey, 2017).

Despite this wide-reaching range of ES applications and research endeavours, the underlying mechanism by which the therapeutic effect is achieved or pursued is the same in all cases: Electrical charge is delivered to a target excitable structure in order to influence voltage gated channels, usually to generate action potentials, and thereby to control the release of neurotransmitters.

This injected charge creates an artificial potential field between the poles of the stimulation source, altering the state of voltage-gated ion channels affected by that field. This modulation effect can either be inhibitory or excitatory, and can in the latter case, if sufficiently intense, evoke self-propagating action potentials leading to neurotransmitter release at the axonal terminals. While some electrical stimulation therapies are claimed to be “subthreshold”, the targeted control of neurotransmitter release provides the basis for the therapeutic effects of most well-studied ES applications. Increased neurotransmitter release may for example be used to activate muscle fibres and thus generate locomotion or to provide visual or auditory perception. A decreased neurotransmitter release can be achieved by blocking action potential conduction pathways. Such a block can be achieved both with kilohertz frequency alternating current (KHFAC) or with direct current (DC) and may be used to inactivate or downregulate the nervous system (Bhadra and Kilgore, 2018), e.g. to reduce spasticity or chronic pain.

Besides a general introduction of the above outlined mechanisms underlying ES, in this chapter the principal technical components and parameters of ES systems will be discussed. This discussion includes the general topologies of stimulator output stages, waveforms commonly used for neural stimulation, principal electrode arrangements and the electrode-tissue interface as well as electrochemical processes that may occur at the latter. Lastly, some important relationships between stimulation parameters such as stimulus duration and amplitude, charge injection, and energy consumption at a given activation threshold will be introduced.

Prior to these technical discussions it will be useful to introduce some basic terminologies, physical quantities and the laws describing their relations.

1.3.1 Basic terminologies and physical quantities

Electric charge is a fundamental property of matter, causing it to experience a force when placed in an electromagnetic field. Electric charge, quantified in the SI unit[5] coulomb, can either be positive or negative. Charge can neither be generated nor destroyed, but it can be separated. Like charges exert a repulsive force on each other, while opposite charges attract each other. For our discussion of processes occurring during extracellular stimulation, atomic or molecular carriers of electric charge, so-called ions, will have a central place. The amount of work required to move an electric charge through an electromagnetic field, which can also be understood as energy carried per unit of charge, is termed voltage and its SI unit is volt. The rate of charge flow (coulomb per second) through a specific point or region is the electric current, quantified in ampere, and is one of the seven SI base quantities. Conventional current flow is defined as movement of positive charge, from the positive pole (i.e. the anode) of a stimulation source to the negative pole (i.e. the cathode). Electrons flow in the opposite direction, from the cathode to the anode.

The terms cathode and anode are grounded in the electrochemical processes occurring at physical electrodes at a specific time. In extracellular electrical stimulation the anode is the electrode through which conventional current (positive charge) is applied and at which, following the increased positive valence, oxidation reactions take place. The cathode is defined as the electrode at which conventional current is removed, which represents a decreased positive valence or an electron gain, and at which reduction occurs. In practical applications of ES, it is important not to confuse these terms, as sadly often is the case even in peer-reviewed literature, with physical electrode descriptions such as active, return or stimulation electrode. As we elaborate below, most waveforms used for neural stimulation are biphasic, meaning that they are comprised of a cathodic (typically first) and anodic phase to achieve charge balance. This means that both physical

[5] The International System of Units (SI) is comprised of the seven base units: kilogram, second, metre, ampere, candela, kelvin, and mole for the base quantities mass, time, length, electric current, luminous intensity, temperature, and amount of a substance. These units are the backbone of the modern metric system and the basis for all derived units.

electrodes of the stimulation system will act as a cathode as well as an anode at some point during the stimulation.

Further, possible misunderstandings can be avoided when we clearly differentiate the terms monophasic and biphasic from monopolar and bipolar. As we started to outline above, the terms monophasic and biphasic describe waveform characteristics. A monophasic pulse is comprised of charge injection with only one polarity, while a biphasic pulse has a positive and a negative phase (Chapter 1.3.5). The terms monopolar and bipolar on the other hand describe two principal electrode configurations used for ES and will be explained in more detail in Chapter 1.3.4.

1.3.2 Electrically evoked action potentials

For this introduction of the mechanisms leading to action potential generation through ES, we assume that an electrical charge is injected at the active electrode, which can be idealized as a point source, in the extracellular space[6] near the target nervous structure and returned over a large, remotely placed return electrode. This stimulation electrode arrangement, which is called monopolar, is the configuration used in most early experiments and computational models of ES and is the operational mode of many contemporary ES applications. The electric potential field that arises between both electrodes during the injection of a negative (i.e. cathodic) charge has its highest field density at the active electrode near the target nerve. Here the injected negative charge (electron gain) counters the predominantly positive charge at the outside of the nerve membrane. The less positive charge at the outside of the membrane leads to a flow of negative charge on the inside, along the long axis of the axon and away from the site of (extracellular) stimulation. This displacement of negative charge along the axon, away from the site of stimulation can effectively be understood as a positive charge crossing

[6] Action potentials can also be electrically evoked using intracellular injection of positive (i.e. anodic) charge, as was done in many early electro-neurophysiology investigations. Most famously, based on Cole's voltage clamp experiment, Hodgkin and Huxley inserted microelectrodes inside giant squid axons to study how ionic currents give rise to the action potential, a work for which they received the 1963 Nobel Prize in Physiology or Medicine. However, intracellular stimulation has obvious limitations for its clinical use in human subjects as the diameter of mammalian axons, unlike the axons of the giant squid which have diameters of up to 1mm, ranges only from 0.2 to 20µm. Since both principal ES electrode types that find clinical application in human subjects, transcutaneous surface electrodes and implanted electrodes, stimulate nerve or muscle fibres extracellularly, we will focus on extracellular charge injection.

the membrane from the inside to the outside. This is called *capacitive current*, as the stimulation pulse discharges the membrane capacitance. The capacitive current predominately flows through the uninsulated part of the axon membrane, i.e. the node of Ranvier, closest to the stimulating electrode. The equalizing, inward flowing currents are distributed over the adjacent nodes at reduced current densities. The transmembrane currents flowing through the nodes of Ranvier, with the highest current density at the node closest to the stimulation electrode, change the transmembrane potential. In our example of an extracellular cathodic charge injection, leading to a positive capacitive current with the highest density at the node closest to the stimulation electrode, the negative transmembrane resting potential is reduced (i.e. depolarized) at the site of stimulation. The reduced transmembrane potential increases the probability of activatable voltage gated Na^+ channels, which are found in their highest spatial density of 2000 channels/μm^2 at the nodes of Ranvier, to transition to the open state. Na_V channel opening is a stochastic event and an increased probability for transitioning to the open state (of the tens of thousands of Na_v channels in a single node of Ranvier) results in an increased influx of Na^+ ions following both the potential and the concentration gradient. If the influx of Na^+ ions exceeds the net outward flow of K^+ ions sufficiently to reduce the transmembrane potential below the threshold of approximately -55mV, a rapid opening of all activatable Na_v channels takes place and thus a self-propagating action potential is generated. The peripherally evoked action potential travels (in both directions) along the stimulated axon and leads to a release of neurotransmitters at the neuron's terminals.

If the membrane depolarization following the cathodic charge injection is insufficient to reach the threshold membrane, no self-propagating action potential is evoked, and the stimulation is called *subthreshold*.

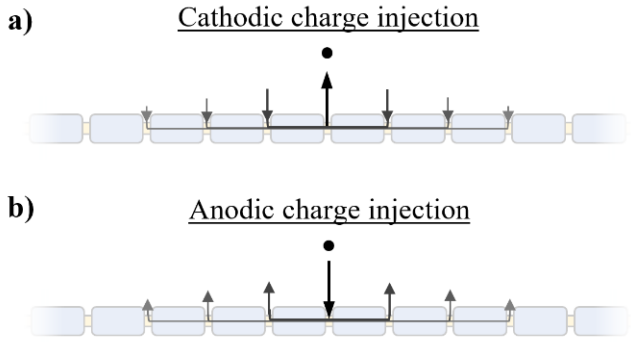

Figure 1.7 Model of extracellular charge injection with a monopolar stimulation point source. a) An injection of cathodic (negative) charge in the extracellular space results in a depolarization (i.e. a reduction of the transmembrane potential) of the axon's membrane at the central node of Ranvier. **b)** The injection of anodic (positive) charge in the extracellular space leads to a hyperpolarization (i.e. an increase of the transmembrane potential) at the central node. These changes in the transmembrane potential can be understood as capacitive currents across the membrane, positive charge crossing the membrane from the inside to the outside are visualized as upward arrows, and currents of positive charge entering the cell are indicated by downward arrows. Equalizing currents through the adjacent nodes have opposite directions and reduced current densities than the capacitive currents through the central node of Ranvier.

As described above, the highest density of transmembrane capacitive current occurs at the node closest to the stimulation electrode. In the case of cathodic stimulation this was the location where the action potential was elicited following a chain of events set in motion by that maximal capacitive current density. However, this is not always the case. If we inject a positive (i.e. anodic) charge in the extracellular space, we find that the capacitive current profile along the axon is inverted. The highest current density will still be through the membrane of the node closest to the stimulation electrode, only this time it is equivalent to an inward flow of positive charge, causing a hyperpolarization at this location. Equalizing this capacitive inward flow, less dense outward currents will flow through the adjacent nodes on both sides, creating zones of depolarization. Given sufficient strength of the anodic stimulation, the potential across the membrane in those zones of depolarization can be reduced to reach the threshold and action potentials are elicited.

Another mechanism that can lead to the electrical elicitation of action potentials is the so-called *anodic break excitation*. Here, an excitatory (positive) capacitive current flows through the central node of Ranvier following the electric field change after termination of a prolonged anodic pulse. The anodic pulse hyperpolarizes the membrane (increases the transmembrane potential) under the stimulation electrode which causes the majority

of Na_v deactivation gates to fully open[7] and thus renders the membrane more excitable (Grill and Mortimer, 1995). The termination of the anodic pulse can be understood as a cathodic field transition, re-establishing the resting potential. This cathodic field transition finds the nerve membrane in its hyperexcitable (nearly 100% of Na_v channels are activatable) state and causes Na_v channel opening, leading to increased Na^+ influx. If this influx is not countered by K^+ outward currents, and depolarizes the membrane sufficiently to reach the threshold, an action potential is elicited.

Even though a detailed discussion of computational approaches to describe these mechanisms leading to excitation would exceed the scope of the present thesis, the above considerations of capacitive currents along the axon during extracellular stimulation lead to the introduction of an important concept of numerical nerve simulations: the *activating function*.

The activating function is a mathematical description of the transmembrane potential change induced by an applied stimulation. It is derived from the McNeal cable model (McNeal, 1976) and based on the second difference quotient of the extracellular field along the axon (Rattay, 1986).

$$\boldsymbol{V_{e,n-1} - 2V_{e,n} + V_{e,n+1}} \tag{1.8}$$

In this generalized form of the activating function, $V_{e,n}$ represents the magnitude of the extracellular potential at the central node of Ranvier, while $V_{e,n-1}$ and $V_{e,n+1}$ represent these measures for the adjacent nodes respectively. Where the activating function is positive, the membrane at that location experiences a depolarizing effect, while a negative activating function represents a hyperpolarization respectively. The potential generated by the stimulation point source at any point (in the two-dimensional space) is proportional to $1/r$, where r is the radial distance from the electrode:

$$\boldsymbol{r = \sqrt{z^2 + x^2}} \tag{1.9}$$

The essential influence of the activating function on simulation of peripheral nerve stimulation will be illustrated in brief to provide a mechanistic explanation for an

[7] At resting state, the inactivation variable h is approximately 0.8, meaning that the probability for the deactivation gate of a Na_V channel to be open is 80%. Upon hyperpolarization of the membrane this value approaches 1 so that the membrane becomes hyperexcitable (Grill and Mortimer, 1995).

experimental observation called *inverse recruitment*, that describes how electrical stimulation tends to recruit large diameter fibres first, which are physiologically recruited at last[8].

Figure 1.8 shows segments of two myelinated axons of different sizes. Importantly, the internodal spacing scales proportionally with myelin outer diameter and equals approximately 100 times that diameter (Hursh, 1939; Rushton, 1951). For larger fibres, the increased internodal distance results in increased radial distance of the adjacent nodes n_{-1} and n_{+1} from the stimulation electrode and thus decreases their influence in the activation function of the central node of Ranvier n. This results in lower activation threshold for peripheral stimulation of larger diameter axons and thus in an inverse order of recruitment.

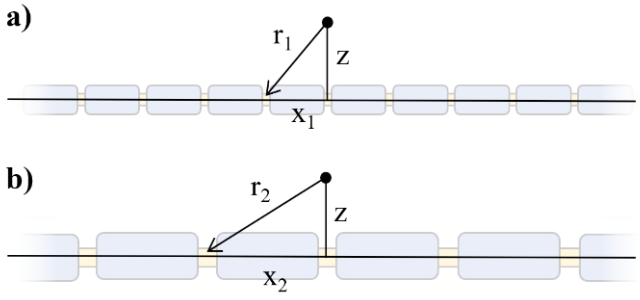

Figure 1.8 Axon-size influence on activating function for extracellular stimulation. Two axons are stimulated via a monopolar stimulation point source, centrally located over a node of Ranvier at distance *z*. The smaller diameter axon **a)** has a proportionally smaller internodal distance x_1 than the larger diameter axon **b)** with internodal distance x_2. The magnitude of the potential at the central node $V_{e,n}$ is equal for both axon sizes (since *z* is equal). However, due to the larger radial distance of the adjacent nodes to the stimulation source for the larger diameter axon ($r_2>r_1$), the magnitude of the extracellular potential at these neighbouring nodes $V_{e,n-1}$ and $V_{e,n+1}$ is reduced in case of the larger axon. This reduction of $V_{e,n-1}$ and $V_{e,n+1}$ increases the activating function at the central node for larger diameter axons, rendering them more excitable to extracellular stimulation than smaller axons and results in lower thresholds for activation.

[8] Physiologically, the neuromuscular system first recruits small motor neurons that innervate fatigue resistant slow twitch muscle fibres and only later, if that higher twitch force is required, large diameter motor neurons that innervate the less fatigue resistant fast twitch muscle fibres. This neuromuscular recruitment order is known as Henneman's size principle. Inverse recruitment describes a recruitment of large diameter nerve fibres prior to smaller diameter fibres, such as is the case with ES of peripheral efferent nerves. This inversed order of recruitment presents challenges to neuromuscular stimulation endeavours because the large fibres that are preferably activated generate intense muscle twitches, unfit for many fine locomotive operations and are prone to fatigue early.

1.3.3 Electrical stimulators

The electrical stimulator is the central piece of hardware of any ES system. Its main tasks are the generation and amplification of the simulation pulses that are then applied over the electrodes to the target excitable structure. The basic elements comprising an electrical stimulator are the pulse generation circuitry, a voltage supply, and an output stage. While many contemporary stimulators combine all these elements in a single device, the ongoing endeavour to miniaturize stimulation implants lead to numerous developments of stimulators that receive power wirelessly from an external power supply. Moving on from the original proposal of the wirelessly powered BION micro-stimulation implants (Loeb *et al.*, 1991), *passive* stimulation implants are under development that do not contain any active circuitry and instantly convert the wirelessly received energy (e.g. via acoustic waves, infrared light, or radio frequency) into an electrical impulse for neural stimulation (Sahin and Pikov, 2011). Independent of those design differences regarding the separation of power supply, active and passive circuitry components, a main functional distinction can be made based on the output stage topology.

Voltage-controlled stimulation

Voltage-controlled stimulation output stages deliver the desired stimulation pulse, independent of the load impedance and output current, as a voltage waveform. Figure 1.9 illustrates the controlled voltage across as well as the resulting current through the stimulation electrodes qualitatively for basic waveforms.

Generally, the design of output stages for voltage-controlled stimulation is simpler than that of current-controlled stimulators as most power sources (e.g. batteries, mains electricity) are voltage sources. Basic output stages for voltage-controlled stimulation can be comprised of a simple network of switches, disconnecting and connecting the voltage source in the desired polarity (and with appropriate patient coupling, e.g. over capacitors) with the electrodes. Such low circuit complexity results in higher energy efficiency compared to output stages that incorporate operational amplifiers. Stimulation amplitude modulation can be achieved with linear or with switching regulators. While linear regulators are the simpler solution, their inherent low energy efficiency represents a major disadvantage for battery powered stimulation systems, where energy consumption is a main performance parameter.

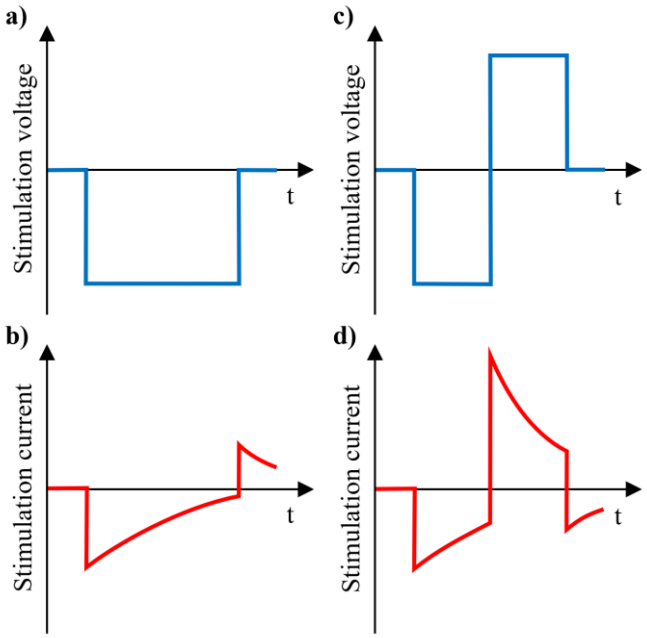

Figure 1.9 Voltage-controlled stimulation. a) Voltage profile and **b)** resulting current flow of monophasic rectangular voltage-controlled stimulation. **c)** Voltage-controlled biphasic rectangular waveform and **d)** resulting current profile. The capacitive portions of the stimulated load (electrode-tissue interface) distort the associated current waveforms b) and d).

Voltage-controlled stimulation offers some advantages for transcutaneous stimulation in terms of safety, as commonly occurring variations in the electrode-skin-interface (e.g. partial detaching of the skin electrodes, uneven pressure) will not result in dangerous current densities (Merrill, Bikson and Jefferys, 2005; Peckham and Knutson, 2005). However, using voltage-controlled stimulation, normal changes in the electrode-tissue impedance over time will result in changes of the induced electrical field and thus influence the stimulation thresholds (Merrill, Bikson and Jefferys, 2005). Varying thresholds are disadvantageous and can represent challenges to the therapeutic success of many ES applications, especially where “finely tuned” selective stimulation of specific fibre populations is pursued.

Current-controlled stimulation

Current-controlled stimulation output stages deliver ES pulses as defined current waveforms that are not affected by changes in the load impedance. Figure 1.10 shows monophasic and biphasic rectangular current waveforms as well as the resulting voltage profile across the stimulation electrodes. Current-controlled output stages generally require more complex circuitry components than voltage-controlled, such as operational amplifiers (OPAs), and this increased complexity results in increased energy overhead. A major advantage of current-controlled stimulation is that variations of the electrode-

tissue impedance, which represents a load in series, do not influence the delivered current flow through the electrodes. As this results in an increased stability of the potential field created within the tissue and thus in an increased security of effective stimulation because of stable thresholds (Peckham and Knutson, 2005; Mortimer and Bhadra, 2018), current-controlled output stages are the preferred choice for many contemporary ES applications.

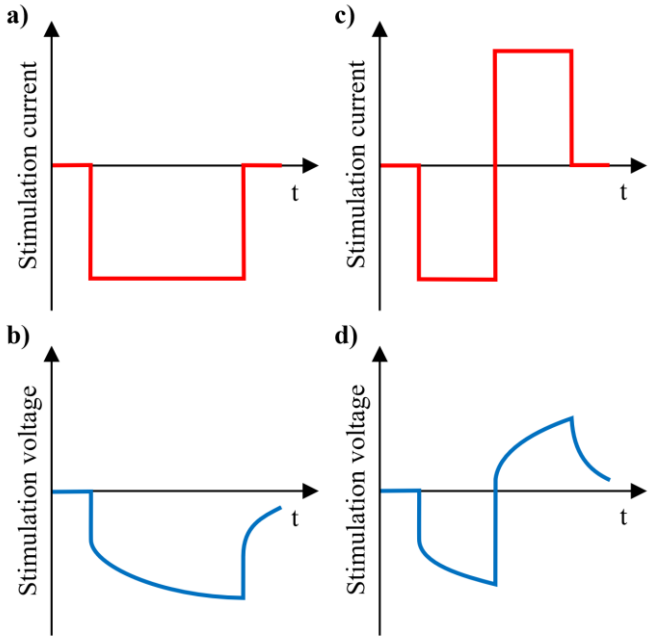

Figure 1.10 Current-controlled stimulation. a) Current-controlled monophasic rectangular waveform and **b)** resulting voltage across the stimulation electrodes. **c)** Current profile and **d)** resulting voltage of biphasic rectangular current-controlled stimulation. The capacitive portions of the stimulated load (electrode-tissue interface) influence the voltage output b) and d) non-linearly.

1.3.4 Electrodes for electrical stimulation

Electrodes used for stimulation of excitable tissue are as diverse as the applications of ES. Figure 1.11 gives an overview of approaches in which electrodes are used as an interface to the nervous system and weighs their inherent risks and potential benefits. Generally, a greater risk is associated with increased invasiveness of an electrode. These increased risks portray a sum of all risks during electrode placement, ES operation and, in some cases, replacement or removal of the electrodes. The surgery necessary to place an intracortical electrode for deep brain stimulation (DBS), for example, carries a significantly greater risk than the placement of a peripheral nerve cuff electrode. Similarly, injuries caused by a faulty stimulation output, e.g. a prolonged and uncontrolled DC current following a stimulator hardware failure, can cause more severe

impairments when they occur with the more invasive electrode. However, as the more invasive electrodes enable a more intimate interface with the specific target neural structure, the potential benefit with those electrodes is increased (Tyler, 2018).

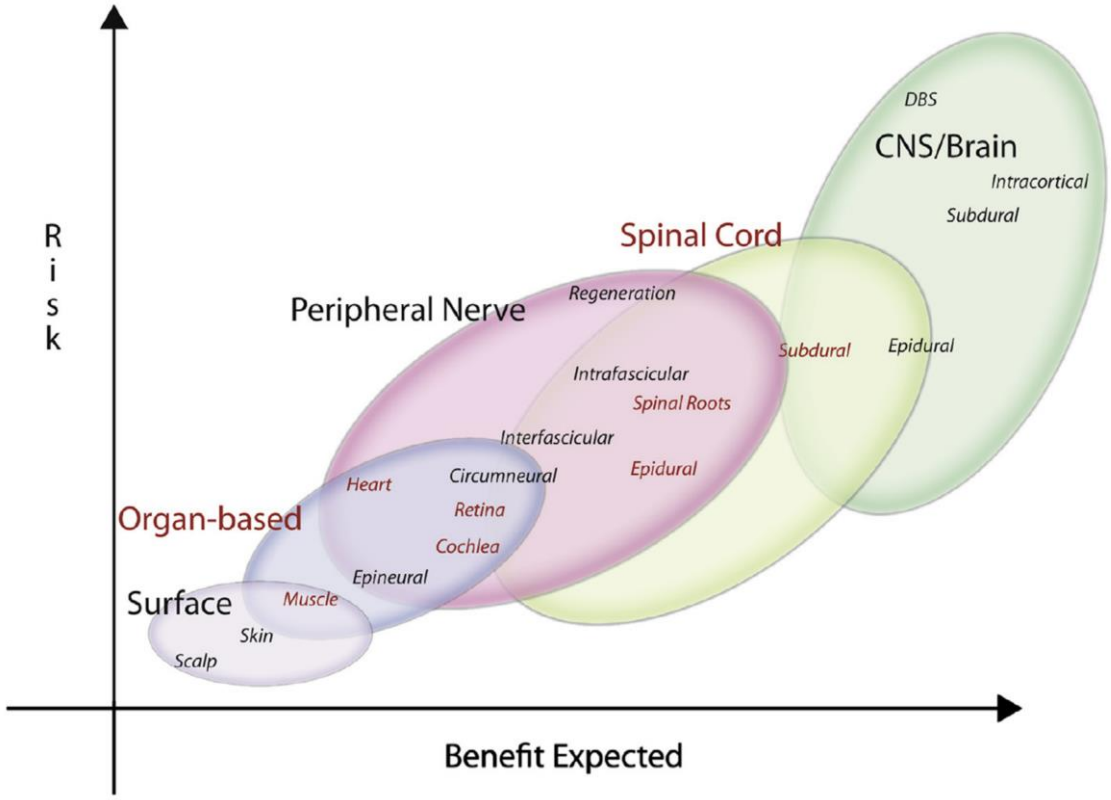

Figure 1.11 Risk versus potential benefit of neural stimulation electrodes. Greater invasiveness of the interface with the nervous system allows for increased selectivity of ES and thus correlates with an increased expected benefit. However, as the electrodes are more invasive, they have greater associated risk. (Tyler, 2018) Copyright by Elsevier. Reprint with permission.

Besides this first categorization based on the invasiveness of the electrodes, further distinctions can be made regarding practical electrode configurations and design as well as the choice of electrode material. Choices made in these categories influence the performance of the neural interface and can have an impact on stimulation safety and stimulation induced tissue damage.

Electrode configurations

ES relies on charge injection to apply artificial potential fields that act on ion channels in the membranes of excitable tissue. An injection of charge, however, is only possible when both poles of the stimulator are connected via the tissue, i.e. when the electrical circuit is closed. The arrangement of these two poles of the stimulator, in relation to the excitable target structure, is referred to as *electrode configuration* or *mode*.

While there is a broad range of proposed electrode configurations for neural stimulation, monopolar and bipolar stimulation configurations are by far the most commonly used modes in contemporary neuromodulation devices (Fallon and Carter, 2016).

Monopolar

In a monopolar stimulation configuration, the stimulation waveform is applied via an active electrode which is typically in close proximity to the target structure. Despite the name *mono*polar, it is important to remember that charge injection can only be achieved when both poles, active and return, of the stimulator are connected. In monopolar configurations the charge is returned over a large, typically remotely placed electrode. Often this charge return is achieved via the conductive casing of the stimulator itself. Advantages of monopolar configurations are that, in many applications, the high field density at the (usually small) active electrode (near the target excitable structure) results in lower thresholds for activation. Monopolar electrode configurations have been the standard mode for most of the early ES devices, such as cardiac pacemakers, and are still used in many contemporary applications. Also, most early computational investigations of extracellular nerve stimulation, like the landmark studies by McNeal (1976) and Rattay (1986), have modelled the stimulation electrode as a monopolar point source.

Bipolar

In the bipolar configuration however, the stimulation pulses are delivered between two electrodes of similar size and typically similar proximity to the targeted structure. This creates a much more contained potential field within the tissue, allowing for finer adjustments of the activating field and thus reducing unwanted co-activation. Thresholds for activations in terms of current or voltage are generally higher with bipolar compared to monopolar stimulation, which results in increased energy consumption and thus represents a disadvantage, especially for battery powered devices. While in some contemporary applications, e.g. those operating with electrode arrays like cochlear implants or epidural spinal cord stimulators, one can typically choose between using the monopolar and the bipolar configuration, in other cases application specific parameters predetermine the electrode configuration. For example, in the emerging field of miniaturized bioelectronic implants, so called electroceuticals (Famm *et al.*, 2013; Birmingham *et al.*, 2014), the electrodes are envisioned as integral with the stimulator. The small overall device size does not allow substantial electrode separation, and so the stimulation configuration is inevitably bipolar.

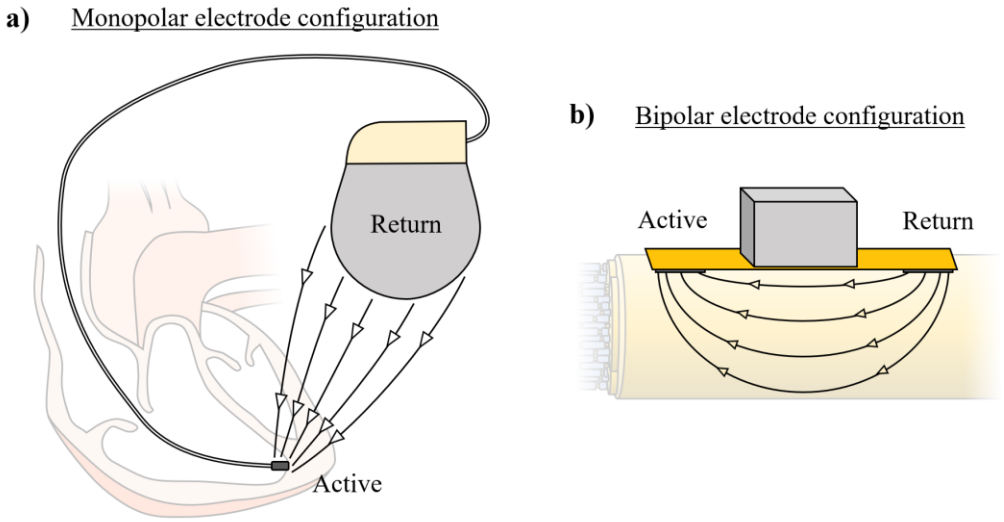

Figure 1.12 Principal stimulation electrode configurations. a) Many past and present electrical neuromodulation devices and research studies have used monopolar electrode configurations often with the implantable pulse generator itself as the return electrode. In this configuration the electric field between the single active electrode near the target excitable structure and the remotely placed return electrode area can be idealized as an electrical monopole. **b)** Due to the small overall device size, both electrodes of proposed electroceutical devices are in similar proximity to the target structure and the generated electric field resembles an electric dipole.

Implantable electrode design examples

The practical design of implantable electrodes for ES strongly depends on the specific application and the degree of invasiveness (Figure 1.11), and in many cases electrodes are specifically designed based on the anatomical morphology of a single application. Although the following list is far from exhaustive, here we highlight two principal designs of implantable extraneural[9] electrodes for peripheral nerve stimulation.

Epineural electrodes

Electrodes that are placed in close proximity to a nerve or are sewn onto the epineurium that serves as an external covering to the nerve are referred to as epineural. Epineural electrodes are the least invasive group of extraneural electrodes (Tyler, 2018) and examples of their application include implanted peroneal nerve stimulators to treat drop foot (Strojnik *et al.*, 1987) and phrenic nerve stimulation for diaphragm pacing (Glenn

[9] Extraneural electrodes do not penetrate any structures of the targeted nerve. They are less invasive than interfascicular electrodes that penetrate the epineurium, or intrafascicular electrodes that penetrate both epineurium and perineurium (Figure 1.2).

and Phelps, 1985). They are advantageous in applications where whole peripheral nerves are to be stimulated, e.g. to activate synergistic muscle groups, like the dorsiflexors in the example of drop foot stimulators, rather than single muscles. The benefits of relatively low invasiveness, however, are bought at the expense of limited selectivity of the induced electrical field. This presents challenges when only a subpopulation of a nerve is to be stimulated and increases the potential for unwanted coactivation of nearby nervous structures.

Circumneural electrodes

Circumneural, or nerve cuff, electrodes encircle a peripheral nerve and thus create an intimate interface between that nerve and multiple electrode contacts incorporated into the inner surface of the cuff. The cuffs are made of an insulating material, typically silicone, which confines the electrical field within them. Selective stimulation with cuff electrodes has been demonstrated in various clinical applications including standing systems in paraplegic subjects (Fisher *et al.*, 2006) and control of the upper extremity in human subjects (Polasek *et al.*, 2007). The increased invasiveness of cuff electrodes compared to other extraneural electrodes is associated with greater risks. A major challenge of circumneural electrode interfaces is the risk of squeezing the nerve and thus restricting blood flow. In order not to exceed safe levels of intraneural pressure (Rydevik, Lundborg and Bagge, 1981) self-sizing spiral (Naples *et al.*, 1988) and helix (Agnew *et al.*, 1989) electrode cuffs have been developed. These cuffs can accommodate some swelling of the nerve, which might, for example, occur during an inflammation, without dangerously increasing intraneural pressure, while maintaining a tight fit after the swelling is gone.

Materials for implantable stimulation electrodes

Besides the general requirements regarding biocompatibility that many biomedical implants have in common, materials for implantable neural stimulation electrodes must be electrochemically stable under pulsed conditions. Gold for example, a material that exhibits a good general biocompatibility and is used in many medical implants, is not suitable to be used as stimulation electrode material, as it readily dissolves when its potential is raised a few hundred millivolts above the resting potential (Fallon and Carter, 2016). The main parameter that determines the performance of chronically implanted electrodes under pulsed condition is the reversible charge storage capacity (CSC), that is the amount of charge that may be stored at the electrode-tissue interface without causing

irreversible electrochemical processes, such as the formation of toxic molecular species. Craggs et al. highlighted the central role of the electrode resting potential and introduced the electrode limit-voltage plane to predict the maximum safe charge injection with a given electrode without the formation of noxious molecular species (Craggs, Donaldson and Donaldson, 1986).

Table 1.3 Reversible charge storage capacity and other parameters in electrode material selection. (Merrill, Bikson and Jefferys, 2005) Copyright by Elsevier. Reprint with permission.

	Reversible charge storage capacity ($\mu C/cm^2$)	**Reversible charge injection processes**	**Corrosion characteristics**	**Mechanical characteristics**
Platinum	300-350 r[a]; AF, 200µs: 50-100 g[b]; CF, 200µs: 100-150 g[b]	Double layer charging, hydrogen atom plating, and oxide formation and reduction	Relatively resistant; greatly increased resistance with protein	Relatively soft
Platinum-iridium alloys	Similar CSC to Pt			Stronger than Pt
Iridium	Similar CSC to Pt			Stronger than Pt
Iridium oxide	AF: ±2200 g[c,d]; CF: ±1200 g[c,d]; AB: ±3500 g[c,d,e]	Oxide valency changes	Highly resistant[e,f]	
316LVM stainless steel	40-50 g	Passive film formation and reduction	Resistant in passive region; rapid breakdown in trans-passive region	Strong and flexible
Tantalum/tantalum pentoxide	700 g[g]; 200 g[h]	Capacitive only	Corrosion resistant[i,j,k,l]	

r = real area; g = geometric area; AF = anodic first, charge-balanced; CF = cathodic first, charge-balanced; AB = cathodic first, charge-balanced, with anodic bias.

[a] (Brummer and Turner, 1977).

[b] (Rose and Robblee, 1990).

[c] (Beebe and Rose, 1988).

[d] (Kelliher and Rose, 1987).

[e] (Agnew *et al.*, 1986).

[f] (Robblee, 1983).

[g] (Guyton and Hambrecht, 1973, 1974).

[h] (Rose, Kelliher and Robblee, 1985).

[i] (Bernstein *et al.*, 1977).

[j] (Donaldson, 1974).

[k] (Johnson *et al.*, 1977).

[l] (Lagow, Sladek and Richardson, 1971).

Merrill el al. (2005) reviewed biocompatible materials that exhibit suitable reversible charge storage capacities and other parameters of interest for neural stimulation electrodes (Table 1.3). Most commercially available electrodes are manufactured from electrochemically stable noble metals such as platinum, titanium or iridium.

Stimulation induced tissue damage

Although the exact mechanisms leading to stimulation induced tissue damage are yet be fully understood, they have been categorized into detrimental electrochemical reactions at the electrode-tissue interface and electrotoxicity (Cogan, Hara and Ludwig, 2018).

Stimulation electrodes that are operated within their specific charge injection capacity achieve the desired charged injection by means of capacitive, non-faradaic, processes in which no species are oxidised or reduced. If limits for charge injection are exceeded, faradaic, irreversible reactions occur at the electrode-tissue interface. These reactions can cause the formation of species, for example through oxidation or reduction of water molecules, that are damaging to neural tissue as they induce local pH-changes. Further, a disintegration of the electrode material itself might not only lead to failure of the stimulation system over time, but dissolution products of common electrode materials such as platinum or titanium nitride have been shown to induce neurotoxicity (Guenther *et al.*, 1999; Kumsa *et al.*, 2017).

Mechanisms of tissue damage induced by electrotoxicity are less well understood than these detrimental electrochemical reactions. For example, they can occur at intensities below maximum charge injection capacities and might thus not be related to the formation of noxious species (McCreery *et al.*, 1988). Investigations incorporating anaesthetic suppression of nerve activity showed that stimulation of a silenced nerve, at intensities where damage would occur in activatable nerves, caused little to no electrotoxic damage and suggest that these mechanisms are directly related to nerve hyperactivity (Agnew *et al.*, 1990).

A mathematical description to predict the safety of electrical charge injection, the Shannon equation (1.10), has been developed based on empirical data (Shannon, 1992):

$$\boldsymbol{log\left(\frac{Q}{A}\right) = k - log(Q)} \tag{1.10}$$

Here Q/A is the charge density and Q the injected charge. The adjustable parameter k is typically between 1.5 and 2. Charge density - charge combinations to the left and below the so-called *Shannon line* are deemed safe, whereas values to the right and above the line

are predicted to be damaging (Cogan *et al.*, 2016). Limitations and applicability of the Shannon model are discussed in detail by Cogan *et al.* (2016).

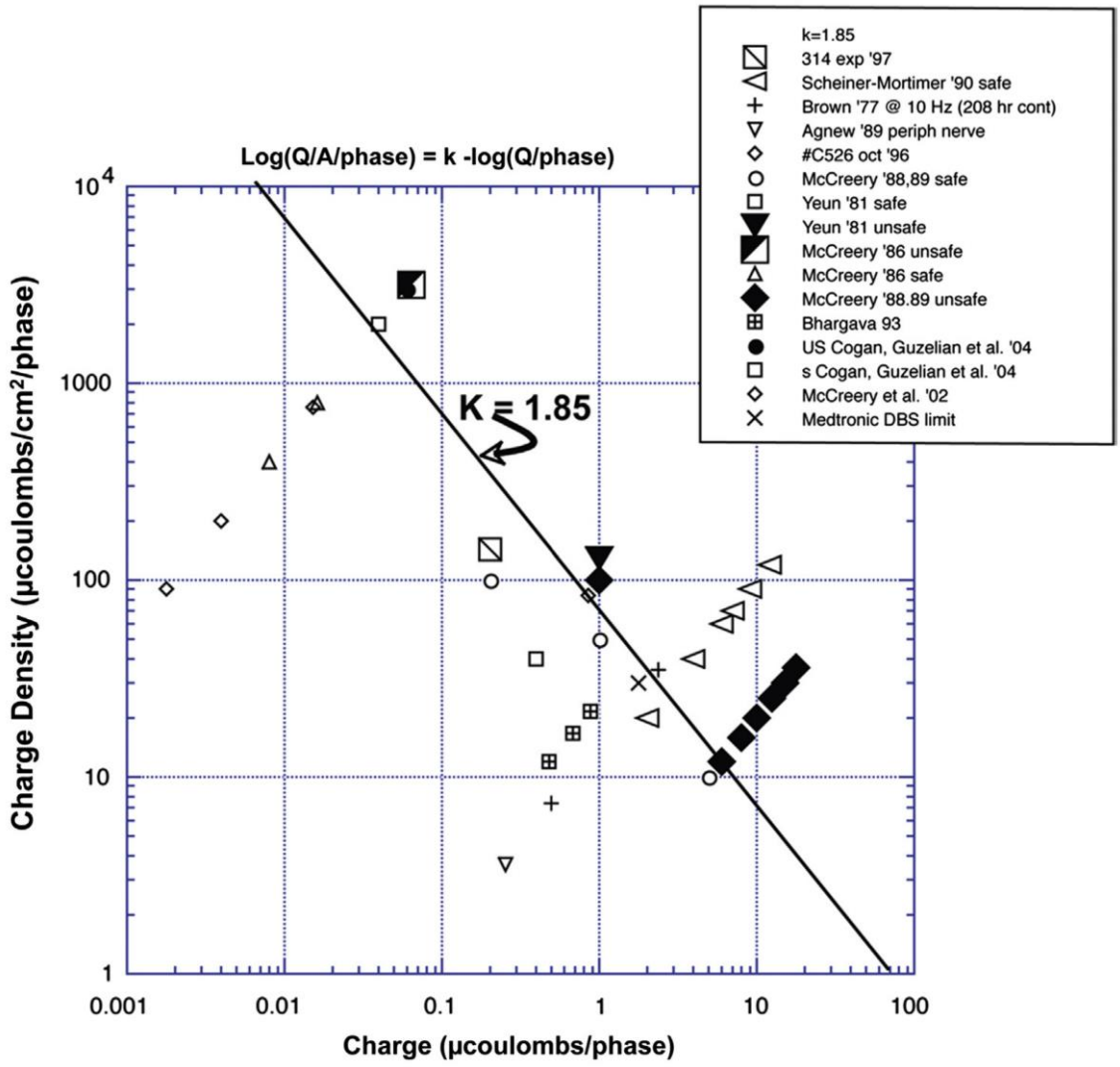

Figure 1.13 Plot of Shannon equation for safe stimulation. Data shown here are derived from published and unpublished experiments. Filled symbols were deemed unsafe by the investigators, whereas open symbols indicate safe stimulation parameters. (Mortimer and Bhadra, 2018) Copyright by Elsevier. Reprint with permission.

1.3.5 Stimulation waveforms

Some of the earliest devices used for electrical stimulation were alternating current (AC) generators that used sinusoidal waveforms to activate nerve and muscle tissue. However, most present neuromodulation devices use, not least because of the ease of generating them with simple electronic circuits, rectangular stimulation waveforms. While monophasic rectangular pulses may be used to achieve neural stimulation with charge injection of only one polarity, in order to reduce detrimental electrochemical reactions at the electrode-tissue interface, biphasic charge-balanced pulses are commonly

incorporated in contemporary ES devices (Merrill, Bikson and Jefferys, 2005). Stimulation pattern comprised of such monophasic or symmetrical biphasic rectangular pulses are further parameterised by the stimulation amplitude, the duration of the phase(s), often referred to as phase width (PhW), and the frequency of pulse delivery in Hz or pulses per second (pps).

It has been shown that variations of the rectangular biphasic pulse such as interphase gaps (IPGs) (van den Honert and Mortimer, 1979; Gorman and Mortimer, 1983), charge balanced asymmetric pulses, and subthreshold conditioning pre-pulses (Grill and Mortimer, 1993, 1995, 1997) can be used to increase stimulation efficiency or selectivity. Merrill *et al.* (2005) reviewed the findings of studies that investigated rectangular pulse shape variations (Gorman and Mortimer, 1983; Scheiner, Mortimer and Roessmann, 1990) in monopolar stimulation configurations. However, the significant influence of the electrode configuration on the efficiency of stimulation waveforms is highlighted by our own experimental work presented in Chapter 3.

Besides these variations in rectangular pulse shapes, non-rectangular waveforms have also been investigated in the pursuit of energy efficient neural stimulation. These non-rectangular waveforms include exponentially rising or decaying pulses (Jezernik and Morari, 2005), sinusoidal and Gaussian pulses, as well as linearly rising or decaying ramps (Sahin and Tie, 2007). While some waveforms performed better than others with regard to energy efficiency, these benefits were accompanied with decreased performance in other measures of efficiency (such as charge or peak power), so that no one waveform was found to be simultaneously optimal in all measures of efficiency (Wongsarnpigoon, Woock and Grill, 2010). Further, it was recognized that the optimal (with regard to a specific measure of efficiency, e.g. energy efficiency) stimulation waveform may depend on phase width.

Promisingly three recent computational studies identified Gaussian-shaped stimulation waveforms independently, and using different approaches, to use the least amount of electrical energy to activate nerves (Wongsarnpigoon and Grill, 2010; Forger, Paydarfar and Clay, 2011; Krouchev *et al.*, 2014). We have investigated these predictions in a rodent *in-vivo* nerve-muscle model (Chapter 3.3).

1.3.6 Recruitment and pulse duration relationships

Recruitment behaviour

For an ES pulse of any given waveform (e.g. monophasic, cathodic rectangular) to evoke an action potential, it needs to be of sufficient intensity. The stimulation intensity of single stimuli depends on the stimulation amplitude and duration (or phase width). For a fixed stimulation phase width one can thus define the stimulation amplitude required to evoke an action potential (in the target excitable fibre) as a *threshold* (Lapicque, 1907). An amplitude below the threshold is insufficient to elicit excitation and is termed *subthreshold*, whereas an amplitude above this minimum required intensity for activation is called *suprathreshold*. While reaching the threshold for activation, and thus action potential generation, is an all-or-none event for a single fibre, activation happens gradually, i.e. over a range of threshold amplitudes, in a stimulated population of fibres. As we have discussed for myelinated axons in Section 1.3.2, two main determinants for activation (via the magnitude of the extracellular potential) are the distance of the central NoR from the electrode and the internodal distance, which is correlated to axon diameter. In a homogenous nerve both these parameters, electrode distance to central NoR for individual fibres and individual fibre diameter, are normally distributed and the recruitment is thus typically described by a sigmoidal curve (Figure 1.14). For stimulation of a whole nerve one can thus express relative activation as a percentage threshold, e.g. the 50% activation threshold $I_{th50\%}$ is the amplitude required to activate 50% of the individual nerve fibres in that nerve. Further, dynamic ranges, e.g. the range of amplitudes between 5 and 95% relative activation, which are of interest for many ES applications that seek to stimulate specific subpopulations selectively, can be determined (Figure 1.14.b).

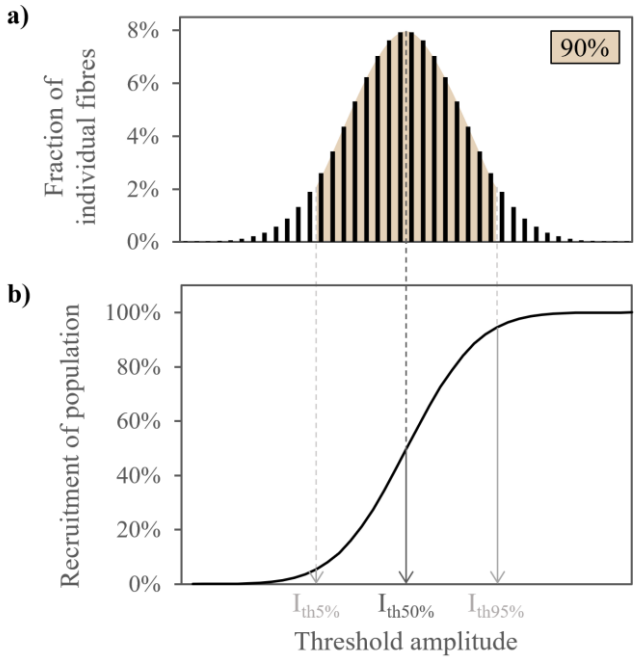

Figure 1.14 Recruitment behaviour of a homogeneous fibre population. a) The normally distributed thresholds for individual fibres of a homogeneous population cumulate to a **b)** characteristic sigmoidal recruitment curve. Percentage threshold for activation of the population $I_{th5\%}$, $I_{th50\%}$, and $I_{th95\%}$ are indicated.

Pulse duration relationships

The relationship of the pulse width PW and threshold amplitude I_{th} is called *strength-duration relationship*. For monophasic rectangular pulses and a single excitable fibre, this relationship can mathematically be described by the Lapicque equation

$$\boldsymbol{I_{th}(PW) = \frac{I_r}{1-e^{-\left(\frac{PW}{ln(2)*T_c}\right)}}}, \tag{1.11}$$

where I_r is the *rheobase*, that is the minimum amplitude required to activate the fibre with an infinitely long pulse, and T_c is the *chronaxie* (Lapicque, 1907). The chronaxie T_c is defined as the pulse duration at which the target fibre is activated with an amplitude of twice the rheobase I_r (Figure 1.15.a).

Although this relationship was originally developed for stimulation of a single excitable fibre with monophasic rectangular pulses, the SD curve is often used to determine rheobase and chronaxie values for stimulation of whole nerves and muscles (Geddes, 1999; Ashley *et al.*, 2005), e.g. at a specific percentage activation threshold, and also for different waveforms (Sahin and Tie, 2007).

The linear charge-duration curve can be attained by integrating the threshold currents over the pulse duration (Figure 1.15.b). The amount of charge injection Q_{th} required to

reach threshold, and thus, when extrapolated to the whole stimulated excitable structure, to achieve the desired neuromodulation effect, is a critical parameter. Since charge injection is a main determinant of stimulation safety (compare Shannon model, Figure 1.13) and scales directly proportional to pulse duration, many ES applications typically use the shortest feasible pulses.

$$\boldsymbol{Q_{th}(PW) = \int_0^{PW} I_{th}(PW)\,dt.} \tag{1.12}$$

Integration of the power at threshold, which is proportional to I_{th} squared for a given load Z, over the pulse duration gives us the electrical energy E_{th} which is "consumed" to reach the threshold for activation:

$$\boldsymbol{E_{th}(PW) \propto \int_0^{PW} I_{th}(PW)^2\,dt.} \tag{1.13}$$

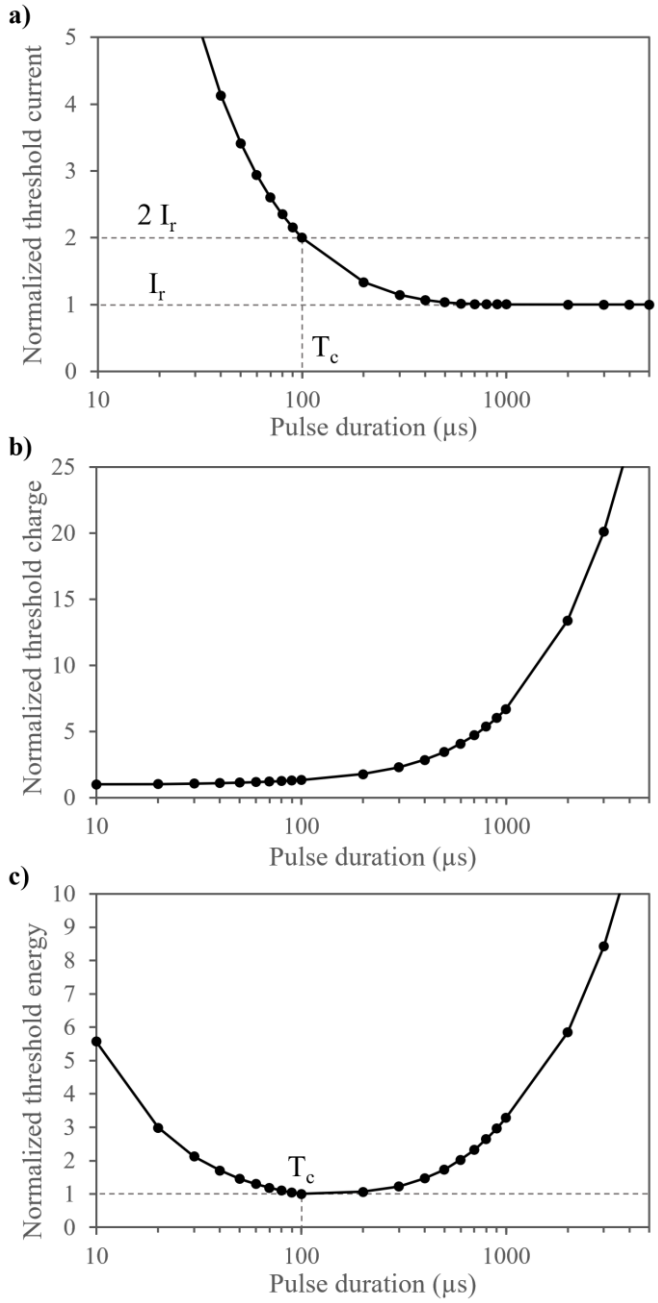

Figure 1.15 Pulse duration relationships. a) Strength-duration curve as described by the Lapicque equation (1.11), normalized to multiples of the rheobase I_r. The pulse duration at which twice I_r is required to reach threshold is termed chronaxie T_c. **b)** Normalized charge-duration curve and **c)** normalized energy-duration curve with local minimum at T_c are based on the threshold current I_{th} determined with (1.11).

An important characteristic of the energy-duration relationship (Figure 1.15.c) is that it has a local minimum at a pulse duration equal to the chronaxie T_c. Using the least amount of electrical energy to achieve neural activation is desired in many battery powered ES implants, as the energy consumption per pulse directly impacts the battery life for a given battery technology and volume. More energy efficient stimulation would therefore enable increased battery life and/or reduced battery volume (and thus overall implant volume).

2 GENERAL METHODS

The development and refinement of a rodent nerve-muscle model, a sophisticated neural stimulation and recording system, and effective methods for data normalization as well as analysis of complex bioelectric signals were main parts of my three-year PhD journey and are summarized below. This chapter describes the general methods that were used in our *in-vivo* experiments to attain and analyse the data presented in Chapters 3 to 5. The "Materials and Methods" sections of published and unpublished studies in those chapters are reduced to brief summaries of the study-specific methods.

2.1 Surgical procedure

Experiments were carried out in adult Wistar rats under adherence to the Animals (Scientific Procedures) Act of 1986. All procedures were approved by the Home Office under the project licence (PPL 40/3743).

Animals were anaesthetised with isoflurane in oxygen at an initial concentration of 3%. For analgesia 0.05 mg kg^{-1} of Buprenorphine (Temgesic, Indivior, Slough, UK) was administered intra muscularly in the quadriceps of the contralateral (right) hindlimb. In order to maintain a stable deep level of anaesthesia throughout the experimental procedures, respiration rates were monitored and the isoflurane concentration was adjusted accordingly between 1.5% and 2%. Thus, the respiration rate was kept between 40 and 60 breaths per minute, approximately 50% of the normal respiratory rate of awake and undisturbed rats. The animals were placed on an adjustable heat pad (E-Z Systems Corporation, Palmer, Pennsylvania, USA) to keep the body core temperature between 37-38°C which was monitored using a rectal temperature probe. While *hypothermia* is, due to the relatively large ratio of animal surface area to body mass, a common concern in small animal anaesthesia, preventing malignant *hyperthermia*, which may lead to muscle rigidity and even death, was crucial as well. We found that, besides close monitoring of the body core temperature and adjusting of the heat pad, using the least concentration of isoflurane, while maintaining a deep and stable level of anaesthesia, and setting the oxygen flow rate to at least 1 L min^{-1} reduced the risk of hyperthermia.

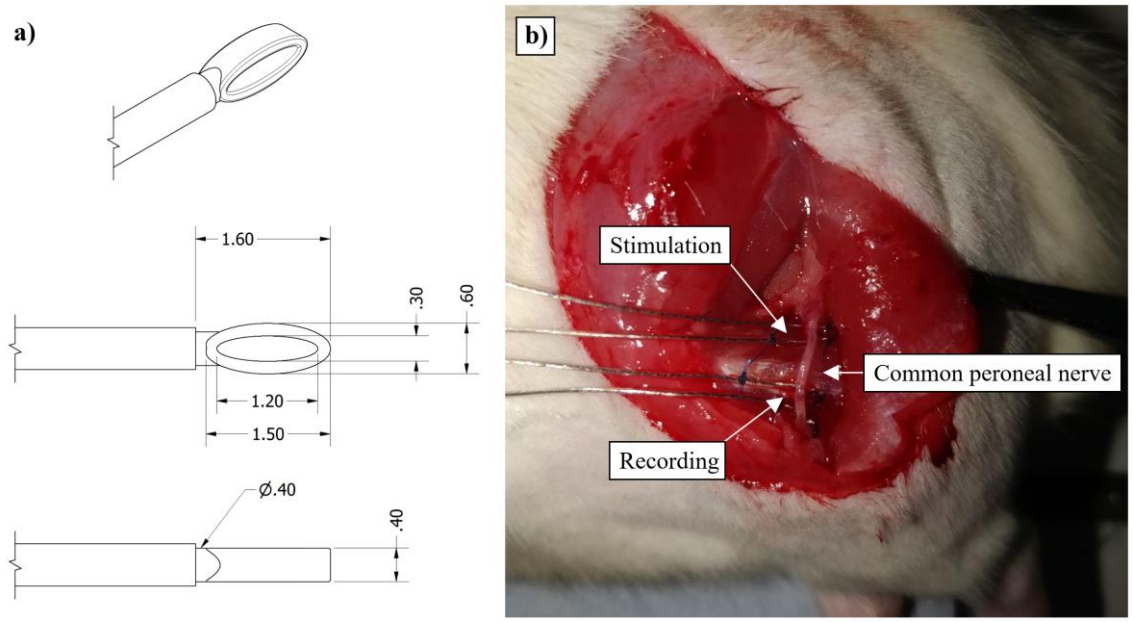

Figure 2.1 Loop electrodes for neural stimulation and recording. **a)** Sketch of elongated loop electrodes in isometric projection, top view, and side view. All dimensions are approximations in mm. Drawn in Autodesk ® Inventor ® Professional 2019 (Autodesk, Inc, San Rafael, California, USA). **b)** Two bipolar pairs of loop electrodes implanted at the common peroneal nerve: proximal electrode pair is for stimulation and distal electrodes are for ENG recording.

For stimulation and electroneurogram (ENG) recordings, loop electrodes with an inner diameter of approximately 1mm were formed from the uninsulated ends of 40-strand stainless steel electrode wire (Electrode wire AS634, Cooner Sales Company, Chatsworth, California, U.S.A.). When the electrode wire geometry is simplified and assumed to be a single strand, the uninsulated loop areas have an exposed electrode area of approximately 0.025-0.03cm^2. The electrode surface area is an important parameter for electrical stimulation electrodes as it determines the maximum reversibly injectable charge for any given material (Table 1.3) as well as the safety limits for charge injection per phase (Figure 1.13). The loop electrodes were placed in the tissue immediately underneath the common peroneal nerve (CPN) and were elongated to an oval form during placement and fixation (Figure 2.1). The stimulation electrodes were placed approximately 5mm distal from the point where the CPN branches from the sciatic nerve. The more proximal stimulation electrode was used as return electrode for bipolar stimulation and the distal electrode, separated by 2mm from the return, was used as active electrode. In some experiments, a second pair of electrodes, also with an inter electrode separation of 2mm, was placed approximately 10mm distally to the stimulation electrodes to record a distal ENG of the stimulated nerve. After placing the nerve electrodes, the muscle and skin were closed to prevent the nerve from drying out. A hypodermic needle

(21G x 1-1/2") was placed in the dorsal skin of the animals and was used as return electrode for the monopolar configuration. In some early experiments an additional loop electrode, fixed to the muscle tissue approximately 10mm away from the CPN, served as return electrode in the monopolar configuration. This configuration can also be called "near monopolar" and was replaced in later experiments by the hypodermic needle, as the high current density at the near monopolar loop return electrode could lead to unwanted coactivation.

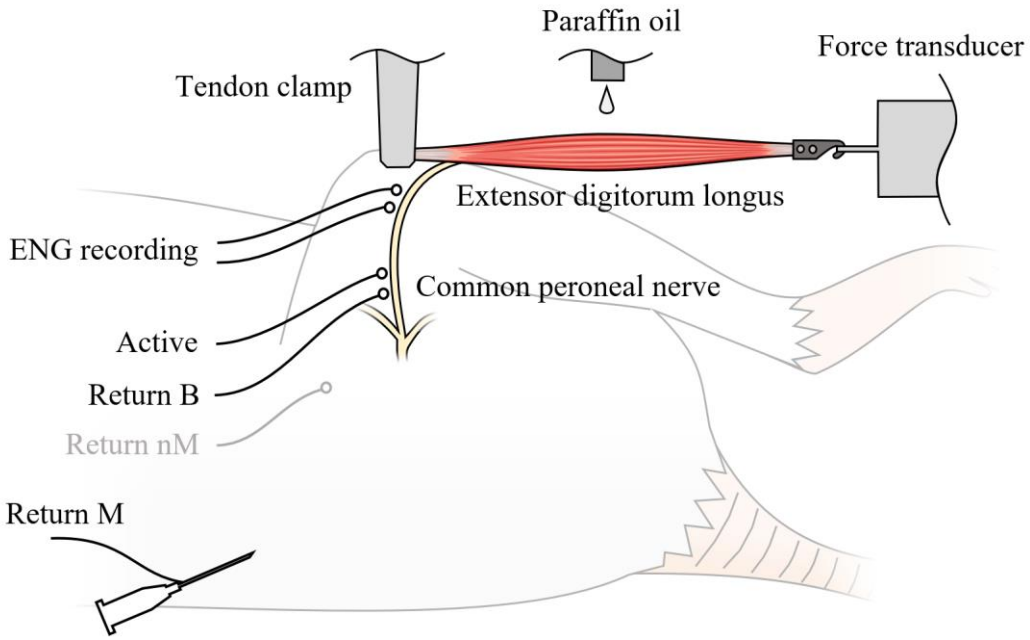

Figure 2.2 Rodent in-vivo nerve-muscle preparation with both principal stimulation electrode configurations. The common peroneal nerve (CPN) in anaesthetized rats is stimulated and the isometric twitch force response of the extensor digitorum longus (EDL) muscle recorded. Depending on which return electrode is connected, the stimulation setup is either monopolar (with Return M) or bipolar (with Return B). In some early experiments a loop electrode, approximately 10mm away from the CPN long axis was used as "near monopolar" return electrode (Return nM). ENG recordings of the CPN were measured distally to stimulation.

To access the extensor digitorum longus (EDL) muscle, the distal tendon of the tibialis anterior muscle was cut and the muscle belly carefully blunt dissected from the deeper lying EDL. The proximal EDL tendon was exposed and clamped with a sturdy artery forceps that was firmly mounted on the experimental steel table. The distal EDL tendon was dissected and connected with a miniature titanium alloy hook to a force transducer (Gould Inc, Statham Instrument Division, Oxnard, California, U.S.A.) which was also mounted on the steel table. Thus, the EDL was mechanically isolated and held in an isometric condition while innervation and blood supply were preserved (Figure 2.2). The ideal muscle length was set by increasing it from slack in 0.5mm increments to that length

at which the developed isometric twitch force response to single stimuli was maximal but without excessive passive muscle tension (compare Figure 1.6). Heated liquid paraffin oil was delivered by a peristaltic pump (Watson-Marlow Ltd., Falmouth, Cornwall, UK) at a rate of 0.1ml min^{-1} to the EDL muscle surface to maintain physiological temperature and to prevent the muscle from drying. Normal fluid loss during the experimental procedures was replaced by administering approximately 1ml of sterilized saline solution (OXOID Ltd., Basingstoke, Hampshire, UK) per hour subcutaneously.

2.2 Stimulation

Stimulation pulses were generated in a custom written LabVIEW™ 2016 (National Instruments Corporation, Austin, Texas, U.S.A.) program (Appendix 1) and delivered at 1MS/s resolution over the analog output of a NI PCIe 6351 Data Acquisition Card (National Instruments Corporation, Austin, Texas, U.S.A.) to a galvanically isolated voltage-to-current converter. The pulses were delivered to the active electrode at the CPN at a rate of one pulse every three seconds. In some experiments, where a series of strong twitch forces were elicited or where spinal reflex activity was investigated, this rate was reduced up to one pulse every ten seconds to allow for full recovery and prevent neuromuscular fatigue. A relay unit switched under computer control between the return electrode at the nerve (for bipolar stimulation) and the hypodermic needle acting as return electrode under the dorsal skin (for monopolar stimulation). In some early experiments, the return electrodes were disconnected and connected manually between recording periods. However, this made it difficult to distinguish between small threshold changes due to electrode configuration and normal variations due to depth of anaesthesia, fatigue, or body temperature that might occur between one recording period and another.

Pulses with combinations of the pulse parameters to be tested (e.g. amplitude, phase widths, interphase gap, and return electrode configuration) were delivered in randomized order. This means recruitment curves were assembled from test pulses that were randomly placed from start to finish of a recording period. Every 20 test stimulations a control pulse which was set to elicit full neural activation was delivered to use for normalization. The control pulses were standard biphasic rectangular pulses with 200µs phase width, cathodic phase first and amplitudes set for each experiment separately (typically 1mA) to elicit maximal isometric twitch force. Twitch force responses to the test stimulations were measured relative to the control pulses and thus normalized. The randomized order of test stimulation parameter delivery and normalization with control pulses allowed us to attain

recordings that produced meaningful relationships within the parameter space and that were not affected by progressive or cyclic variations in body temperature, depth of anaesthesia or fatigue.

The shorter the duration of one recording period, that is of one set containing all stimulations (in randomized order) that comprise the recruitment curves that are to be compared against each other, the better and smoother are the recorded recruitment curves. We found that recording periods of 20 minutes and below are ideal because they resulted in data with a steady normalization level (i.e. data with minor influence of fatigue or cyclic variations in depth of anaesthesia), while still enabling to compare several pulse shape variations. With a pulse delivery rate of one pulse every 3 seconds and one control pulse every 20 test pulses, a 20-minute recording session allows to test 380 pulses. With typically 20 pulses comprising one recruitment curve, one such 20-minute recording period enables to record and later compare 19 recruitment curves. To further reduce variations within those recording periods and thus increase the data quality, we found it helpful to precede all recording periods by a brief series of approximately 10 warmup pulses at the normal rate of one pulse every 3 seconds. These warmup pulses were not part of the recording period and the rationale for their incorporation was that the first few twitch force responses after a pause were generally weaker than during the recording.

2.3 Recording and data analysis

The isometric twitch force of the EDL muscle was used as main indication of motor pool activation with CPN stimulation. To verify the correlation between EDL twitch force and CPN nerve activation and to further investigate temporal aspects of AP elicitation, in most later experiments, an electroneurogram (ENG) recording was added distal to the site of stimulation (Figure 2.2). This additional ENG was used to analyse the root mean square (RMS) of the evoked compound action potential (eCAP) in the CPN. The RMS is the square root of the average power across the electrical signal or wave, and it is commonly used to report the amplitude of bioelectric signals[10]. The ENG RMS correlates closely with isometric EDL twitch force (Figure 2.3). validate the use of EDL twitch force as indication of CPN activation.

[10] While there is no clearly defined standard for analysing epineural ENG recordings, RMS is a standard method for reporting EMG data (Merletti, 1997), which is a similar bioelectric signal.

In experiments that were conducted to investigate the energy consumption required to achieve neural activation with different stimulation waveforms (Chapter 3.3), stimulation voltage across the electrodes and stimulation current through a resistor in series were recorded in addition.

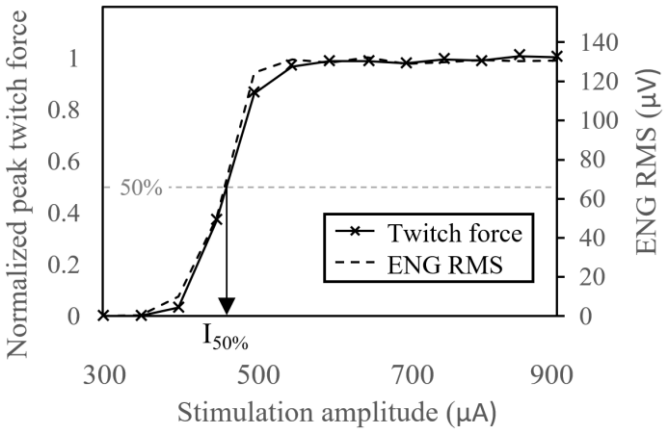

Figure 2.3 EDL twitch force correlates with CPN eCAPs. One representative normalized recruitment curve for 200µs biphasic stimulation in the monopolar electrode configuration. 50% activation threshold is determined by linear interpolation. Normalized peak twitch force and ENG root mean square (RMS) are correlated.

2.3.1 Isometric twitch force

The isometric twitch force responses of the extensor digitorum longus (EDL) muscle were recorded at a sample rate of 100kS/s. Triggered by the stimulation system, the signals were recorded with a PowerLab 16/35 (ADInstruments Pty Ltd, Bella Vista, New South Wales, Australia) and stored, pre-processed and exported using LabChart 7 Pro (ADInstruments Pty Ltd, Bella Vista, New South Wales, Australia). The developed isometric twitch force was determined by subtracting the passive muscle tension (typically between 0.05 and 0.1N) from the peak recorded muscle tension (Figure 2.4).

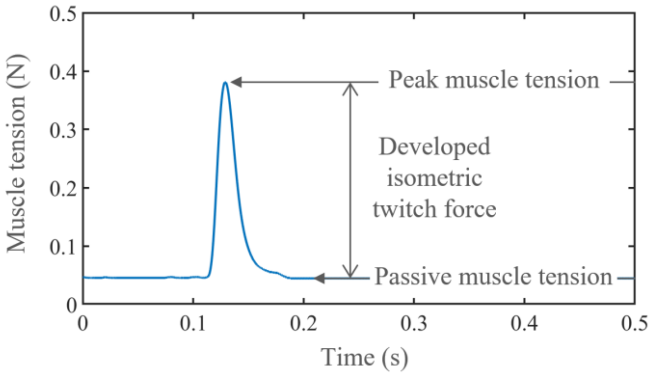

Figure 2.4 Developed isometric twitch force responses of the EDL are determined by subtraction of the passive muscle tension from the peak recorded muscle tension during stimulation.

As introduced in Section 2.2, to minimize any effects of variations in depths of anaesthesia, temperature or fatigue on the recordings, test stimulations were delivered in randomized order. Force responses to each test stimulation were normalized by division by the interpolated control pulse level (dashed line in Figure 2.5.a) at the time of that stimulation.

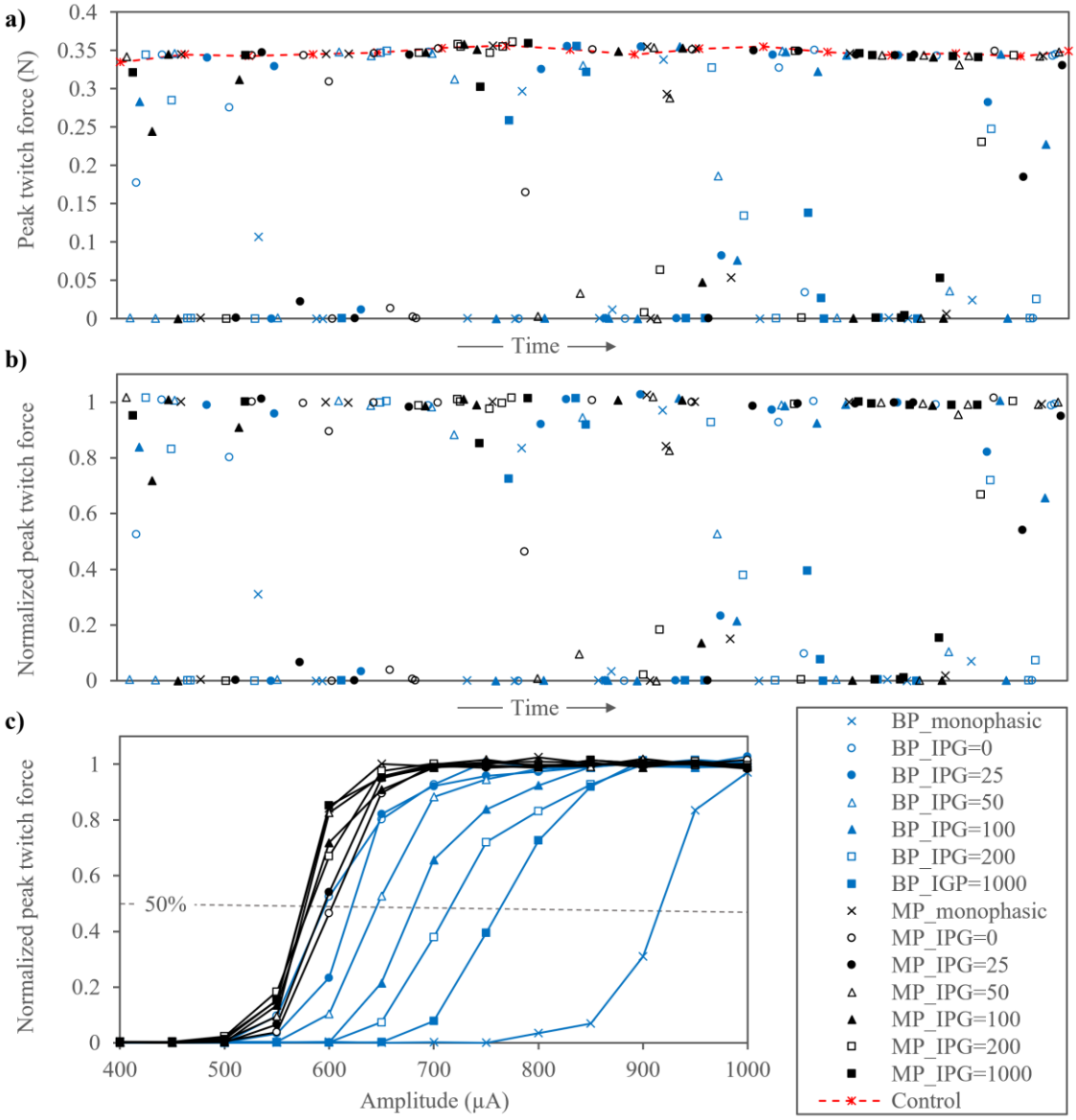

Figure 2.5 Determination of 50% activation thresholds. a) Test stimulation were delivered in randomized order and control pulses were incorporated in regular intervals: one control pulse every 20 test stimuli. Linear interpolation between the control pulses provides a control level (red dashed line) for full neuromuscular activation. **b)** Developed twitch force values are normalized in relation to the normalization level before they are **c)** sorted to reveal the recruitment curves for the tested pulse variations. 50% activation thresholds are determined by linear interpolation of the recruitment data points. Data is from one representative recording period that compared monophasic and biphasic pulses with and without interphase gaps in the monopolar (black) and bipolar (blue) electrode configuration.

The normalized twitch force responses (Figure 2.5.b) are sorted by ascending stimulation amplitude and thus build the recruitment curves (Figure 2.5.c). By linear interpolation of the experimental data points the 50% activation thresholds were determined for all tested pulses shape variations (MATLAB code in Appendix 2). This allowed us to express the efficiencies of tested pulse shape variations, such as interphase gaps (IPGs), as a

percentage difference, e.g. in amplitude required, to reach 50% activation compared to a standard comparator pulse shape. In the exemplary data from Figure 2.5.c for instance, in the bipolar electrode configuration (blue traces) adding and increasing the length of IPGs increased the amplitude required to reach 50% activation up to approximately 28% with 1ms IPG (compared to the amplitude required with biphasic pulses without IPG in that same electrode configuration).

2.3.2 Electroneurogram

In most later experiments, an electroneurogram of the CPN was recorded approximately 10mm distal to the site of stimulation. The purpose of incorporating ENG recordings was to investigate fine temporal aspects of action potential generation, in particular, to identify the part or field transition within the stimulation waveform at which neural excitation occurs. Since most commonly used waveforms for neural stimulation have phase widths of 200µs and less, identifying such small temporal differences in the mechanical muscle twitch response, which even for the fast type EDL muscle that we studied was about 30-50ms in duration (Figure 2.4), is not practical. Analysis of the shift in the recorded bioelectric eCAP signal, which has a duration of approximately 1ms, allowed for identification of such fine temporal aspects. We concede that the signals we recorded, and that we call *ENG*, might have (in some cases, e.g. in Figures 2.6 and 2.7) a substantial interference from the electrical activity of the surrounding muscle tissue (EMG). While this EMG influence would prohibit the direct assessment of nerve conduction velocities, as long as the recorded signal shape is consistent, it allows for analysis of shifts in the signal-to-artifact latency and thus to evaluate what part of the stimulation pulse elicited excitation. Possible ways to reduce the EMG interference are increased insulation, e.g. by using cuff electrodes with conductive shield layers (Sabetian *et al.*, 2017), silencing of the surround muscle tissue by denervation, or using pulse doublets to harness differences in nerve and muscle refractory periods and mask out the EMG. Since, as we outlined above, the potential EMG interference did not prohibit us to analyse relative differences in signal-to-artifact latencies, we did not take any of those steps in the experiments presented in this thesis.

The ENG was recorded at a sample rate of 100kS/s with a PowerLab 16/35 (ADInstruments Pty Ltd, Bella Vista, New South Wales, Australia) and stored, pre-processed and exported using LabChart 7 Pro (ADInstruments Pty Ltd, Bella Vista, New South Wales, Australia). The ENG recordings were filtered to extract the 50Hz noise and

stimulation artifacts were removed. For short stimulation pulses (Figure 2.6) this artifact reduction was achieved automatically with a custom written MATLAB code (Appendix 3a).

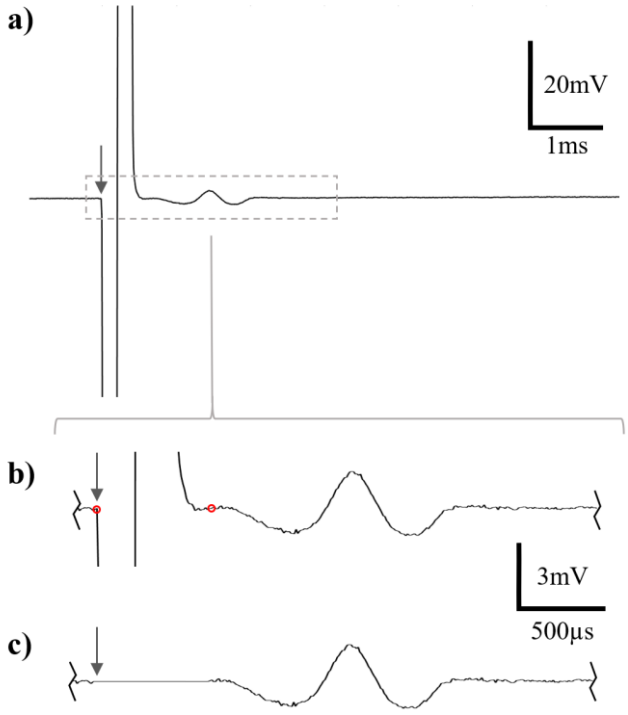

Figure 2.6 Artifact removal of short stimulation pulses. a) ENG recording during stimulation of the CPN with short biphasic rectangular pulse (phase width 200µs). Artifact and eCAP are not merged so that the former can easily be removed. **b)** The stimulation artifact onset can automatically be detected (first red circle) and a fixed interval (to second red circle) from there (here 600µs) is identified as stimulation artifact and **c)** removed from the ENG recording. Arrows indicate stimulation onset.

For stimulations with longer phase widths (Figure 2.7.a), the eCAPs were merged with the stimulation artifacts, often on the slopes of capacitive charging/discharging during the stimulation phases, as in Figure 2.7.b. These artifact characteristics do not scale purely proportional with stimulation amplitude and vary strongly between experiments, and so manual input was necessary to fit a spline as baseline on which the eCAP laid (Figure 2.7.c) and which was then used to remove the artifact (Appendix 3b). As this method of artifact removal relied strongly on user input, the resulting eCAP recordings (Figure 2.7.d) might be biased and where therefore not used for further quantitative analysis, such as determination of precise eCAP-latencies. ENG plots were typically smoothed with a 10-sample moving average MA-filter. All ENG processing and plotting was done in MATLAB (MATLAB (R2018a), The MathWorks Inc., Natick, MA, USA).

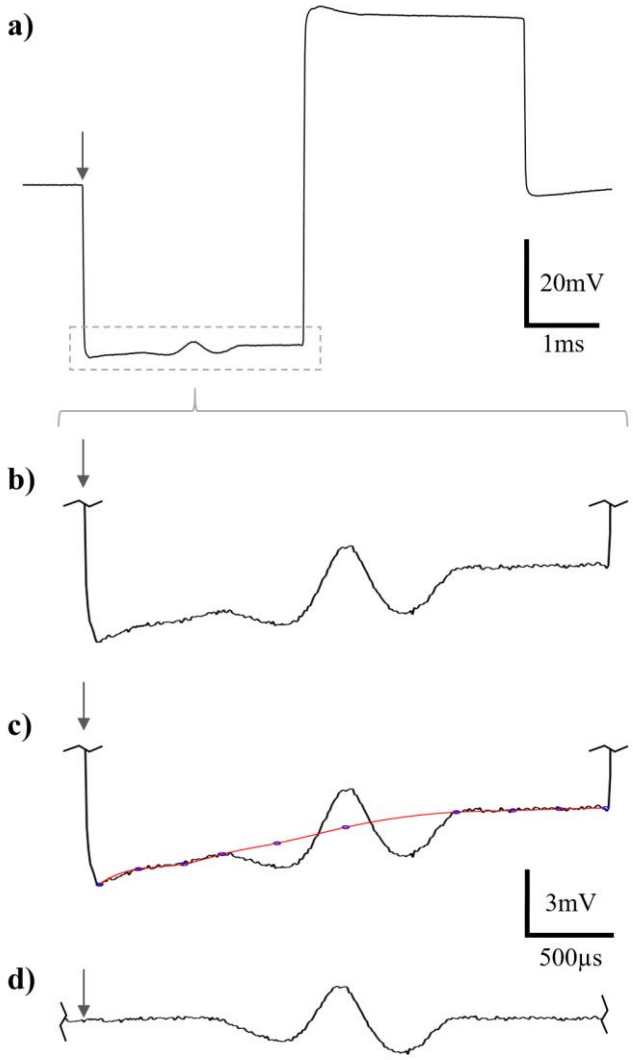

Figure 2.7 Artifact removal of long stimulation pulses. a) ENG recording during stimulation of the CPN with long biphasic rectangular pulse (phase width 3ms). **b)** eCAP is merged with the stimulation artifact and **c)** manual input (blue circles) is required to fit a spline (red trace) on the slope of the artifact. **d)** The fitted spline is subtracted from the merged signal and thus the artifact is removed from the ENG recording. Arrows indicate stimulation onset.

3 WAVEFORMS FOR NEURAL STIMULATION

Extensive research has been carried out to investigate the influence of stimulation waveforms on efficiency, selectivity, and safety of electrical neuromodulation. While most published literature in this field is concerned with waveforms that are variations of rectangular pulses, as these are the standard waveform shapes used in many past and present stimulation devices, some studies investigated non-rectangular stimulation waveforms. The research summarized in this chapter focuses on detailed re-examinations of four proposed waveforms:

- Subthreshold conditioning pre-pulses have been suggested to selectively alter the thresholds for activation of fibre populations that are, due to fibre size or proximity to the stimulation electrode, activated first when standard rectangular pulses are used. However, since their original proposal in the mid-1990s, published literature on the effect of subthreshold pre-pulses is contradictory. Our experimental efforts described in Chapter 3.1 provide an explanation for this two-decade longstanding controversy in published literature and show how the choice of the practical electrode configuration influences the effect of those pre-pulses.
- Based on these findings we extended our investigations to interphase gaps (IPGs) and asymmetric biphasic pulses with reduced anodic amplitude, two of the most suggested and used pulse shape variations. This study (Chapter 3.2) shows how the effect of those waveforms, that have previously predominantly been studied using monopolar electrode configurations, is opposite in the bipolar compared to the monopolar stimulation mode. This finding is of particular relevance to many miniature stimulation systems, such as the envisioned field of electroceuticals, where the small overall device size does not allow for substantial separation of the electrodes, so that they inevitably operate in a bipolar mode.
- Gaussian shaped stimulation waveforms have recently been identified by three independent computational studies to require the least amount of energy to activate nerves. However, there has not been a comprehensive *in-vivo*

investigation of these findings. We studied the efficiency of Gaussian shaped stimulation waveforms in our rodent model (Chapter 3.3) and found that only moderate energy savings are achievable with this novel pulse shape. In addition, further challenging the proposed benefits of this waveform, we found that those limited energy savings were accompanied by substantial increases of the maximum instantaneous power required to activate a target nerve.

3.1 Subthreshold conditioning pre-pulses

The study presented in this chapter is published and copyrighted:

The only main differences between the published article and the present chapter are:

- Figure and equation numbers were adjusted to match the thesis chapter numbering.
- Parts of the "Materials and Methods" section, such as the surgical procedure, which are described in detail in the General Methods (Chapter 2), are left out and the omissions are indicated by "[…]". Instead, key methodological information such as number of animals, electrode configurations, and recording sampling rates are summarized in inserted boxes.
- To avoid redundant chapter names, the paper section-headings such as "Introduction", "Results", and "Discussion" have been replaced by brief summarizing descriptions of each section's main message.

(Abstract)

Objective: Published research on nerve stimulation with sub-threshold conditioning pre-pulses is contradictory. Like most early research on electrical stimulation (ES), the pioneer work on the use of pre-pulses was modelled and measured only for monopolar electrodes. However, many contemporary ES applications, including miniaturized neuromodulation implants, known as electroceuticals, operate in bipolar mode. Methods: We compared depolarizing (DPPs) and hyperpolarizing (HPPs) pre-pulses on neural excitability in rat nerve with monopolar and bipolar electrodes. The rat common peroneal nerve was stimulated with biphasic stimuli with and without ramp and square DPPs or HPPs of 1, 5 and 10ms duration and 10% - 20% of the amplitude of the following pulse.

Results: The effects were opposite for the monopolar and bipolar configurations. With monopolar electrodes DPPs increased the amplitude required to activate 50% of the motoneuron pool (between 0.7% and 10.3%) and HPPs decreased the threshold (between 1.7% and 4.7%). With bipolar electrodes both pre-pulse types had the opposite effect: DPPs decreased thresholds (between 1.8% and 5.5%) whereas HPPs increased thresholds (between 0.5% and 4.1%). Electroneurograms from the stimulated nerve revealed spatial and temporal differences in action potential generation for monopolar and bipolar electrodes. In bipolar biphasic stimulation, excitation first occurred at the return electrode as a response to the transition between the cathodic and anodic phase. Conclusion: These data help to resolve the contradictions in the published data over two decades. Significance: They also show that fundamental research carried out in monopolar configuration is not directly applicable to contemporary bipolar ES applications.

Index Terms — Action potential, Bipolar stimulation, Electrical stimulation, Sub-threshold pre-pulses

3.1.1 Published literature on pre-pulses is contradictory

(I. Introduction)

Electrical stimulation (ES) is a neuromodulation technique that applies artificial electrical stimuli to alter the activity of target nervous structures. The stimuli are delivered via an active electrode near the target nerve. The charge can either be returned via a second electrode, often of similar size and situated in similar proximity to the target structure, this configuration is clinically called bipolar. If the charge is returned over a large, remotely placed electrode area, such as the casing of an implant, the configuration is known as monopolar. Although there are other electrode configurations, such as focused multipolar electrodes, monopolar and bipolar setups are the most commonly used in contemporary neuromodulation devices (Fallon and Carter, 2016). For some applications of ES either electrode setup might be used, but for others specific requirements predetermine the electrode configuration. For example, in the emerging field of miniaturized neuromodulation implants, so called “electroceuticals” (Horn, Ardell and Fisher, 2019) the electrodes are envisaged as integral with the stimulator. The small device size does not allow substantial electrode separation, so the configuration is inevitably bipolar. The same limitation applies to electrode arrays in which the maximum separation of electrodes is not much greater than the size of the target neural structure.

Beside the fundamental function of ES, to activate (or block) the target nerve, stimulation safety, selectivity and efficiency are key performance requirements (Grill, 2018). The pursuit of stimulation selectivity, that is the activation of a specific neuronal population without coactivation of other fibers (for example, activation of sensory in preference to motor fibers, or slow motoneurons in preference to fast motoneurons), led to numerous investigations of ES with waveforms varying from standard rectangular pulses. One such modification is the addition of a sub-threshold conditioning pre-pulse immediately prior to the stimulating pulse. Sub-threshold means that the pre-pulse alone does not elicit action potentials (APs). Published data on the effect of such sub-threshold pre-pulses in computer simulations and various experimental settings are apparently contradictory (Vargas Luna, Mayr and Cortés-Ramirez, 2018). Mortimer and Grill described in 1995 an effect of hyperpolarizing pre-pulses (HPPs) to decrease threshold (Grill and Mortimer, 1995) and an effect of depolarizing pre-pulses (DPPs) to increase threshold for activation (Grill and Mortimer, 1993, 1995, 1997). Over the following two decades, several studies agreed with these original findings (Blumenthal, Burnett and Swerdlow, 2001; Deurloo, Holsheimer and Bergveld, 2001; Poletto and Van Doren, 2002), but other research groups reported opposing results, describing a decrease of stimulation threshold with DPPs (Hennings, Arendt-Nielsen and Andersen, 2005; Willand and de Bruin, 2008; Vastani *et al.*, 2013; Vargas Luna, Mayr and Cortés-Ramirez, 2018).

Like most early research on pulse shaping or fundamental mechanisms underlying electrical stimulation, the pioneer work by Mortimer and Grill was modelled and carried out only for the monopolar electrode configuration. To the best of our knowledge the transferability of findings from these investigations of the effect of DPPs and HPPs in monopolar electrode configurations to the bipolar case has not been studied. This represents a procedural gap in knowledge in the scientific literature on the effect of pre-pulses, especially in the light of the emerging field of miniaturized, and thus bipolar, neuromodulation devices.

The aim of this study was to investigate the effect of DPPs and HPPs on motor nerve recruitment. The pre-pulses were studied under conditions relevant to neuromodulating implants: The stimulation pulses preceded by DPPs and HPPs were biphasic and of a phase width near the chronaxie, that is, near the stimulus duration that uses the least energy to activate the nerve. Both principal electrode configurations, bipolar and monopolar, were tested and for the first time, detailed comparisons of the distal electroneurogram (ENG) of the stimulated nerve were made.

3.1.2 Comprehensive range of pre-pulse parameters to be tested

(II. Materials and Methods)

Surgical Procedure

Experiments were carried out in n=5 adult Wistar rats.

Home Office project licence: PPL 40/3743.

Stimulation electrodes: Active electrode distal, bipolar return electrode proximal, and hypodermic needle in dorsal skin as monopolar return electrode (return electrode switched by relay unit).

Recording electrodes: Approximately 10mm distal to stimulation electrodes.

[…]

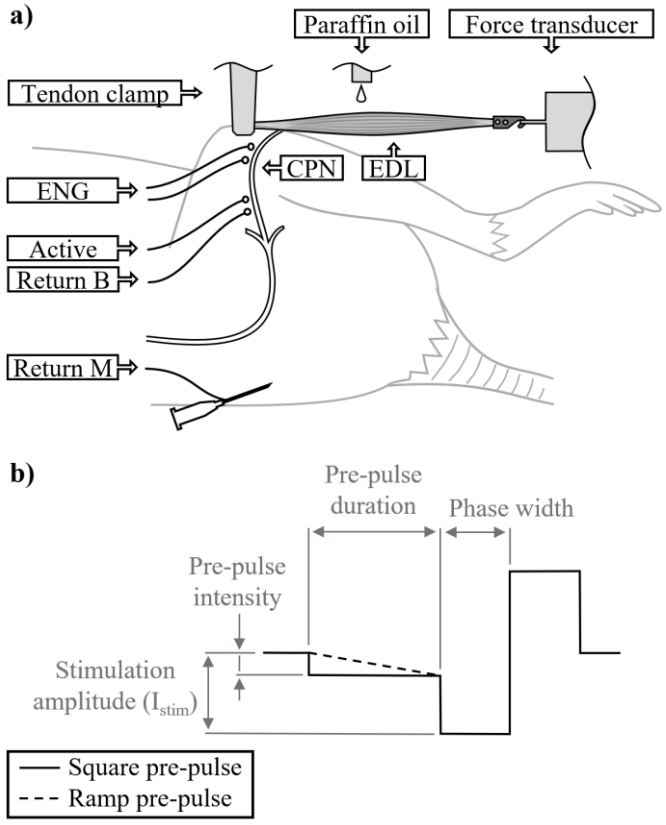

Figure 3.1 Experimental model: **a)** Nerve-muscle-preparation of Common Peroneal Nerve (CPN) and Extensor Digitorum Longus (EDL). Electrodes: A pair of ENG recording electrodes (reference most distal) was placed distal to the bipolar stimulation electrode pair (active electrode more distal). For monopolar stimulation, the nerve return electrode (Return B) was disconnected and a hypodermic needle (Return M) under the dorsal skin of the animal was used as return electrode. **b)** Parameterization of pre-pulses: Square (solid line) and ramped (dashed line) pre-pulses are parameterized by pre-pulse duration of 1, 5 or 10ms and intensities of 10 or 20% of the stimulation amplitude (waveform is not to scale). […]

Stimulation

[…] The maximal stimulation amplitude was capped at 2mA, which was sufficient in every one of the five experiments and with every tested waveform to elicit full nerve activation.

Subthreshold Pre-pulses

Terminology: Pre-pulses were defined by the current waveform at the active, charge injecting, electrode (Figure 3.2, left column). The injection of negative charge, i.e. a cathodic phase, decreases the transmembrane potential and thus depolarizes the membrane of axons near the active electrode (Figure 3.2.a, left). The injection of a positive, anodic charge increases the transmembrane potential at the site of injection and thus hyperpolarizes the membrane (Mortimer and Bhadra, 2018). Hence a pre-pulse in the cathodic phase (at the active electrode) is referred to as a depolarizing pre-pulse (DPP) and a pre-pulse in the anodic phase as a hyperpolarizing pre-pulse (HPP).

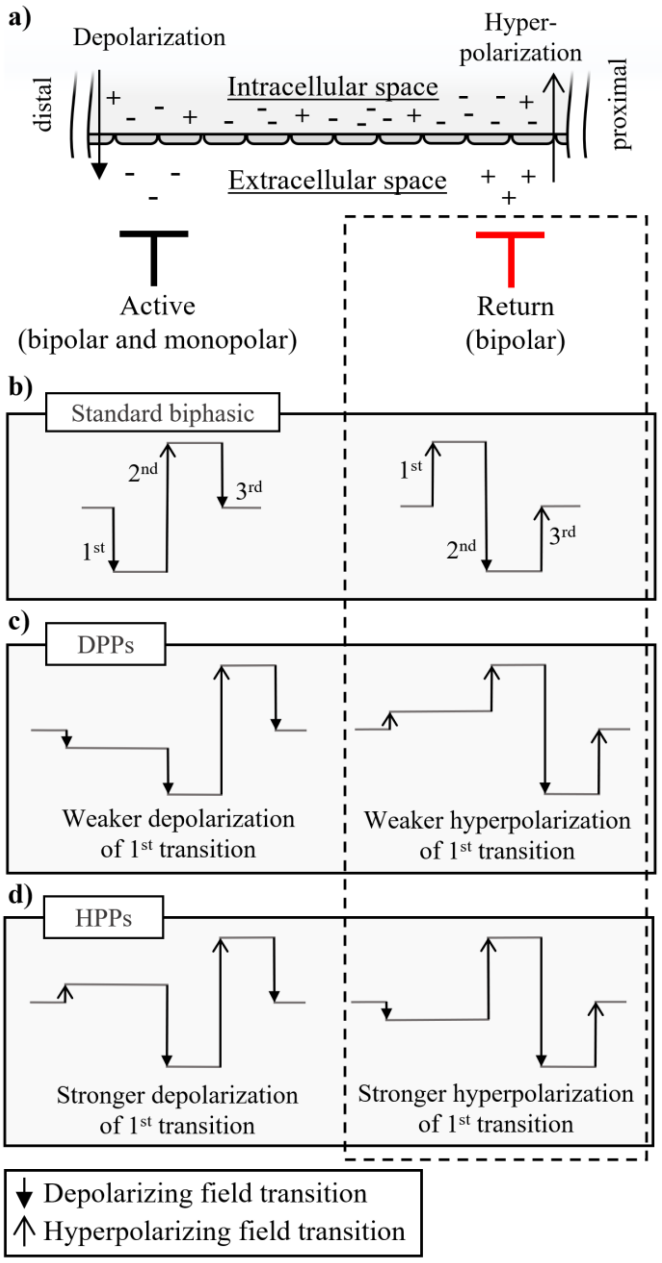

Figure 3.2 Electrical fields introduced during monopolar and bipolar extracellular nerve stimulation at the active (left column) and return (right column) electrode. **a)** The injection of a negative or cathodic charge (electron gain) at the active electrode depolarizes the membrane of an axon near that location from its negative resting potential. The charge-return during that same stimulation (electron loss) hyperpolarizes the membrane near the return electrode for the bipolar electrode configuration. The effect of the field transitions within **b)** standard biphasic pulses (cathodic phase first), **c)** biphasic pulses with DPPs, and **d)** biphasic pulses with HPPs on the membrane of an axon can either be categorized as depolarizing (full arrowheads) or hyperpolarizing (open arrowheads). Waveforms not to scale.

Test pulses: All test pulses were biphasic rectangular pulses with 40µs phase width, cathodic phase first (Figure 3.1.b). The test pulses were delivered during four successive stimulation sessions, subdivided by pre-pulse polarity (DPPs and HPPs) and intensity (10% and 20% of subsequent test pulse). The four test stimulation sets were: 10% DPPs,

20% DPPs, 10% HPPs, and 20% HPPs. Within each of these recording sessions, the following pulse parameters were tested: Pre-pulse type (no pre-pulse, ramp, and square), pre-pulse duration (1, 5, and 10ms), and electrode configuration (monopolar and bipolar). For each parameter combination, e.g. 5ms square DPPs of 20% stimulus intensity applied via monopolar electrode configuration, a full recruitment curve in 20 steps of 50µA stimulation amplitude (typically ranging from 400-1350µA) was recorded (Figure 3.3.a). All combinations of these stimulation parameters were applied in randomized order.

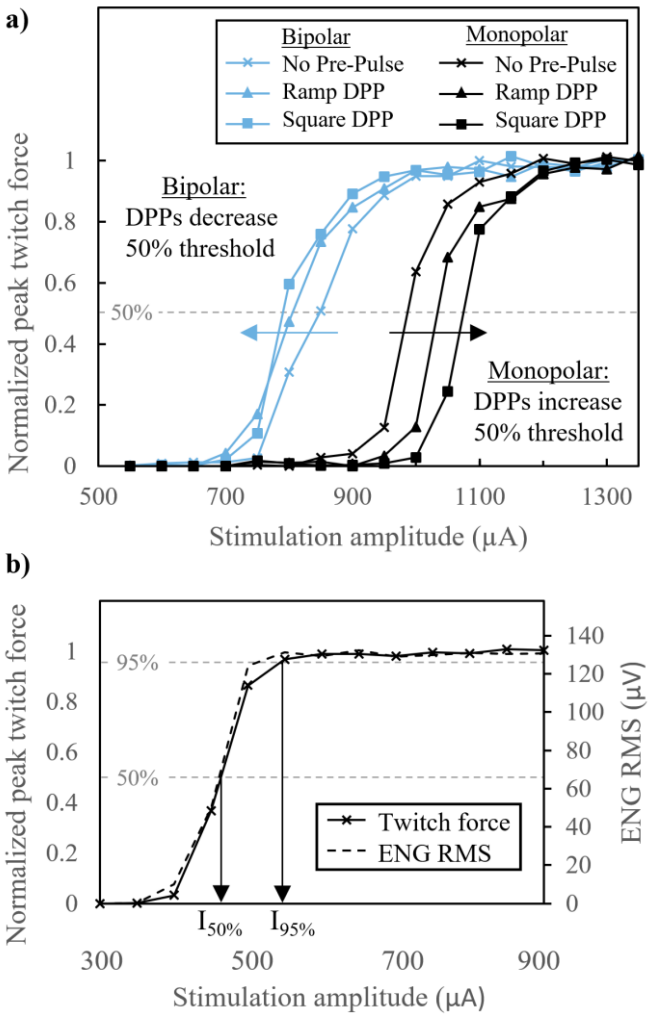

Figure 3.3 Recruitment curves a) Recruitment curves for 40µs biphasic stimulation with and without 5ms DPPs of 20% stimulus intensity in monopolar (black) and bipolar (blue) setup. Force responses of test stimulations were normalized to the closest control pulse (in total n=16 control pulses (mean=0.39N, SD=0.01N) were used for normalization of this exemplary data set). **b)** Recruitment curve for 200µs biphasic stimulation in monopolar electrode configuration. Arrows indicate 50% and 95% thresholds ($I_{50\%}$ and $I_{95\%}$) determined by linear interpolation of normalized peak twitch force. Root mean square (RMS) of ENG recordings of the stimulated nerve correlate with isometric peak twitch force.

The upper limit of pre-pulse intensity (20% of subsequent test pulse) was chosen based on strength duration curves as a value with which no excitation was to be expected. To verify that all tested pre-pulses were indeed sub-threshold, the ENG recording of the stimulated nerve was checked. No early excitations as a response to the pre-pulse were observed, proving their amplitude never reached threshold. […]

Supramaximal amplitude stimulation

In two animals, temporal differences in action potential generation between monopolar and bipolar electrode configurations were investigated. Amplitudes that ensured 95% neural activation ($I_{95\%}$), that is 95% of maximal isometric twitch force, were determined for phase width 100 and 200µs standard biphasic stimulations (without pre-pulses). Ten repetitions of biphasic stimulation at this 95% activation threshold $I_{95\%}$ were recorded for both phase widths and both electrode configurations. Further repeated recordings were made during stimulation at supramaximal amplitudes in 50µA increments up to $I_{95\%}$+350µA.

Recording

Extensor digitorum longus muscle twitch force recorded at 100kS/s. Common peroneal nerve ENG recorded at 100kS/s.

[…]

Data analysis and statistics

Force responses

[…] The effect of each pre-pulse on the 50% activation threshold was expressed as the percentage difference between $I_{50\%}$ without pre-pulse (i.e. standard biphasic stimulation) and $I_{50\%}$ with that pre-pulse.

Paired t-tests were performed for each pre-pulse duration (1, 5 and 10ms), polarity (DPPs and HPPs) and intensity (10 and 20%) to search for significant differences between the changes in 50% threshold in the monopolar and bipolar electrode configurations. The data for both pre-pulse shapes (square and ramp) were grouped together for these statistical tests. […]

3.1.3 Pre-pulses have opposite effects in bipolar compared to monopolar stimulation mode

(III. Results)

Subthreshold Pre-pulses

The dataset presented here is generated from 5900 individual responses, 1180 from each of the five experiments. The data is consistent, has only minor influence of fatigue or cyclic variations in depth of anaesthesia (Figure 3.3 - Figure 3.5) and demonstrates the value of computer-controlled experiments to extract a large amount of well controlled data from a small number of preparations, and thus achieve a reduction in the use of animals.

To ensure that all tested pre-pulses were indeed sub-threshold, the ENG recording of the CPN distal to the stimulation electrodes was checked. No early excitations as a response to the pre-pulse were observed, proving their amplitude never reached threshold.

Depolarizing Pre-pulses

DPPs increased the 50% activation thresholds in the monopolar electrode configuration and decreased stimulation thresholds in the bipolar configuration (Figure 3.4). On average across subjects, DPPs (square and ramp; 1, 5, and 10ms duration) with 10% of the stimulation pulse amplitude increased thresholds in the monopolar configuration between 1.2% and 6.0% and decreased thresholds between 1.8% and 3.5% in the bipolar configuration. The difference of the effect of 10% DPPs with monopolar and bipolar electrode configuration was significant for all tested pre-pulse durations ($p<0.001$). Larger average threshold changes between 0.7% and 10.3% increase in monopolar and between 3.9% and 5.5% decrease in bipolar configurations were observed across subjects when the DPP amplitude was set to 20% of the stimulus amplitude. For all tested pre-pulse durations, the percentile threshold changes with DPPs of 20% stimulus intensity were found to be significantly different between monopolar and bipolar electrodes (1ms: $p=0.002$, 5ms, and 10ms $p<0.001$).

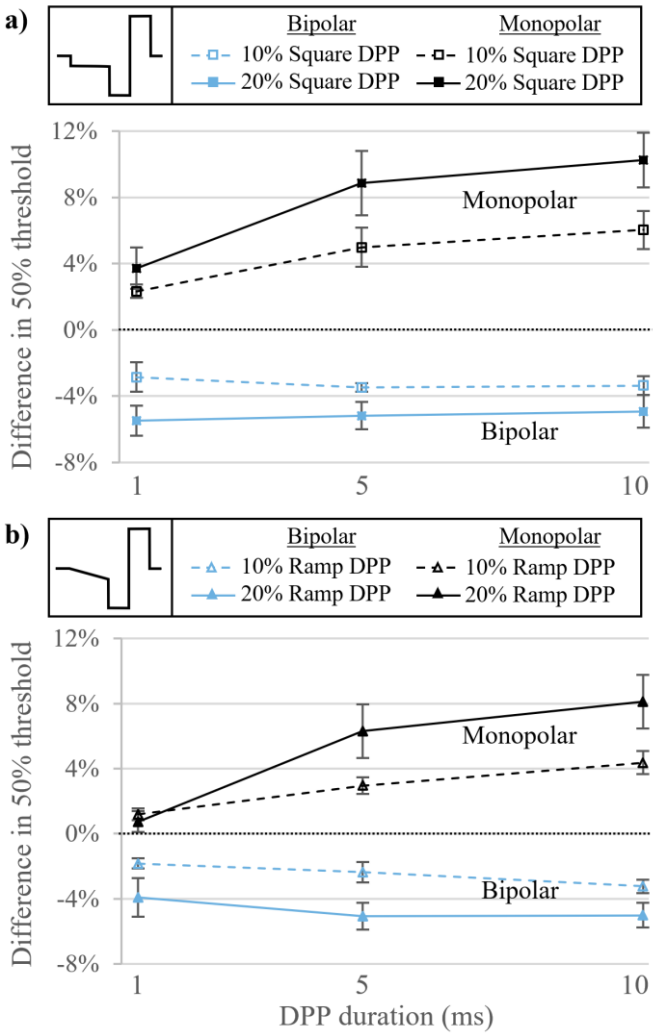

Figure 3.4 Changes in 50% activation threshold with DPPs. Threshold changes with **a)** square and **b)** ramp 10% and 20% DPPs of 1, 5 and 10ms duration in monopolar (black) and bipolar (blue) setup. Negative values of "Difference in 50% threshold" indicate that the activation threshold with biphasic stimulation phase width=40µs decreased with the tested pre-pulse compared to stimulation without pre-pulse. Dashed lines represent mean ±SEM for 10% DPPs, solid lines represent mean ±SEM for 20% DPPs of n=4 animals (except for 5ms and 10ms 10% DPPs with n=5). 0% (dotted line) represents the baseline of 50% thresholds with biphasic pulses without pre-pulse. Waveforms in legend not to scale.

Hyperpolarizing Pre-pulses

HPPs decreased stimulation thresholds in monopolar and increased thresholds in bipolar configurations (Figure 3.5). The average threshold decreases across subjects with 10% HPPs (square and ramp; 1, 5, and 10ms duration) ranged from 1.7% to 3.3% for monopolar stimulation. The same pre-pulses increased thresholds on average between 0.5% and 4.1% in the bipolar case. 10% HPPs of 5ms and 10ms duration showed significant differences in the threshold changing effect between the two compared electrode configurations ($p<0.01$). On average across subjects, thresholds were decreased

between 1.7% and 4.7% in monopolar and increased between 1.2% and 2.5% in bipolar setup, when HPPs of 20% stimulus amplitude were used. The effect of 20% HPPs was significantly different in monopolar compared to bipolar stimulation for all tested pre-pulse durations (1ms: p=0.017, 5ms: p=0.003, 10ms: p<0.001).

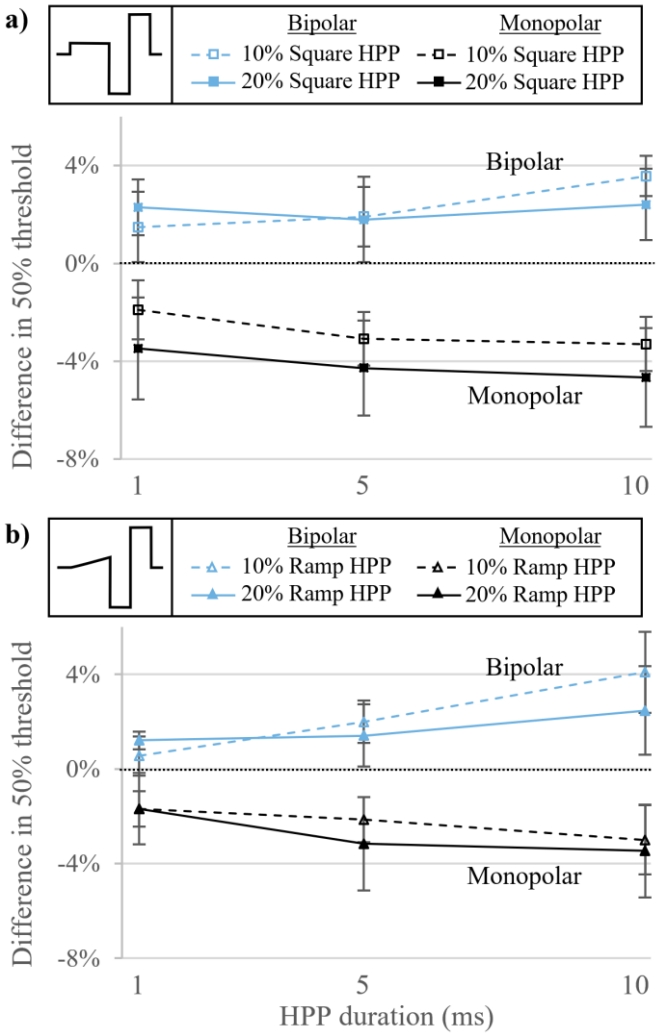

Figure 3.5 Changes in 50% activation threshold with HPPs. Threshold changes with **a)** square and **b)** ramp 10% and 20% HPPs of 1, 5 and 10ms duration in monopolar (black) and bipolar (blue) setup. Negative values of "Difference in 50% threshold" indicate that the activation threshold with biphasic stimulation phase width=40µs decreased with the tested pre-pulse compared to stimulation without pre-pulse. Dashed lines represent mean ±SEM for 10% HPPs, solid lines represent mean ±SEM for 20% HPPs of n=4 animals. 0% (dotted line) represents the baseline of 50% thresholds with biphasic pulses without pre-pulse. Waveforms in legend not to scale.

ENG during supramaximal amplitude stimulation

ENG recordings of compound action potentials (CAPs) evoked by 100µs biphasic stimulation at 95% activation threshold $I_{95\%}$ had an average delay of 1.67ms ±7.2µs of the peak of the prominent first downward signal deflection from the stimulus artifact with monopolar electrodes, and an approximately one phase width greater delay of 1.78ms ±4.9µs with bipolar electrodes (Figure 3.6.a). Higher stimulation amplitudes led to shorter delays between artifact and ENG. In Monopolar stimulation the delay decreased by up to 60µs to 1.61ms ±6.4µs with 250µA above $I_{95\%}$. In the bipolar configuration the delay shortened by up to 170µs to 1.61ms ±6.5µs with stimulation amplitudes 300µA above $I_{95\%}$ (Figure 3.6.b), so that there was no difference between monopolar and bipolar.

Biphasic stimulation with 200µs phase width at 95% activation threshold $I_{95\%}$ led to a delay of 1.73ms ±6.2µs in the monopolar and 1.91ms ±4.7µs, approximately one phase width greater, in the bipolar setup (Figure 3.6.c). Stimulation amplitude exceeding $I_{95\%}$ led to shorter delays between artifact and signal in both electrode configurations. In the monopolar case the delay shortened up to 69µs to 1.67ms ±7.8µs at 250µA above $I_{95\%}$ and in the bipolar case greater reductions of the delay of up to 245µs to 1.67ms ±7.5µs at 350µA above $I_{95\%}$ were observed (Figure 3.6.d). Thereby, difference in response delay between monopolar and bipolar electrode setup diminished with increasing suprathreshold stimulation amplitude.

These are the data for one of the two rats in which ENG recordings were performed. Although absolute latency values differed, the general finding of activation one phase width later in bipolar compared to monopolar stimulation, as well as the reduction of this difference with increasing supramaximal amplitude was observed in both animals.

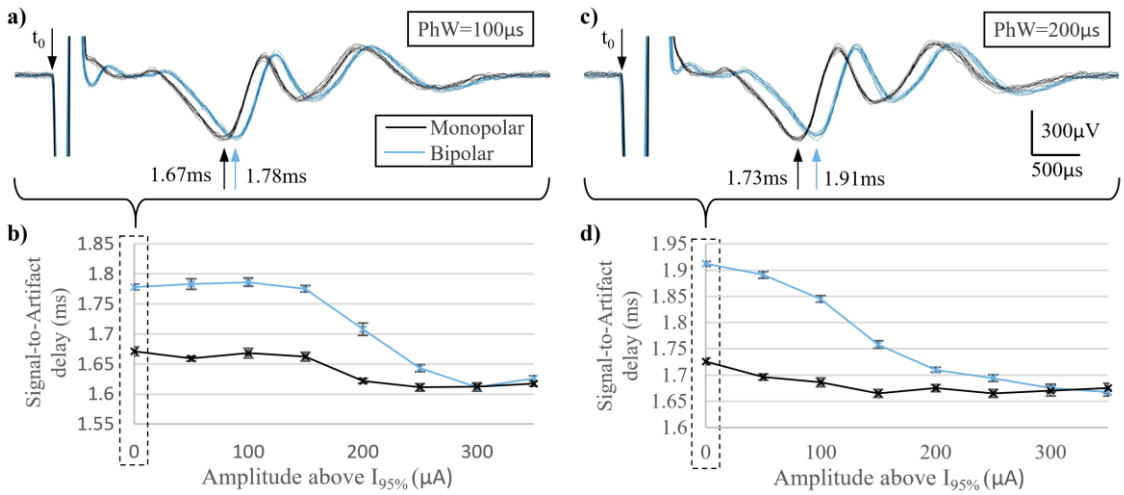

Figure 3.6 Electroneurogram recordings of compound action potentials recorded in one example during standard biphasic **a)** phase width 100µs and **c)** 200µs stimulation without pre-pulse at 95% activation threshold $I_{95\%}$. Ten repeated recordings are superimposed, arrows indicate the mean delay of the first prominent downward deflection towards the stimulation artifact t_0. Signal-to-Artifact delays of **b)** phase width 100µs and **d)** 200µs decrease with increasing supramaximal amplitude above $I_{95\%}$. Data represents mean ±SEM of 10 repeated ENG recordings at each amplitude and phase width in monopolar (black) and bipolar (blue) electrode configuration. With phase width of 100µs (a and b) $I_{95\%}$ corresponds to 1000µA in bipolar and 750µA in monopolar configuration, for phase width of 200µs (c and d) $I_{95\%}$ corresponds to 900µA in bipolar and 600µA in monopolar configuration.

3.1.4 In the bipolar configuration, excitation first occurs at the return electrode

(IV. Discussion)

Our data on the effects of DPPs and HPPs to alter the excitability of the nerve to a subsequent stimulus in monopolar electrode configuration are in good agreement with the original research by Mortimer and Grill. In their first publication on subthreshold pre-pulses, the authors used a cable model of the mammalian myelinated axon with 500µs monophasic stimuli applied via a monopolar point source. They reported increased thresholds when the stimulation pulse was preceded by 500µs DPPs of 95% threshold amplitude (Grill and Mortimer, 1993). Further computer simulations employed a single space-clamped Node of Ranvier as well as a compartment cable model of a mammalian nerve fiber, both modelled exclusively with a monopolar stimulation point source and described threshold increases with 500µs DPPs of 90% threshold amplitude and threshold decreases with similarly parametrized HPPs (Grill and Mortimer, 1995). The authors root these effects of sub-threshold pre-pulses in their influence on the inactivation variable h: DPPs decrease h and thus render the neural membrane less excitable, whereas HPPs

increase h which increases the membrane excitability. In later in-vivo experiments on cat sciatic nerve, Mortimer and Grill demonstrated that 500µs DPPs of 90% threshold amplitude applied via a monopolar electrode contact selectively increased stimulation thresholds of nerve fibers that otherwise showed the lowest threshold for recruitment (Grill and Mortimer, 1997).

Using the bipolar electrode configuration that is relevant to stimulation via many nerve cuffs, electrode arrays and proposed electroceutical devices, we observed opposite effects of pre-pulses on stimulation threshold that are also in line with other published literature that does not follow the pioneer work by Grill and Mortimer (Hennings, Arendt-Nielsen and Andersen, 2005; Willand and de Bruin, 2008; Vastani *et al.*, 2013; Vargas Luna, Mayr and Cortés-Ramirez, 2018). Most of these studies were carried out with human transcutaneous stimulation, either in a clearly bipolar configuration (Hennings, Arendt-Nielsen and Andersen, 2005; Willand and de Bruin, 2008) or in a monopolar setting in which the reference electrode was relatively close to the stimulated nervous structure (Vargas Luna, Mayr and Cortés-Ramirez, 2018).

The consistent differences of pre-pulse effects in monopolar and bipolar electrode setup in both the data described in the present study and in previously published literature, led to the hypothesis that the return electrode might be the effective electrode in bipolar stimulation setups at near threshold conditions. This hypothesis of threshold excitation at the return electrode provides a satisfying explanation for the opposite effects of pre-pulses in bipolar versus monopolar stimulation described in this study. Since the stimulation waveform is inverted at the return electrode, not only do the stimulation phases have opposite effects here but also the pre-pulses: DPPs (defined by the current waveform injected at the active electrode, compare methods section “Subthreshold Pre-pulses”) have a hyperpolarizing effect and thus decrease thresholds in the tissue surrounding the return electrode (Figure 3.2.c), whereas HPPs have depolarizing effects that render the membrane less excitable at this location (Figure 3.2.d). The ENG recordings support our hypothesis by showing a shift correlating to the duration of one phase width between responses elicited by monopolar and bipolar stimulation setups at amplitudes near full activation threshold $I_{95\%}$ (Figure 3.6.a & .c). It was interpreted that while in monopolar stimulation excitation occurred near the active electrode as a response to the cathodic (first) phase (Figure 3.2.b, left), for the bipolar setup the return electrode was the effective electrode during the second phase, which here acts cathodically (Figure 3.2.b, right). In the bipolar case, the first phase effectively acts as a HPP at the return electrode and

increases the resting potential of nerve fibers in proximity to this electrode. The subsequent middle field transition acts from this increased resting potential with a strong depolarizing influence on the axons in the field (compare 2nd field transition in Figure 3.2.b, right). The hypothesis is further supported by the changes in delay of elicited CAPs at supramaximal stimulation intensities (Figure 3.6.b & .d). For both tested phase widths, the reductions in the delay with increasing amplitude in monopolar setup were less than one phase width. This implies that the threshold for excitation was first reached late within the cathodic (first) phase and then gradually synchronized with the transition edge at the beginning of that phase as the amplitude increased. In bipolar stimulation however, the observed CAP delays consistently shifted more than one phase width with increasing supramaximal stimulation amplitude. This greater reduction in CAP delay supports our hypothesis that excitation begins at the return electrode during the second phase and shifts with increasing amplitude to the first phase and the more distal active electrode (compare Figure 3.2.b). The smooth nature of the curve of reduction of delay with increasing amplitude must represent the variation among the population of motoneurons. This provides a potent explanation for the differences in pre-pulse effects that were observed between monopolar and bipolar configurations in this study. Furthermore, the possibility of excitation at the return electrode explains work in which an “unexpected” reduction of stimulation thresholds with DPPs has been reported with bipolar electrodes (Hennings, Arendt-Nielsen and Andersen, 2005; Willand and de Bruin, 2008).

In one experiment, 5ms and 10ms HPPs of 20% stimulation intensity led, against the generally observed trend, to lower stimulation thresholds in bipolar configuration. This caused the average threshold changes across subjects with 20% HPPs to be smaller than those observed with 10% HPPs in bipolar setup. The rationale for this might be that some aspect of the electrode configuration in this specific preparation caused the HPP to increase the stimulation thresholds at the return electrode sufficiently (and decrease thresholds at the active electrode respectively) to shift the site of AP generation from the proximal return to the distal active electrode.

Especially in the bipolar case, no significant effect of increasing the pre-pulse duration above 1ms could be observed. The rationale for this could be the separation of the pre-pulse from the effective part of stimulation (i.e. the middle field transition) by the first phase of the stimulation pulse. In this case, the pre-pulse effect might predominantly originate in a decrease (with DPPs, Figure 3.2.c) or increase (with HPPs, Figure 3.2.d) of the first pulse transition. As this transition has a hyperpolarizing effect on axons near the

return electrode, a decrease of this transition edge will result in decreased thresholds for activation, as was in fact observed with DPPs in bipolar configuration. The same explanation applies to HPPs in bipolar electrode configuration: Independent from pre-pulse duration the HPPs increase the inhibitory effect of the first pulse transition (compare Figure 3.2.d, right) at the return electrode and thus lead to increased stimulation thresholds. The general finding of limited influence of increasing pre-pulse durations above 1ms is in agreement with the model-based work by Grill and Mortimer, who showed that increasing the DPP duration from 0.5ms to 1ms had little to no effect on the stimulation threshold of a space clamped Node of Ranvier (Grill and Mortimer, 1997). In the same study, using a nerve cuff to stimulate the sciatic nerve in cat, the investigators described a diminishing additional effect of increasing pre-pulse duration above 5ms. All studies that tested multiple pre-pulse durations and describe a significant effect of increasing it above a duration of approximately 5ms were conducted using transcutaneous stimulation (Hennings, Arendt-Nielsen and Andersen, 2005; Willand and de Bruin, 2008; Vargas Luna, Mayr and Cortés-Ramirez, 2018), where the tissue separating the target nerve from the electrodes is likely to influence these temporal aspects.

In general, the presented data suggests that the principal effect of any given pre-pulse may chiefly depend on the intensity and polarity of that pre-pulse at the effective location of AP generation (i.e. at the effective physical or virtual electrode). This would imply that the depolarizing effect of a sub-threshold pre-pulse at this location would also increase stimulation thresholds for other waveforms, such as monophasic or biphasic pulses with inverse phase order.

3.1.5 Implications for devices operating in bipolar mode warrant further research

(V. Conclusion)

The present study is the first to investigate the effect of DPPs and HPPs on activation thresholds with biphasic stimulation under conditions of direct relevance to contemporary miniature implantable neuromodulation devices. The significant and consistent finding of reversed pre-pulse effects in bipolar setup due to excitation at the return electrode not only helps to resolve two decades of conflicting data in the published literature on pre-pulses, but also stresses the strong influence of electrode configuration on the effect of variations in pulse shape. While the generation of action potentials at the return electrode of a bipolar electrode pair is the subject of recent research in the field of clinical nerve

conduction studies (Leote, Pereira and Valls-Sole, 2017), it has not yet been studied in terms of its influence on the performance of implantable neuromodulation devices. A better understanding of the differences between monopolar and bipolar stimulation is of particular relevance to the emerging field of miniaturized neuromodulators, so called *electroceuticals*, where the small implant size does not allow for substantial separation of the electrodes. Most published data on well-established pulse shape variations such as inter phase gaps (van den Honert and Mortimer, 1979; Gorman and Mortimer, 1983), like the pioneer literature on subthreshold pre-pulses, is based on the monopolar case and therefore not directly applicable to these bipolar scenarios. We report major differences in spatial and temporal mechanisms of excitation between stimulation with monopolar and bipolar electrode positions. These findings must be taken into account when designing activation patterns delivered by miniaturized neuromodulation devices. Further investigations of action potential generation at the return electrode of a bipolar pair and its influence on the performance of implantable neuromodulators are warranted.

3.2 Interphase gaps (IPGs) and asymmetric pulses

(Abstract)

Interphase gaps (IPGs) are among the most commonly suggested pulse shape variations to try to enhance neural stimulation efficiency by reducing the action potential (AP) suppressing effect of an early anodic hyperpolarization. The majority of published literature on the effect of IPGs is based on investigations of monopolar stimulation configurations. However, many contemporary neuromodulation applications including the emerging field of electroceutical devices must operate in a bipolar electrode configuration. We investigated the effect of IPGs and asymmetric biphasic pulses with reduced anodic amplitude on neural activation thresholds in both principal electrode configurations in a rodent in-vivo nerve muscle preparation. In the monopolar electrode configuration, our findings of 10.9 ± 1.5% decreased activation thresholds with 200µs IPGs in biphasic pulses of 40µs phase width are in agreement with published literature in this configuration. Surprisingly, using the bipolar electrode configuration, opposite effects of IPGs were observed and activation thresholds were increased up to 18.6 ± 3.1% (phase width 100µs, IPG=1000µs). Electroneurogram (ENG) recordings of the stimulated nerve revealed temporal and spatial differences in AP generation between the monopolar and bipolar configuration. In the bipolar configuration excitation first occurred at the return electrode in response to the middle field transition of biphasic pulses. This is the first study to report consistently increased activation thresholds with IPGs in a bipolar stimulation configuration. Our findings must be taken into consideration when designing stimulation waveforms for neuromodulation devices that operate in a bipolar mode to avoid increased amplitude requirements that result in increased energy consumption

3.2.1 Authoritative literature on the effect of IPGs investigated only monopolar stimulation configurations

(I. Introduction)

Electroceuticals are miniature neuromodulation devices in development to treat a wide array of medical conditions by selectively delivering electrical stimuli to specific target neural structures (Famm *et al.*, 2013). Recent research assesses the potential of this novel therapeutic strategy to treat a range of diseases including type 2 diabetes (Sacramento *et al.*, 2018; Fjordbakk *et al.*, 2019), renal fibrosis, and hypertension (Okusa, Rosin and Tracey, 2017). The high degree of selectivity necessary to target specific populations of nerve fibres or specific brain circuits is a major challenge to the success of these therapies.

One approach to work toward this selectivity is by means of device miniaturization, especially of the electrodes via which the electrical stimuli are applied, to close the gap between the size of the target neural structure and the electrodes. This ongoing trend for device miniaturization has led to a number of remarkable developments of millimetre-scale implantable devices, most prominently of the so-called "neural dust" or "stim dust" for recording and stimulation of nerves (Neely *et al.*, 2018; Piech *et al.*, 2020). Moving on from the original proposal of the wirelessly powered BION micro-stimulation implants (Loeb *et al.*, 1991), implantable stimulators with ever smaller dimensions have been developed (Luo *et al.*, 2013; Freeman *et al.*, 2017; Tanabe *et al.*, 2017; Charthad *et al.*, 2018; Lee *et al.*, 2018). The smallest neural stimulator using wireless transfer of stimulating energy that has been reported and tested in-vivo has an overall volume of less than 0.01 mm^3 (Khalifa *et al.*, 2019).

The underlying principle of these novel bioelectronics is the same as in other electrical neuromodulation devices that already find broad clinical application such as cochlear implants, pacemakers, and spinal cord stimulators: electrical pulses are used to alter the generation and/or transmission of action potentials (APs) in the target excitable tissues. Modulation of nerve activity can either be to reduce pathological activity, for example to treat chronic pain or reduce spasticity in spinal cord injured subjects, or to elicit desired therapeutic neural activity, for example, the stimulation of the auditory nerve to restore the sense of hearing. Beside the main objectives to activate or block a target population of nerve fibres, stimulation efficiency, selectivity and safety are key requirements of electrical neuromodulation applications (Grill, 2018). Biphasic waveforms are essential to achieve charged balanced stimulation which is a critical safety requirement to minimise tissue damage and electrode disintegration that is caused by unbalanced charge injection through electrochemical processes at the tissue-electrode interface (Merrill, Bikson and Jefferys, 2005). Not least because they are easy to generate, rectangular biphasic stimulation pulses have commonly been used. Although it has been shown that non-rectangular waveforms can have advantages in terms of stimulation efficiency (Sahin and Tie, 2007; Wongsarnpigoon, Woock and Grill, 2010; Eickhoff and Jarvis, 2019), most contemporary devices use variations of the standard biphasic rectangular waveform. One of the most widely used pulse shape variations is the introduction of an interphase gap (IPG), sometimes also referred to as an interphase interval, between the cathodic and anodic phases of the biphasic rectangular pulse.

In their pioneer research on IPGs, van den Honert and Mortimer (van den Honert and Mortimer, 1979) studied a single voltage-clamped Node of Ranvier (NoR) (Frankenhauser, 1957) and showed how an AP elicited by the cathodic (first) phase can be abolished in near threshold conditions by an anodic (second) phase. Separation of the two stimulation phases by an IPG removed the suppression by the anodic phase. The authors tested their finding in an in-vivo experiment stimulating the tibialis anterior muscle of cat with a monopolar intra-muscular electrode and reported increased motor unit recruitment (that is, increased force) with increasing IPG durations from 0 to 100µs. In a later study, the laboratory confirmed these findings of decreased activation thresholds with the introduction of IPGs in biphasic pulses in a computational model of myelinated axons (McNeal, 1976) stimulated via a monopolar point source, as well as in-vivo experiments on monopolar tibial nerve stimulation in cat (Gorman and Mortimer, 1983).

Although conducted four decades ago and using exclusively monopolar electrode configurations, these studies still stand, as far as we can determine, as the only authoritative literature on the basic principles underlying the effect of IPGs for neural stimulation. While the effect of IPGs has been studied in numerous applications including the stimulation of the auditory nerve (Shepherd and Javel, 1999; McKay and Henshall, 2003; Carlyon *et al.*, 2005; Prado-Guitierrez *et al.*, 2006a; Kim *et al.*, 2010; Ramekers *et al.*, 2014; Schvartz-Leyzac and Pfingst, 2016; Hughes, Choi and Glickman, 2018), transcutaneous neuromuscular stimulation (Kaczmarek *et al.*, 2010; Springer *et al.*, 2014; Vargas Luna *et al.*, 2017), and epiretinal prostheses (Weitz *et al.*, 2014), the majority of these studies investigated only the monopolar case (Figure 3.7.a). Although it is commonly assumed that IPGs are advantageous in any stimulation configuration, there has not been any research to test the transferability of the early investigations of IPGs in the monopolar configuration (van den Honert and Mortimer, 1979; Gorman and Mortimer, 1983) to the bipolar configuration. This represents a fundamental gap in knowledge especially in view of the emerging field of electroceutical devices and electrode systems that due to their small size do not allow for substantial electrode separation and are therefore inevitably bipolar, that is, the interelectrode distance is of a similar size to the structure to be activated (Figure 3.7.b). Closing this gap in the scientific literature is a crucial first step toward the development of stimulation pattern that are optimized for next generation bioelectronic devices.

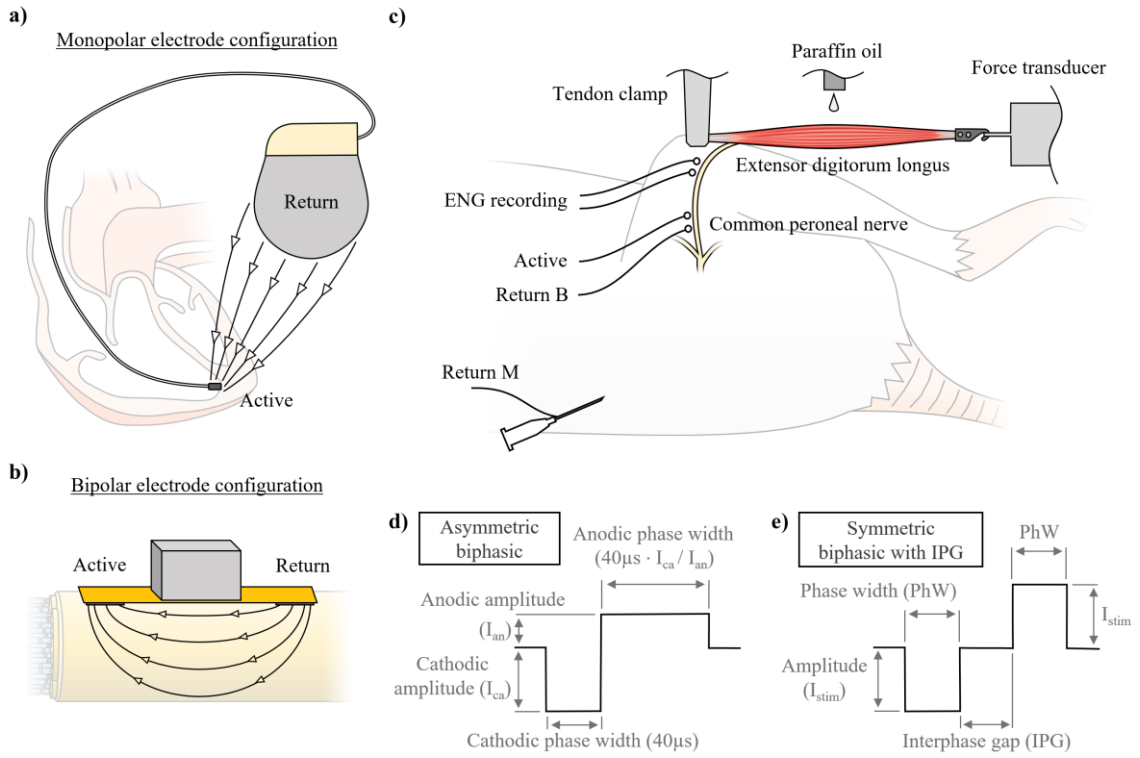

Figure 3.7 Electrode configurations and stimulation waveforms. (a) Many past and present electrical neuromodulation devices and research studies have used monopolar electrode configurations often with the implantable pulse generator itself as the return electrode. In this configuration the electric field between the single active electrode near the target excitable structure and the remotely placed return electrode area can be idealized as an electrical monopole. **(b)** Due to the small overall device size, both electrodes of proposed electroceutical devices are in similar proximity to the target structure and the generated electric field resembles an electric dipole. **(c)** In our experimental model, a rodent *in-vivo* nerve-muscle preparation, we compared both principal electrode configurations. The common peroneal nerve (CPN) in anaesthetized rats was stimulated and the isometric twitch force response of the extensor digitorum longus (EDL) muscle recorded. Depending on which return electrode was connected, the stimulation setup was either monopolar (with Return M) or bipolar (with Return B). ENG recordings of the CPN were measured distally to stimulation. We investigated the influence of different **(d)** asymmetric stimulation waveforms as well as different **(e)** IPG durations on neural activation thresholds.

We designed our study specifically to meet this need and to catalyse a re-examination of published pulse shaping strategies for their transferability to novel neuromodulation applications. We studied the effect of biphasic charge balanced pulses with a range of amplitudes of the anodic (second) phase and with different IPG durations on neural activation thresholds in an in-vivo nerve-muscle preparation in anesthetized rats (Figure 3.7.c). Under computer control our stimulation system switched between the monopolar electrode configuration (so that we can put our findings into perspective with the pioneer research on IPGs (van den Honert and Mortimer, 1979; Gorman and Mortimer, 1983)) and the bipolar electrode configuration, to inform the emerging field of miniaturized

neuromodulation implants. In 5 adult Wistar rats, we recorded the isometric twitch force response of the extensor digitorum longus muscle (EDL) to monophasic and biphasic charge balanced stimulation of the common peroneal nerve (CPN).

First, following the approach of van den Honert and Mortimer (van den Honert and Mortimer, 1979), we investigated the AP suppressive effect of anodic (second) phases of biphasic pulses, when they were not separated by an IPG. Biphasic pulses with cathodic (first) phase widths of 40µs and anodic (second) phases of 1, 2, 3, 4, and 8 times lower amplitude than the first phase, were tested (Figure 3.7.d). The reduction in amplitude of the anodic phase was compensated to achieve charge balance by a proportionally longer phase width. Further we examined neural activation thresholds using biphasic symmetric pulses with phase widths of 40, 100, 200, and 1000µs with and without IPGs of 25, 50, 100, 200, and 1000µs duration in both principal electrode configurations (Figure 3.7.e). The EDL force response gives a reliable estimation of neural recruitment in the CPN (Eickhoff and Jarvis, 2020b). In one representative nerve preparation, electroneurogram (ENG) recordings during monopolar and bipolar stimulation with maximal (95% activation threshold) and supramaximal amplitudes were analysed and presented here to investigate the temporal aspects of AP generation in both electrode configurations and to explain the differences found between the monopolar and bipolar cases.

3.2.2 Experimental model to test waveform variations in both principal electrode configurations

(II. Materials and Methods)

A detailed description of the experimental model, surgical procedures, and recording/stimulation instrumentation can be found in Chapter 2.

Experiments were carried out in n=5 adult Wistar rats.
Home Office project licence: PPL 40/3743.
Stimulation electrodes: Active electrode distal, bipolar return electrode proximal, and hypodermic needle in dorsal skin as monopolar return electrode (return electrode switched by relay unit).
Recording electrodes: Approximately 10mm distal to stimulation electrodes.

Stimulation protocol

Pulses with combinations of the pulse parameters to be tested (amplitude, phase widths, asymmetric amplitude ratio, IPG, and return electrode configuration) were delivered in

randomized order. This means recruitment curves were assembled from test pulses that were randomly placed from start to finish of a recording period. Every 20 test stimulations a control pulse which was set to elicit full neural activation was delivered to use for normalization. The control pulses were standard biphasic rectangular pulses with 200µs phase width, cathodic phase first and amplitudes set for each experiment separately (typically 1mA) to elicit maximal isometric twitch force. Twitch force responses to the test stimulations were measured relative to the closest control pulse and thus normalized. The randomized order of test stimulation parameter delivery and normalization with control pulses allowed us to attain recordings that produced meaningful relationships within the parameter space and are not affected by progressive or cyclic variations in body temperature, depth of anaesthesia or fatigue.

Biphasic asymmetric pulses: In order to investigate the influence of the anodic (second) phase of a charge balanced biphasic stimulation pulse, various ratios of cathodic to anodic amplitude I_{ca}/I_{an} were tested. The cathodic phase duration was set to 40µs, a typical chronaxie value (i.e. the phase duration at which neural activation can be achieved with minimum energy consumption) for our nerve-muscle preparation. The anodic phase duration was 40µs multiplied by the asymmetry ratio I_{ca} / I_{an} in order to achieve charge balance. Symmetric biphasic pulses (amplitude ratio $I_{ca}/I_{an}=1$) provided baseline values for activation threshold in both electrode configurations separately. Asymmetric biphasic pulses with ratios of I_{ca}/I_{an} of 2, 3, 4, and 8 as well as monophasic cathodic pulses were tested in both monopolar and bipolar electrode configurations. For every tested pulse shape variation (e.g. asymmetric biphasic pulses with amplitude ratio $I_{ca}/I_{an}=4$ in monopolar electrode configuration) a full recruitment curve in 20 steps of 50µA was recorded. In each of the 5 comprehensive animal experiments, all 240 test pulses for this investigation of asymmetric pulses were applied in one recording period in randomized order and interspersed with control pulses as described above.

Biphasic symmetric pulses with IPGs: The effect of IPGs on neural activation thresholds in bipolar and monopolar electrode configuration was tested in four different stimulation phase widths. Biphasic symmetric pulses of phase width 40, 100, 200, and 1000µs were tested with IPGs of 0 (standard biphasic pulses as baseline), 25, 50, 100, 200, and 1000µs. For each combination of phase widths, IPG duration and electrode configuration (e.g. phase width of 100µs with 50µs IPGs applied via bipolar electrodes), a full recruitment curve in 20 steps of 50µA was recorded. The four phase widths were tested in separate recording periods, each consisting of 240 test pulses. All test pulses within each recording

period were applied in randomized order and interspersed with control pulses as described above.

Maximal and Supramaximal stimulation: In two nerve-muscle preparations, temporal aspects of AP generation were investigated in detail in monopolar and bipolar electrode configurations. In both electrode setups thresholds for full motor unit activation ($I_{95\%}$) were determined for standard biphasic pulses of 100µs and 200µs phase width. First using stimuli with phase width of 100µs, ten maximal amplitude ($I_{95\%}$) stimulations were applied at a rate of one pulse every 3 seconds in monopolar electrode configuration, followed by ten repetitions at $I_{95\%}$ in bipolar configuration. Amplitudes were increased to supramaximal intensities in 7 steps of 50µA up to $I_{95\%}$ + 350µA. For every amplitude increment, ten repetitions were applied in monopolar and bipolar configuration. The same procedure was repeated for biphasic stimuli with phase widths of 200µs.

Data analysis and statistical tests

For every tested pulse shape variation (e.g. an IPG of 200µs duration), the difference of the 50% threshold with that specific variation was compared to the 50% threshold with standard symmetric biphasic pulses (cathodic phase first) in the same electrode configuration. The difference in 50% threshold for each tested pulse shape variation was expressed as a percentage, negative values representing a reduction of the amplitude required to reach 50% neural activation. Paired t-Tests were performed on the percentage threshold changes between bipolar and monopolar electrode configurations.

3.2.3 IPGs and pulse asymmetry have opposite effects in bipolar compared to monopolar stimulation mode

(III. Results)

The data on the effect of asymmetric biphasic pulses (Figure 3.8) and symmetric biphasic pulses with IPG (Figure 3.9) on neural activation threshold presented here were generated from 6300 individual recordings, 1260 from each of the 5 comprehensive experiments. The data exhibits only minor influence of fatigue or cyclic variations in depth of anaesthesia and thus demonstrates the value of computer-controlled stimulation protocols in which we used a randomized order of stimulus parameter delivery as well as control pulses for normalization across the duration of the experiment. These aspects of our model are crucial to answer relevant research questions with a small number of experimental animals.

Absolute amplitude values used in the experiments presented here ranged from 50 to 2000µA and the absolute amount of charge injected per phase did not exceed 1µC. This means the maximum charge density per phase was below 40µC/cm^2, so the stainless steel electrodes were operated safely (Shannon, 1992) and within their specific charge injection capacity (Merrill, Bikson and Jefferys, 2005). Monophasic pulses (maximum phase width 40µs) were separated by at least 3 seconds to allow charge dissipation.

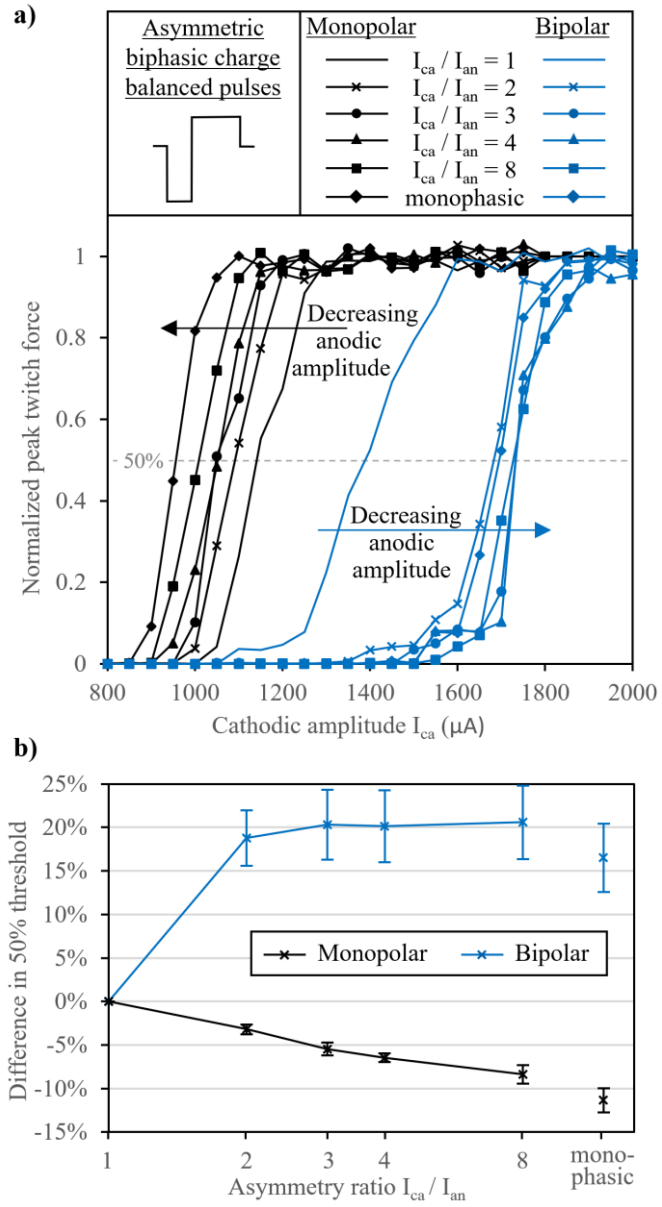

Figure 3.8 Effect of decreasing the anodic amplitude from biphasic symmetric pulses over different ratios of asymmetric charge balanced pulses to monophasic stimulation. **(a)** Recruitment curves from one representative experiment: Decreasing the anodic amplitude decreases neural activation thresholds in monopolar (black) configuration but surprisingly increases thresholds in bipolar (blue) electrode configuration. Waveform in legend not to scale. **(b)** Average change of 50% activation threshold across subjects. A negative percentage change means that a lower amplitude is needed to activate 50% of the motoneuron pool. Data represents mean of n=5 animals ± SEM.

Asymmetric biphasic charge balanced pulses.

Decreasing the amplitude of the anodic (second) phase of a biphasic pulse below the absolute amplitude of the cathodic phase (biphasic symmetric pulse) to 2, 3, 4, and 8 times lower values and finally to zero (monophasic pulse) led to decreased neural activation thresholds with the *monopolar* electrode configuration (Figure 3.8). The average

threshold reduction across subjects increased with decreasing anodic amplitude ratio up to 8.4 ± 1.1% with 8 times lower anodic amplitude. Monophasic stimulation achieved neural activation with 11.4 ± 3.9% lower thresholds than those required with symmetric biphasic pulses in monopolar configuration. Surprisingly, the same relative reduction of the anodic amplitude consistently increased threshold for neural activation when the electrode configuration was *bipolar* (Figure 3.8): Asymmetric biphasic pulses with 8 times lower anodic amplitudes showed 20.6 ± 4.2% higher thresholds than biphasic symmetric pulses. Stimulation with monophasic pulses led to 16.5 ± 3.9% higher neural activation thresholds than for biphasic symmetric pulses. The difference in threshold (from the baseline threshold with biphasic symmetric pulses) of all tested asymmetry ratios as well as monophasic stimulation was significant between monopolar and bipolar electrode configuration ($p<0.01$).

Symmetric biphasic pulses with IPGs.

The introduction of IPGs in between the cathodic (first) and anodic (second) phases of symmetric biphasic stimulation pulses decreased stimulation thresholds in monopolar electrode configuration (Figure 3.9) in agreement with the common expectation based on van den Honert and Mortimer's original work (van den Honert and Mortimer, 1979). This threshold decreasing effect was more profound for short phase widths and decreased with increasing phase durations. Increasing IPG durations above 50µs did not significantly enhance this threshold lowering effect in the monopolar configuration. With 40µs phase width IPGs lowered the activation threshold by 10.9 ± 1.5% (IPG=200µs, n=5). We observed lower threshold reductions of 4.9 ± 0.8% for phase width of 100µs (IPG=1000µs, n=5) and up 2.9 ± 0.9% with phase width of 200µs (IPG=100µs, n=5). With the longest tested stimulation phase width of 1000µs no consistent effect to change threshold was observed.

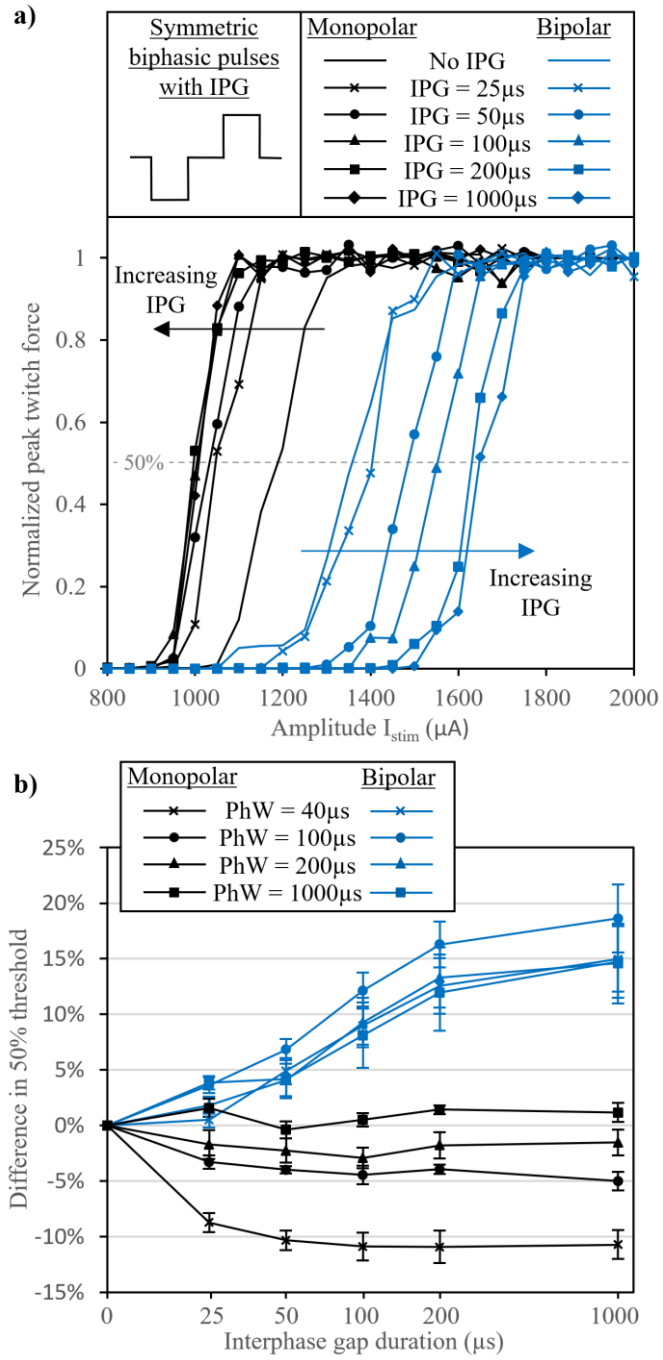

Figure 3.9 Effect of introducing IPGs of different durations between cathodic (first) and anodic (second) phase on neural activation thresholds. **(a)** Recruitment curves from a representative experiment with 40µs phase width: Introducing IPGs and increasing IPG duration decreases neural activation thresholds in the monopolar (black) configuration but surprisingly increases thresholds in the bipolar (blue) electrode configuration. Waveform in legend not to scale. **(b)** Average change of 50% activation threshold across subjects. A negative percentage change means that a lower amplitude is needed to activate 50% of the motoneuron pool. Data represents mean of n=5 animals ± SEM.

Opposite effects of IPGs on neural activation thresholds were observed in the bipolar electrode configuration: With all four tested phase widths, the introduction of IPGs between the cathodic and anodic phases consistently increased stimulation thresholds

(Figure 3.9). This effect increased with increasing IPG duration and elevated thresholds by 14.9 ± 2.9% (IPG=1000µs, n=5) with 40µs phase width stimuli. The longest IPG duration of 1000µs increased thresholds by 18.6 ± 3.1% (IPG=1000µs, n=5) for 100µs phase width pulses, 14.6 ± 3.6% (IPG=1000µs, n=5) for 200µs phase width stimuli, and 14.7 ± 3.2% (IPG=1000µs, n=5) for 1000µs phase width pulses.

The effect of IPGs on the 50% activation threshold was significantly different ($p<0.05$) between the monopolar and bipolar electrode configurations for all combinations of phase width and IPG duration except for phase width 200µs with 25µs IPGs and phase width 1000µs with 25, 50, and 100µs IGPs. The divergence between monopolar and bipolar increased with increasing IPG (Figure 3.9.b).

Electroneurography during biphasic stimulation at supramaximal amplitude.

ENG recordings during repeated monopolar and bipolar stimulation with maximal (95% activation threshold $I_{95\%}$) and supramaximal amplitudes are presented here from a representative nerve preparation (Figure 3.10). The compound action potentials (eCAP) evoked with biphasic pulses of 100µs phase width at maximal amplitude $I_{95\%}$ were recorded and had a latency of 1.67 ± 0.007ms (mean of n=10, ± SEM) between the stimulation artifact and the first prominent downward deflection of the eCAP with the monopolar electrode configuration (Fig. 4.a). With the bipolar electrode configuration, maximal amplitude stimulation ($I_{95\%}$) elicited eCAPs with an approximately one phase width greater latency of 1.78 ± 0.005ms. Increasing the amplitude in 50µA increments from $I_{95\%}$ to $I_{95\%}$ +350µA reduced the delay by 60µs to 1.61 ± 0.006ms with monopolar electrode configuration and by 170µs us to 1.61 ± 0.007ms with bipolar electrodes, so that there was no longer a difference in the eCAP latencies between monopolar and bipolar stimulation (Fig. 4.i).

Stimulation with 200µs phase width biphasic pulses at 95% activation threshold elicited eCAPs with a latency of 1.73 ± 0.006ms in the monopolar case, whereas the delay was 1.91 ± 0.005ms, approximately one phase width greater with bipolar configuration (Figure 3.10.e). Increasing the stimulation amplitude to $I_{95\%}$ +350µA decreased the eCAP latencies in monopolar stimulation by 69µs to 1.67 ± 0.008ms and by 245µs to 1.67 ± 0.008ms with bipolar electrode configuration. To summarize, the approximately one phase width difference in eCAP delay between monopolar and bipolar stimulation progressively decreased between maximal and supramaximal stimulation amplitudes (Figure 3.10.j).

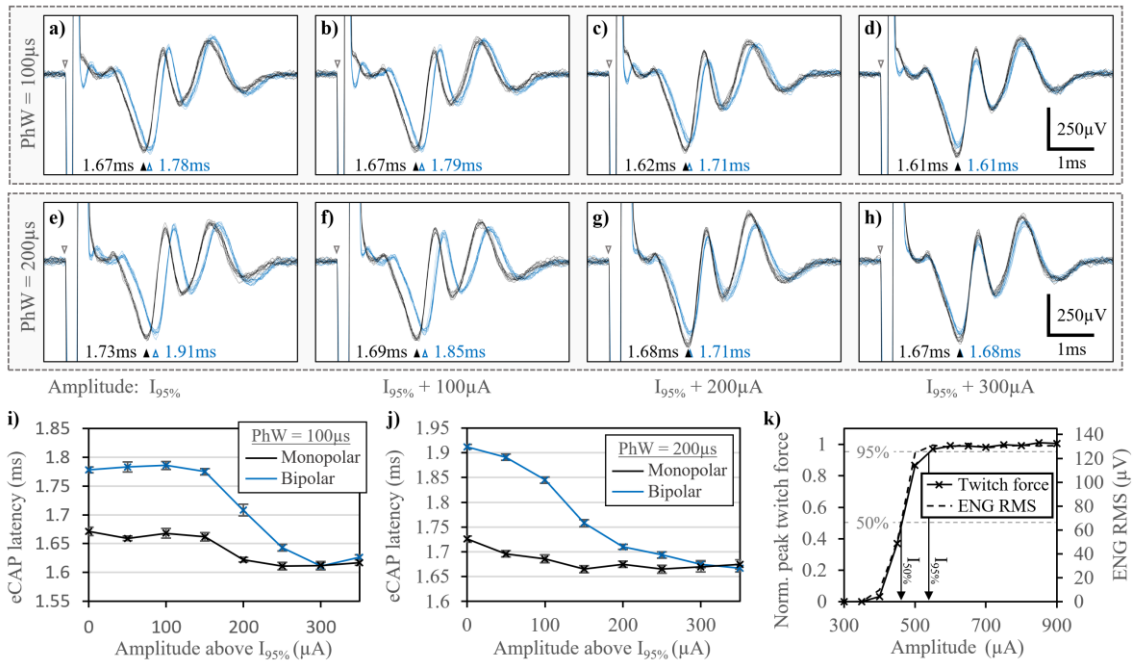

Figure 3.10 ENG recordings during maximal ($I_{95\%}$) and supramaximal amplitude stimulation. eCAPs were recorded during stimulation with standard biphasic rectangular pulses with phase width 100µs and amplitude **a)** $I_{95\%}$, **b)** $I_{95\%}$+100µA, **c)** $I_{95\%}$+200µA, and **d)** $I_{95\%}$+300µA and with phase width 200µs and amplitude **e)** $I_{95\%}$, **f)** $I_{95\%}$+100µA, **g)** $I_{95\%}$+200µA, and **h)** $I_{95\%}$+300µA. Each plot shows ten superimposed ENG recordings for stimulation via monopolar (black) and bipolar (blue) electrode configuration. Arrowheads indicate mean eCAP latencies. Mean eCAP latencies of stimulation with amplitudes equal to $I_{95\%}$ are approximately one phase width greater with bipolar (blue) than with monopolar (black) electrode configuration. The difference in eCAP latencies between the two electrode configurations diminishes progressively as the amplitude increases for phase widths **i)** 100µs and **j)** 200µs. Data represents mean ±SEM of n=10 recordings. **k)** One representative normalized recruitment curve for 200µs biphasic stimulation in the monopolar electrode configuration. 50% and 95% activation thresholds are determined by linear interpolation. Normalized peak twitch force and ENG root mean square (RMS) are correlated. (Eickhoff and Jarvis, 2020b) Copyright by IEEE. Adapted with permission.

3.2.4 Excitation at the bipolar return electrode explains opposite effects of pulse shaping

(IV. Discussions)

We investigated the effects of decreasing the anodic (second) amplitude of a biphasic pulse and introducing IPGs in biphasic pulses on neural activation thresholds in the monopolar and bipolar electrode configurations. In agreement with the pioneering research on IPGs (van den Honert and Mortimer, 1979; Gorman and Mortimer, 1983), we observed an AP suppressing effect of the secondary anodic phase of a biphasic pulse when we used a monopolar electrode configuration. Thresholds were decreased for neural activation with asymmetric biphasic pulses that had reduced anodic amplitudes (Figure 3.8, black traces) and with separation of the anodic phase from the cathodic phase by an IPG (Figure 3.9, black traces). Furthermore, our data obtained with the monopolar stimulation configuration are remarkably concurrent with earlier observations that the benefit of an IPG is greater for short phase width stimulation (Gorman and Mortimer, 1983) and that there is little additional advantage in increasing IPG durations above approximately 100µs (van den Honert and Mortimer, 1979; Shepherd and Javel, 1999). The rationale for both these observations is the so-called vulnerable period of axons that just reached activation threshold in response to the cathodic (first) stimulation phase. During this period, an early anodic phase can suppress self-propagating APs. Once the IPG sufficiently separates the onset of the anodic phase from the timepoint of AP elicitation during the cathodic phase, the AP has “escaped” the stimulation site and can not be easily abolished by hyperpolarisation through the anodic phase. Further increasing of IPG duration does not bring any additional advantage. As this separation is already achieved by the relatively long phase widths of standard biphasic pulses (approximately 100µs or greater), there is limited practical benefit in introducing IPGs to such pulses.

Surprisingly in the bipolar electrode configuration that is most relevant to many contemporary neuromodulation implants, especially to the emerging field of miniaturized bioelectronic devices, we observed opposite and therefore detrimental effects of the pulse shape variations that we tested. When we reduced the amplitude of the anodic (second) phase of biphasic stimuli (Figure 3.8, blue traces) or introduced an IPG (Figure 3.9, blue traces) both changes consistently led to *increased* stimulation thresholds for neural activation.

As both of these pulse shape variations reduce the effective slope and/or amplitude of the middle field transition of biphasic pulses (compare Figure 3.11.c-e), we formed the

hypothesis that in the bipolar electrode configuration excitation is first elicited by this middle transition. While the middle field transition of a standard biphasic (cathodic phase first) pulse has a hyperpolarizing effect at the active electrode, the same transition of the mirrored or inverted current waveform at the return electrode has a strong depolarizing effect (Figure 3.11.c). In addition, at the return electrode the first stimulation phase might act as a hyperpolarizing pre-pulse, which has been shown to render axons more excitable (Grill and Mortimer, 1995; Eickhoff and Jarvis, 2020b). Since in the bipolar configuration both electrodes were placed at the same distance from the nerve, which setup resembles the operational mode of many miniaturized implanted systems, the preconditioning effect of the first phase followed by the strongly depolarizing middle field transition supports our hypothesis of excitation at the return electrode.

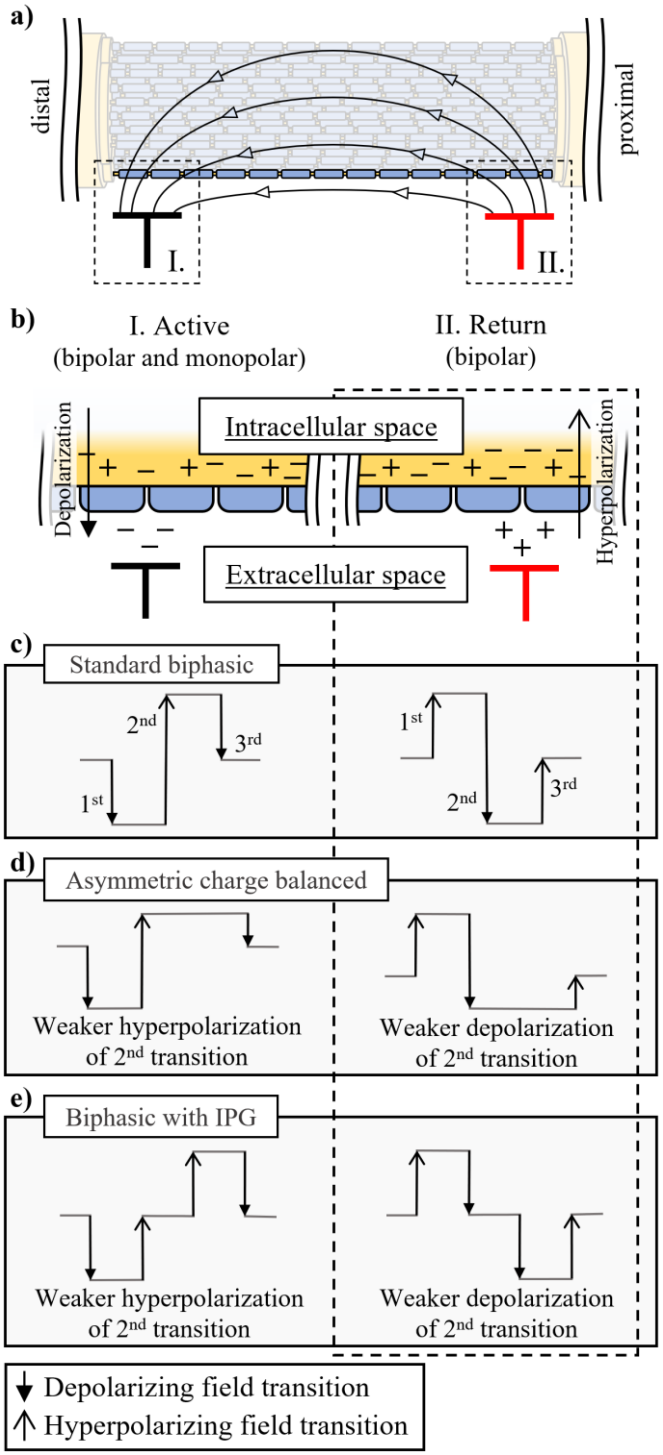

Figure 3.11 Model of extracellular stimulation with practical electrode configurations. a) Electrical field induced during cathodic stimulation in bipolar electrode configuration. **b)** Cathodic stimulation leads to an extracellular electron gain at the active electrode (I.) which results in depolarization of the neural membrane, whereas the charge return causes an increased positive valence at the return electrode (II.) which hyperpolarizes the membrane. Thus, the effect of the field transitions within a **c)** standard biphasic, **d)** asymmetric charge balanced, and **e)** biphasic pulse with IPG on neural stimulation is the opposite at the return as compared to the active electrode. Full arrowheads indicate depolarizing effects of field transition, open arrowheads represent hyperpolarizing effects.

In order to test this hypothesis, we analysed ENG recordings distal to the stimulation site during maximal ($I_{95\%}$) and supramaximal stimulation with standard biphasic pulses in two nerve-muscle preparations. The results were consistent, and representative records are presented from one of the preparations. During maximal stimulation amplitude $I_{95\%}$, the eCAP latencies were consistently greater with the bipolar than with the monopolar electrode configuration. The difference in eCAP latency was very close to the duration of one stimulation phase, verifying the hypothesis that APs in the bipolar configuration were elicited first in response to the second phase or the middle transition. Following our hypothesis, this implies that in the bipolar configuration excitation first occurred at, or near to, the return electrode. When amplitudes were increased above $I_{95\%}$, the eCAP latencies progressively decreased. In the case of monopolar stimulation this decrease in delay was less than one phase width, indicating that the threshold for activation was first reached late in the first phase and then gradually synchronized with the onset of that first phase (i.e. the first field transition). In the bipolar configuration we consistently observed a reduction of the delay greater than one phase width. The rationale for this observation may be that in this electrode setup excitation threshold was first reached within the second phase at the return electrode. Upon increasing the supramaximal intensity, the event of AP generation shifted temporally to the beginning of the first phase and spatially, according to our hypothesis, from the return to the more distal active electrode. The progressive nature of these shifts in delay must represent the distribution of threshold values among the motoneuron population.

Due to the small size of our nerve preparation, an experimental verification of the site (i.e. the electrode) of AP generation, e.g. by flipping the electrode polarities or changing the inter electrode spacing, is not practical in our rodent model. With an interelectrode distance of 2mm and a typical range of motor neuron conduction velocities of 70 to 120m/s, the difference in conduction time of an eCAP elicited at the more proximal return electrode and one generated at the more distal active electrode would be between 28 and 16µs. These calculations are based on the assumption that the activated NORs are located centrally over the electrode; if they are located towards the inside of the bipolar pair, which is where the electrical field is likely to exhibit its highest density, the temporal differences due to conduction velocity would be even smaller. This investigation of the exact location of eCAP elicitation would however be an interesting follow up study in a larger preparation such a human median nerve stimulation experiment. Here a greater interelectrode separation would be possible and thus a reduction of the relative error due

to uncertainties such as the location of the activated NORs relative to the electrode location as outlined above.

Despite the extensive body of scientific literature on the incorporation of IPGs in waveforms for direct neural stimulation, this is the first study to report significantly increased stimulation thresholds with IPGs in biphasic pulses in the bipolar electrode configuration. A thorough review of the published literature on IPGs reveals that the majority of these studies, including the early pioneer research in this field (van den Honert and Mortimer, 1979; Gorman and Mortimer, 1983), investigated the effect of IPGs only in the monopolar stimulation configuration (McKay and Henshall, 2003; Kim *et al.*, 2010; Ramekers *et al.*, 2014; Weitz *et al.*, 2014; Schvartz-Leyzac and Pfingst, 2016; Hughes, Choi and Glickman, 2018). The common conclusion of these studies of reduced thresholds for neural activation with IPGs is in agreement with our findings in the monopolar electrode configuration. Fewer studies have investigated the effect of IPGs on neural stimulation thresholds in bipolar the configuration (Shepherd and Javel, 1999; Prado-Guitierrez *et al.*, 2006b; Cappaert *et al.*, 2013), and only two studies examined both principal electrode configurations (Carlyon *et al.*, 2005; Maciejasz *et al.*, 2015). The general consensus of these studies is that lower thresholds for neural activation may also be achieved with IPGs in the bipolar electrode configuration. These therefore oppose our findings in this configuration, but a number of methodological differences weaken this opposition. First, as in many auditory nerve stimulation studies, the study by Prado-Guitierrez et al. (Prado-Guitierrez *et al.*, 2006b), and in one group of cochlear implant users in the study by Carlyon et al. (Carlyon *et al.*, 2005), biphasic pulses with 8µs IPG instead of biphasic pulses without IPG were used as baseline. From this baseline both studies describe decreasing thresholds with increasing IPG duration. This short IPG might already have elevated the threshold for activation at the return electrode sufficiently, so that the mechanism of activation as a response to the middle field transition, as we describe it, could not be observed. Furthermore, although a detailed comparison of IPG effects in the different electrode configurations was not the authors main objective and so it was not subjected to further discussion or statistical tests, Carlyon et al. describe less IPG effect in bipolar than in monopolar electrode mode (Carlyon *et al.*, 2005). The rationale for this could be that in bipolar configuration a subset of axons was excited at the return electrode, where the increasing IPG weakens the depolarizing effect of the middle field transition (compare Figure 3.11.e), and another subset of axons was excited at the active electrode where the IPG reduces the AP abolishing effect of the anodic

(second) phase. Maciejasz et al. investigated the effect of IPGs in asymmetric pulses consisting of a rectangular cathodic phase and a passive capacitive discharge as the anodic phase (Maciejasz *et al.*, 2015). As this passive discharge only reached a peak amplitude of approximately 20% of the cathodic phase, the middle field transition of these asymmetric pulses might not have been sufficient to elicit any activation at the return electrode.

Our findings of increased thresholds for neural activation with biphasic pulses with reduced anodic amplitude and IPG in the bipolar configuration are of direct importance for many neuromodulation devices that operate in a bipolar mode. If these findings are not considered in the design of stimulation patterns, the desired benefit of adding an IPG or reducing the anodic amplitude might, depending on the electrode configuration, represent a significant disadvantage. As the energy consumption per pulse is a crucial parameter for neuromodulation devices that are battery powered or rely on wireless energy transmission, we present two example calculations of this parameter to illustrate the potential disadvantage. Since the electrical energy consumption per pulse is proportional to the square of the stimulation current (Eickhoff and Jarvis, 2019), the threshold increase of 12.2% that we observed with biphasic pulses with phase width 100µs and 100µs IPG (compared to standard biphasic pulses of phase width 100µs and *no* IPG) in the bipolar configuration would increase the energy required to elicit the same neural activation by 25%. Similarly, the 20% threshold increase we report for asymmetric biphasic pulses with a ratio of $I_{ca}/I_{an} = 3$ compared to symmetric biphasic pulses in the bipolar configuration would lead to 44% increased energy consumption. These increased energy requirements clearly oppose the ambition of device (and battery) miniaturization as well as the reduction of recharge frequency or even battery replacement surgeries.

However, we argue that an understanding of the different mechanisms of AP generation in the bipolar electrode configuration (that is details about the effective transition within the stimulation waveform as well as the effective electrode) can not only prevent possible disadvantages, but might also be harnessed to *improve* stimulation selectivity. As we have demonstrated for asymmetric pulses and IPGs, any given pulse shape variation will (due to the inverted current profile at the bipolar return electrode) have opposite effects at the two bipolar electrodes. This effectively creates a zone of lower activation thresholds near one electrode while at the same time thresholds for activation are elevated near the other electrode and thus might offer a twofold opportunity for improved selectivity. Utilization of this principle might offer crucial advantages for selective stimulation of

morphologically or physiologically complex neural structures that carry an array of functions, such as in recent explorations to stimulate the carotid sinus nerve as treatment for type 2 diabetes (Sacramento *et al.*, 2018; Fjordbakk *et al.*, 2019).

Besides the relative threshold changing effect of the investigated pulse shape variations (i.e. the percentile difference from a baseline with standard biphasic pulses), which was the main objective of the present study, in some experiments we observed significant differences in absolute thresholds between the monopolar and the bipolar stimulation configuration. In the data presented in Figure 3.8.a and Figure 3.9.a, for instance, stimulation with monopolar configuration required less amplitude to elicit neural activation than stimulation in the bipolar mode. Although we stated that miniaturized electroceutical implants must, due to their small, operate in the bipolar configuration, it can be argued that even with very small implants electrode arrangements could be used that exhibit features of the classical monopolar stimulation mode. The miniaturized implants could, for instance, be oriented so that one electrode is in contact with the nerve while the other electrode surface is pointed away from it. Further, as long as maximal charge density limits are not exceeded, the electrode design could incorporate a smaller active electrode surface area and a larger return electrode area. These and other electrode design parameters for miniaturized implants should be investigated in future research as they might be beneficial in applications where (like in the representative data in Figure 3.8.a and Figure 3.9.a) stimulation with monopolar electrodes achieves activation with lower amplitudes than stimulation in bipolar mode.

3.2.5 IPGs could significantly decrease battery life of stimulation implants operating in bipolar mode

(V. Conclusion)

We examined the transferability of earlier published studies on the effect of IPGs for neural stimulation thresholds that were predominantly carried out in monopolar electrode configuration, to the bipolar stimulation configuration that is the operational mode of many contemporary and future devices, such as the proposed class of electroceuticals. Surprisingly we found opposite effects of IPGs in the bipolar compared to the monopolar electrode configuration. This is the first study to report consistently *increased* thresholds for neural activation with IPGs in the bipolar mode. We identified temporal differences of AP generation as the cause for opposite effects of IPGs and biphasic asymmetric pulses in the two principal electrode configurations. In the bipolar configuration excitation first

occurred in response to the middle field transition. This experimental observation supports our hypothesis that, in the bipolar case, APs were first generated at the return electrode. These findings must be taken into consideration when designing stimulation patterns for neuromodulation devices that operate in bipolar mode to avoid increased activation thresholds and thus over 40% increased energy consumption. Further research is warranted to bridge the apparent gap between the findings of this study and earlier published work that described a threshold lowering effect of IPGs for bipolar stimulation of the auditory nerve (Shepherd and Javel, 1999; Carlyon *et al.*, 2005; Prado-Guitierrez *et al.*, 2006a). Furthermore, a deeper understanding of the opposite threshold changing effects of pulse shape variations that we describe at the active compared to the return electrode of a bipolar stimulation configuration, may enhance selectivity of neural stimulation and should be investigated in further research.

3.3 Gaussian shaped pulses

The study presented in this chapter is published and copyrighted:

The only main differences between the published article and the present chapter are:

- Figure and equation numbers were adjusted to match the thesis chapter numbering.
- Parts of the "Materials and Methods" section, such as the surgical procedure, which are described in detail in the General Methods (Chapter 2), are left out and the omissions are indicated by "[…]". Instead, key methodological information such as number of animals, electrode configurations, and recording sampling rates are summarized in inserted boxes.
- To avoid redundant chapter names, the paper section-headings such as "Introduction", "Results", and "Discussion" have been replaced by brief summarizing descriptions of each section's main message.

(Abstract)

Objective: Previous computational studies predict that Gaussian shaped waveforms use the least energy to activate nerves. The primary goal of this study was to examine the claimed potential of up to 60% energy savings with these waveforms over a range of phase widths (50-200µs) in an animal model. Methods: The common peroneal nerve of anaesthetized rats was stimulated via monopolar and bipolar electrodes with single stimuli. The isometric peak twitch force of the extensor digitorum longus muscle was recorded to indicate the extent of neural activation. The energy consumption, charge injection and maximum instantaneous power values required to reach 50% neural activation were compared between Gaussian pulses and standard rectangular stimuli. Results: Energy savings in the 50-200µs range of phase widths did not exceed 17% and were accompanied by significant increases in maximum instantaneous power of 110-200%. Charge efficiency was found to be increased over the whole range of tested phase widths with Gaussian compared to rectangular pulses and reached up to 55% at 1ms phase width. Conclusion: These findings are surprising in light of the claims of up to 60%

energy savings with Gaussian like stimulation waveforms. The moderate energy savings achieved with the novel waveform are accompanied with considerable increases in maximal instantaneous power. Larger power sources would therefore be required, and this opposes the trend for implant miniaturization. Significance: This is the first study to comprehensively investigate stimulation efficiency of Gaussian waveforms. It sheds new light on the practical potential of such stimulation waveforms.

Index Terms—Electrical stimulation, Gaussian waveform, Energy efficiency, Charge efficiency, Peak power

3.3.1 Computational studies identified Gaussian shaped waveforms as energy optimal

(I. Introduction)

Electrical stimulation (ES) of excitable tissues successfully finds application in a number of therapeutic systems and medical devices such as the cochlear implant, the cardiac pacemaker, deep brain and spinal cord stimulators. Electrical impulses are used to activate or inhibit activation in a target excitable structure, which might be a block of cardiac tissue, a region of the brain, or a peripheral nerve. This can be achieved using voltage- or current-controlled stimulation waveforms: the latter has the benefit of eliminating threshold variations that result from changes in electrode-tissue impedance and is therefore commonly used today.

While the basic requirement of a stimulation waveform is to activate (or block) the target structure, energy efficiency as well as stimulation selectivity and safety are of high importance (Grill, 2018). In view of the many implantable ES devices and the trend towards miniaturized applications such as so-called electroceutical systems for stimulation of the autonomic nervous system (Horn, Ardell and Fisher, 2019), energy efficient stimulation is important to the whole field as it enables increased battery lifetime or the use of smaller batteries. There are recent early successes in wireless power delivery, for example to a passive miniature radio-frequency identification (RFID) tag placed inside a central organ of pigs (Ma *et al.*, 2018). However, the higher amounts of electrical energy required by active implants such as neural stimulators as well as the safety limits of human exposure to radio frequency electromagnetic fields (IEEE, 2006) indicate that the need to optimize stimulation efficiency remains. Superficially placed implants, such as cochlear implants, that use transcutaneous power transmission can also benefit from

increased energy efficiency. Although not as critical as for devices with implanted batteries, a more economical use of energy allows reduction in size and fewer recharge cycles from an external power source. Although it is not often mentioned as a key parameter of electrical stimulation, charge efficiency is also an important cofactor as it can influence both selectivity and safety. An increased charge efficiency, that is, a reduction of the charge injection required to activate a nerve, can increase the stimulation safety due to reduced charge density at the electrode-tissue interface and/or increase selectivity because electrode size may be reduced without exceeding safe limits for charge density. Furthermore, the maximum instantaneous electrical power delivered via the stimulation electrodes is an important criterion for implantable stimulators. Battery size scales directly proportionally with maximum power since the specific power (W/kg) is constant for any specific battery technology.

In many cases, rectangular current waveforms are used in electrical nerve stimulation, not least because of the ease of generating them with simple electronic circuits. They are often biphasic so that the overall net charge injection is near zero. Many studies have been conducted to investigate variations of the rectangular biphasic waveform such as interphase gaps (IPGs), asymmetric pulses (van den Honert and Mortimer, 1979; Gorman and Mortimer, 1983; Reilly and Diamant, 2011) and pre pulses (Sassen and Zimmermann, 1973; Grill and Mortimer, 1995, 1997; Vargas Luna, Mayr and Cortés-Ramirez, 2018). Some of these studies sought to discover whether non-rectangular stimulation waveforms might have an advantage in terms of efficiency or selectivity. Several programmes also incorporated computational simulations. Employing the Hodgkin-Huxley nerve membrane model (Hodgkin and Huxley, 1952a; McNeal, 1976) Jezernik and Morari predicted that an exponentially rising stimulation waveform would provide the best energy efficiency (Jezernik and Morari, 2005). Comparing this and other non-rectangular waveforms to standard rectangular stimuli applied to a computational model of a single mammalian axon (Sweeney, Mortimer and Durand, 1987), exponentially rising and decaying waveforms were found to be most charge efficient across the whole range of phase widths. When the threshold charge was expressed as a fraction of the charge injection capacity with practical titanium nitride microelectrodes, exponential and linearly decreasing (i.e. reverse ramp) waveforms were most charge efficient. Both exponential waveforms were most energy efficient at long phase durations (>250µs). Gaussian shaped stimuli achieved the best energy efficiency at shorter phase widths (Sahin and Tie, 2007). Using a more sophisticated computational simulation of a

population of mammalian myelinated axons (McIntyre, Richardson and Grill, 2002) as well as *in vivo* experiments, the apparent superiority of exponential waveforms in terms of charge and energy efficiency at long phase widths was shown to be misleading and therefore over-estimated because the waveform shape became insensitive to the phase duration since only the low amplitude 'tail' of the computed current waveform grew with increasing phase width. Furthermore, exponential waveforms had significantly higher peak power requirements than rectangular stimuli and triangular pulses were most charge efficient for phase widths $\leq 200\mu s$. It was shown that none of the tested rectangular, exponential or ramp waveforms was simultaneously most efficient in terms of energy, charge and peak power (Wongsarnpigoon, Woock and Grill, 2010).

Promisingly, three recent studies independently found a Gaussian shaped stimulation waveform to be optimal in terms of minimized energy consumption using model-based approaches probed by a genetic algorithm (Wongsarnpigoon and Grill, 2010), the calculus of variation (Forger, Paydarfar and Clay, 2011) and the least action principle (Krouchev *et al.*, 2014). While these studies agree that a Gaussian stimulation waveform shows increased energy efficiency over rectangular stimuli, there are considerable differences in the claimed potential to save energy by replacing simple rectangular waveforms with modified pulses. The largest claim of 5-60% increased energy efficiency over a clinically relevant range of phase widths (~ 50-200µs) can be found in the genetic algorithm study of Wongsarnpigoon and Grill, based on the outcome of their computational and *in vivo* work (Wongsarnpigoon and Grill, 2010). However, these studies on Gaussian shaped stimulation waveforms recognize that the energy costs of generating such complex waveforms may decrease the achievable benefit in energy efficiency of neuro stimulators and conclude that more practical investigations of the incorporation of Gaussian waveforms are warranted. We here respond to this challenge.

To the best of our knowledge, the practical implementation of the Gaussian stimulation waveform has not been studied further till now. The primary goal of our study was to explore the findings of these recent computational studies in an animal model. Single electrical stimuli were used to activate the common peroneal nerve (CPN) of anaesthetized rats via monopolar or bipolar electrodes. The isometric peak twitch force of the extensor digitorum longus muscle (EDL) was recorded to indicate the extent of neural activation. To bring the detailed computational findings closer to practical application, we reduced the phase-width-dependent variation of the optimal waveforms. Only one fixed Gaussian waveform, which was chosen to closely resemble the waveforms

used by (Wongsarnpigoon and Grill, 2010) in the range of 50-200µs phase widths, was compared to rectangular stimulation. Since charge balance is a key requirement of most electrical stimulation applications, only biphasic stimuli were incorporated in this study. As well as a comparison of energy efficiency between Gaussian and rectangular stimuli, charge efficiency and peak power of stimulation with these waveforms were also investigated, as these are important parameters of stimulation for the design of implantable devices.

3.3.2 In-vivo experiment design

(II. Materials and Methods)

Experiments were carried out in n=7 adult Wistar rats.
Home Office project licence: PPL 40/3743.
Stimulation electrodes: Active electrode distal, bipolar return electrode proximal, and monopolar return electrode (in 3 animals) 10mm away from the CPN long axis (return electrode switched manually between recordings).

Surgical procedure

[…]

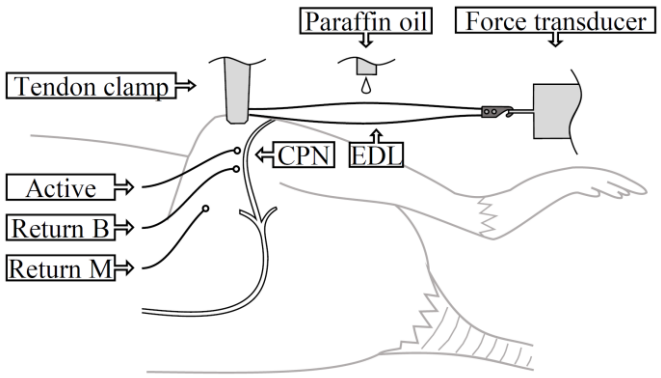

Figure 3.12 Experimental model: Nerve-muscle-preparation with Common Peroneal Nerve (CPN) and Extensor Digitorum Longus (EDL). Electrodes: The active electrode was placed most distal at the CPN. For bipolar stimulation "Return B" was used, for monopolar stimulation "Return M" served as return electrode.

Stimulation

[…] To achieve charge balanced stimulation, all impulses were biphasic with the cathodic phase first. The kurtosis of the Gaussian waveform is described by

$$I(t) = e^{-\frac{\left(\frac{t}{PhW}-0.5\right)^2}{0.045}}, \quad (3.1)$$

as this current profile was a close match to the waveforms used by Wongsarnpigoon and Grill in what they called the clinically relevant range of phase widths (Wongsarnpigoon and Grill, 2010). Recruitment curves (that is peak muscle force plotted against pulse amplitude, see Figure 3.13.a) for phase widths of 40, 60, 80, 100, 120, 140, 160, 180, 200, 250, 325, 425, 550, 775 and 1000µs were recorded with 100µA amplitude increments for biphasic Gaussian and rectangular pulses. For both waveforms and both electrode configurations, the different combinations of stimulation parameters, that is, amplitudes and phase widths, were applied in randomized order. Every 20 test stimulations a standard control stimulation pulse (biphasic rectangular, 200µs PhW), with an amplitude set for each subject to elicit supramaximal nerve recruitment (typically 1mA) was delivered and the resultant force recorded.

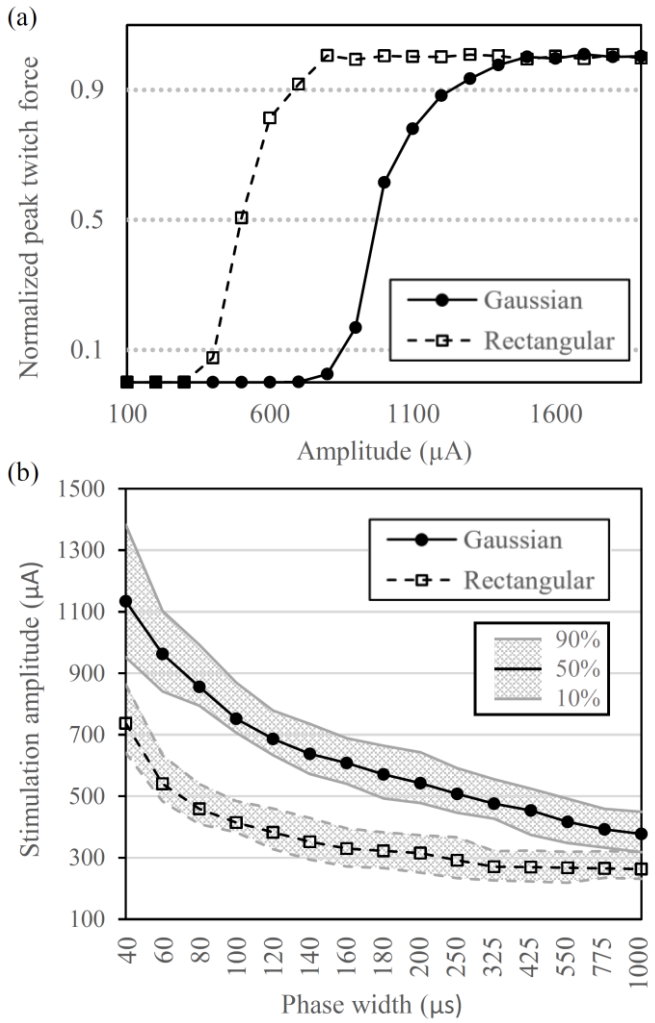

Figure 3.13 Exemplary recruitment data for Gaussian and rectangular pulses with bipolar electrodes. a) Normalized recruitment curves for PhW=60µs. 10%, 50%, and 90% of maximum isometric twitch force were determined by linear interpolation of experimental measurement points. **b)** Strength-duration curves for 50% activation (black traces) and dynamic ranges (gray area) between 10% (lower traces) and 90% (upper traces) activation levels. Data are means of n=7.

Recording

Extensor digitorum longus muscle twitch force recorded at 100kS/s.

[…] We wished to record the electrode current at a higher sample rate, so stimulation current through a resistor in series and stimulation voltage across the electrodes, were recorded separately at 500kS/sec with an NI PCIe 6351 Data Acquisition Card, which was also used for stimulation.

Data analysis and statistics

The isometric peak twitch force values elicited by the randomly applied test stimulations were normalized to the force response of the nearest control pulse. The normalized peak

force values were then sorted by pulse shape, phase width and stimulation amplitudes, to reveal the normalized recruitment data. Thus, the final recruitment curves were assembled from test pulses that were placed randomly from start to end of the respective recording period, and therefore are not affected by variations of temperature, level of anaesthesia or fatigue. Linear interpolation between data points was used to determine the 50% activation thresholds of all recruitment curves (Figure 3.13.a). The energy consumption (3.2) and charge injection (3.3) values for all applied stimuli were attained by integration of the electrical stimulation recordings:

$$\boldsymbol{E = \int_{0}^{2PhW} V(t) I(t) dt,} \tag{3.2}$$

$$Q = \int_{0}^{2PhW} |I(t)|\, dt. \tag{3.3}$$

Energy and charge values at 50% activation level were scaled according to the threshold interpolation. Furthermore, the percentage differences in energy consumption (3.4) and charge injection (3.5) with Gaussian pulses compared to rectangular stimuli at 50% activation threshold were calculated:

$$\textbf{Difference in energy} = \left(\mathbf{1} - \frac{\boldsymbol{E_{gaus}}}{\boldsymbol{E_{rect}}}\right) * \mathbf{100}\%, \tag{3.4}$$

$$\text{Difference in charge} = \left(1 - \frac{Q_{gaus}}{Q_{rect}}\right) * 100\%. \tag{3.5}$$

In addition to these integrated measures of stimulation efficiency, the maximum instantaneous power across the electrodes was also calculated

$$\boldsymbol{P(t) = V(t) * I(t)} \tag{3.6}$$

for both tested waveforms and expressed as a percentage difference between the response to rectangular and Gaussian pulses:

$$\textbf{Diff. in max. inst. power} = \left(\mathbf{1} - \frac{\boldsymbol{P_{gaus}}}{\boldsymbol{P_{rect}}}\right) * \mathbf{100}\%. \tag{3.7}$$

Figure 3.14 shows an example of the electrical recordings (stimulation current and voltage) as well as of the computed efficiency measures (energy, charge, and maximum instantaneous power) with rectangular and gaussian pulses of 100µs PhW near 50% activation level.

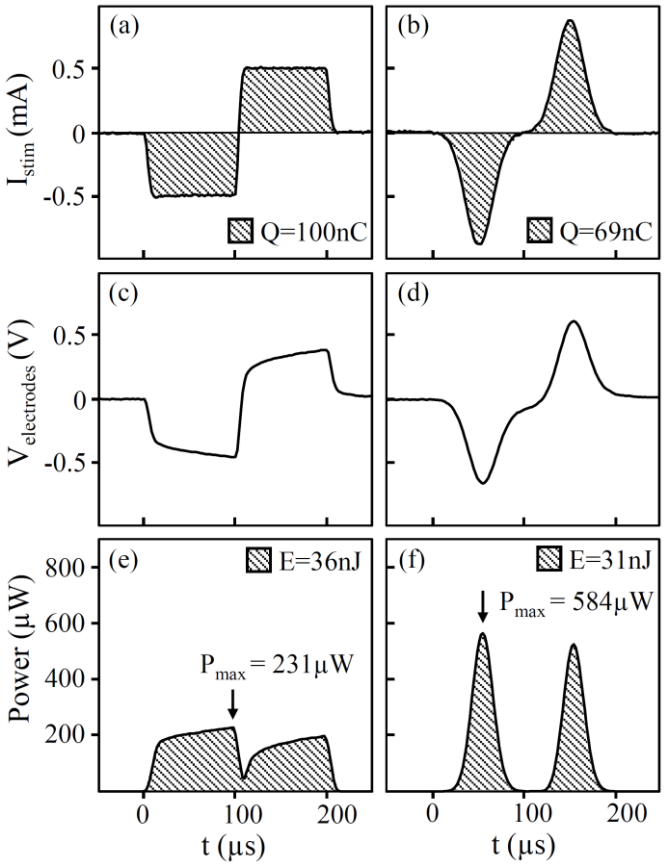

Figure 3.14 Electrical recordings of rectangular (left column: a, c, e) and Gaussian (right column: b, d, f) stimulation (PhW=100µs) near 50% activation threshold. Stimulation current and charge: **a)** Rectangular stimulus with 500µA amplitude and 100nC overall charge injection; **b)** Gaussian pulse with 900µA amplitude and 69nC (31% reduction) charge injection. Stimulation voltage across electrodes during rectangular **c)** and Gaussian **d)** stimulation. Instantaneous power and energy consumption: **e)** Rectangular pulse consumes 36nJ energy and has a max. inst. power of 231µW; **f)** Gaussian pulse consumes 31nJ energy (14% reduction) and has a max inst. power of 584µW (153% increase).

A two-way repeated measures analysis of variance (ANOVA) was performed for each measure of stimulation efficiency separately. The dependent variable was the normalized charge, energy or maximum instantaneous power value at 50% activation level. The independent variables were waveform (rectangular or Gaussian), PhW, and rat (subject). Where the effect of the waveform was found to be significant ($p<0.05$), Sidak's multiple comparisons were conducted post hoc for the means of the respective efficiency measure (charge, energy or power) of Gaussian and rectangular stimuli at each PhW separately.

3.3.3 Moderate energy savings with Gaussian waveform are accompanied with substantially increased power requirements

(III. Results)

The recruitment data underlying the calculations of the efficiency measures exhibit only minor influence of fatigue or cyclic variations in depth of anaesthesia. Figure 3.13.a shows examples of typical recruitment curves with their characteristic sigmoidal shape. Strength-duration curves at 50% activation level as well as the dynamic ranges (10% to 90% activation) exhibit the characteristic hyperbolic shapes (Figure 3.13.b).

Energy efficiency

Bipolar case: The energy-duration curves for 50% activation with Gaussian and rectangular stimuli applied via bipolar electrodes (in n=7 animals) intersect at a phase width between 60 and 80µs (Figure 3.15.a). After this intersection the energy consumption values of Gaussian stimuli increase less with increasing PhWs than for rectangular stimulation. This implies an increasing energy efficiency of Gaussian compared to rectangular pulses with increasing PhW (Figure 3.15.c). The effect of waveform on energy efficiency was significant ($P<0.001$). However, stimulation with Gaussian pulses of the shortest tested phase width of 40µs required on average 17.7% (±4.8% SEM) more energy than rectangular stimuli of the same PhW. In the range of 50-200µs PhWs the differences in mean energy efficiency of Gaussian compared to rectangular pulses ranged from -5.8% (±1.4% SEM) at 60µs to +17.1% (±2.4% SEM) at 200µs. At the longest tested PhW of 1000µs, excitation with Gaussian pulses was achieved with 46.7% (±5.9% SEM) less energy than with rectangular impulses (Figure 3.15.c).

Monopolar case: Energy duration curves for stimulation via a monopolar electrode configuration (in n=3 animals) intersect at a phase width of 100µs; for shorter pulses rectangular stimulation appear to require less energy while Gaussian stimuli are more energy efficient at PhWs over 100µs (Figure 3.15.b), although ANOVA revealed no significant effect of waveform ($P=0.11$). At 40µs PhW stimulation with Gaussian pulses was on average 17.6% (±4.7% SEM) less energy efficient than stimulation with rectangular pulses. As the energy duration curves intersect within the range of 50-200µs PhWs, the energy efficiency of Gaussian compared to rectangular pulses ranged from -7.5% (±4.9% SEM) at 60µs to +17.5% (±5.9% SEM) at 140µs. The highest difference in energy efficiency of 61.6% (±3.9% SEM) was observed at 1000µs (Figure 3.15.d).

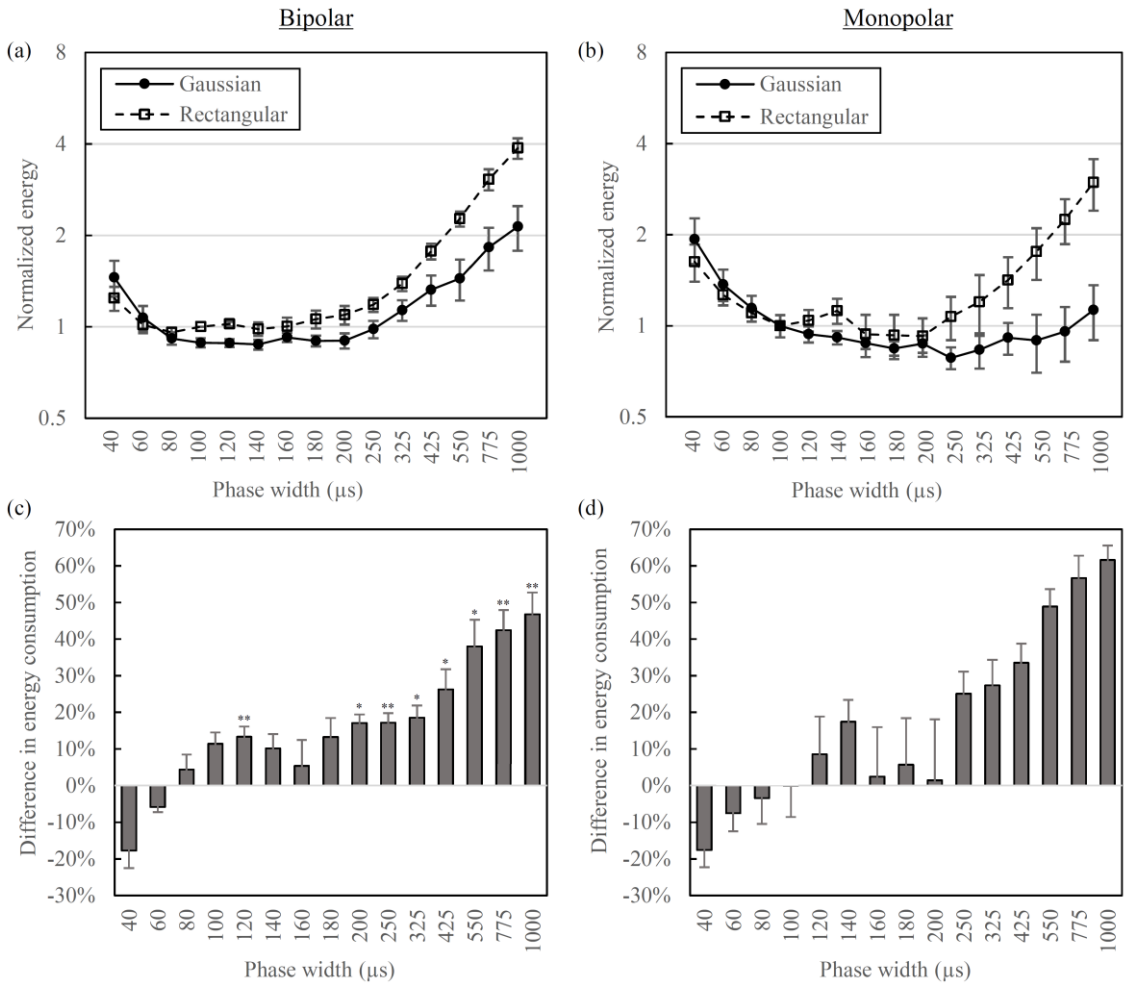

Figure 3.15 Energy efficiency of biphasic Gaussian waveform compared to biphasic rectangular stimuli. Data for 50% of maximal isometric twitch force with bipolar (left column: a, c) and monopolar electrodes (right column: b, d), mean +/- SEM (bipolar n=7, monopolar n=3). **a)**, **b)** Energy-duration curves normalized to energy consumption with rectangular pulses of PhW=100µs. **c)**, **d)** Energy consumption of Gaussian waveform compared with rectangular; positive values of "Difference in energy consumption" indicate that Gaussian pulses were more energy efficient.

Charge efficiency

For both electrode configurations the charge injection values required to elicit 50% of the maximum isometric twitch force are remarkably linear functions of the stimulation phase width (Bipolar: Figure 3.16.a, Monopolar: Figure 3.16.b). In both electrode setups and throughout the whole range of tested phase widths (40-1000µs), Gaussian stimulation required less charge injection than standard rectangular pulses to activate the target nerve. Absolute charge injection values never exceeded 0.5µC per phase, so the charge density per phase was always below 20µC/cm^2. This means the stainless-steel stimulation electrodes were operated within the limits of their specific charge injection capacity (Merrill, Bikson and Jefferys, 2005) and within the safe operating range (Shannon, 1992).

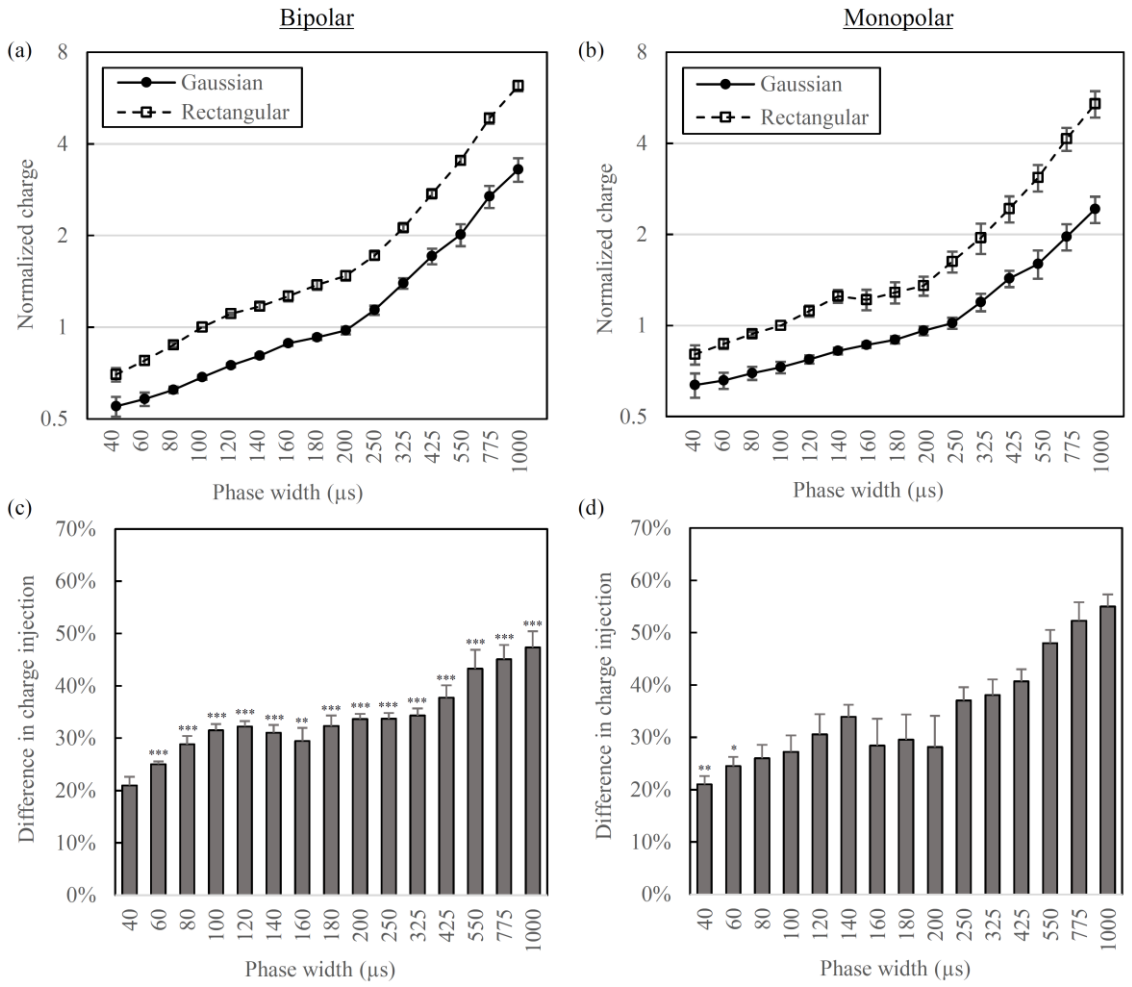

Figure 3.16 Charge efficiency of biphasic Gaussian waveform compared to biphasic rectangular stimuli. Data for 50% of maximal isometric twitch force with bipolar (left column: a, c) and monopolar electrodes (right column: b, d), mean +/- SEM (bipolar n=7, monopolar n=3). **a)**, **b)** Charge-duration curves normalized to charge injection with rectangular pulses of PhW=100µs. **c)**, **d)** Charge injection of Gaussian waveform compared with rectangular; positive values of "Difference in charge injection" indicate that Gaussian pulses were more charge efficient.

Bipolar case: The superiority of Gaussian pulses in terms of lower charge injection requirements compared to rectangular stimuli (in n=7 animals) was highly significant ($P<0.001$). Gaussian stimulation with the shortest tested phase width of 40µs required on average 20.9% (±1.6% SEM) less charge than rectangular pulses of the same duration. In the range of 50-200µs PhWs, the reduction in charge injection with Gaussian pulses ranges from 25.1% (±0.5% SEM) at 60µs to 33.7% (±0.9% SEM) at 200µs. In stimulation with the longest tested phase width of 1000µs Gaussian pulses needed on average 47.4% (±3.1% SEM) less charge than rectangular stimuli (Figure 3.16.c).

Monopolar case: The reduction of charge injection with Gaussian pulses in monopolar stimulation (in n=3 animals) was significant ($P=0.013$). At 40µs phase width Gaussian

pulses needed 21.0% (±1.6% SEM) less charge than rectangular stimuli to elicit the same force response. The average charge reduction achieved within the range of 50-200µs PhWs ranged from 24.5% (±1.8% SEM) at 60µs to 33.9% (±2.3% SEM) at 140µs. Stimulation with 1000µs phase width was on average 54.9% (±2.3% SEM) more charge efficient with Gaussian pulses (Figure 3.16.d).

Peak power

Throughout all tested phase widths and in both electrode configurations, the Gaussian stimulation waveforms were less power efficient, i.e. they required a higher maximal instantaneous power than the rectangular stimuli. ANOVA revealed the effect of waveform to be significant in both electrode configurations (bipolar: $P<0.001$, monopolar: $P=0.017$). The difference in maximum power between the compared waveforms decreased with increasing phase duration from approximately 230% at 40µs to 31.1% (±14.7% SEM, bipolar in n=7 animals) or 7.5% (±10.9% SEM, monopolar in n=3 animals) at 1000µs (Figure 3.17).

These substantially increased values of maximal instantaneous power are due to the higher stimulation amplitudes required with Gaussian pulses. The exemplar recordings in Figure 3.14 show two pulses (phase width 100µs) near the 50% threshold. The rectangular pulse has a stimulation amplitude of 500µA (Figure 3.14.a), whereas the Gaussian pulse needed 900µA to elicit the same level of neural activation (Figure 3.14.b). The increased current is associated with a higher voltage across the electrodes for the Gaussian (Figure 3.14.d) than for the rectangular pulse (Figure 3.14.c). As the instantaneous power across the electrodes is the product of stimulation current and voltage (see Equation 3.6), it scales approximately quadratically with the current. In the exemplary data of Figure 3.14, the higher stimulation amplitude led to a 153% increase in maximum instantaneous power. It increased from 231µW with the rectangular pulse (Figure 3.14.e) to 584µW with the Gaussian pulse (Figure 3.14.f).

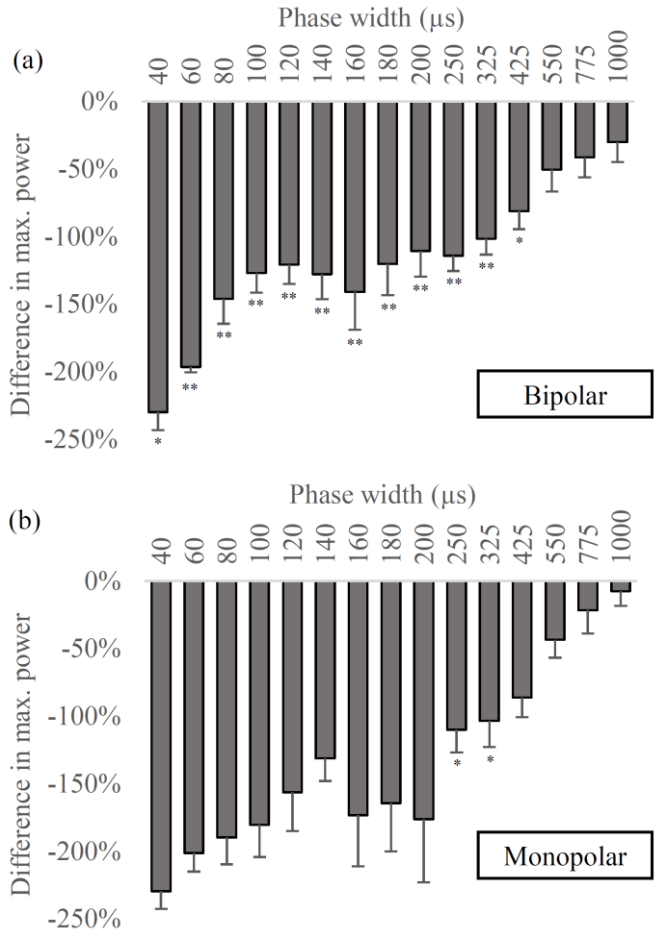

Figure 3.17 Difference in maximum instantaneous power of Gaussian waveform compared to rectangular in **a)** bipolar (n=7 animals) and **b)** monopolar stimulation (n=3 animals). Negative values of "Difference in max. power" indicate that Gaussian pulses had higher values of max instantaneous power.

3.3.4 Experimental findings set into perspective with published literature on non-rectangular waveforms

(IV. Discussion)

Following the findings of recent computational studies on energy optimal stimulation waveforms (Wongsarnpigoon and Grill, 2010; Forger, Paydarfar and Clay, 2011; Krouchev *et al.*, 2014), Gaussian shaped stimuli were compared against standard rectangular stimulation in a nerve-muscle preparation in anaesthetized rats in terms of energy, charge and peak power efficiency. In order to attain results that can be applied for practical applications such as cochlear implants or neuromuscular prosthetics, both commonly used electrode configurations, monopolar and bipolar stimulation, were tested. To further bring this investigation closer to practical implementation, instead of duration-dependent pulse shapes only one fixed Gaussian waveform was used for all phase widths and all tested stimuli were biphasic and charge balanced. In both electrode configurations,

Gaussian stimulation was found to be less energy efficient than rectangular pulses at short phase widths. However, at phase durations above approximately 80µs the Gaussian waveform becomes more energy efficient than the traditionally used rectangular stimulus. This superiority of the Gaussian pulse in terms of energy efficiency increases with increasing stimulation phase width up to 46.7% in bipolar and 61.6% in monopolar stimulation at the upper end of tested phase durations of 1ms. Energy savings in the so-called clinically relevant range of phase width (50-200µs) were less than the claims made in previous papers and did not exceed 17%. Furthermore, these energy savings did not take the additional energy requirement to generate such gaussian waveforms into account, so the realistically achievable savings might be even lower. We found that charge efficiency of Gaussian shaped stimuli was significantly greater than that for standard rectangular pulses with both electrode configurations. Neuronal activation was achieved with 21-55% less charge injection with the Gaussian waveform. In the range of 50-200µs PhWs a 25-33% reduction of charge injection was realised. However, the maximum instantaneous power was greater for Gaussian than rectangular stimuli over the whole range of phase widths. This disadvantage in peak power, which ranged from approximately -200% to -110% in the range of 50-200µs PhWs, decreased with increasing phase duration (Figure 3.17).

The general finding of increased energy and charge efficiency with Gaussian compared to rectangular stimuli fits well with the data from single axon models, which predicted Gaussian stimuli to be more charge efficient throughout all phase widths and more energy efficient at phase durations over approximately 60µs (Sahin and Tie, 2007). However, the observed extent of energy savings in the range of 50-200µs PhWs of only up to 17% is surprising in light of the predicted energy benefit of up to 60% with Gaussian stimulation waveforms in this so-called clinically relevant range (Wongsarnpigoon and Grill, 2010). The lower energy savings described in the present study might have partially originated from differences in the fixed Gaussian waveform used here (Equation 3.1) with the PhW dependent waveforms used by Wongsarnpigoon et al. Since we chose our Gaussian waveform to best match the average pulse shape used by Wongsarnpigoon et al. in the range of 50-200µs PhW, we expect little influence of PhW depend shape variations with our results in this range. However, the biphasic pulses generated by their genetic algorithm were not perfectly symmetrical, but the peak of the cathodic phase was shifted further away from the anodic phase (Wongsarnpigoon and Grill, 2010), which was not the case in the pulses used here (Equation 3.1). The asymmetrical shifting of the peak

effectively introduces a greater interphase gap (IPG) than a symmetric Gaussian pulse would have. It is known that the anodic phase of a biphasic pulse can abolish action potentials in near threshold scenarios at short PhWs (van den Honert and Mortimer, 1979; Gorman and Mortimer, 1983). Thus, the introduction of a (greater) IPG might lead to greater stimulation efficiency. It might be argued that the (limited) energy savings with biphasic Gaussian pulses at short PhWs are also a result of the separation of the stimulation phases compared to a biphasic rectangular pulse without IPG (compare Figure 3.14.a-b). Investigations of this hypothesis would require new experiments.

We found that the increase in energy and charge efficiency was accompanied by a increased peak power requirements, which extends the finding of Wongsarnpigoon et al. that no rectangular, exponential or ramp waveform was at the same time most efficient for energy, charge and power (Wongsarnpigoon, Woock and Grill, 2010). The benefits in charge efficiency in the range of 50-200µs PhWs with the Gaussian waveform were greater than those reported by Wongsarnpigoon et al., who found ramp pulses to be most charge efficient for 20-200µs phase duration with 5-18% less charge injection than required with standard rectangular pulses. Energy savings at long phase widths were similar to those reported for exponential waveforms based on a population model and *in vivo* work (Wongsarnpigoon, Woock and Grill, 2010). However, due to certain constraints in pulse shaping the effective part of the exponential pulses used in that study did not change as the phase width increased over approximately 0.3ms. The results were therefore misleading for longer phase durations as the authors conceded. By contrast, the Gaussian waveform used in the present study was scaled to fill the whole phase duration (compare Figure 3.14.b).

3.3.5 Gaussian shaped stimulation waveforms not beneficial for neuromodulation implants

(V. Conclusion)

The results of this study in terms of improved energy efficiency with Gaussian stimulation waveforms must surprise any dispassionate researcher in light of the predicted range of up to 60% energy savings in a so-called clinically relevant range of phase widths (50-200µs) (Wongsarnpigoon and Grill, 2010) since only moderate savings of up to 17% were observed. Furthermore, the comparison of maximum instantaneous power required with Gaussian and rectangular stimuli revealed that in the range of 50-200µs PhWs, these moderate energy savings were accompanied with profound increases in peak power.

While the energy savings could (if the additional instrumentational energy consumption is neglected) increase the number of pulses that a given battery can deliver by up to 17%, the 110% to 200% higher maximum power requirements would necessarily lead to an undesired increase in battery size. Thus, the tested Gaussian waveform is not advantageous to improve performance of implanted stimulation devices that operate at the range of 50-200µs phase widths. The need for a larger energy source clearly opposes the ambition for device miniaturization.

As all three measures of stimulation efficiency improved with increasing phase duration (in the case of peak power, a decrease in the disadvantage) we conclude that the implementation of the Gaussian stimulation waveform may have great potential especially for applications with long phase widths such as stimulation of denervated or partially denervated muscle (Salmons *et al.*, 2005; Kern, 2014). And for stationary therapeutic devices, where energy efficiency might not be as crucial as it is for battery powered devices, the significant increase of charge efficiency could increase stimulation selectivity by allowing electrode size to be reduced without exceeding safe limits of charge density. The significant improvement in charge efficiency of over 50% which we observed at 1ms phase width would allow the safe use of electrodes only half the size of those required with conventional stimuli. Such a reduction in electrode size would enable major improvements in applications like laryngeal (Cheetham *et al.*, 2015) or facial stimulation (Targan, Alon and Kay, 2000), where space is highly limited and coactivation of nearby innervated structures is undesired and may be painful.

This study provides promising results and limitations related to the practical implementation of Gaussian stimulation waveforms.

3.3.6 Addendum: Gaussian and "Gaussian-like" waveforms

Following the publication of the above study of neural stimulation efficiency with Gaussian shaped stimulation waveforms, the discussion of this subject was further advanced, commenced by a Letter to the Editor (Grill and Wongsarnpigoon, 2020). In their letter Grill and Wongsarnpigoon, authors of one of the three computational studies that identified Gaussian shaped waveforms as energy optimal, claiming up to 60% energy savings (Wongsarnpigoon and Grill, 2010), who also hold an U.S. patent for their method of deriving these Gaussian shaped stimuli with a genetic algorithm (GA) (Grill and Wongsarnpigoon, 2015), raised the following point:

The waveforms used in our study (Eickhoff and Jarvis, 2019) are so different from their GA waveform, that the limited extend of energy savings we reported does not challenge their predicted range of 5-60% relative energy savings with GA waveforms (Wongsarnpigoon and Grill, 2010). The differences between the waveforms are:

- Phase widths dependency: We used a fixed, phase widths independent Gaussian waveform, whereas their optimal GA waveform was phase widths dependent.
- Kurtosis: The peaks of the Gaussian waveform studied in our investigation were "less sharp" than those of the GA waveforms. The tails of our Gaussian waveforms approached zero, while their GA waveforms were truncated.
- Symmetry: We studied symmetrical biphasic Gaussian pulses, whereas the biphasic GA waveforms were coupled to rectangular anodic phases for charge balance.

Our response to their letter reiterates that we did neither intend nor claim to have used the *exact* GA waveforms described in their study (Eickhoff and Jarvis, 2020a). We discuss that our findings of only up to 17% relative energy savings are, despite of the described differences in the studied waveforms, very surprising in light of the predicted range of "5-60%" energy savings and propose further research to reconcile the reported ranges of potential energy savings.

The editorial letter presented below is published and copyrighted:

The only main differences between the published article and the present chapter are:

- Figure and equation numbers were adjusted to match the thesis chapter numbering.
- In the following letter we repeatedly refer to specific figures in our study as well as in the genetic algorithm study by (Wongsarnpigoon and Grill, 2010). For the sake of readability, we substituted the figure references to our study with cross references to the same figures as they appear in the present thesis. References to figures in the study by Wongsarnpigoon and Grill are indicated by an asterisk (e.g. *Fig 7.a-b).

Dear Editor,

We thank Professors Grill and Wongsarnpigoon for their detailed responses prompted by our recent publication (Eickhoff and Jarvis, 2019) in this journal. We welcome the opportunity we have had for discussion and thank the Editor for his invitation to make this further contribution.

We made our experiments partly in the light of the statements in the abstract of their relevant paper (Wongsarnpigoon and Grill, 2010) that energy optimal genetic algorithm (GA) waveforms *"resembled truncated Gaussian curves"* and that *"if used in implantable neural stimulators, GA-optimized waveforms could prolong battery life, thereby reducing the frequency of recharge intervals, the volume of implanted pulse generators, and the costs and risks of battery-replacement surgeries."*

The authors discussed the practical consequences of both a 5% increase and a 60% increase in energy efficiency in the final statement of the paper and acknowledged that to include the cost of generating the GA waveforms might change the predicted optimal shape. Although mentioned only once, a claim of up to 60% relative energy savings is of great interest to those who design and use neural stimulators. Based on our *in-vivo* investigation of neural stimulation efficiency with biphasic Gaussian waveforms, we reported an upper potential of 17% energy savings over rectangular biphasic pulses. Furthermore, we added the consideration of instantaneous power requirement in our paper to further inform this discussion. This is a crucial parameter, especially to set the practical performance of the sharp-peaked GA waveforms into perspective, given that they deliver the majority of the cathodic charge in a time much shorter than the nominal phase duration.

Gaussian-like stimulation waveforms

We examined the practical implications of three recent independent computational studies that identified Gaussian-like waveforms as energy optimal (Wongsarnpigoon and Grill, 2010; Forger, Paydarfar and Clay, 2011; Krouchev *et al.*, 2014). We chose our waveform based on the cathodic GA waveform in the *"clinically relevant range"*, identified by Wongsarnpigoon and Grill, of 50-200µs phase width (PhW). However our intention, as we described in the study, was not to rebuild the *exact* GA waveforms but rather *"to explore the findings of these recent computational studies in an animal model."*

Selection of waveform kurtosis

The waveform we tested was modeled on the kurtosis of the effective (cathodic charge injecting) part of the biphasic GA waveforms shown in *Fig 6, as nearly as they could be reconstructed from that figure. While the monophasic GA waveforms were truncated at the tails (*Fig 2), this was not the case for the biphasic GA waveforms (*Fig 6) which approached zero amplitude towards the tails and based on which we modeled our biphasic Gaussian waveforms (Figure 3.14.b). Although the waveform defined by equation (3.1) was a close match for the effective part of the GA waveforms in the range of 50-200µs phase width and we expected *"little influence of PhW dependent shape variations with our results in this range"*, we did not claim to have used the exact GA waveforms but rather stated the differences between the waveforms.

Differences to GA waveforms

We acknowledge the differences between the Gaussian and GA waveforms and discussed the main variations between the waveforms in our paper:

Pulse symmetry

The *"biphasic pulses generated by their genetic algorithm were not perfectly symmetrical, but the peak of the cathodic phase was shifted further away from the anodic phase (Wongsarnpigoon and Grill, 2010), which was not the case in the pulses used"* in our study (Eickhoff and Jarvis, 2019) and *"The asymmetrical shifting of the peak effectively introduces a greater interphase gap (IPG) than a symmetric Gaussian pulse would have."* The IPGs introduced by the near zero amplitude tails are most pronounced in longer duration GA waveforms that deliver the majority of the cathodic charge in a time much shorter than the nominal phase duration. This is not the case in our symmetric Gaussian pulses, that were *"scaled to fill the whole phase duration."*

Phase width dependency

"To bring the detailed computational findings closer to practical application, we reduced the phase-width-dependent variation of the optimal waveforms" to *"one fixed Gaussian waveform"*. We acknowledged that *"the lower energy savings described in the present study might have partially originated from differences in the fixed Gaussian waveform used here (Eickhoff and Jarvis, 2019) with the PhW dependent waveforms used by Wongsarnpigoon et al."*

Because of these differences in the waveforms studied, we carefully chose our words to recognize that earlier predictions of up to 60% energy savings with Gaussian-like waveforms are still worth exploring.

Although we mentioned these differences between our fixed symmetrical waveform and the phase width dependent, asymmetrical waveforms used by (Wongsarnpigoon and Grill, 2010), we did not explicitly discuss the difference in shape of the anodic charge balancing phase. The biphasic GA waveforms used by Wongsarnpigoon and Grill had *"rectangular charge-balancing anodic pulses"*, whereas we investigated symmetrical biphasic Gaussian pulses. Especially in light of the gap between the reported upper limits for relative energy savings (17% vs. 60%) with similar Gaussian-like cathodic waveforms, we believe further exploration of this detail as follows might be helpful to reconcile the two reported ranges of energy savings.

Further analysis to reconcile reported ranges of energy saving

Origin of 17% upper energy saving potential (Eickhoff and Jarvis, 2019)

We compared the energy consumption to reach 50% neural activation with biphasic Gaussian compared to biphasic rectangular pulses of same phase durations in a murine *in-vivo* model. All pulses were symmetric with equal cathodic and anodic phase durations, and the polarity was cathodic phase first. The kurtosis of the Gaussian waveform is described by equation (3.1) and was chosen based on the effective (cathodic charge injecting) part of the biphasic GA waveforms (*Fig. 6). The greatest relative energy savings of Gaussian pulses (in the 50-200µs range) of 17.1 ± 2.4% (mean of n=7, ± SEM) were observed with phase width of 200µs (Eickhoff and Jarvis, 2019).

Origin of 5-60% energy saving range (Wongsarnpigoon and Grill, 2010)

Although the authors provided calculations on the implications for battery replacement surgeries with this 60% figure, it was not stated in the paper whether this figure is based on *in-vivo* or computational investigations, nor if it was attained with monophasic or

cathodic GA paired with rectangular anodic stimuli. As we understand the paper, it does not originate from the *in-vivo* experiments, in which monophasic GA waveforms were compared against monophasic conventional waveforms and realized a maximum relative energy saving (in the 50-200µs range) of approximately 22% at 200µs phase width (*Fig. 5.b). Therefore, we assumed that the 60% figure might rather be rooted in the examination of biphasic GA waveforms in the computational population model (*Fig 7.c-d). Here the relative energy savings with cathodic GA waveforms (*Fig 6, $PW_{anodic}/PW_{cathodic} = 1$) coupled to *"rectangular charge-balancing anodic pulses"* were investigated (compare Figure 3.18.a). Cathodic phase first (*Fig 7.d) reached maximum energy savings of almost 50% and the highest energy savings achieved with anodic phase first (*Fig 7.c) appear to be approximately 70% compared to symmetrical rectangular pulses.

Proposed further investigations

Although the full biphasic waveforms are not depicted in the paper, in order to illustrate the following considerations, we reconstructed the GA waveforms from *Fig. 6 and added rectangular anodic pulses of the same nominal phase duration and equivalent amount of charge injection.

When energy consumption, which is proportional to I^2, is calculated across both phases of the biphasic GA pulses (as was the case in (Wongsarnpigoon and Grill, 2010)) it becomes apparent that the overall energy consumption of these waveforms is highly asymmetric with limited contribution of the anodic phase (Figure 3.18.b). This is not the case for conventional waveforms, such as the (symmetric) biphasic rectangular pulse, which Wongsarnpigoon and Grill used as comparator (*Fig 7.c-d), nor was it the case in our energy comparison of symmetric Gaussian versus symmetric rectangular waveforms (Figure 3.14.e-f) in which both phases contributed similarly to the overall energy consumption.

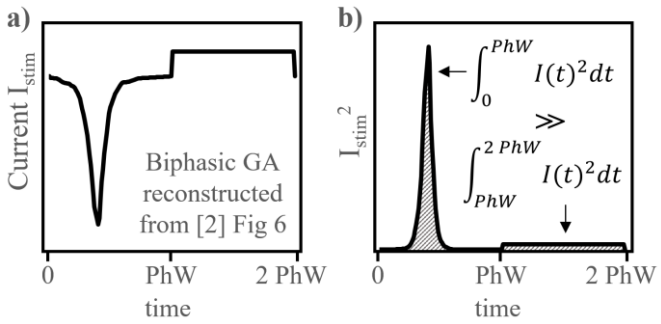

Figure 3.18 Biphasic GA waveform. a) Biphasic GA current waveform delivers the majority of its cathodic charge in a time frame much shorter than the nominal PhW, while using the whole nominal PhW for low anodic amplitude charge balancing (reconstructed from *Fig 6, $PW_{anodic}/PW_{cathodic}$ = 1, PhW=0.1ms, cathodic phase first). **b)** Integration of $I_{stim}2$, which is proportional to energy consumption, reveals a strong asymmetry with limited influence of the anodic phase to the overall energy consumption.

The anodic phase of the GA waveform has such low energy consumption because of its lower anodic amplitude. The use of this lower anodic amplitude is made possible by the effectively shorter cathodic phase width of the GA waveform. The GA waveform therefore delivers its cathodic charge in a time frame much shorter than the nominal phase width. Most biphasic GA waveforms delivered over 90% of the cathodic charge in much less than half of the nominal phase duration, while during the rest of the phase charge injection was near zero. It is well known that the energy-duration relationship has a minimum at the so-called chronaxie, and so the use of the term *"phase width"* is more than just a matter of nomenclature. It could be argued that the comparison made in *Fig 7.c-d (which may be the origin of the 60% energy saving figure) is a comparison of pulses of different phase widths, with the GA waveforms being closer to chronaxie. We agree with the authors, that the charge delivery in a time shorter than the nominal phase width can not be the sole mechanism by which GA waveforms perform better than conventional waveforms, because as they state *"one would expect that at a given PW, the GA could produce any waveform that was produced at a shorter PW bounded by tails of zero amplitude"*, which was not observed (Wongsarnpigoon and Grill, 2010).

For charge balance however, the biphasic GA waveforms harness the whole anodic phase duration, and thus achieve a low anodic amplitude resulting in a very low anodic energy consumption. This explanation for the much larger energy savings in *Fig 7.c-d is further supported by the fact that once the phase duration ratio (PWanodic/PWcathodic) was increased, the anodic energy consumption of all waveforms was reduced (*Fig 7.e-h). In this case, the superiority in energy efficiency of the biphasic GA waveforms was

significantly reduced and closer to the range reported for monophasic GA waveforms (up to approx. 22% at 200µs phase width *Fig. 5.b) or symmetrical Gaussian waveforms (17.1 ± 2.4% at 200µs phase width (Eickhoff and Jarvis, 2019)).

Conclusion

In order to reconcile the gap between the reported upper ranges of energy saving potential with Gaussian and Gaussian-like stimulation waveforms (17% vs 60%), we have highlighted the differences between our Gaussian stimuli and the GA waveforms used in previous computational investigations (*Fig 6). Further we explore the principle that the benefit of biphasic GA waveforms (*Fig 7.c-d) of up to 60% energy savings might partially be the outcome of an effectively shorter (and thus closer to chronaxie) cathodic phase width, while still using the whole nominal phase width (which determines the comparator symmetrical rectangular pulse) for low amplitude anodic charge balance.

Both these pulse variations (shorter effective phase width and asymmetric, low amplitude charge balance) are not, we would argue, properties of a particular waveform. To discriminate between the effect to reduce energy consumption of a particular waveform kurtosis or other waveform variations such as IPGs, asymmetric low amplitude anodic phases and phase duration, further research is warranted (Figure 3.19).

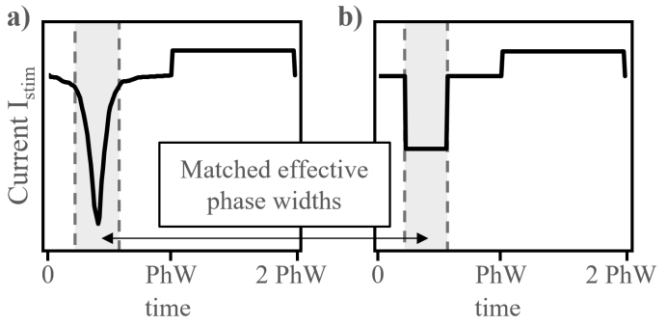

Figure 3.19 Proposed further comparison to discriminate between the effect to lower energy consumption of a particular cathodic kurtosis and other waveform variations. a) Biphasic GA waveform effectively delivers majority of its cathodic charge in a time much shorter than the nominal PhW (90% charge injection highlighted in dashed bars), has an IPG and an asymmetric low amplitude anodic phase (reconstructed from *Fig 6, $PW_{anodic}/PW_{cathodic}$ = 1, PhW=0.1ms, cathodic phase first). In order to assess the performance of a particular cathodic waveform kurtosis, the ideal conventional comparator pulse **b)** should perhaps have other waveform variations such as IPG, effective PhW and anodic amplitude in common.

Further, the above considerations clearly illustrate why we feel it is crucial to take into account and to report maximum instantaneous power as well as energy consumed. The

concentration of charge delivery into a small part of the phase width inevitably increases this parameter, which has implications for battery size or voltage multiplication circuitry.

Jonathan C. Jarvis, PhD

Professor of Sport and Exercise Sciences

Liverpool John Moores University

J.C.Jarvis@ljmu.ac.uk

Steffen Eickhoff, M.S.

PhD Candidate in Biomedical Engineering

Liverpool John Moores University

S.Eickhoff@2017.ljmu.ac.uk

4 DENERVATED MUSCLE STIMULATION

In this chapter, a series of 7 terminal rat experiments is presented that investigated properties of the denervated extensor digitorum longus muscle as well as strategies to use electrical stimulation to activate such muscle in the absence of innervation. Many findings reported here are of preliminary nature and raise some fundamental research questions. The summary of our first observations and unanswered questions in this chapter is intended to encourage future investigations.

The stimulation of denervated muscle will require the use of muscle surface electrodes, a configuration dissimilar from the general methods (as described in Chapter 2) used in the nerve stimulation studies. Therefore, in order to relate the observations with muscle surface electrodes with the body on knowledge attained with nerve stimulation (Chapters 3 and 5), two initial experiments were conducted in healthy rats without nerve impairment.

In the first experiment recruitment curves for monophasic rectangular pulses with amplitudes from 50 to 1000µA (in steps of 50 µA) and 100µs phase width applied over monopolar electrode configurations were recorded. We compared monopolar nerve stimulation of the CPN, monopolar EDL muscle surface stimulation with a centrally placed stainless steel disk electrode (diameter of 4mm), and monopolar intramuscular stimulation with an approximately 5mm long inserted uninsulated stainless steel electrode wire (Figure 4.1.a). A relay unit was used to switch between the active stimulation electrodes under computer control while the return electrode was in all cases a hypodermic needle under the dorsal skin of the animal.

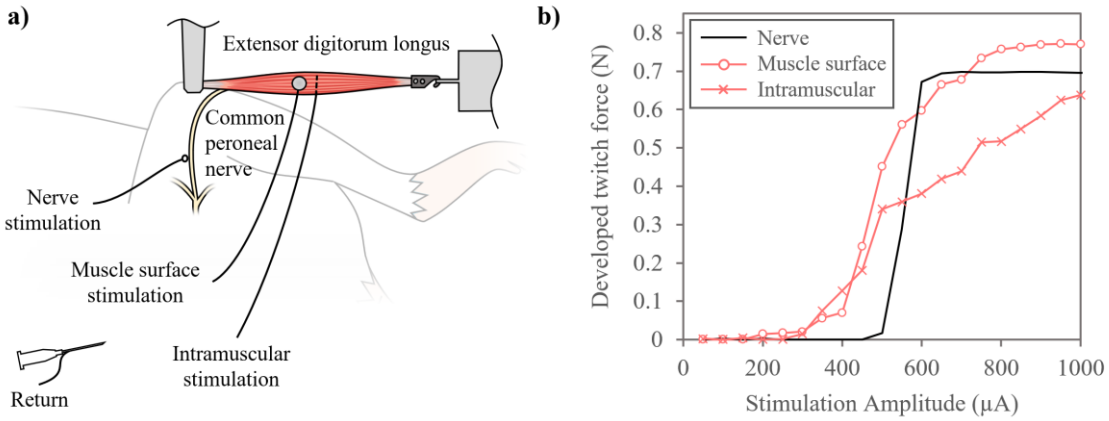

Figure 4.1 Monopolar nerve versus muscle surface versus intramuscular stimulation in a healthy preparation. a) Experimental setup to compare stimulation via a monopolar loop electrode at the CPN against stimulation with a monopolar circular (4mm) EDL muscle surface electrode and a monopolar intramuscular electrode wire. **b)** Recruitment curves for monophasic 100µs stimulation with nerve (black) and muscle (red) electrodes. Twitch force responses to nerve stimulation reach a stable full recruitment plateau at approximately 0.7N. Stimulation via muscle electrodes begins to elicit neuromuscular recruitment at lower amplitudes (200-500µA). Stimulation with muscle surface electrodes exceeds the full activation plateau of nerve stimulation at high amplitudes (of approx. 700µA and above).

In the second experiment with a healthy rat, a bipolar pair of loop electrodes was placed at the common peroneal nerve, approximately 5mm distal to the point it branches off the sciatic nerve. The more distal electrode was used as active stimulation electrode and the charge was returned over the more proximal nerve electrode. For muscle surface stimulation, a bipolar pair of circular electrodes (diameter of 4mm) was manufactured from thin stainless steel sheet metal and placed opposite to each other, centrally on the EDL muscle (Figure 4.2.a). A relay unit was used under computer control to switch between the muscle surface and nerve electrodes. Monophasic rectangular pulses with phase widths of 200, 400, 600, 800, and 1000µs and amplitudes from 200µA to 5mA (in increments of 200µA) were applied in random order via both sets of stimulation electrodes (Figure 4.2.b).

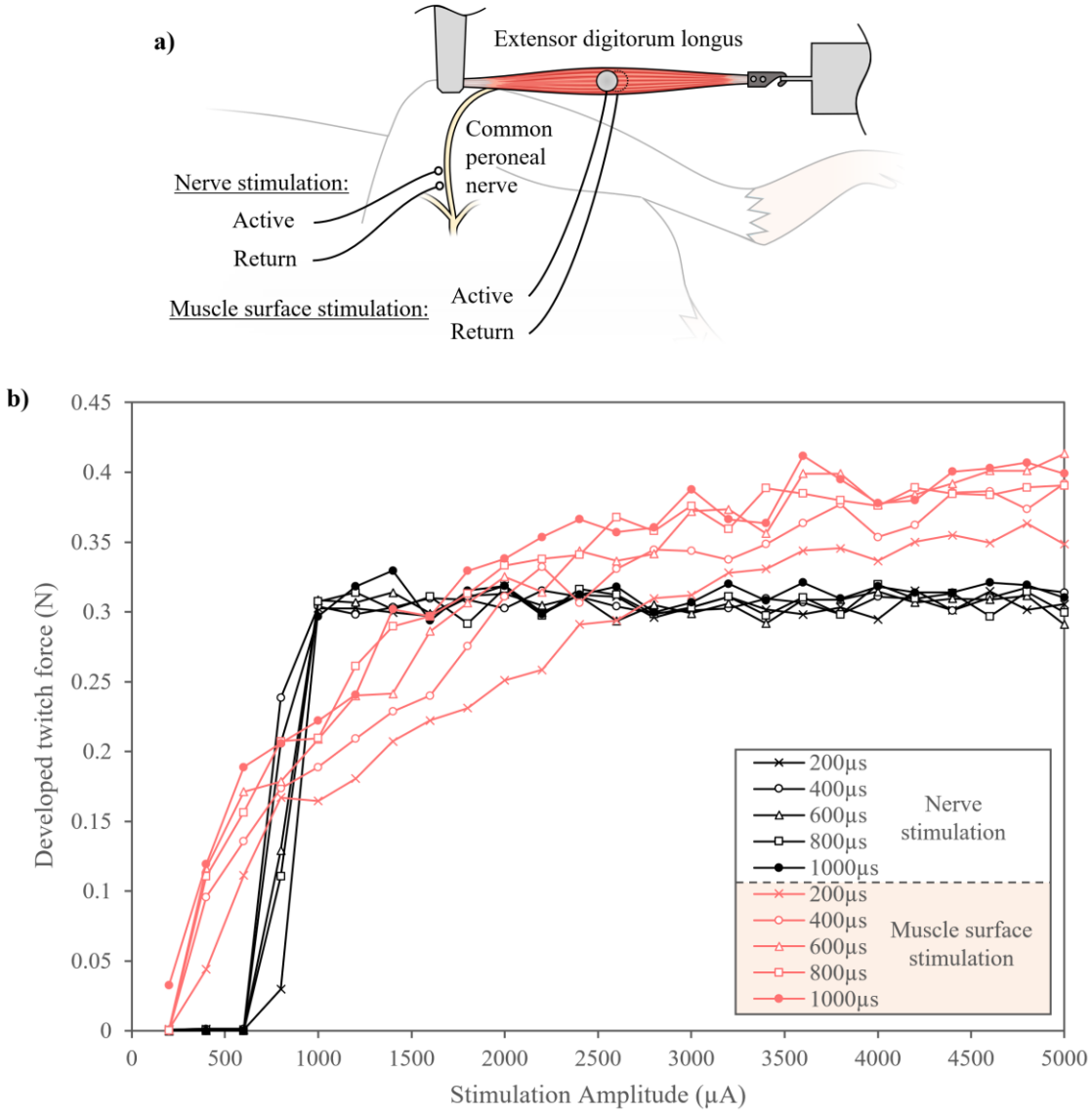

Figure 4.2 Nerve versus muscle surface stimulation in a healthy preparation. a) Experimental setup to compare stimulation via a bipolar pair of loop electrodes at the CPN against stimulation with a bipolar pair of circular (4mm) muscle surface electrodes. **b)** Recruitment curves for stimulation with nerve (black) and muscle surface (red) electrodes. Twitch force responses to nerve stimulation reach a stable full recruitment plateau at approximately 0.3N. Stimulation via muscle surface electrodes begins to elicit neuromuscular recruitment at lower amplitudes (200-600µA) and exceeds the full activation plateau of nerve stimulation at high amplitudes (of approx. 2mA and above).

Stimulations applied over the nerve electrodes resulted in the characteristic recruitment behaviour which we regularly observed using this configuration. Upon increasing the amplitude, the elicited twitch force increases until it reaches a full activation plateau which it does not exceed, not even at very high supramaximal intensities. The recruitment behaviour in Figure 4.2.b appears to be rather step-like than sigmoidal, but this is only due to the wide amplitude increments of 200µA that we chose in order to probe a wide

parameter space in a well-controlled timeframe. Finer amplitude increments would result in the typical sigmoidal recruitment curve but would require a higher number of pulses and thus a longer recording period.

The recruitment behaviour with stimulations applied over the muscle electrodes surprised us in multiple ways. Due to the lower charge density with the larger surface electrodes (5mm uninsulated length of the intramuscular electrode and 4mm diameter of the muscle surface electrodes), we expected to activate the terminal nerve branches at higher amplitudes than those required with the smaller nerve loop electrodes. Further it was anticipated that the partial covering of the EDL with the relatively small muscle surface electrodes (the two circular 4mm electrodes of experiment 2 (Figure 4.2) covered approximately 10% of the EDL surface) would lead to would lead to partial motor pool activation and lower twitch force responses. However, the experimental observations dismissed both these expectations as the threshold for activation was lower with muscle surface (and intramuscular) stimulation and the elicited twitch force responses exceeded those with nerve stimulation (in case of the muscle surface electrodes). Further, and this observation represents some challenges to the experiments with denervated muscle stimulation that are described below, no clear full activation plateau was reached with muscle surface stimulation. Both, increasing phase width and stimulation amplitudes, even up to the instrumentational limit of 5mA, continued to increase the generated twitch force. This makes it difficult to determine control pulse parameter for normalization, as no obvious full activation level can be defined.

These fundamental questions remain open and further research towards answering them be strongly encouraged:

- What causes the lower thresholds for activation with muscle surface compared to (smaller) nerve loop electrodes in a healthy preparation? In healthy neuromuscular preparations, stimulation at the muscle surface (and intramuscular stimulation) will lead to activation of the terminal nerve branches rather than direct activation of muscle tissue as the later has significantly higher threshold for activation. Might the epineurium connective tissue sheath have an electrically shielding effect at the proximal nerve stimulation site and thus lead to higher activation threshold than compared to stimulation at the muscle surface? Further research could investigate this hypothesis by carefully dissection of the connective tissue at the nerve stimulation site.

- Why does stimulation with muscle surface electrodes elicit higher twitch force values, even with very partial muscle coverage? Maybe the greater spatial distribution of the terminal nerve branches at the muscle surface leads to a temporally less synchronous activation than with stimulation of the CPN. This asynchronicity of individual motor unit activations might lead to higher "fused" twitch forces that one synchronous activation of all motor units that is anticipated with nerve stimulation. Future investigations could study the influence of electrode size and position (especially in relation to the motor point (i.e. the location of innervation with highest motor endplate density).
- Why did we not observe a stable force plateau with muscle surface stimulation? Once all motor units are recruited, the twitch force response should not increase further? How can we explain the "more is always better" phenomenon that we observed (in terms of both phase width and amplitude). Maybe the electrical field of the stimulation, besides activating terminal nerve branches, directly influences calcium release mechanisms in the muscle membrane?

Besides exploring the general recruitment behaviour with single pulses applied over surface electrodes, we used one of these healthy innervated preparations to attain a baseline value for stimulation with doublets. For fast twitch muscle such as the EDL it has been shown that an ideally spaced doublet, that is with an ideal interpulse interval (IPI), can generate more than twice the twitch force-time integral (FTI) of a single pulse (Kwende, Jarvis and Salmons, 1995). This phenomenon has been labelled the *"doublet effect"* and can be harnessed to start a stimulation burst of a given frequency (e.g. 30-50Hz for tetanic contraction) with an ideal IPI doublet to increase stimulation efficiency. Temporal aspects of calcium ion release and the momentum required to overcome the elastic series element titin have been suggested as rationale for this doublet effect in fast type muscles (Kwende, Jarvis and Salmons, 1995).

Doublets of monophasic pulses (phase width of 100µs and amplitude of 5mA) with IPIs from 10µs to 150ms have been tested in this one healthy preparation with stimulation via muscle surface electrodes and in random order. The normalized force-time integral (nFTI) was determined by division of the FTI of the tested doublets by the FTI of a single pulse. Figure 4.3 shows a characteristic plot for nFTI over IPI for a healthy fast muscle. Doublet with IPIs of less than approximately 1ms do not elicit nFTIs of greater than 1 (Figure 4.3.b), as the neuromuscular preparation is in absolute refractory period (ARP). Upon further increase of the IPI the second pulse of the doublet "leaves" the ARP, becomes

effective and elicits a second muscle activation and thus a higher fused twitch force. The doublets elicit largest nFTIs above 3.5 with IPIs between 3 and 8ms (Figure 4.3.c). IPIs of 10ms and above lead to a separation of the two single twitches and the nFTI decreases to a value of 2 (Figure 4.3.d).

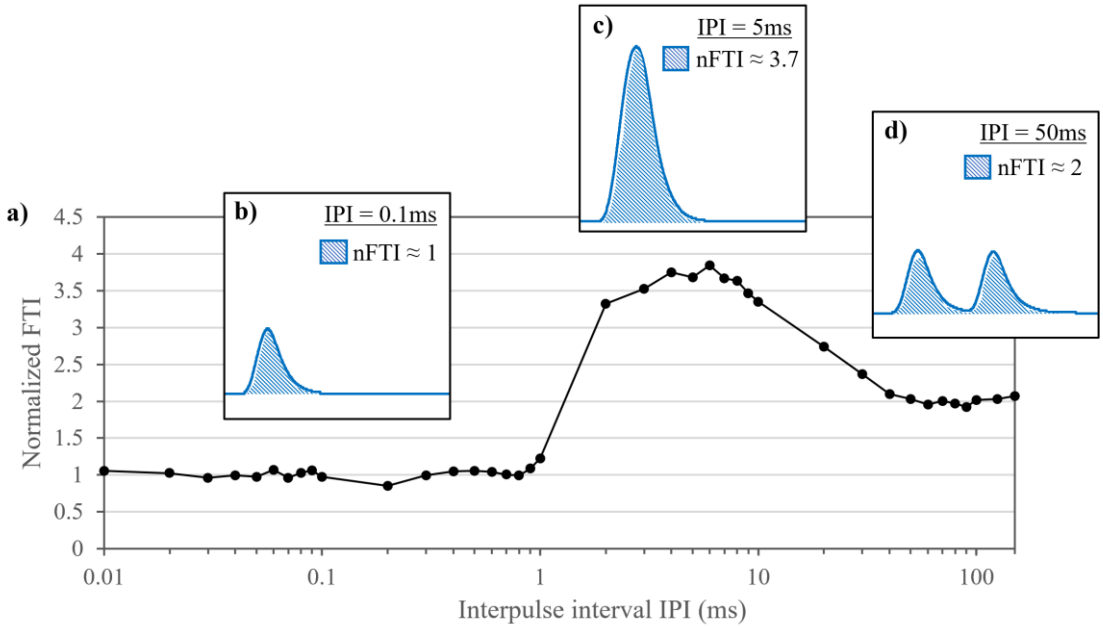

Figure 4.3 Doublet stimulation in a healthy preparation with muscle surface stimulation. **a)** Doublets (monophasic pulses, phase widths 100µs, 5mA amplitude) with interpulse intervals (IPIs) between 10µs and 150ms were tested in randomized order. **b)** Doublets with IPIs below 1ms elicit normalized force-time integrals (nFTIs) of 1, indicating that the second pulse of the doublet falls into the absolute refractory period (ARP). **c)** IPIs of 3 to 8ms result in ideally fused twitches with maximal nFTIs above 3.5, whereas **d)** greater IPIs lead to separation of the two twitches and nFTIs of 2.

4.1 Time course of denervation of the rat hindlimb dorsiflexors

The two tests described above (recruitment curves for wide range of phase widths with nerve versus muscle stimulation (Figure 4.2), and doublet test with muscle surface stimulation (Figure 4.3)) on the example of one healthy preparation have been repeated in two animals with motor nerve injury.

A crush injury of the common peroneal nerve (CPN) was created using a standardized method (Vareĵao *et al.*, 2004) of clamping the nerve just distal to where it branches from the sciatic nerve for 30 seconds with a Castroviejo needle holder (approximately 2mm wide jaws). In one animal (Figure 4.4.a.c) the nerve crush injury was introduced 24 hours prior to the stimulation experiment, in the second animal (Figure 4.4.b.d) the injury was created 72 hours before stimulation.

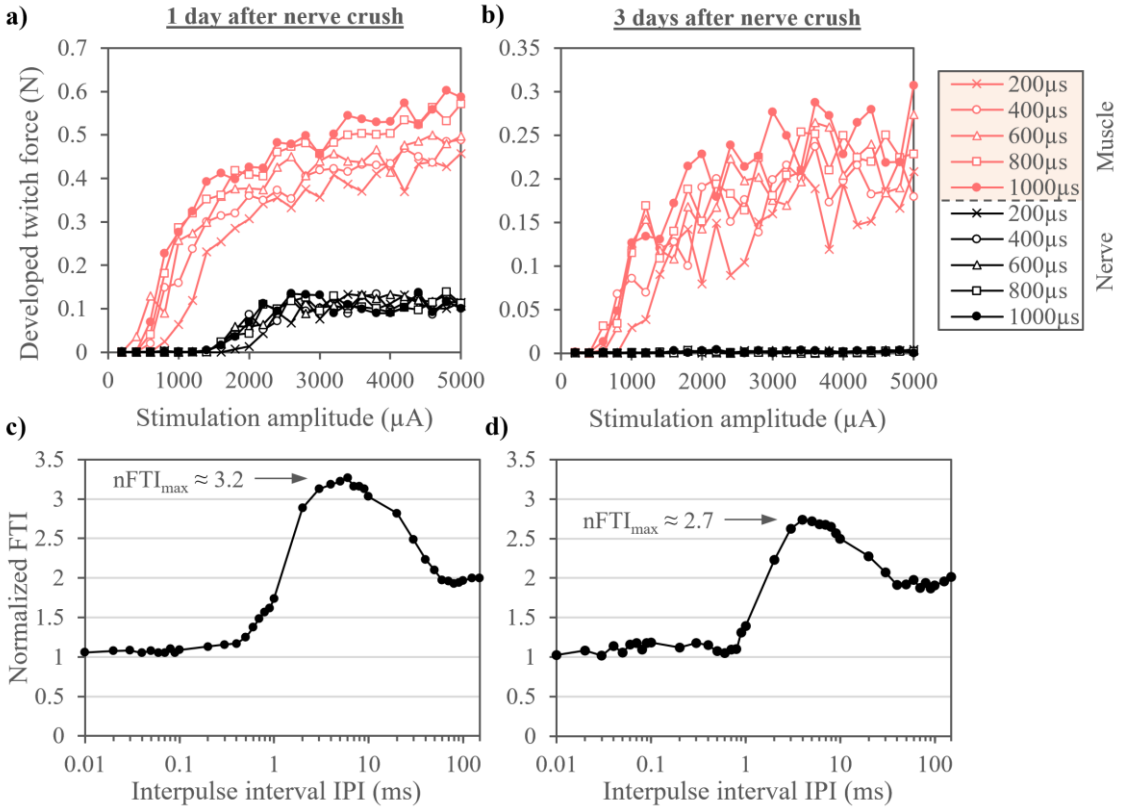

Figure 4.4 Recruitment curves and doublet test 1 and 3 days after nerve crush injury a) and **b)** recruitment curves for stimulation with phase width 200 to 1000µs via muscle surface electrodes (red) and nerve electrodes (distal to nerve crush injury, black). Excitation via nerve stimulation is strongly reduced 24 hours after nerve crush injury, and completely lost 72 hours after the injury. Doublet test with muscle surface stimulation indicates a decrease of the achievable doublet effect with increasing time after nerve crush injury. **c)** One day after nerve injury the nFTI reaches a maximum of approximately 3.2, whereas **d)** the maximum nFTI after three days lowered to approximately 2.7.

24 hours after the introduction of the CPN crush injury, excitability via nerve stimulation (approximately 5mm distal to the nerve injury) was already drastically reduced to approximately 25% of the twitch force generated with muscle surface stimulation (Figure 4.4.a). After 72 hours no muscle twitch could be elicited with nerve stimulation (Figure 4.4.b), indicating that the motor axons have fully degenerated by that time. A doublet test with muscle surface stimulation further revealed gradual changes in the maximal achievable nFTI (Figure 4.4.c-d). One day after the nerve crush injury a maximal nFTI of 3.2, a value still in the range of typical healthy preparations as we will show below (Figure 4.5.b), was achievable with an ideal IPI of 6ms. Three days after the injury, the maximal nFTI decreased to approximately 2.7, indicating that the denervated muscle transitions to the physiological behaviour of slow twitch muscle.

While it is a well-established fact that, following spinal cord injury, muscles lose their characteristic mosaic type I and type II fibre pattern and become composed predominantly of fast (type II) fibres, this fibre re-composition does not take place immediately. Reviewing the literature on analyses of biopsies obtained from various muscles of human spinal cord injured subjects, Castro et al. describe an almost complete absence of type I (slow) fibres 2–11 years after the injury. However, there was no clear evidence that any significant fibre type transformation occurred in the first 1 to 6 months after injury (Castro *et al.*, 1999). While there is not a comprehensive body of literature on the acute physiological changes of denervated muscle within the first days of injury with regard to single twitch to tetanic contraction ratios, the shift toward slow twitch characteristics that we describe agrees well with an earlier report by Yeagle et al. In their study on the contractile properties of denervated fast twitch rodent muscle, the authors reported significantly increased contraction times (that are characteristic for slow twitch muscle) within the first 8 to 11 days following nerve injury and discuss the possibility of a decreased muscle fibre conduction velocity (MFCV) as rationale for this observation (Yeagle, Mayer and Max, 1983). Decreased MFCV might explain the early changes in muscle twitch characteristics towards those of slow twitch muscle that we observed three days after the nerve injury, as lower MFCV has been identified as one of the earliest changes in denervated muscle (Wu *et al.*, 2014). Further investigations, including MFCV measurements and twitch force recordings, ideally in a time course from acute nerve injury over complete denervation to fully reinnervated muscle, are warranted to test this assumption.

With increasing time of denervation, it became increasingly difficult to identify a sensible force value that might represent full motor pool activation with muscle surface stimulation. For this reason, in the following experiments described below (that studied ten day denervated muscles), a qualitative comparison was sought by studying both the denervated test muscle and the healthy control muscle of the contralateral (right) hindlimb.

4.2 N-let stimulation of denervated muscle

While we observed a complete loss of excitability with nerve stimulation three days after the nerve crush injury, literature on denervation of the rat hindlimb suggests that functional and morphological changes are most severe 1 to 2 weeks after the nerve injury (Vareĵao *et al.*, 2004). Therefore, the following study that seeks to investigate optimal stimulation strategies for fully denervated muscle was carried out in three rats ten days after a nerve crush injury to the left CPN. The aim of the experiments described below was to identify if ideally spaced doublets, 3-lets, and 4-lets can be used to optimize stimulation patterns to activate denervated muscles most efficiently. The following tests were conducted on both the ten day denervated test muscle (left EDL) and the contralateral, healthy control muscle (right EDL).

First, a strength duration curve was probed for the first visible twitch force response with biphasic rectangular pulses. This allowed to measure the rheobase amplitude and thus to determine the chronaxie. A typical chronaxie value for the denervated test muscle was 2ms, significantly higher than for the healthy control muscle with chronaxie values of 100 to 200µs. This observation is in line with published literature on denervated muscle stimulation, reporting that longer phase widths (of even up to several hundred milliseconds in severe, long term denervation) are required to activate denervated muscle (Hofer *et al.*, 2002; Mayr *et al.*, 2002). In Chapter 5 we summarize a study of the influence of such long stimulation pulses, used to active denervated muscle tissue, on nerves.

Once the chronaxie time was determined, a recruitment curve was recorded to identify the amplitude at which full neuromuscular activation (i.e. maximal twitch force) was achieved. As discussed above (Figure 4.2.b), the determination of this full activation level for muscle surface stimulation was complicated as the twitch force did not plateau but kept increasing even at very high amplitudes. For this reason, we typically chose the maximum deliverable amplitude (due to instrumentational limitations) of 5mA as "full activation" amplitude when no other value could sensibly be chosen.

Pulses parameterized with these two values, phase width equal to the chronaxie time and the amplitude set to reach full recruitment, were now used to determine the ideal interpulse intervals (IPIs) for doublets, 3-lets, and 4-lets. First, in randomized order, doublets with varying IPIs between 100µs and 150ms were tested and the value resulting in the largest nFTI identified as ideal doublet. This doublet was then used as basis for the 3-let test, where a third pulse with varying IPI was added. Again, the ideal IPI was

determined and used as basis for the 4-let test. On the 10 day denervated test side, ideal IPIs were typically between 30 and 100ms but with very little increase in the achievable nFTI. Never did the nFTI of an additional pulse add more than 1 to the nFTI of the previous n-let, in other words, in denervated muscle no doublet effect was observed (Figure 4.5.a). On the healthy control muscle however, ideal IPIs were shorter, typically between 3 and 20ms, and achieved significant increases in nFTI in this "sweet spot" (Figure 4.5.b). The ideal IPI was shorter for the first pulse pair, i.e. the initial doublet, with values between 3 and 10ms. This observation is in line with previous reports of the benefit of a single high frequency doublet at the beginning of a fixed frequency stimulation burst (e.g. 50Hz = 20ms IPIs) to activate healthy muscle (Kwende, Jarvis and Salmons, 1995).

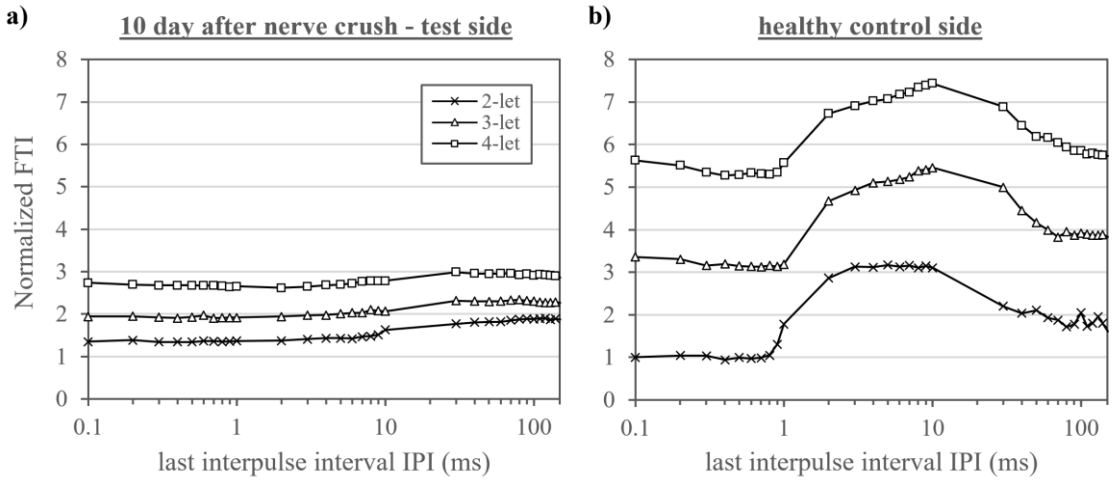

Figure 4.5 N-let test in **a)** 10 day denervated EDL and **b)** healthy control EDL muscles. IPIs between 0.1 and 150ms were tested in randomized order and the IPIs resulting in the largest normalized force-time integral (nFTI) were used as basis for the next n-let. Data are mean of n=3 animals.

The data presented in Figure 4.5 stresses the physiological differences between healthy and denervated muscle and shows that there is no benefit in using a high frequency doublet at the beginning of a stimulation burst to enhance the activation of denervated muscle. The maximal nFTI of an ideally spaced 4-let only reaches a value of approximately 3 in denervated muscle, whereas it exceeds 7 in the healthy control muscle. As these values are normalized by the FTI of a single twitch, they can also be understood as twitch to (n-let) tetanus ratios in terms of force-time integral. Figure 4.6 shows force frequency plots of the ten day denervated and the healthy control muscle for one representative experiment. The 10 day denervated muscle shows many properties that are

characteristics for a slow twitch muscle such as higher (i.e. more complete) single twitch force responses, longer relaxation times, and lower peak tetanus to single twitch ratio.

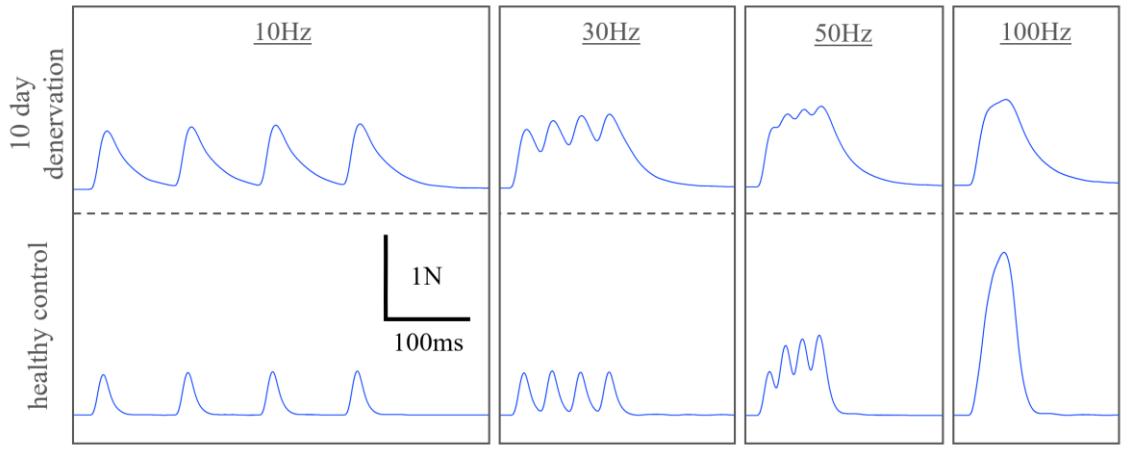

Figure 4.6 4-let force-frequency test in (top) 10 day denervated EDL and (bottom) healthy control EDL muscles. The 10 day denervated muscle has higher single twitch force responses, longer relaxation times, and a lower tetanic peak force than the healthy control muscle.

5 THE INFLUENCE OF LONG PULSE DURATION ON NERVE ACTIVATION

5.1 Observation of additional neuromuscular recruitment with long duration pulses

(I. Introduction)

Electrical stimulation (ES) is a collective term for the application of electrical charge to modify the activity of a target excitable tissue. This target tissue can either be a central or peripheral nervous structure or a muscle. The modulatory effect is achieved by the interaction of the electric field, induced by the (extracellular) charge injection, with voltage gated ion channels in membranes within the excitable target. Electrical nerve stimulation finds broad application in medical devices and therapies such as cochlea stimulation for hearing loss, cardiac pacemaking to correct arrythmias, and therapeutic and functional spinal cord and deep brain stimulation. Electrical stimuli are delivered via implanted or transcutaneous electrodes and are typically biphasic to achieve zero net charge injection, and thus to reduce detrimental electrochemical processes at the electrode-tissue interface (Shannon, 1992), (Merrill, Bikson and Jefferys, 2005). Besides overall charge balance, stimulation waveform, frequency and phase duration (or phase width) are important parameters that influence the efficiency and safety of ES protocols (Grill, 2018). Phase widths commonly used for nerve stimulation are below 1ms and typically, to allow to use the least amount of electrical charge (which is the product of phase duration and amplitude) to activate the nervous target, one chooses the shortest feasible stimulation phase width. This feasibility depends on a function called “strength/duration-curve” and is limited by the amplitude that the stimulator can safely deliver. Usually in commercially available nerve stimulation devices the range of phase widths between approximately 90-200µs finds application and a wider range of phase widths is investigated in ES research.

In ES applications to activate muscle contractions, it is important to recognize the known difference between stimulation of healthy (i.e. innervated) and denervated muscle. Because nerve tissue has much lower thresholds for activation with ES than muscle tissue, in the innervated case, even if the stimulation is directly applied to a muscle belly, the electric field is considered first to activate the terminal nerve branches which then activate the muscle fibres of their respective motor units. Since in such scenarios the electric field does not directly activate muscle tissue but actually elicits activity in neural tissue, even though muscle contraction is desired, such applications are to be categorized as nerve stimulation. Direct activation of muscle tissue with ES is relevant in absence of neural innervation, i.e. in the case of denervated muscle. Direct stimulation of denervated muscle requires significantly higher stimulation amplitudes (Ashley *et al.*, 2005; Cheetham *et al.*, 2015) and longer stimulation durations of, in cases of severe denervation, up to several hundred milliseconds (Hofer *et al.*, 2002; Mayr *et al.*, 2002). This latter parameter represents a major challenge when the aim is to elicit tetanic contractions, e.g. for muscle training to prevent or reverse atrophy, as these long stimulation durations limit the maximal possible pulse frequency (Salmons *et al.*, 2005). Our laboratory investigated the influence of rectangular and non-rectangular waveform variations, such as subthreshold pre-pulses (Eickhoff and Jarvis, 2020b), interphase gaps and Gaussian shaped pulses (Eickhoff and Jarvis, 2019), on neural stimulation efficiency (Chapter 3). For these investigations we used a rodent *in vivo* nerve muscle preparation, stimulating the nerve and measuring the muscle force or in some cases the distal ENG signal to measure neural activation, and studied a range of stimulation phase widths from 20 to 1000µs. While for most of this range the neuromuscular recruitment behaviour followed the characteristic sigmoidal dose-response relationship, at the upper end of the investigated range of phase widths we consistently observed unexpected additional recruitment, above the level of full motor unit activation. We conducted a series of experiments to try to explain this observation and here we report 5 experiments that represent milestones on our investigative journey. We discuss potential implications of these findings for stimulation of denervated and partially denervated muscle, where long duration electrical pulses are used. Further, these observations represent a challenge to state-of-the-art biophysical computational models of extracellular nerve stimulation.

5.2 Experimental journey to investigate the additional recruitment

(II. Materials and Methods)

Animals and surgical Procedure.

Experiments were carried out in n=5 adult Wistar rats.

Home Office project licence: PPL 40/3743.

Stimulation electrodes: Active electrode distal, bipolar return electrode proximal, and hypodermic needle in dorsal skin as monopolar return electrode (in Experiment 5).

Recording electrodes: Approximately 10mm distal to stimulation electrodes (in Experiments 4 and 5).

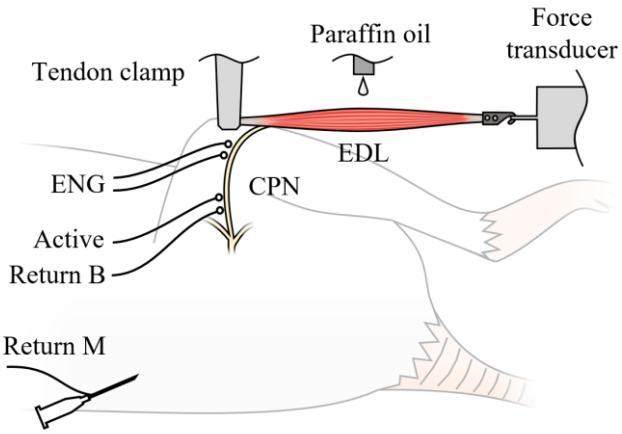

Figure 5.1 Experimental setup: In-vivo nerve muscle preparation in anaesthetized rats. Electrical stimulation was applied to the common peroneal nerve (CPN) via an active electrode. In the bipolar electrode configuration, charge was returned via Return B at the CPN. In the monopolar electrode configuration (in experiment 5) Return B was disconnected and a hypodermic needle under the dorsal skin served as return electrode. In experiments 4 and 5 electroneurograms (ENGs) of the CPN were recorded distal to the site of stimulation. The isometric twitch force of the extensor digitorum longus (EDL) muscle was recorded via a force transducer.

Stimulation setup.

In experiments 1 to 4 the stimulation charge was returned over the (more proximal) nerve electrode, creating a bipolar electrode arrangement. In experiment 5, we added a hypodermic needle (21G x 1-1/2") under the dorsal skin of the animal which in this case served as return electrode to create a monopolar stimulation configuration. All stimulation pulses were biphasic rectangular, with cathodic phase first except for a subset of

experiment 4, where monophasic (cathodic) rectangular pulses were used. Stimulation pulses were applied at a rate of one pulse every 3 seconds.

Recording settings.

Extensor digitorum longus muscle twitch force recorded at 100kS/s. Common peroneal nerve ENG recorded at 100kS/s (in Experiments 4 and 5).

Stimulation protocols and experiment-specific methods.

Experiment 1 represents a typical measurement conducted in our lab to examine the efficiency of Gaussian compared to rectangular waveforms for neural activation (Eickhoff and Jarvis, 2019). In this experiment we recorded recruitment curves for biphasic pulses with phase widths of 20, 40, 60, 80, 100, 120, 140, 160, 180, 200, 250, 325, 425, 550, 775, and 1000µs in 100µA amplitude increments. The single pulses that comprise these 16 recruitment curves were delivered in randomized order via a bipolar stimulation configuration.

Experiment 2 investigated the possibility that some unexpectedly high twitch force responses, that we observed at long stimulation phase widths in Experiment 1, might have been additional activation as a result of spinal reflex activity. Here we dissected the CPN proximal to the site of stimulation where it branches from the sciatic nerve to eliminate direct afferent activation of spinal circuits. We stimulated the nerve with biphasic pulses of 1ms phase width and amplitudes ranging from 100µA, in 100µA increments, to 5mA. For amplitudes 100µA to 3mA we recorded 3 repetitions at each stimulation intensity, for amplitudes above 3mA we recorded a single repetition. All pulses were applied in randomized order and via bipolar stimulation electrodes.

Experiment 3 was conducted to attain insight into the recruitment behaviour with a wider range of stimulation phase widths. In two separate recording sessions we recorded recruitment curves, first for biphasic and later for monophasic (cathodic) pulses of phase widths ranging from 200µs, in 200µs increments, to 4ms. For every phase width, stimulation intensities from 200µA, in 200µA increments, to 5mA were used. All combinations of phase widths and amplitudes were tested in randomized order. Following every 20 of these test stimulations a fixed control stimulation was delivered (2mA, phase width 200µs), set to elicit one full nerve activation. Following these two recording sessions we conducted a doublet test to probe the time course of refractoriness of our preparation. For this test we stimulated with pulse doublets comprised of two biphasic

pulses (5mA, phase width 100µs) separated by inter pulse intervals (IPIs) of durations from 10µs up to 500ms. Doublets with this range of IPI values were tested in randomized order and control pulses were delivered at regular intervals. All pulses for this experiment were delivered via the bipolar stimulation electrode configuration.

Experiment 4 investigated the hypothesis that a biphasic, long duration (phase width above absolute refractory period) pulse might be substituted with a triplet, comprised of three separate short pulses, spaced at the field transitions of the longer pulse to achieve equivalent neuromuscular recruitment. Recruitment curves for single biphasic pulses of phase widths 3ms and 200µs as well as for a pulse triplet comprised of three biphasic pulses of phase width 60µs and IPI 2880µs were recorded for amplitudes from 100µA, in 100µA increments, to 5mA. All combinations of pulse-type and amplitude were tested in randomized order and every 20 test stimulations a fixed control stimulation (2mA, phase width 200µs) was delivered. Additionally, we conducted a doublet test to probe the time course of escape from the refractory period. Doublets of two biphasic pulses (1.5mA, phase widths 60µs) with IPIs of duration from 100µs to 20ms were tested in randomized order with control pulses delivered at regular intervals. In addition to the isometric twitch force, in this experiment we recorded the ENG from the stimulated nerve distal to the stimulation site. All pulses were applied via bipolar electrode configuration.

Experiment 5 was conducted to probe thresholds for activation with a higher resolution (i.e. smaller stimulation amplitude increments) and to investigate differences between monopolar and bipolar electrode configuration. Biphasic pulses of 5ms phase width and amplitudes from 50µA to 2mA (in 50µA increments) were tested in ascending order first in the bipolar and afterwards in the monopolar configuration. Isometric twitch force and the distal ENG responses were recorded.

Data analysis and normalization. The developed isometric peak twitch force was determined by subtracting the passive muscle tension, which was typically between 0.05 and 0.1N, from the peak recorded force value. For the longer stimulation and recording periods in experiments 3 and 4, in order to minimize any effects of variations in depths of anaesthesia, temperature or fatigue on the recordings, force responses to test stimulations were normalized by division by the response to the nearest control pulse.

The ENG recordings were filtered to extract the 50Hz noise and stimulation artifacts were removed. For short stimulation pulses this artifact reduction was achieved automatically with a custom written MATLAB code (MATLAB (R2018a), The MathWorks Inc.,

Natick, MA, USA). For stimulations with longer phase widths, where the eCAPs were merged with the stimulation artifacts (often on the slopes of capacitive charging/discharging during the stimulation phases), manual input was necessary to fit a spline as baseline on which the eCAP laid and which was then used to remove the artifact. The ENG plots were smoothed with a 10-sample moving average MA-filter. All ENG processing and plotting was done in MATLAB (MATLAB (R2018a), The MathWorks Inc., Natick, MA, USA).

5.3 Transitions within biphasic long duration pulses can elicit up to 3 separate APs

(III. Results)

Experiment 1: The recruitment curves for biphasic pulses with phase widths from 20µs to 1ms are of the typical sigmoidal shape, which is characteristic for stimulation of healthy, homogeneous nerves (Figure 5.2.a). All recruitment curves plateau at an isometric peak twitch force level between 0.4 to 0.5N, typical values for this nerve-muscle preparation (Eickhoff and Jarvis, 2019). Stimulation with pulses of the three longest tested phase widths (550, 775, and 1000µs) elicited additional twitch force, exceeding this plateau, at high amplitudes.

Experiment 2: The recruitment curve for biphasic 1ms phase width pulses, applied distal to a complete dissection of the CPN, shows three distinct plateaus between zero and 5mA (Figure 5.2.b). Pulses with amplitudes between 400µA and 1.3mA elicited twitch forces of approximately 0.4N, typical values for full activation of all motor units in this preparation. The second plateau of approximately 0.75N was evoked by stimuli with amplitudes between 1.8 and 2.7mA. The last plateau is comprised of force responses to stimuli with amplitudes above 3.3mA which elicited approximately 0.87N peak twitch force.

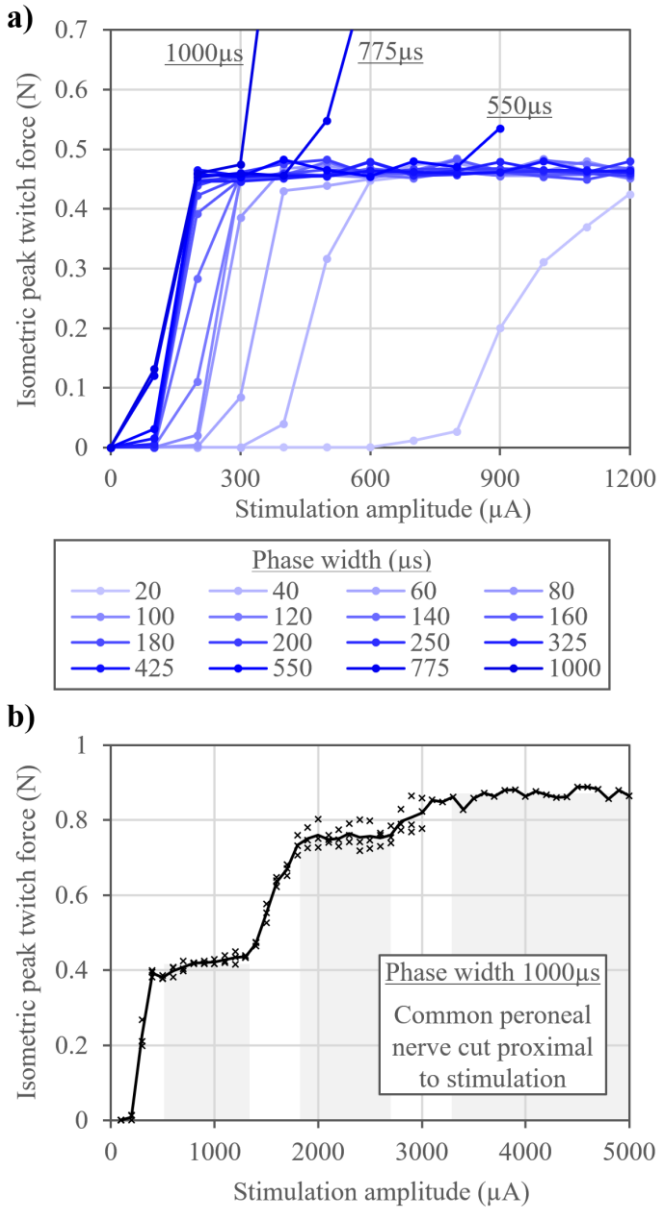

Figure 5.2 Recruitment curves for biphasic rectangular stimulation in bipolar electrode configuration recorded in steps of 100µA. **a)** Experiment 1: Recruitment curves for pulses with phase widths ranging from 20µs to 1000µs. Isometric peak twitch force plateaus between 0.4N and 0.5N. Pulses of the three longest tested phase widths (550, 775, and 1000µs) exceed this plateau at high amplitudes and elicit additional twitch force. **b)** Experiment 2: Recruitment curve for phase width 1000µs pulses with CPN cut proximal to the site of stimulation. Developed peak twitch force approached three distinct plateaus, indicated by grey bars. Data represents mean of 3 repetitions for amplitudes 100µA to 3mA, and a single repetition for amplitudes above 3mA.

Experiment 3: Stimulation with monophasic cathodic pulses elicited muscle responses with two distinct plateaus in the normalized recruitment curves. All monophasic pulses with phase widths equal or below 1ms elicited twitch force responses that formed a surprisingly stable plateau at the level of normalization (control pulses for normalization elicited 0.31N, mean of n=52, SD=0.01N). Longer pulses (phase width above 1ms)

elicited additional normalized force responses and stimulation with phase widths above 2ms formed the second plateau at approximately 2.9 (Figure 5.3.a-b). Biphasic pulses lead to normalized twitch force responses in three distinct steps. The shortest pulses of phase widths 200, 400 and 600µs formed a plateau at the normalization level 1 (control pulses for normalization elicited 0.44N, mean of n=51, SD=0.05N). With increasing amplitude, biphasic pulses above approximately 2ms phase width lead to two additional steps in normalized force responses. The second step was at 2.8 and the third plateau formed at approximately 3.5 times normalization (Figure 5.3.c-d). Doublets with IPIs below 1ms did not elicit additional peak twitch force above the level of normalization (control pulses for normalization elicited 0.32N, mean of n=6, SD=0.01N), signifying that the nerve-muscle preparation is still in absolute refractory period (ARP). Doublets with longer IPIs gradually resulted in additional twitch force up to approximately 2.7 to 2.9 with IPIs between 2 and 10ms, indicating that two ideally spaced single activations (of all motor units) elicit an isometric twitch force almost 3 times higher than with a single activation (Figure 5.3.e).

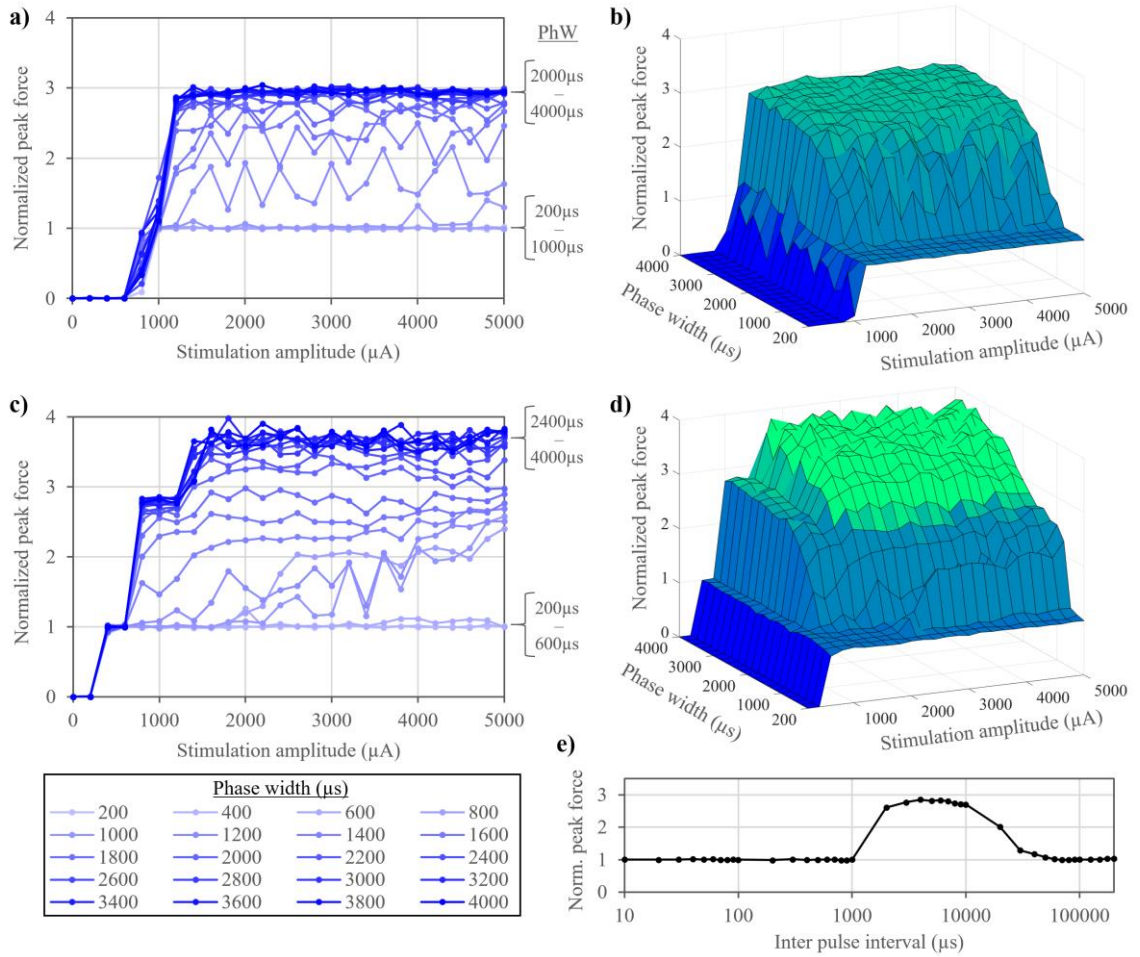

Figure 5.3 Results Experiment 3: Normalized recruitment curves for phase widths from 200µs to 4ms and amplitudes from 200µA to 5mA in 200µA increments. Stimulation presented in the bipolar electrode configuration. Recruitment curves for monophasic stimulation represented in the classical two-dimensional plot **(a)** and as surface plot **(b)**. Normalized peak force approached two distinct plateaus: The first plateau is formed by all monophasic pulses of phase width equal or below 1ms, the second plateau is formed by pulses of approximately 2ms phase widths and above at sufficiently high amplitudes. Panels (c) and (d) show recruitment data for biphasic stimulation represented as a two-dimensional plot **(c)** and as a surface plot **(d)**. Normalized peak force approached three distinct plateaus: The first plateau is formed by the responses to all biphasic pulses of phase width equal to or below 600µs, the second and third plateaus are formed by pulses of approximately 2.4ms phase width and above at sufficiently high amplitudes. **(e)** Doublet test with two biphasic 100µs pulses of high amplitude (5mA) and varying inter pulse interval (IPI) presented in the bipolar electrode configuration. The second pulse of doublets with less than 1ms IPI does not elicit any additional twitch force, indicating that this value is near the absolute refractory period for the preparation. Doublets with IPIs between 2ms and 10ms elicit maximal normalized peak force of approximately 2.7 to 2.9.

Experiment 4: Stimulation with biphasic pulses with phase width 200µs evoked stable twitch force responses at the level of normalization (Figure 5.4.a). The recruitment curve for biphasic 3ms pulses, shows 2 steps above this level of normalization, the first at approximately 2.1 and the second at 2.5. Recruitment with triplets of biphasic 60µs

pulses, modelled to match the transitions within a biphasic 3ms pulse, lead to similar twitch forces at a level of 2.5 times normalization (control pulses for normalization elicited 0.52N, mean of n=12, SD=0.02N). Force responses to doublets with IPIs below 1ms did not exceed the normalization level (control pulses for normalization elicited 0.6N, mean of n=8, SD=0.07N). Doublets with 3ms IPI elicited normalized force responses of 2.1 (Figure 5.4.b). Distal ENG recordings during stimulation with biphasic 3ms pulses show up to 3 evoked compound action potentials (eCAPs) elicited with a single pulse. The earliest (that is lowest threshold) eCAP is elicited as a response to the middle transition of the biphasic pulse at an amplitude of 400µA. At 500µA, an additional eCAP is elicited at the first transition and a third eCAP gradually develops at amplitudes above 1.3mA after the third transition of the biphasic pulse (Figure 5.4.c). ENG recordings during stimulation with the triplet of short pulses start to show three submaximal eCAPs at an amplitude of 600µA, which reach maximal peak-to-peak amplitude at 700µA stimulation intensity (Figure 5.4.d). ENGs recorded during stimulation with single biphasic pulses of 200µs phase width exhibit maximal eCAPs at amplitudes of 500µA and above (Figure 5.4.e). Latencies of the eCAP onset (i.e. delay of the start of the first eCAP deflection to the respective triggering field transition) were constant for all maximal eCAPs and across all pulses at approximately 600 to 700µs.

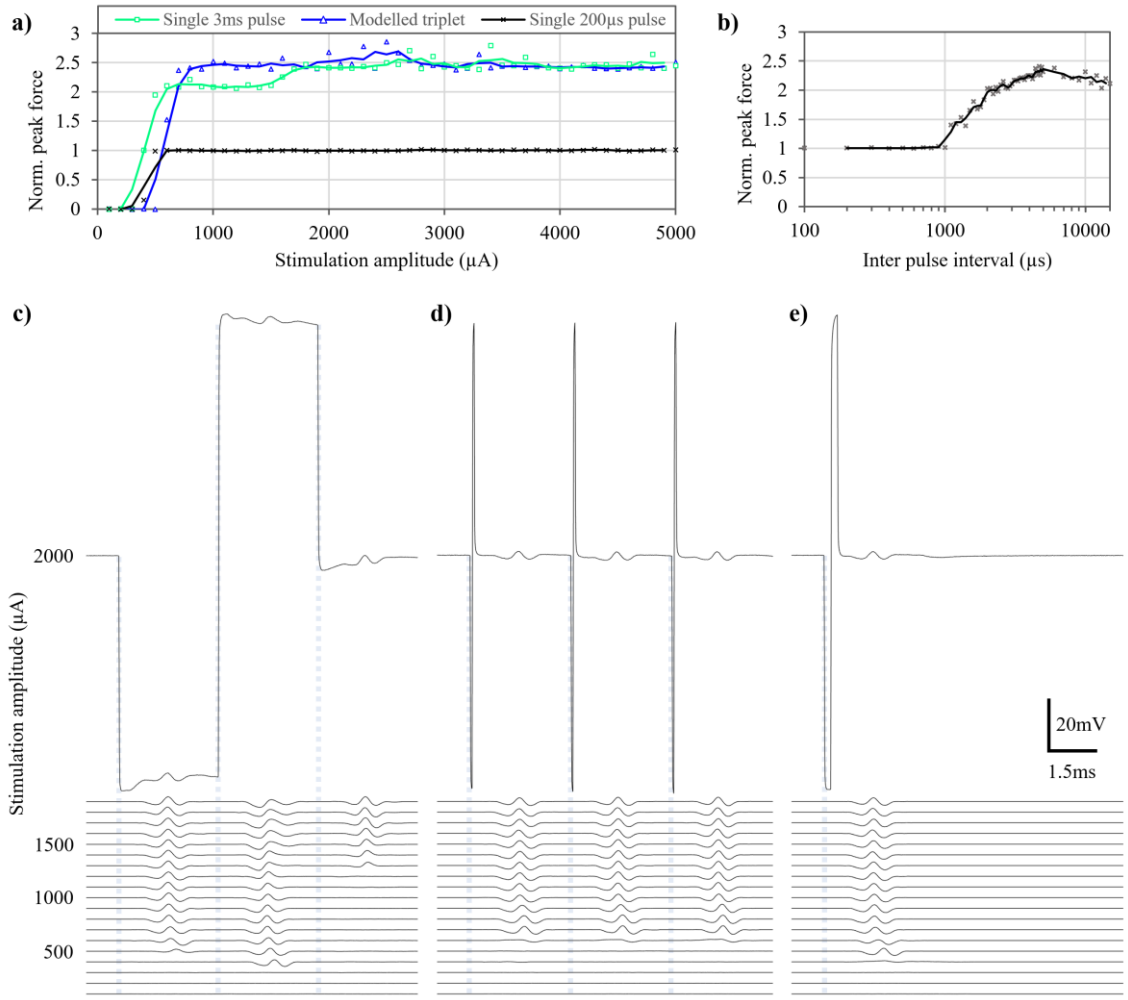

Figure 5.4 Results Experiment 4: **a)** Normalized recruitment data for single 3ms biphasic stimuli (green), triplet consisting of three biphasic 60µs pulses every 3ms (blue), and single 200µs biphasic stimuli (black) presented in the bipolar electrode configuration. **b)** Doublet test with two biphasic 60µs pulses of maximal amplitude and varying inter pulse interval (IPI). The second pulse of doublets with IPI less than 1ms does not elicit any additional twitch force, indicating that this value is near the absolute refractory period for the preparation. Doublets with 3ms IPI elicit normalized peak force of 2.1. ENG recordings of the CPN during stimulation with amplitudes from 100µA to 2mA with **c)** single 3ms biphasic stimuli, **d)** triplet consisting of three biphasic 60µs pulses every 3ms, and **e)** single 200µs biphasic stimuli. ENG recordings for 2mA amplitude stimulation are raw recordings (filtered) consisting of stimulation artifact and evoked compound action potentials (eCAPs). Stimulation artifacts have been removed from ENGs for amplitudes below 2mA and dashed lines indicate position of artifact onset or transitions within the artifact in case of c). Curves a) and b) have been fitted using a 3-sample moving average filter.

Experiment 5: Recruitment curves for biphasic stimulation with 5ms phase width lead to force responses in three steps (Figure 5.5.a). Stimulation via bipolar electrodes gradually reached a first level of just below 0.5N at amplitudes of 550 to 650µA, a second step of approximately 1.3N with amplitudes ranging from 850 to 1150µA, and a third force level of approximately 1.8N at amplitudes above 1.5mA. Stimulation delivered via a

monopolar electrode arrangement reached a first stable force plateau of just above 0.5N with amplitudes between 450 and 950µA. The second short plateau in the elicited force response was at 1.25N with stimulation amplitudes of 1200 to 1250µA before the twitch force reached the third plateau of 1.8N with amplitude above approximately 1.5mA. ENG recordings during stimulation via bipolar and monopolar electrode configurations exhibited up to three separate eCAPs for a single stimulation. The first eCAPs were elicited at the second field transition within the biphasic pulse at an amplitude 450µA, the second eCAPs started to develop with amplitudes above 650µA as a response to the first pulse transition, and the third eCAPs start to develop with amplitudes above 1150µA after the third pulse transition (Figure 5.5.b). Applying stimulation via a monopolar electrode configuration, eCAPs were first elicited at the first pulse transition with amplitudes of 350µA. Stimulation with amplitudes of 950µA and above started to elicit a second eCAP after the middle field transition of the biphasic pulse. The third eCAPs gradually develop as a response to the third pulse transition at amplitudes above 1.3mA (Figure 5.5.c).

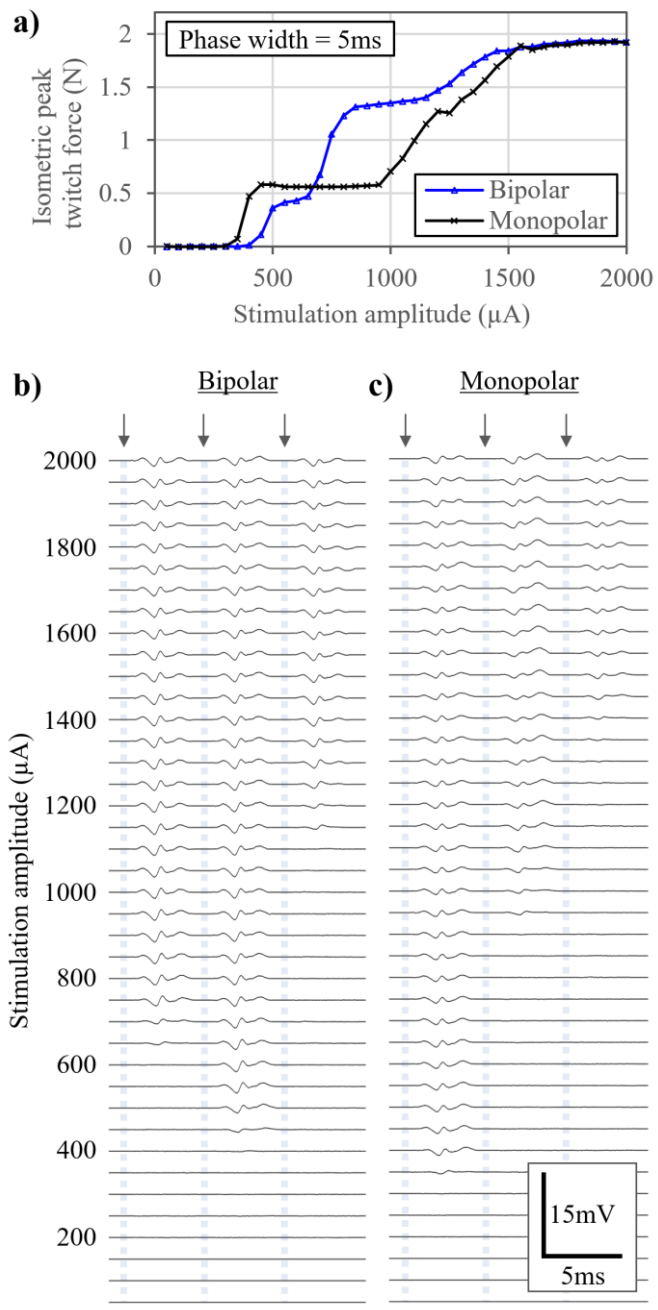

Figure 5.5 Results Experiment 5: **a)** Recruitment data for single 5ms biphasic stimuli, applied in the monopolar (black) and in the bipolar electrode configuration (blue). ENG recordings during stimulation with biphasic 5ms phase width pulses in the bipolar **b)** and in the monopolar stimulation configuration **c)**. Stimulation artifacts have been removed from the ENG. Arrows and dashed lines indicate the position of the transitions within the biphasic pulses. In the bipolar configuration, the first eCAP was elicited by the middle transition, while the activation started at the first transition in the monopolar configuration.

5.4 Discussion and implication for stimulation of (partially) denervated muscle

(IV. Discussion)

Experiments 1 clearly illustrates an unexpected yet consistent observation of our electrical stimulation experiments using an *in vivo* nerve-muscle preparation (Eickhoff and Jarvis, 2019, 2020b): biphasic stimulation with phase widths below approximately 550µs showed a characteristic sigmoidal recruitment behaviour, followed by a stable full recruitment level, whereas longer pulses elicited additional muscle twitch force at high amplitudes (Figure 5.2.a). In order to understand this consistent observation, we conducted a series of experiments.

First the hypothesis was tested that long phase width pulses might elicit a spinal reflex (H-reflex) at high amplitudes (Gozariu *et al.*, 1998). In order to test this hypothesis, in Experiment 2 the CPN was dissected proximal to the site of stimulation, just distal to where it branches from the sciatic nerve. As stimulation with biphasic pulses of 1ms phase width still showed additional twitch force above the first plateau (at a typical twitch force value for full recruitment of approx. 0.4N), we could reject the hypothesis that this observation might derive from central reflex activity (Figure 5.2.b). Further, we extended the amplitude range and observed that the elicited twitch force response not only exceeded the *first* plateau, which represents full activation for all phase widths below 550µs, but instead approached *three* distinct plateaus.

This surprising observation led us to form the hypothesis that the three field transitions within a single biphasic stimulation pulse can elicit three separate nerve activations, if separated enough not to fall within the preparation's refractory period and given sufficient amplitude. This would provide an explanation for the observations so far: with a typically anticipated ARP for fast twitch motor units of approximately 1ms, biphasic pulses of 550µs phase widths would be among the shortest pulses to elicit more than a single nerve activation (compare Figure 5.2.a), as the first and the last field transition are separated by more than 1ms. Longer biphasic pulses with phase widths above the ARP could elicit up three activations as the separation of each field transition to the next one allows for (partial) recovery from refractoriness (compare Figure 5.2.b).

The findings of Experiment 3 strongly support this hypothesis. Monophasic pulses of phase widths of 1ms and below did not exceed the level of normalization (i.e. the force response representing one full neuromuscular recruitment), whereas an additional

recruitment was evidenced with monophasic pulses of longer phase durations (Figure 5.3.a-b). This additional recruitment formed a remarkably stable second plateau in the normalized force response at approximately 2.9. The rationale for both, the minimum phase width at which additional recruitment can take place as well as the amount of normalized twitch force at which the second plateau forms, can be attained from the doublet test (Figure 5.3.e). First, it is shown that the minimum phase width at which additional recruitment can take place with monophasic stimuli correlates with the ARP of our preparation of approximately 1ms. Secondly, the doublet test shows that two ideally spaced motor nerve activations, in this case with an IPI of 2 to 10ms, elicit twitch force responses of approximately 2.7 to 2.9 times normalization level, correlating with the "height" of the second force plateau (compare Figure 5.3.b). These are typical values for fast twitch motor units (Burke, 1967), of which the EDL is predominantly comprised (Green *et al.*, 1984; Larsson and Yu, 1997), and the rationale for the high relative peak twitch force of an ideally spaced doublet is rooted in calcium release mechanics of fast twitch muscle fibres (Kwende, Jarvis and Salmons, 1995). Using biphasic stimulation, a maximum now of three distinct activation levels could be observed, correlating with the three field transitions within a biphasic pulse (Figure 5.3.c-d). Again, the phase widths at which no additional activation (above normalization level) occurred, correlated with approximately *half* of the ARP. Once the phase widths of biphasic pulses exceeded 600µs, meaning that the first pulse transition was separated by more than 1.2ms from the third transition which thus did not fall within the ARP anymore, additional recruitment above the level of normalization was observed.

The addition of ENG recordings distal to the site of stimulation in Experiments 4 and 5 shed further light on our observations. In Experiment 4 we proved that the threefold neuromuscular activation elicited by biphasic pulses of 3ms phase width can reliably be replicated using triplets consisting of three short pulses located at the field transitions of the 3ms biphasic pulse (Figure 5.4.a). Again, the doublet test illustrates how a doublet of 3ms IPI elicits force responses correlating to those elicited at intermediary amplitude (600-1500µA) with biphasic 3ms pulses that evoke two of the possible three activations (compare Figure 5.4.b and .c). While triplets elicit eCAPs at all three pulses at the same amplitude (Figure 5.4.d), the thresholds for activation at the three transitions of the biphasic 3ms are not equal (Figure 5.4.c). Interestingly, the lowest threshold, i.e. the "part" of the biphasic pulse at which the first eCAP is evoked, is the middle field transition, followed first by the first transition and later by the third transition. This is in

line with earlier findings from our laboratory, that the middle field transition of biphasic pulses can be the effective transition in the bipolar electrode configuration (Eickhoff and Jarvis, 2020b). In this configuration, the cathodic (first) phase of the biphasic pulse acts as hyperpolarizing pre-pulse at the return electrode, rendering the nerve membrane more excitable in this location (Grill and Mortimer, 1995), and the middle field transition depolarizes the nerve at the bipolar return electrode where the current profile is inverted (Eickhoff and Jarvis, 2020b).

Experiment 5 provides further insight into the different thresholds for activation at the three field transitions within biphasic stimuli in the monopolar and bipolar electrode configuration. In contrast to the order of thresholds in the bipolar configuration described above, with a monopolar electrode arrangement excitation first occurred at the first field transition followed by the middle and later by the third field transition (Figure 5.5.c). Further, the finer amplitude increments of 50µA used in Experiment 5 allow for an exploration of the different mechanisms leading to excitation at the different field transitions and in different electrode configurations. For this exploration we will compare the dynamic ranges, i.e. the range of amplitudes from the elicitation of the first APs to a complete activation of all motor units, at different transitions within the biphasic pulse in both electrode configurations (Figure 5.5.b-c). This dynamic range, which can also be assessed by examining the slope of the steps in the recruitment curves (Figure 5.5.a), is greater for the second and third activation in the monopolar configuration and the third activation in the bipolar configuration than it is for the first activation in the monopolar and the first and second activations in the bipolar configuration. The rationale for this could be that the activations exhibiting a greater dynamic range represent activation by anodic excitation, where APs are not elicited at the central (i.e. closest to the respective electrode) nodes of Ranvier but rather at adjacent nodes. At these adjacent nodes, the extracellular field density is reduced (Rattay, 1986) so that the here effectively smaller stimulation increments could be the origin of the greater dynamic range. In-depth investigation of the mechanisms leading to excitation at the different field transitions warrants further experimental and computational research.

These observations of multiple activations with single, long duration electrical stimulations have implications for medical devices and therapies that seek to activate partially or complete denervated muscle. Especially in scenarios where innervated structures are nearby the denervated stimulation target, a single twitch activation of the denervated muscle might be accompanied by an undesired strong (effectively up to

threefold) coactivation of the innervated structures. Further research could investigate the effect of different “slopes” of the field transitions within biphasic stimuli or altogether different waveforms, such as variations of the sawtooth shape, on those multiple activations.

Further, an ongoing collaboration with the Scientific Computing research group around Prof. Frank Ratty (Vienna University of Technology) investigates parameters of state-of-the-art biophysical stimulation models that might enable those models to predict the threefold activations we observed. With none of the well-studied and described computational models, a practical straight forward prediction of three separate activations as response to the three field transitions within a biphasic ES pulse seems to be possible. However, preliminary results of this ongoing research collaboration suggest that implementation of the stimulator output stage circuitry, along with the capacitive properties of the tissue-electrode interface may be of central importance to model such triple activations.

6 FUTURE WORK

In this chapter, the development and testing of two experimental devices for future use is described. Besides some exemplary recordings during bench testing, no data is included in this thesis.

6.1 Cell stimulation system

To support the research group around Dr Daniel Owens that seeks to investigate the influence of vitamin D on metabolic adaptation to endurance training in muscle cell cultures, a cell stimulation system was developed and tested. Based on the design of commercially available electrode rigs for cell culture stimulation, such as the C-Dish (IONOPTIX LLC, Westwood, MA, USA), an electrode array was built using the lid of a 6-well cell culture plate. Electrodes were manufactured from a thin stainless-steel sheet metal, cut into 15mm wide and 10mm high pieces that were fixed to the cell culture plate lid with an offset approximately 1mm from the bottom of the wells when the lid is placed on a plate. All active and return electrodes were connected in parallel to achieve an even voltage field in all wells (Figure 6.1). Both, the parallelly connected active and the parallelly connected return electrodes have 2 terminals, one for connection with the stimulator and one for recording.

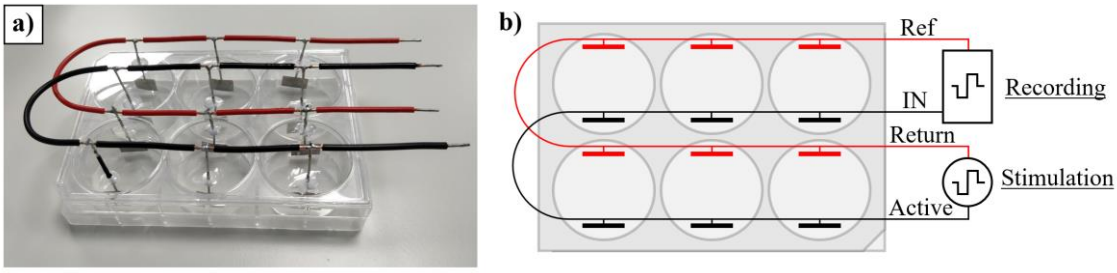

Figure 6.1 Cell culture stimulation system. a) Custom made 6-well cell culture stimulation electrode array. Two 15mm wide stainless-steel electrodes, one active electrode and one return electrode, are placed in each of the six wells. When the wells are filled with conductive cell-culture medium an even voltage field is created in all wells in parallel. **b)** The electrode array has two terminals for active and for return electrodes to connect to the simulator and to a recording system.

For stimulation and recording of the stimulation artifact, a PowerLab 16/35 (ADInstruments Pty Ltd, Bella Vista, New South Wales, Australia) was used. For the first tests, following stimulation protocols suggested in literature (Son *et al.*, 2019), rectangular voltage pulses of ±10V amplitude and 1ms phase width were delivered over one of the PowerLab analog outputs at a rate of 10Hz. The PowerLab 16/35 analog output can drive a maximum output current of ±50mA so that 10V stimulation amplitude can be delivered to any load of 200Ω or greater. To verify that the stimulation pulses were indeed delivered at full amplitude, a scheduler was set up to record a 10-second block of stimulation artifacts every 10 minutes during the whole duration of the 3 or 24-hour experiments (Figure 6.2). Recordings were made at a sample rate of 100kS/s. Pulse generation as well as artifact recordings were done using macros (Appendix 4) in LabChart 7 Pro (ADInstruments Pty Ltd, Bella Vista, New South Wales, Australia).

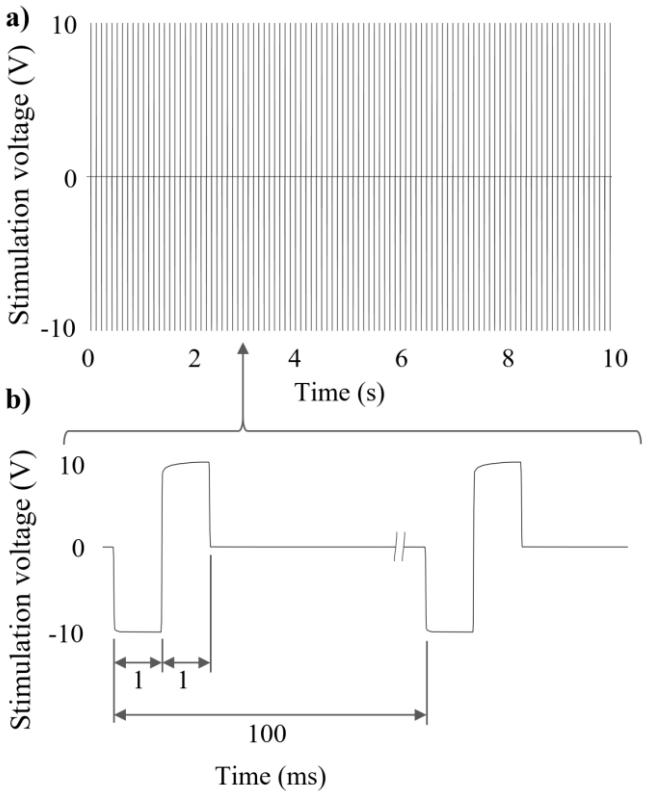

Figure 6.2 Cell culture stimulation artifact recording. a) One representative 10-seconds recording block. **b)** Single stimulation artifacts during 10Hz stimulation with biphasic rectangular pulses of 1ms phase widths and 10V amplitude.

6.2 Development of an electroporator

For a later stage of the joint research project with the group around Dr Daniel Owens, an electroporation device was developed and tested. Electroporation is a technique that uses artificial electrical fields to temporarily increase cell membrane permeabilities, e.g. to introduce foreign DNA. The parameters of these electrical pulses vary depending on the specific application between short and intense (>100V, few ms) pulses used for electroporation of bacteria and milder pulse conditions (10-50V, 20-100ms) for electroporation of higher organism cells (Bullmann *et al.*, 2015). While commercially available electroporators are expensive (above 10.000$), the principal technology required to generate rectangular voltage pulses is rather simple. A DC voltage supply of the desired stimulation amplitude can easily be achieved by connecting 9V block batteries in series. Depending on the maximal stimulation voltage and amplitude, as well as the pulse width and maximal operation frequency, a high-specification reed relay unit can be chosen to connect and disconnect the voltage supply to the electroporation electrodes (typically tweezer electrodes). An adjustable voltage regulator (e.g. a LM317) circuit may additionally be used to limit the maximal stimulation current to a value that guarantees safe relay and electrode operation (Bullmann *et al.*, 2015).

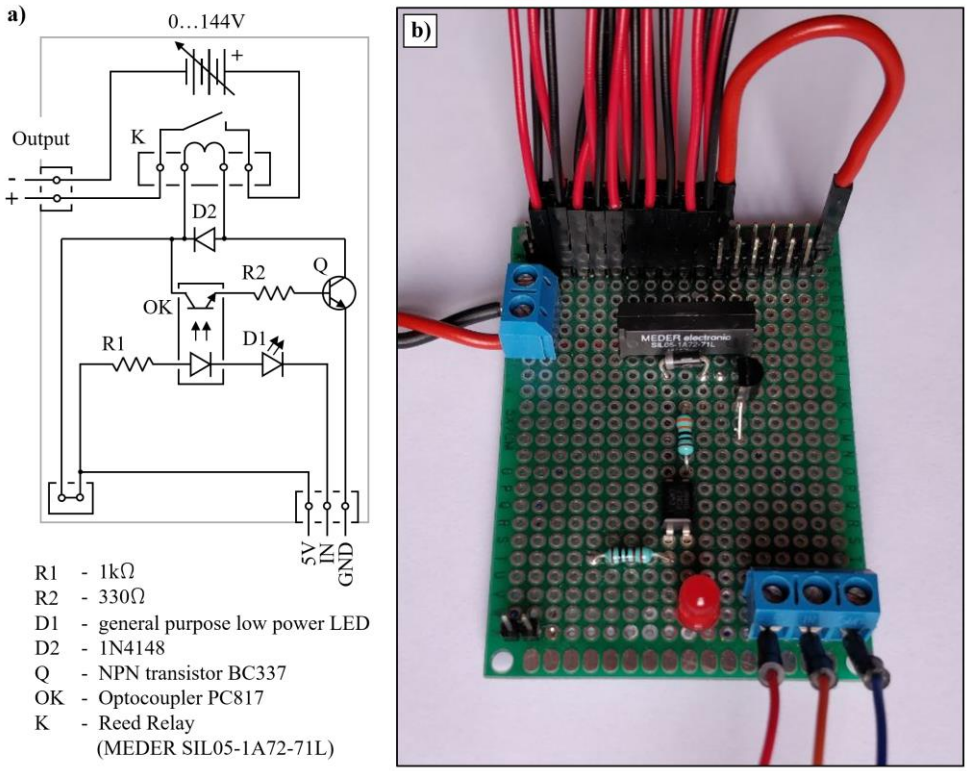

Figure 6.3 Electroporator. a) Electronic schematic and **b)** circuit board of electroporator. A digital input can be used to switch the reed relay K and connect the adjustable supply voltage to the electroporation electrodes.

To cover a wide range of possible stimulation parameters, we designed a simple circuit with a high-quality reed relay, capable of switching up to 200VDC or 500mA (maximum of 10W) with a operation time of 0.7ms and a release time of 0.05ms. While connections have been prepared to attach up to 16 9V block batteries in series (maximum supply voltage of 144V), with the upper limit of typical operation range of 50V (Bullmann *et al.*, 2015) a maximum current of 200mA can be switched. The relay is controlled by the digital output of a NI PCIe 6351 Data Acquisition Card (National Instruments Corporation, Austin, Texas, U.S.A.) Figure 6.4 shows a basic LabVIEW™ 2016 (National Instruments Corporation, Austin, Texas, U.S.A.) program as well as a bench top setup to test the electroporation device with five 9V block batteries connected. The relay unit is switched and thus connects the supply voltage with the electrodes and outputs a monophasic 48V stimulation[11] with pulse width of 50ms.

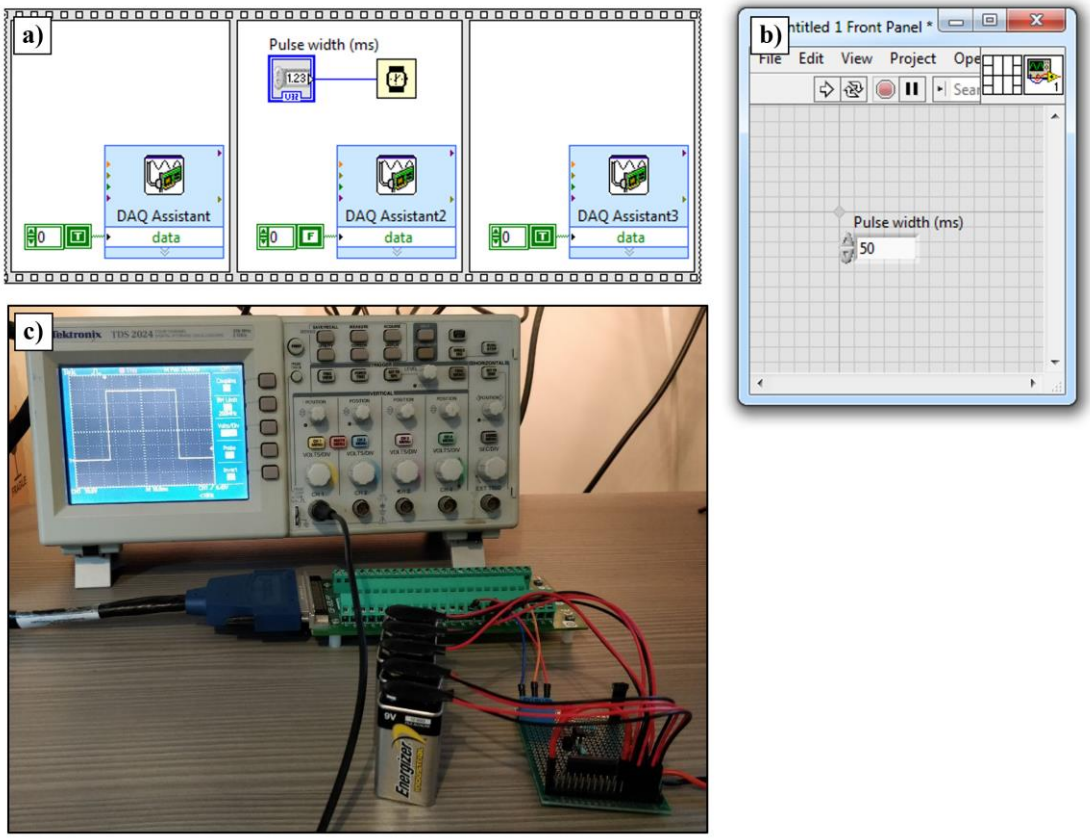

Figure 6.4 Bench testing of the electroporator. a), b) A basic LabVIEW program provides a digital input signal to control the reed relay and thus **c)** connected the supply voltage of 48VDC for the controlled pulse width of 50ms with the electroporation output. Oscilloscope divisions are 10V (vertical) and 10ms (horizontal).

[11] The 9V block batteries used for this test were new and had voltages of approximately 9.6V each. The stimulation amplitude with five such batteries in series was therefore approximately 48V.

7 CONCLUSION AND OUTLOOK

The research summarized in this thesis sheds important new light on the effect of many pulse shape parameters and variations, commonly suggested to enhance the efficiency of ES. We identified that most original research and published, authoritative literature on the effect of these pulse shape variations was modelled and conducted only for the monopolar electrode configuration that is different from the bipolar stimulation mode in which many contemporary ES devices operate. Therefore, in the design of our experimental *in-vivo* model (Chapter 2) to re-examine the effect of these ES waveforms, a special focus was laid on methods to compare the monopolar and the bipolar electrode configuration.

A comprehensive comparison of the effect of subthreshold pre-pulses in both principal configurations revealed opposite effects of those pre-pulses with monopolar compared to bipolar stimulation (Chapter 3.1). The rationale for this surprisingly strong influence of the return electrode position (and thereby of the stimulation configuration) was identified by analysis of the distal ENG of the stimulated nerve. As it is commonly anticipated, in the monopolar configuration, we observed AP elicitation at the active electrode as a response to the first (cathodic) field transition of biphasic pulses. Using the bipolar configuration however, excitation first occurred at the return electrode in response to the middle field transition of biphasic pulses. This study helps to explain the apparent contradictions of over two decades of published literature on the effect of subthreshold pre-pulses. We extended our investigation and reported that by the same mechanisms of excitation, the effect of interphase gaps (IPGs) and asymmetric biphasic pulses (with lower anodic amplitude) is opposite in the monopolar compared to the bipolar stimulation mode (3.2). These are two of the most commonly suggested pulse shape variations and their use in ES devices operating in bipolar mode could significantly *decrease* energy efficiency as they result in higher excitation thresholds than standard biphasic rectangular pulses. Further research is warranted to study this effect of activation at the bipolar return electrode, and thus reversed effects of pulse shape variations such as IPGs, asymmetric pulse ratios, and pre-pulses, with commercially used cuff and array electrodes. In addition, future research could investigate the influence of the bipolar inter-electrode

separation, as well as of the electrode areas on the described effect of activation at the bipolar return.

Among the non-rectangular ES waveforms, Gaussian-like pulses have been identified by three independent computational studies to consume the least amount of electrical energy and predictions of up to 60% energy saving potential with this waveform have been made. In the study presented in Chapter 3.3, we investigated these claims in a comprehensive series of *in-vivo* experiments and not only reported lower energy saving potentials of only up to 17%, but further, for the first time, reported major disadvantages in terms of peak power requirements with these novel stimulation waveforms. We proposed further research to reconcile the surprising gap between predicted energy savings of up to 60% and our moderate energy saving observations of only up to 17% in section 3.3.6.

In Chapter 4 a series of experiments is highlighted that investigated the time course of loss of excitability with nerve stimulation following a standardized nerve crush injury. All excitability over the injured motor nerve was lost 3 days after the nerve crush. Further, we report how the complete denervated EDL muscle changed its physiological characteristics towards that of a slow twitch muscle after 10 days of the nerve crush injury. As we demonstrate on experiments investigating ideal n-let spacings, such changes in the denervated muscle's physiological behaviour lead to significant differences in the optimal ES strategies to activate these muscles. While in healthy fast twitch muscle, a high frequency doublet may be used at the beginning of a stimulation burst to enhance the efficiency of ES to generate tetanic contractions, we show that this so called "doublet effect" is lost in fully denervated muscle. Another difference in the stimulation strategies to activate denervated muscle, and one that is already well known and described in literature, is the need for longer stimulation pulse durations. However, the effect of those long duration pulses on nerves has not been studied comprehensively. In Chapter 5 we highlighted a series of experiments, demonstrating how biphasic pulses with phase durations greater than the refractory period of nerves (approx. 1ms) can elicit up to 3 separate eCAPs. These findings are of interest for ES applications and therapies that seek to activate denervated muscles with innervated structures nearby. These innervated structures might experience an undesired, up to threefold coactivation for a single activation of the denervated stimulation target. Further research could extend this investigation and test long duration pulses with different field transition slopes, e.g. a series of slopes from rectangular to a *"sawtooth"* waveform, and their effect on denervated muscle as well as on nerves.

8 REFERENCES

Agnew, W. F. *et al.* (1986) 'Histopathologic evaluation of prolonged intracortical electrical stimulation', *Experimental Neurology*. doi: 10.1016/0014-4886(86)90132-9.

Agnew, W. F. *et al.* (1989) 'Histologic and physiologic evaluation of electrically stimulated peripheral nerve: Considerations for the selection of parameters', *Annals of Biomedical Engineering*. doi: 10.1007/BF02364272.

Agnew, W. F. *et al.* (1990) 'Local anaesthetic block protects against electrically-induced damage in peripheral nerve', *Journal of Biomedical Engineering*. doi: 10.1016/0141-5425(90)90004-7.

Ashley, Z. *et al.* (2005) 'Determination of the chronaxie and rheobase of denervated limb muscles in conscious rabbits', *Artificial Organs*. doi: 10.1111/j.1525-1594.2005.29037.x.

Beebe, X. and Rose, T. L. (1988) 'Charge Injection Limits of Activated Iridium Oxide Electrodes with 0.2 ms Pulses in Bicarbonate Bufered Saline', *IEEE Transactions on Biomedical Engineering*. doi: 10.1109/10.2122.

Bentivoglio, M. (2014) 'Ramón y Cajal, Santiago', in *Encyclopedia of the Neurological Sciences*. 2nd edn, pp. 1061–1065.

Bernstein, J. (1868) 'Ueber den zeitlichen Verlauf der negativen Schwankung des Nervenstroms', *Pflüger, Archiv für die Gesammte Physiologie des Menschen und der Thiere*. doi: 10.1007/BF01640316.

Bernstein, J. (1902) 'Untersuchungen zur Thermodynamik der bioelektrischen Ströme - Erster Theil', *Pflüger Archiv für die Gesammte Physiologie des Menschen und der Thiere*. doi: 10.1007/BF01790181.

Bernstein, J. *et al.* (1977) 'Electrical stimulation of the cortex with Ta2O5 capacitive electrodes.', in Hambrecht, F. and Reswick, J. (eds) *Functional electrical stimulation*. New York: Marcel Dekker, pp. 465–77.

Bertorini, T. (2008) 'Neuromuscular Anatomy and Function', in *Neuromuscular Case Studies*, pp. 1–25. doi: https://doi.org/10.1016/B978-0-7506-7332-7.50005-2.

Bhadra, N. and Kilgore, K. L. (2018) 'Fundamentals of Kilohertz Frequency Alternating

Current Nerve Conduction Block of the Peripheral Nervous System', in *Neuromodulation*. doi: 10.1016/b978-0-12-805353-9.00010-3.

Birmingham, K. *et al.* (2014) 'Bioelectronic medicines: A research roadmap', *Nature Reviews Drug Discovery*. doi: 10.1038/nrd4351.

Blumenthal, T. D., Burnett, T. T. and Swerdlow, C. D. (2001) 'Prepulses reduce the pain of cutaneous electrical shocks', *Psychosomatic Medicine*. doi: 10.1097/00006842-200103000-00012.

Brummer, S. B. and Turner, M. J. (1977) 'Electrical Stimulation with Pt Electrodes: II–Estimation of Maximum Surface Redox (Theoretical Non-Gassing) Limits', *IEEE Transactions on Biomedical Engineering*. doi: 10.1109/TBME.1977.326179.

Bullmann, T. *et al.* (2015) 'A transportable, inexpensive electroporator for in utero electroporation', *Development Growth and Differentiation*. doi: 10.1111/dgd.12216.

Burke, R. E. (1967) 'Motor unit types of cat triceps surae muscle', *The Journal of Physiology*. doi: 10.1113/jphysiol.1967.sp008348.

Cappaert, N. L. M. *et al.* (2013) 'Efficacy of a new charge-balanced biphasic electrical stimulus in the isolated sciatic nerve and the hippocampal slice', *International Journal of Neural Systems*. doi: 10.1142/S0129065712500311.

Carlyon, R. P. *et al.* (2005) 'Effect of inter-phase gap on the sensitivity of cochlear implant users to electrical stimulation', *Hearing Research*, 205(1–2), pp. 210–224. doi: 10.1016/j.heares.2005.03.021.

Carmeliet, E. (2019) 'From Bernstein's rheotome to Neher-Sakmann's patch electrode. The action potential', *Physiological Reports*. doi: 10.14814/phy2.13861.

Castro, M. J. *et al.* (1999) 'Influence of complete spinal cord injury on skeletal muscle within 6 mo of injury', *Journal of Applied Physiology*. doi: 10.1152/jappl.1999.86.1.350.

Charthad, J. *et al.* (2018) 'A mm-Sized wireless implantable device for electrical stimulation of peripheral nerves', *IEEE Transactions on Biomedical Circuits and Systems*. doi: 10.1109/TBCAS.2018.2799623.

Cheetham, J. *et al.* (2015) 'Effects of Functional Electrical Stimulation on Denervated Laryngeal Muscle in a Large Animal Model', *Artificial Organs*. doi: 10.1111/aor.12624.

Cogan, S. F. *et al.* (2016) 'Tissue damage thresholds during therapeutic electrical stimulation', *Journal of Neural Engineering*. doi: 10.1088/1741-2560/13/2/021001.

Cogan, S. F., Hara, S. and Ludwig, K. A. (2018) ‘The Safe Delivery of Electrical Currents and Neuromodulation’, in *Neuromodulation*. doi: 10.1016/b978-0-12-805353-9.00007-3.

Craggs, M. D., Donaldson, N. de N. and Donaldson, P. E. K. (1986) ‘Performance of platinum stimulating electrodes, mapped on the limitvoltage plane - Part 1 Charge injection in vivo’, *Medical & Biological Engineering & Computing*. doi: 10.1007/BF02442699.

Curtis, H. J. and Cole, K. S. (1942) ‘Membrane resting and action potentials from the squid giant axon’, *Journal of Cellular and Comparative Physiology*. doi: 10.1002/jcp.1030190202.

Deurloo, K. E. I., Holsheimer, J. and Bergveld, P. (2001) ‘The effect of subthreshold prepulses on the recruitment order in a nerve trunk analyzed in a simple and a realistic volume conductor model’, *Biological Cybernetics*. doi: 10.1007/s004220100253.

Donaldson, P. (1974) ‘The stability of tantalum-pentoxide films in vivo’, *Med Biol Eng*, (12), pp. 131–5.

Dwyer, T. (2018) ‘The Electrochemical Basis of Nerve Function’, in *Fundamental Neuroscience for Basic and Clinical Applications*. 5th edn, pp. 34–53.

Eickhoff, S. and Jarvis, J. C. (2019) ‘An Investigation of Neural Stimulation Efficiency with Gaussian Waveforms’, *IEEE Transactions on Neural Systems and Rehabilitation Engineering*. doi: 10.1109/TNSRE.2019.2954004.

Eickhoff, S. and Jarvis, J. C. (2020a) ‘Reply to “Energy Optimal Stimulation Waveforms, Or Not: Comments on ‘An Investigation of Neural Stimulation Efficiency With Gaussian Waveforms’”’, *IEEE Transactions on Neural Systems and Rehabilitation Engineering*, pp. 1–1. doi: 10.1109/TNSRE.2020.2984294.

Eickhoff, S. and Jarvis, J. C. (2020b) ‘The Effect of Sub-Threshold Pre-Pulses on Neural Activation Depends on Electrode Configuration’, *IEEE Transactions on Biomedical Engineering*. doi: DOI: 10.1109/TBME.2020.2964071.

Fallon, J. B. and Carter, P. M. (2016) ‘Principles of Recording from and Electrical Stimulation of Neural Tissue’, in Shepherd, R. K. (ed.) *Neurobionics: The Biomedical Engineering of Neural Prostheses*. Wiley Blackwell, pp. 89–120.

Famm, K. *et al.* (2013) ‘Drug discovery: A jump-start for electroceuticals’, *Nature*. doi: 10.1038/496159a.

Fisher, L. E. *et al.* (2006) ‘Preliminary evaluation of a neural prosthesis for standing after spinal cord injury with four contact nerve-cuff electrodes for quadriceps stimulation’, in *Annual International Conference of the IEEE Engineering in Medicine and Biology - Proceedings*. doi: 10.1109/IEMBS.2006.260833.

Fjordbakk, C. T. *et al.* (2019) ‘Feasibility of kilohertz frequency alternating current neuromodulation of carotid sinus nerve activity in the pig’, *Scientific Reports*, 9(1). doi: 10.1038/s41598-019-53566-8.

Forger, D. B., Paydarfar, D. and Clay, J. R. (2011) ‘Optimal stimulus shapes for neuronal excitation’, *PLoS Computational Biology*. doi: 10.1371/journal.pcbi.1002089.

Frankenhauser, B. (1957) ‘A method for recording resting and action potentials in the isolated myelinated nerve fibre of the frog’, *The Journal of physiology*. doi: 10.1113/jphysiol.1957.sp005729.

Freeman, D. K. *et al.* (2017) ‘A sub-millimeter, inductively powered neural stimulator’, *Frontiers in Neuroscience*. doi: 10.3389/fnins.2017.00659.

Geddes, L. A. (1999) ‘Chronaxie’, *Australasian Physical and Engineering Sciences in Medicine*.

Glenn, W. W. L. and Phelps, M. L. (1985) ‘Diaphragm pacing by electrical stimulation of the phrenic nerve’, *Neurosurgery*. doi: 10.1227/00006123-198512000-00021.

Goldman, D. E. (1943) ‘Potential, impedance, and rectification in membranes’, *Journal of General Physiology*. doi: 10.1085/jgp.27.1.37.

Gorman, P. H. and Mortimer, J. T. (1983) ‘The Effect of Stimulus Parameters on the Recruitment Characteristics of Direct Nerve Stimulation’, *IEEE Transactions on Biomedical Engineering*. doi: 10.1109/TBME.1983.325041.

Gozariu, M. *et al.* (1998) ‘An electrophysiological investigation into the monosynaptic H-reflex in the rat’, *Brain Research*. doi: 10.1016/S0006-8993(97)01402-9.

Green, H. J. *et al.* (1984) ‘Exercise-induced fibre type transitions with regard to myosin, parvalbumin, and sarcoplasmic reticulum in muscles of the rat’, *Pflügers Archiv European Journal of Physiology*. doi: 10.1007/BF00587545.

Grill, W. M. (2018) ‘Waveforms for Neural Stimulation’, in *Neuromodulation (Second Edition)*, pp. 95–102.

Grill, W. M. and Mortimer, J. T. (1993) ‘Selective activation of distant nerve fibers’, in

Proc. 15th Annu. Int. Conf. IEEE Eng. Med. Biol. Soc. IEEE, pp. 1249–1250. doi: 10.1109/iembs.1993.979119.

Grill, W. M. and Mortimer, J. T. (1995) 'Stimulus Waveforms for Selective Neural Stimulation', *IEEE Engineering in Medicine and Biology Magazine*. doi: 10.1109/51.395310.

Grill, W. M. and Mortimer, J. T. (1997) 'Inversion of the current-distance relationship by transient depolarization', *IEEE Transactions on Biomedical Engineering*. doi: 10.1109/10.553708.

Grill, W. M. and Wongsarnpigoon, A. (2015) 'Methods for generating waveform shapes optimized for energy efficiency for treating neurological disorders'.

Grill, W. M. and Wongsarnpigoon, A. (2020) 'Energy Optimal Stimulation Waveforms, Or Not: Comments on "An Investigation of Neural Stimulation Efficiency With Gaussian Waveforms"', *IEEE Transactions on Neural Systems and Rehabilitation Engineering*, pp. 1–1. doi: 10.1109/TNSRE.2020.2984402.

Guenther, E. *et al.* (1999) 'Long-term survival of retinal cell cultures on retinal implant materials', *Vision Research*. doi: 10.1016/S0042-6989(99)00128-5.

Guyton, D. L. and Hambrecht, F. T. (1973) 'Capacitor electrode stimulates nerve or muscle without oxidation-reduction reactions', *Science*. doi: 10.1126/science.181.4094.74.

Guyton, D. L. and Hambrecht, F. T. (1974) 'Theory and design of capacitor electrodes for chronic stimulation', *Medical & Biological Engineering*. doi: 10.1007/BF02477223.

Hennings, K., Arendt-Nielsen, L. and Andersen, O. K. (2005) 'Orderly activation of human motor neurons using electrical ramp prepulses', *Clinical Neurophysiology*. doi: 10.1016/j.clinph.2004.09.011.

Hill, A. V. (1938) 'The Heat of Shortening and the Dynamic Constants of Muscle', *Proceedings of the Royal Society B: Biological Sciences*. doi: 10.1098/rspb.1938.0050.

Hodgkin, A. L. and Huxley, A. F. (1939) 'Action potentials recorded from inside a nerve fibre', *Nature*. doi: 10.1038/144710a0.

Hodgkin, A. L. and Huxley, A. F. (1952a) 'A quantitative description of membrane current and its application to conduction and excitation in nerve', *J Physiol*, 117(4), pp. 500–544. doi: https://doi.org/10.1113/jphysiol.1952.sp004764.

Hodgkin, A. L. and Huxley, A. F. (1952b) ‘A quantitative description of membrane current and its application to conduction and excitation in nerve’, *The Journal of Physiology*. doi: 10.1113/jphysiol.1952.sp004764.

Hodgkin, A. L. and Huxley, A. F. (1952c) ‘Currents carried by sodium and potassium ions through the membrane of the giant axon of Loligo’, *The Journal of Physiology*. doi: 10.1113/jphysiol.1952.sp004717.

Hodgkin, A. L. and Huxley, A. F. (1952d) ‘The dual effect of membrane potential on sodium conductance in the giant axon of Loligo’, *The Journal of Physiology*. doi: 10.1113/jphysiol.1952.sp004719.

Hodgkin, A. L., Huxley, A. F. and Katz, B. (1952) ‘Measurement of current-voltage relations in the membrane of the giant axon of Loligo’, *The Journal of Physiology*. doi: 10.1113/jphysiol.1952.sp004716.

Hodgkin, A. L. and Katz, B. (1949) ‘The effect of sodium ions on the electrical activity of the giant axon of the squid’, *The Journal of Physiology*. doi: 10.1113/jphysiol.1949.sp004310.

Hofer, C. *et al.* (2002) ‘A stimulator for functional activation of denervated muscles’, in *Artificial Organs*. doi: 10.1046/j.1525-1594.2002.06951.x.

van den Honert, C. and Mortimer, J. T. (1979) ‘The response of the myelinated nerve fiber to short duration biphasic stimulating currents’, *Annals of Biomedical Engineering*. doi: 10.1007/BF02363130.

Horn, C. C., Ardell, J. L. and Fisher, L. E. (2019) ‘Electroceutical Targeting of the Autonomic Nervous System’, *Physiology*, 34(2), pp. 150–162. doi: https://doi.org/10.1152/physiol.00030.2018.

Hughes, M. L., Choi, S. and Glickman, E. (2018) ‘What can stimulus polarity and interphase gap tell us about auditory nerve function in cochlear-implant recipients?’, *Hearing Research*. doi: 10.1016/j.heares.2017.12.015.

Hursh, J. B. (1939) ‘CONDUCTION VELOCITY AND DIAMETER OF NERVE FIBERS’, *American Journal of Physiology-Legacy Content*. doi: 10.1152/ajplegacy.1939.127.1.131.

Huxley, A. F. and Niedergerke, R. (1954) ‘Structural changes in muscle during contraction: Interference microscopy of living muscle fibres’, *Nature*. doi: 10.1038/173971a0.

Huxley, A. F. and Stämpfli, R. (1949) ‘Evidence for saltatory conduction in peripheral myelinated nerve fibres’, *The Journal of Physiology*. doi: 10.1113/jphysiol.1949.sp004335.

Huxley, H. and Hanson, J. (1954) ‘Changes in the Cross-striations of muscle during contraction and stretch and their structural interpretation’, *Nature*. doi: 10.1038/173973a0.

IEEE (2006) *IEEE Standard for Safety Levels With Respect to Human Exposure to Radio Frequency Electromagnetic Fields, 3 kHz to 300 GHz, IEEE Std C95.1-2005 (Revision of IEEE Std C95.1-1991)*. doi: 10.1109/IEEESTD.2006.99501.

Jezernik, S. and Morari, M. (2005) ‘Energy-optimal electrical excitation of nerve fibers’, *IEEE Transactions on Biomedical Engineering*. doi: 10.1109/TBME.2005.844050.

Johns, P. (2014) ‘Neurons and glial cells’, in *Clinical Neuroscience*, pp. 61–69. doi: https://doi.org/10.1016/B978-0-443-10321-6.00005-9.

Johnson, P. F. *et al.* (1977) ‘An in vitro and in vivo analysis of anodized tantalum capacitive electrodes: Corrosion response, physiology, and histology’, *Journal of Biomedical Materials Research*. doi: 10.1002/jbm.820110502.

Kaczmarek, P. *et al.* (2010) ‘Investigation of the relationship between stimulus parameters and a human muscle contraction force during stimulation of the gastrocnemius muscle’, *Artificial Organs*. doi: 10.1111/j.1525-1594.2009.00759.x.

Katz, B. (1966) *Nerve, muscle, and synapse*. McGraw-Hill.

Kelliher, E. M. and Rose, T. L. (1987) ‘Evaluation of Charge Injection Properties of Thin Film Redox Materials for use as Neural Stimulation Electrodes’, *MRS Proceedings*. doi: 10.1557/proc-110-23.

Kern, H. (2014) ‘Funktionelle Elektrostimulation paraplegischer Patienten’, *Östereichische Zeitschrift für Physikalische Medizin 1995*. doi: 10.4081/ejtm.2014.2940.

Khalifa, A. *et al.* (2019) ‘The Microbead: A 0.009 mm3 Implantable Wireless Neural Stimulator’, *IEEE Transactions on Biomedical Circuits and Systems*. doi: 10.1109/TBCAS.2019.2939014.

Kim, J. R. *et al.* (2010) ‘The relationship between electrically evoked compound action potential and speech perception: A study in cochlear implant users with short electrode array’, *Otology and Neurotology*. doi: 10.1097/MAO.0b013e3181ec1d92.

Ko, C. P. (2001) ‘Neuromuscular System’, in *International Encyclopedia of the Social & Behavioral Sciences*, pp. 10595–10600. doi: https://doi.org/10.1016/B0-08-043076-7/03482-3.

Koester, J. (1985a) ‘Resting membrane potential and action potential’, in Kandel, E. R. and Schwartz, J. H. (eds) *Principles of Neural Science*. 2nd edn. New York: Elsevier, pp. 49–57.

Koester, J. (1985b) ‘Voltage gated channels and the generation of the action potential’, in Kandel, E. R. and Schwartz, J. H. (eds) *Principles of Neural Science*. 2nd edn. New York: Elsevier, pp. 75–86.

Krouchev, N. I. *et al.* (2014) ‘Energy-optimal electrical-stimulation pulses shaped by the least-action principle’, *PLoS ONE*. doi: 10.1371/journal.pone.0090480.

Kumsa, D. W. *et al.* (2017) ‘Electron transfer processes occurring on platinum neural stimulating electrodes: Pulsing experiments for cathodic-first, charge-balanced, biphasic pulses for $0.566 \leq k \leq 2.3$ in rat subcutaneous tissues’, *Journal of Neural Engineering*. doi: 10.1088/1741-2552/aa7a4a.

Kwende, M. M. N., Jarvis, J. C. and Salmons, S. (1995) ‘The input-output relations of skeletal muscle’, *Proceedings of the Royal Society B: Biological Sciences*. doi: 10.1098/rspb.1995.0136.

Lagow, C. H., Sladek, K. J. and Richardson, P. C. (1971) ‘Anodic Insulated Tantalum Oxide Electrocardiograph Electrodes’, *IEEE Transactions on Biomedical Engineering*. doi: 10.1109/TBME.1971.4502820.

Lapicque, L. (1907) ‘Recherches quantitatives sur l’excitation électrique des nerfs traitée comme une polarisation’, *J. Physiol. Pathol. Gen*. doi: 10.1007/s00422-007-0189-6.

Larsson, L. and Yu, F. (1997) ‘Gender-related differences in the regulatory influence of thyroid hormone on the expression of myosin isoforms in young and old rats’, *Acta Physiologica Scandinavica*. doi: 10.1046/j.1365-201X.1997.559328000.x.

Lee, B. *et al.* (2018) ‘An Implantable Peripheral Nerve Recording and Stimulation System for Experiments on Freely Moving Animal Subjects’, *Scientific Reports*. doi: 10.1038/s41598-018-24465-1.

Leote, J., Pereira, P. and Valls-Sole, J. (2017) ‘Double peak sensory nerve action potentials to single stimuli in nerve conduction studies’, *Muscle and Nerve*. doi: 10.1002/mus.25486.

Liddell, E. and Sherrington, C. (1925) ‘Recruitment and some other features of reflex inhibition’, *Proceedings of the Royal Society of London. Series B, Containing Papers of a Biological Character*. doi: 10.1098/rspb.1925.0016.

Loeb, G. E. *et al.* (1991) ‘Injectable microstimulator for functional electrical stimulation’, *Medical & Biological Engineering & Computing*. doi: 10.1007/BF02446097.

Luo, Y. S. *et al.* (2013) ‘Ultrasonic power/data telemetry and neural stimulator with OOK-PM signaling’, *IEEE Transactions on Circuits and Systems II: Express Briefs*. doi: 10.1109/TCSII.2013.2286000.

Ma, Y. *et al.* (2018) ‘Enabling deep-tissue networking for miniature medical devices’, in. doi: 10.1145/3230543.3230566.

Maciejasz, P. *et al.* (2015) ‘Delaying discharge after the stimulus significantly decreases muscle activation thresholds with small impact on the selectivity: an in vivo study using TIME’, *Medical and Biological Engineering and Computing*. doi: 10.1007/s11517-015-1244-4.

Mayr, W. *et al.* (2002) ‘Functional Electrical Stimulation (FES) of Denervated Muscles : Existing and Prospective Technological Solutions’, *European Journal of Translational Myology*.

McCreery, D. B. *et al.* (1988) ‘Comparison of neural damage induced by electrical stimulation with faradaic and capacitor electrodes’, *Annals of Biomedical Engineering*. doi: 10.1007/BF02368010.

McIntyre, C. C., Richardson, A. G. and Grill, W. M. (2002) ‘Modeling the Excitability of Mammalian Nerve Fibers: Influence of Afterpotentials on the Recovery Cycle’, *Journal of Neurophysiology*. doi: 10.1152/jn.00353.2001.

McKay, C. M. and Henshall, K. R. (2003) ‘The perceptual effects of interphase gap duration in cochlear implant stimulation’, *Hearing Research*, 181(1–2), pp. 94–99. doi: 10.1016/S0378-5955(03)00177-1.

McNeal, D. R. (1976) ‘Analysis of a Model for Excitation of Myelinated Nerve’, *IEEE Transactions on Biomedical Engineering*. doi: 10.1109/TBME.1976.324593.

Merletti, R. (1997) ‘Standards for reporting EMG data’, *Journal of Electromyography and Kinesiology*. doi: 10.1016/s1050-6411(97)90001-8.

Merrill, D. R., Bikson, M. and Jefferys, J. G. R. (2005) ‘Electrical stimulation of excitable

tissue: Design of efficacious and safe protocols', *Journal of Neuroscience Methods*. doi: 10.1016/j.jneumeth.2004.10.020.

Mortimer, J. T. and Bhadra, N. (2018) 'Fundamentals of Electrical Stimulation', in *Neuromodulation*. 2nd edn. Elsevier, pp. 71–82. doi: 10.1016/B978-0-12-805353-9.00006-1.

Naples, G. G. *et al.* (1988) 'A Spiral Nerve Cuff Electrode for Peripheral Nerve Stimulation', *IEEE Transactions on Biomedical Engineering*. doi: 10.1109/10.8670.

Neely, R. M. *et al.* (2018) 'Recent advances in neural dust: towards a neural interface platform', *Current Opinion in Neurobiology*. doi: 10.1016/j.conb.2017.12.010.

Okusa, M. D., Rosin, D. L. and Tracey, K. J. (2017) 'Targeting neural reflex circuits in immunity to treat kidney disease', *Nature Reviews Nephrology*. doi: 10.1038/nrneph.2017.132.

Peckham, P. H. and Knutson, J. S. (2005) 'Functional Electrical Stimulation for Neuromuscular Applications', *Annual Review of Biomedical Engineering*. doi: 10.1146/annurev.bioeng.6.040803.140103.

Piech, D. K. *et al.* (2020) 'A wireless millimetre-scale implantable neural stimulator with ultrasonically powered bidirectional communication', *Nature Biomedical Engineering*. doi: 10.1038/s41551-020-0518-9.

Polasek, K. H. *et al.* (2007) 'Human nerve stimulation thresholds and selectivity using a multi-contact nerve cuff electrode', *IEEE Transactions on Neural Systems and Rehabilitation Engineering*. doi: 10.1109/TNSRE.2007.891383.

Poletto, C. J. and Van Doren, C. L. (2002) 'Elevating pain thresholds in humans using depolarizing prepulses', *IEEE Transactions on Biomedical Engineering*. doi: 10.1109/TBME.2002.803563.

Prado-Guitierrez, P. *et al.* (2006a) 'Effect of interphase gap and pulse duration on electrically evoked potentials is correlated with auditory nerve survival', *Hearing Research*, 215(1–2), pp. 47–55. doi: 10.1016/j.heares.2006.03.006.

Prado-Guitierrez, P. *et al.* (2006b) 'Effect of interphase gap and pulse duration on electrically evoked potentials is correlated with auditory nerve survival', *Hearing Research*. doi: 10.1016/j.heares.2006.03.006.

Ramekers, D. *et al.* (2014) 'Auditory-nerve responses to varied inter-phase gap and phase

duration of the electric pulse stimulus as predictors for neuronal degeneration', *JARO - Journal of the Association for Research in Otolaryngology*. doi: 10.1007/s10162-013-0440-x.

Ramón y Cajal, S. (1911) 'Histologie du systeme nerveux de l'homme et des vertebres', *Paris Maloine*. doi: 10.1109/WiCom.2008.1401.

Rattay, F. (1986) 'Analysis of Models for External Stimulation of Axons', *IEEE Transactions on Biomedical Engineering*. doi: 10.1109/TBME.1986.325670.

Reilly, J. and Diamant, A. (2011) *Electrostimulation: Theory, Applications, and Computational Model*. Artech House Publishers.

Robblee, L. S. (1983) 'Activated Ir: An Electrode Suitable for Reversible Charge Injection in Saline Solution', *Journal of The Electrochemical Society*. doi: 10.1149/1.2119793.

Rose, T. L., Kelliher, E. M. and Robblee, L. S. (1985) 'Assessment of capacitor electrodes for intracortical neural stimulation', *Journal of Neuroscience Methods*. doi: 10.1016/0165-0270(85)90001-9.

Rose, T. L. and Robblee, L. S. (1990) 'Electrical Stimulation with Pt Electrodes. VIII. Electrochemically Safe Charge Injection Limits with 0.2 MS Pulses', *IEEE Transactions on Biomedical Engineering*. doi: 10.1109/10.61038.

Rushton, W. A. H. (1951) 'A theory of the effects of fibre size in medullated nerve', *The Journal of Physiology*. doi: 10.1113/jphysiol.1951.sp004655.

Rydevik, B., Lundborg, G. and Bagge, U. (1981) 'Effects of graded compression on intraneural blood flow: An in vivo study on rabbit tibial nerve', *Journal of Hand Surgery*. doi: 10.1016/S0363-5023(81)80003-2.

Sabetian, P. *et al.* (2017) 'Characterizing the reduction of stimulation artifact noise in a tripolar nerve cuff electrode by application of a conductive shield layer', *Medical Engineering and Physics*. doi: 10.1016/j.medengphy.2016.11.010.

Sacramento, J. F. *et al.* (2018) 'Bioelectronic modulation of carotid sinus nerve activity in the rat: a potential therapeutic approach for type 2 diabetes', *Diabetologia*. doi: 10.1007/s00125-017-4533-7.

Sahin, M. and Pikov, V. (2011) 'Wireless microstimulators for neural prosthetics', *Critical Reviews in Biomedical Engineering*. doi: 10.1615/CritRevBiomedEng.v39.i1.50.

Sahin, M. and Tie, Y. (2007) ‘Non-rectangular waveforms for neural stimulation with practical electrodes.’, *Journal of neural engineering*, 4(3), pp. 227–233. doi: 10.1088/1741-2560/4/3/008.

Salmons, S. *et al.* (2005) ‘Functional electrical stimulation of denervated muscles: Basic issues’, *Artificial Organs*. doi: 10.1111/j.1525-1594.2005.29034.x.

Sassen, M. and Zimmermann, M. (1973) ‘Differential blocking of myelinated nerve fibres by transient depolarization’, *Pflügers Archiv European Journal of Physiology*. doi: 10.1007/BF00592788.

Scheiner, A., Mortimer, J. T. and Roessmann, U. (1990) ‘Imbalanced biphasic electrical stimulation: Muscle tissue damage’, *Annals of Biomedical Engineering*. doi: 10.1007/BF02364157.

Schvartz-Leyzac, K. C. and Pfingst, B. E. (2016) ‘Across-site patterns of electrically evoked compound action potential amplitude-growth functions in multichannel cochlear implant recipients and the effects of the interphase gap’, *Hearing Research*. doi: 10.1016/j.heares.2016.08.002.

Shannon, R. V. (1992) ‘A Model of Safe Levels for Electrical Stimulation’, *IEEE Transactions on Biomedical Engineering*. doi: 10.1109/10.126616.

Shepherd, R. K. and Javel, E. (1999) ‘Electrical stimulation of the auditory nerve: II. Effect of stimulus waveshape on single fibre response properties’, *Hearing Research*. doi: 10.1016/S0378-5955(99)00011-8.

Son, Y. H. *et al.* (2019) ‘Comparative molecular analysis of endurance exercise in vivo with electrically stimulated in vitro myotube contraction’, *Journal of Applied Physiology*. doi: 10.1152/japplphysiol.00091.2019.

Springer, S. *et al.* (2014) ‘The Effect of Electrode Placement and Interphase Interval on Force Production During Stimulation of the Dorsiflexor Muscles’, *Artificial Organs*. doi: 10.1111/aor.12346.

Strojnik, P. *et al.* (1987) ‘Treatment of drop foot using an implantable peroneal underknee stimulator’, *Scandinavian Journal of Rehabilitation Medicine*. doi: 10.1016/0268-0033(87)90024-6.

Sweeney, J. D., Mortimer, J. T. and Durand, D. M. (1987) ‘Modeling of mammalian myelinated nerve for functional neuromuscular stimulation’, *IEEE 9th Annual Conference of the Engineering in Medicine and Biology Society*.

Tanabe, Y. *et al.* (2017) ‘High-performance wireless powering for peripheral nerve neuromodulation systems’, *PLoS ONE*. doi: 10.1371/journal.pone.0186698.

Targan, R. S., Alon, G. and Kay, S. L. (2000) ‘Effect of long-term electrical stimulation on motor recovery and improvement of clinical residuals in patients with unresolved facial nerve palsy’, *Otolaryngology - Head and Neck Surgery*. doi: 10.1016/S0194-5998(00)70248-8.

Tyler, D. J. (2018) ‘Electrodes for the Neural Interface’, in *Neuromodulation (Second Edition)*, pp. 239–274.

Vareĵao, A. S. P. *et al.* (2004) ‘Functional and morphological assessment of a standardized rat sciatic nerve crush injury with a non-serrated clamp’, *Journal of Neurotrauma*. doi: 10.1089/neu.2004.21.1652.

Vargas Luna, J. L. *et al.* (2017) ‘Optimization of Interphase Intervals to Enhance the Evoked Muscular Responses of Transcutaneous Neuromuscular Electrical Stimulation’, *Artificial Organs*. doi: 10.1111/aor.12921.

Vargas Luna, J. L., Mayr, W. and Cortés-Ramirez, J. A. (2018) ‘Sub-threshold depolarizing pre-pulses can enhance the efficiency of biphasic stimuli in transcutaneous neuromuscular electrical stimulation’, *Medical and Biological Engineering and Computing*. doi: 10.1007/s11517-018-1851-y.

Vastani, N. *et al.* (2013) ‘Preconditioning depolarizing ramp currents enhance the effect of sodium channel blockers in primary sensory afferents’, *Neuromodulation*. doi: 10.1111/ner.12031.

Weitz, A. C. *et al.* (2014) ‘Interphase gap as a means to reduce electrical stimulation thresholds for epiretinal prostheses’, *Journal of Neural Engineering*, 11(1). doi: 10.1088/1741-2560/11/1/016007.

Willand, M. P. and de Bruin, H. (2008) ‘Design and testing of an instrumentation system to reduce stimulus pulse amplitude requirements during FES.’, *Conference proceedings : ... Annual International Conference of the IEEE Engineering in Medicine and Biology Society. IEEE Engineering in Medicine and Biology Society. Conference*. doi: 10.1109/IEMBS.2008.4649775.

Wongsarnpigoon, A. and Grill, W. M. (2010) ‘Energy-efficient waveform shapes for neural stimulation revealed with a genetic algorithm’, *Journal of Neural Engineering*, 7(4). doi: 10.1088/1741-2560/7/4/046009.

Wongsarnpigoon, A., Woock, J. P. and Grill, W. M. (2010) 'Efficiency analysis of waveform shape for electrical excitation of nerve fibers', *IEEE Transactions on Neural Systems and Rehabilitation Engineering*, 18(3), pp. 319–328. doi: 10.1109/TNSRE.2010.2047610.

Wu, P. *et al.* (2014) 'Key changes in denervated muscles and their impact on regeneration and reinnervation', *Neural Regeneration Research*. doi: 10.4103/1673-5374.143424.

Yeagle, S. P., Mayer, R. F. and Max, S. R. (1983) 'Contractile properties of rat fast-twitch skeletal muscle during reinnervation: Effects of testosterone and castration', *Experimental Neurology*. doi: 10.1016/0014-4886(83)90407-7.

9 APPENDICES

APPENDIX 1 LABVIEW STIMULATION CODE

LabVIEW stimulation front panel and parameters:

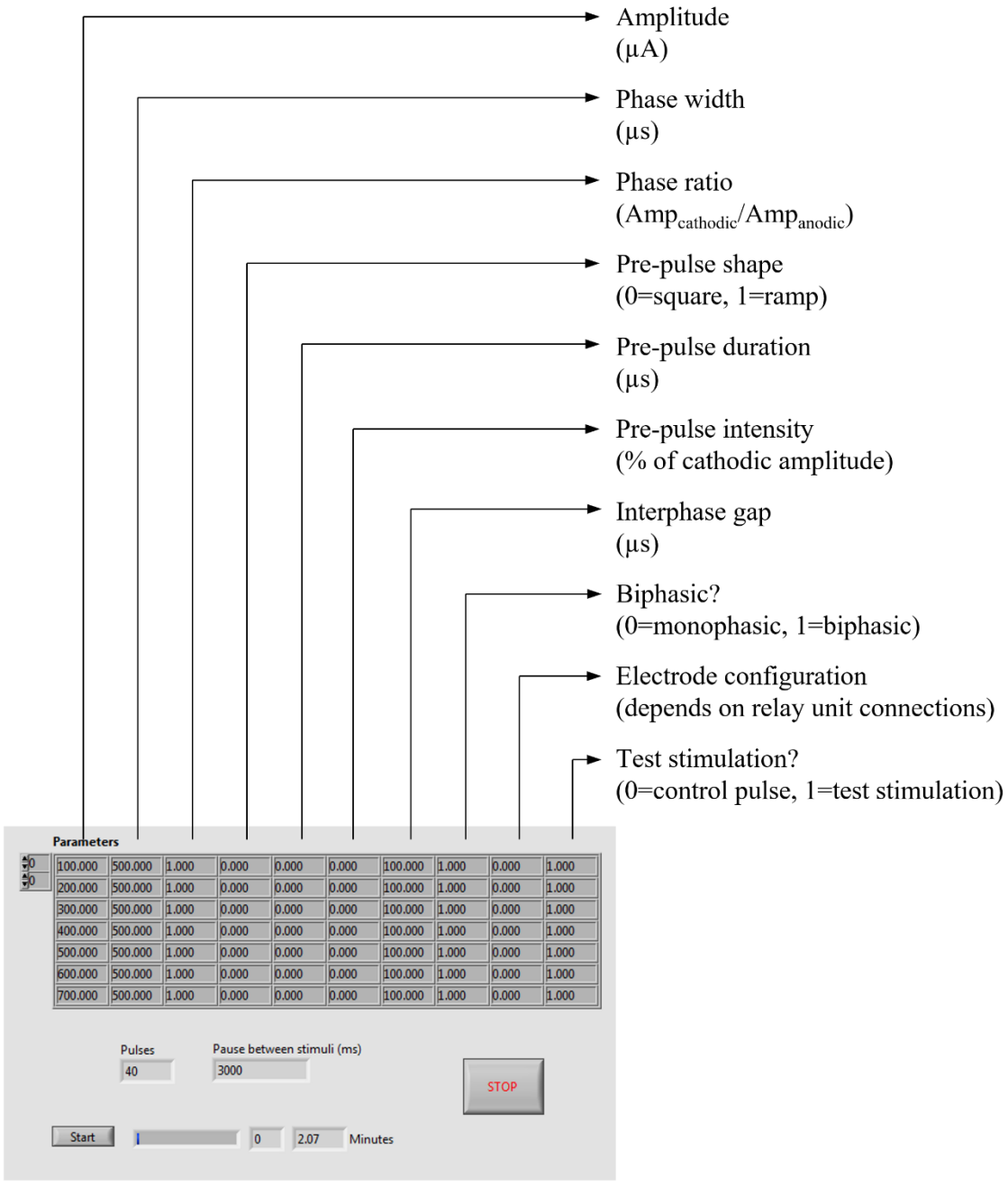

LabVIEW stimulation block diagram (test stimulation):

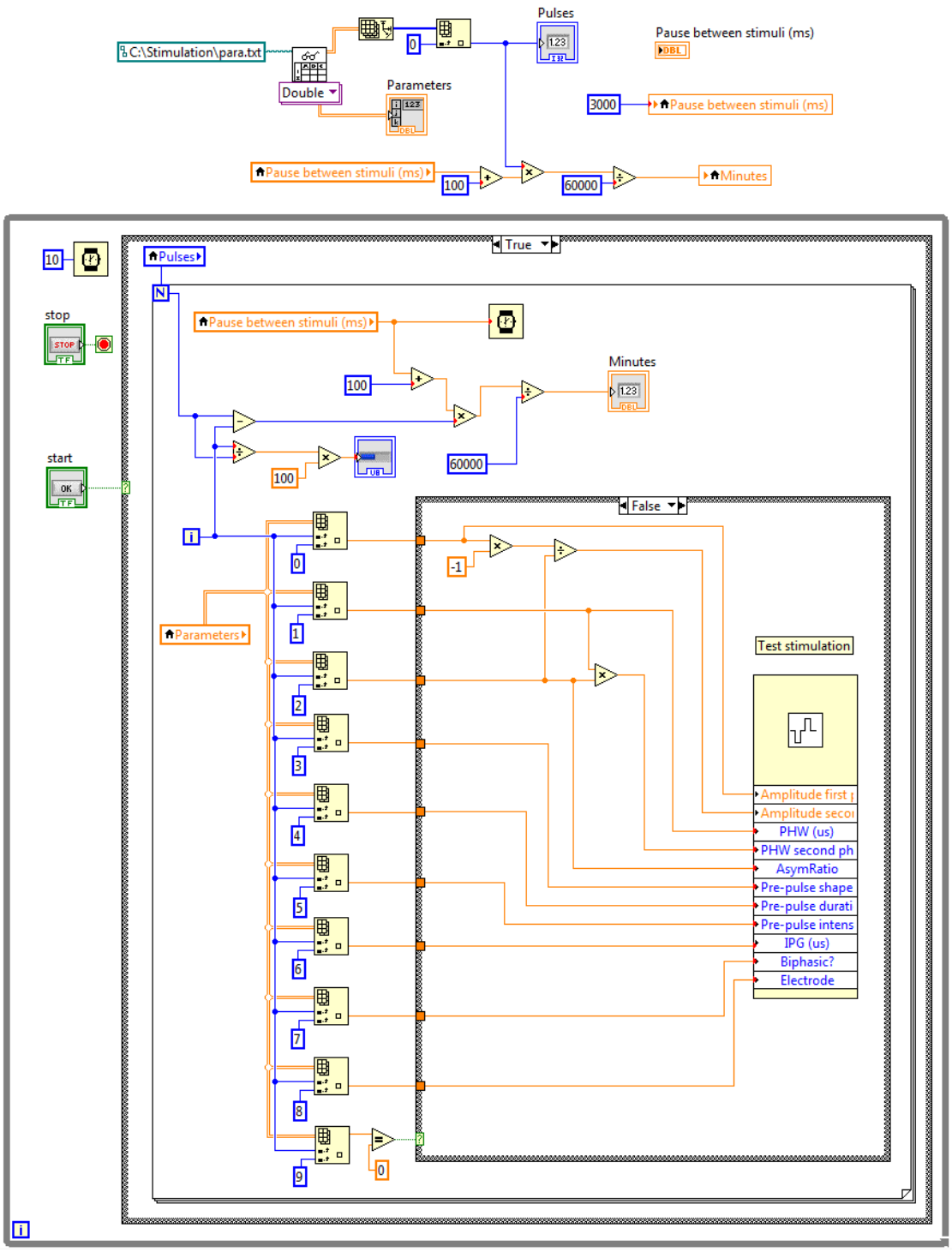

LabVIEW stimulation block diagram (control stimulation):

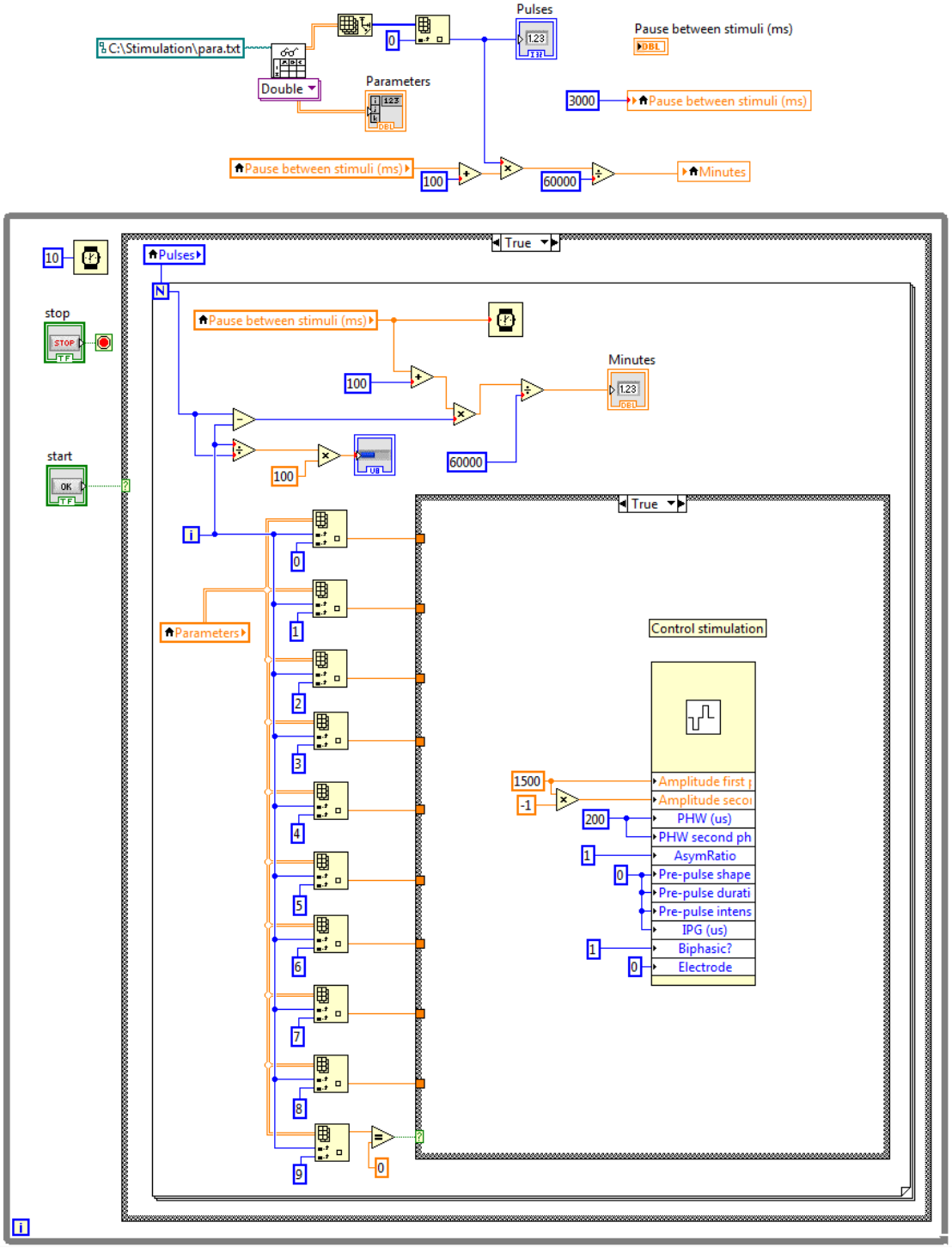

LabVIEW pulse generator sub-VI

(exemplary block diagram for biphasic pulse with square pre-pulses)

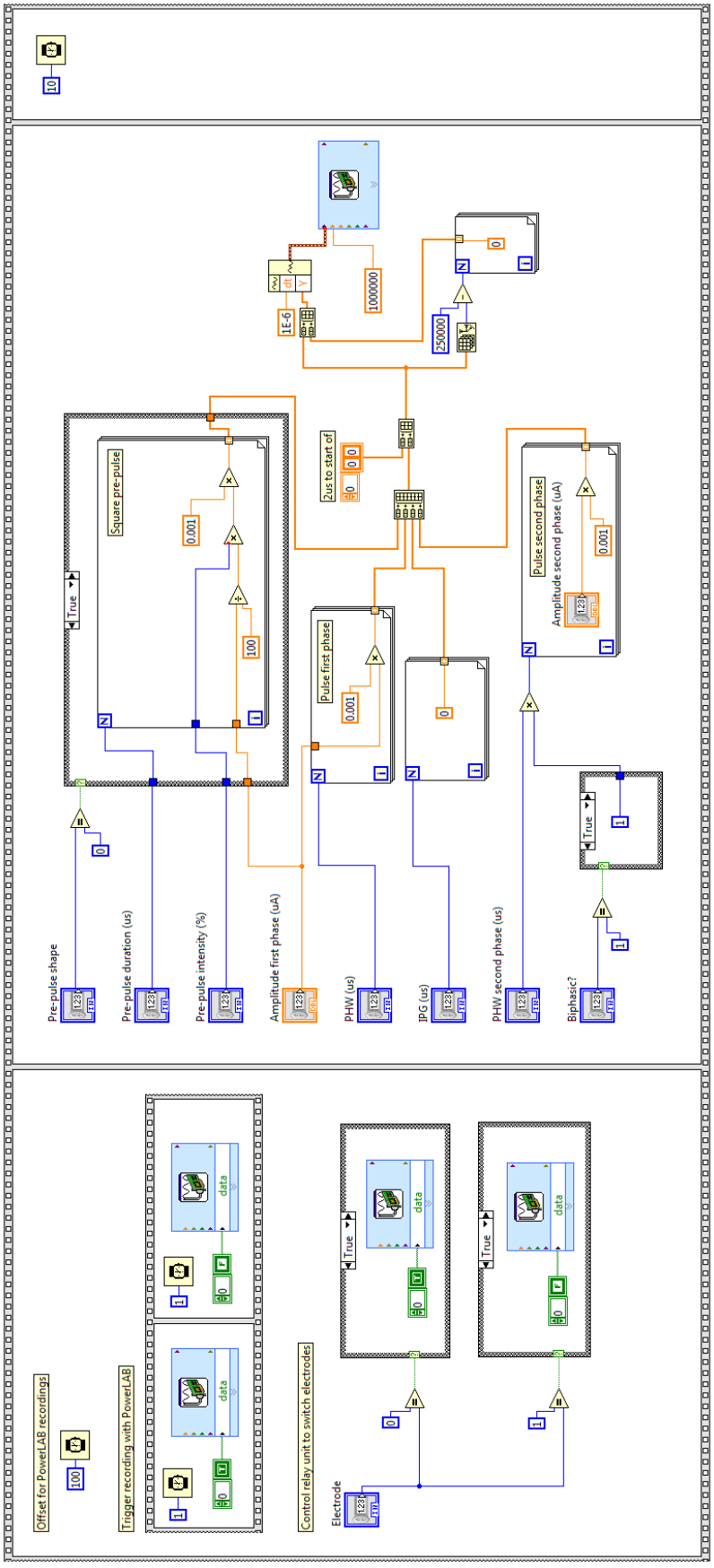

LabVIEW pulse generator sub-VI

(exemplary block diagram for biphasic pulse with ramp pre-pulses)

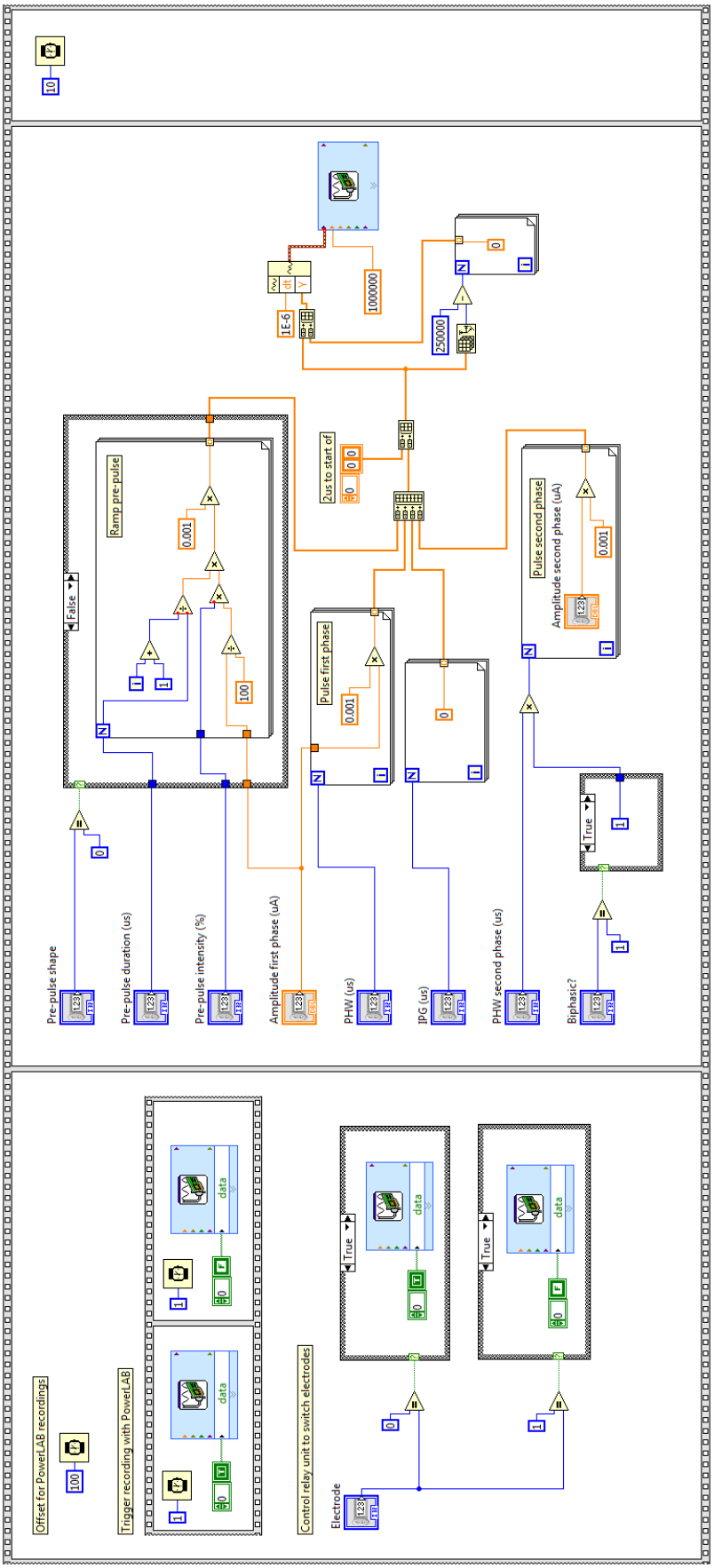

APPENDIX 2 MATLAB TWITCH FORCE ANALYSIS CODES

This first code section analyses the raw twitch force recordings and normalizes the data to the control pulse level:

```
%% read parameter file
[filepath,filefolder]=uigetfile({'*.xlsx'},'Select the parameter xlsx file');
Data_Path=fullfile(filefolder,filepath);

para = xlsread(Data_Path);

%% create data matrices
Num_Stim=length(para);
Data_F=[];

roi_start=8001;                                         %define region of interest (roi) in which to search for the muscle twitch
roi_end=42000;

for i=1:Num_Stim
    Data_F(i,:)=data(datastart(i):dataend(i));
    F_max=max(Data_F(i,roi_start:roi_end));             %find maximal twitch force in roi
    F_pas=mean(Data_F(i,1:roi_start));                  %calculate passive muscle tension before roi
    F_dev(i)=F_max-F_pas;                               %calculate developed twitch force
end

para(:,11)=F_dev.';

%% normalization of force ata
idx_ctrl=find(para(:,10)==0);
ctrl_lin=interp1(idx_ctrl,para(idx_ctrl,11),1:1:Num_Stim).';    %create control pulse level by linear interpolation

for i=1:Num_Stim
    para(i,12)=para(i,11)/ctrl_lin(i);
end

%% plot control pulses
h = figure;
plot(ctrl_lin,'r')
axis([0 length(ctrl_lin) 0 1.1*max(ctrl_lin)])
hold on
plot(idx_ctrl,ctrl_lin(idx_ctrl),'r*')
```

The normalized data set is then, depending on the specific series (i.e. recruitment curves) contained within it, sorted and fed as matrix RC into the following program. This next code section is used to determine the 10, 50, and 90% activation thresholds by linear interpolation of the recorded twitch force measurements:

```
%% properties of recruitment curve (RC) matrix
AMPs_test=[550:50:1700];                                %amplitude increments of RC
Traces=[1:1:12];                                        %numer of recruitment curves

%% linear interpolation of RC
RC_int_lin=interp1(AMPs_test,RC,min(AMPs_test):1:max(AMPs_test));

%find threshold values
for i=1:length(Traces)
    if min(RC_int_lin(:,i))>0.1
        A_10_Thres_lin(i)    = nan;
    elseif max(RC_int_lin(:,i))<0.1
        A_10_Thres_lin(i)    = nan;
    else
    A_10_Thres_lin(i)    = find(RC_int_lin(:,i) >= 0.1, 1, 'first')+min(AMPs_test);     %determine 10% threshold
    end

    if min(RC_int_lin(:,i))>0.5
        A_50_Thres_lin(i)    = nan;
    elseif max(RC_int_lin(:,i))<0.5
        A_50_Thres_lin(i)    = nan;
    else
    A_50_Thres_lin(i)    = find(RC_int_lin(:,i) >= 0.5, 1, 'first')+min(AMPs_test);     %determine 50% threshold
    end

    if min(RC_int_lin(:,i))>0.9
        A_90_Thres_lin(i)    = nan;
    elseif max(RC_int_lin(:,i))<0.9
        A_90_Thres_lin(i)    = nan;
    else
    A_90_Thres_lin(i)    = find(RC_int_lin(:,i) >= 0.9, 1, 'first')+min(AMPs_test);     %determine 90% threshold
    end
end

A_Thresholds =[A_10_Thres_lin;A_50_Thres_lin;A_90_Thres_lin];
```

APPENDIX 3A MATLAB ENG ANALYSIS CODES (SHORT PHW)

```
%% powerLab channel settings
fs=100000;                                                  %sampling rate of ENG recording

%% create data matrix
data_all=[];
data_roi=[];

roi=50000;                                                  %region of interest from beginning of recording
phw_us=200;                                                 %set phase widths in us
phw=phw_us/1000000*fs;

    for i=1:length(blocktimes)
        data_all(i,:)=data(datastart(i):dataend(i));
    end

data_roi=data_all(:,1:roi);

%% find artefact merged with ecap
HZ_50=fs/50;
ecap=[];
idx_th=-0.005;                                              %set threshold for artifact detection in V

    for i=1:size(data_roi,1)
        idx_art=find(data_roi(i,:)<=idx_th,1,'first');
        ecap(i,:)=(data_roi(i,(idx_art+(2*phw+100)):(idx_art+(2*phw+2000))))
        -(data_roi(i,(idx_art+(2*phw+100-HZ_50)):(idx_art+(2*phw+2000-HZ_50))));
    end
```

APPENDIX 3B MATLAB ENG ANALYSIS CODES (LONG PHW)

```
%% powerLab channel settings
fs=100000;                                                                  %sampling rate of ENG recording

%% create data matrix
data_all=[];
data_roi=[];

roi=50000;                                                                  %region of interest from beginning of recording

    for i=1:length(blocktimes)
        data_all(i,:)=data(datastart(i):dataend(i));
    end

data_roi=data_all(:,1:roi);

%% find artefact merged with ecap
HZ_50=fs/50;
ecap_merged=[];
idx_th=-0.005;                                                              %set threshold for artifact detection in V

    for i=1:size(data_roi,1)
        idx_art=find(data_roi(i,:)<=idx_th,1,'first');
        ecap_merged(i,:)=(data_roi(i,(idx_art-99):idx_art+900))-(data_roi(i,(idx_art-99-HZ_50):(idx_art+900-HZ_50)));
    end

%% trace and isolate ecap
ecap_pure=zeros(size(ecap_merged));
figure;

for i=1:size(ecap_merged,1)
clf
plot(ecap_merged(i,:),'k','LineWidth',2)                                    %plot artefact-ecap-comnplex
hold on;
pause                                                                       %pause to allow the user to zoom into the ecap

xs = [];
ys = [];
xold = 0;
yold = 0;
but = 1;

while but == 1
    [xi, yi, but] = ginput(1);                                              %user input to trace ecap
    xs = [xs; xi];
    ys = [ys; yi];
    if xold
        plot([xold xi], [yold yi], 'bo','LineWidth',2);
    else
        plot(xi, yi, 'bo','LineWidth',2);
    end
    xold = xi;
    yold = yi;
end

plot([xi xs(1)], [yi ys(1)], 'g-');
hold off;

xs=round(xs,0);
cs=spline(xs,ys);
xx=(xs(1):1:xs(end));
hold on
plot(xx,ppval(cs,xx),'r','LineWidth',2)

ecap_pure(i,xs(1):1:xs(end))=(ecap_merged(i,xs(1):1:xs(end))-ppval(cs,xx)); %substract artefact from ecap
end
```

APPENDIX 4 LABCHART CELL STIMULATION PROGRAM

(Exemplary settings: 10V amplitude, biphasic, phase width 1ms, 10Hz frequency)